ON MICRODOSIMETRY OF NEUTRONS OF SELECTABLE ENERGY IN MIXED (N,Y) FIELDS

Elias Bin Saion

A Thesis Submitted for the Degree of PhD
at the
University of St. Andrews

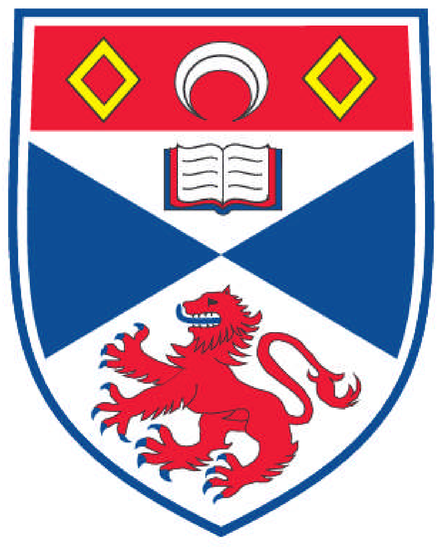

1989

ON MICRODOSIMETRY OF NEUTRONS OF SELECTABLE ENERGY IN MIXED (n,γ) FIELDS

by

ELIAS BIN SAION

BSc. (National Univ., Malaysia) and MSc. (Surrey, U.K.)

A thesis presented for the degree of Doctor of Philosophy

University of St. Andrews

St. Andrews, Fife KY16 9SS

Scotland, United Kingdom.

April, 1989

CONTENTS OF THE THESIS

DECLARATION

I hereby declare that this thesis has been composed by myself, that it is a record of my own work, and that it has not previously been presented for a higher degree.

This research was carried out in the Department of Physics, in the University of St. Andrews under the supervision of Dr. D.E. Watt.

Elias Bin Saion

CERTIFICATE

I hereby certify that the candidate, Elias Bin Saion, has fulfilled the conditions of the Resolution and Regulations of the University of St Andrews appropriate to the Degree of Doctor of Philosophy.

David E. Watt

Research Supervisor

ACKNOWLEDGEMENTS

I wish to express my gratitude to my supervisor, Dr. D.E. Watt (PhD., DSc., F. Inst. P.) for the invaluable guidance, continuing advice and encouragement and stimulating discussions throughout the course of this research.

Thanks are also due to all those who contributed directly or indirectly and particular to

Dr. B.W. East, Dr. T. Preston and Dr. H.M. Banford of the Scottish Universities Research and Reactor Centre for technical supervisons and assistances and providing irradiation facilities during my field work.

Dr. J. Ball, Dr. J. Henderson and Mr. B. Campbell of the Computer Centre for computing advices and services.

Mr. McCraw, Mr. M. Whyte, Mr. T. McQueen and Mr. J. Clark of the Mechanical Workshop for assemble the vacuum system, constructing the main part of the counters and technical assistance in TE film preparation.

Mr. M. Robertson and Mr. J. McWade of the Electronic Workshop for technical assistance and constructing the coincidence/anti-coincidence unit.

The fellow research colleagues for encouragement and understanding.

The Commision of European Communities for financial support under contract no. BIO-A-024-UK.

The Malaysian Government and University of Agriculture Malaysia for financial support.

Lastly, but not the least, I wish to express my gratitute to my mother and immediate family for their continuous support.

With great emphasis, my special thanks is due to my wife and children, to whom I share my happiness and sorrow, for their patience and understanding and also for her continuous support and encouragement, throughout our memorable stay in St. Andrews, the ancient city of Scotland.

ABSTRACT

Biological damage of tissue due to intermediate energy neutrons is generally known to be very important in radiobiology and radiation protection. However, there is no suitable method to determine the quality of these neutrons, in particular, in the working environment of mixed (n,γ) radiation fields. In this thesis, an attempt is made to develop a dosimeter based on microdosimetric principles which has the capability for such a purpose. With this object the basic concepts of microdosimetry are reviewed and discussed with emphasis on their application for radiation protection and in designing of the dosimeter.

Microdosimetry based on low pressure tissue-equivalent proportional counters (TEPCs) is a powerful technique for determining microscopic distributions of energy deposition and quality of ionizing radiations. However the energy deposition spectra of intermediate energy neutrons in mixed fields of fast neutrons can only be measured using TEPC in co-axial double cylindrical form by an appropriate choice for the thickness of the common tissue-equivalent (TE) dividing wall separating the inner and outer counters and by appropriate use of coincidence/anti-coincidence pulse arrangements. An analytical calculation for the response of the inner counter operating in coincidence/anti-coincidence modes with the outer counter was developed. However there will be some events, due to fast neutrons, which will contribute to the signals from intermediate energy neutrons and which cannot be removed by anti-coincidence. For these analytical corrections must be made. Also, the events associated with the dividing wall inherent in the system can contribute to the response of the inner counter and must be corrected by calculation. The calculation was possible due to the fact that recoil particles from intermediate energy neutron interactions have effective stopping powers and projected ranges which differ significantly from the continuous slowing down approximation (CSDA) values. By incorporating these the basic CSDA formulae for energy deposition spectra of neutrons could be extended down to intermediate energy neutrons of about 1 keV.

A prototype co-axial double cylindrical TEPC capable of separating the component of neutrons (≤ 850 keV) in mixed (n,γ) radiation fields was manufactured and tested. The thin wall dividing the inner and outer counters was fabricated from the standard A-150 TE plastic with the thickness equivalent to the range of 850 keV protons. The operational characteristics of the dosimeter were studied to determine its applicability for use in microdosimetry. The gas gain of the inner and outer TEPCs was measured at various simulated mean chord lengths and applied voltages. The results can be expressed according to Campion's equation within a given range of the electric field strength. The resolution of the inner TEPC measured at the operating voltages is in agreement with the theoretical prediction.

A series of microdosimetric experiments were performed with mixed fields of ^{60}Co gamma-rays and neutrons from the UTR-300 nuclear reactor and from ^{252}Cf and ^{241}Am-Be radioactive sources. Discrimination against fast neutrons of energy > 850 keV was achieved using an anti-coincidence unit specially designed for better efficiency of data acquisition. Discrimination against fast electrons due to photon interactions was also achieved. Spectra with anti-coincidence are dominated by slow protons and electrons. Their mean lineal energies are higher than those of spectra without anti-coincidence. The quality factor and dose equivalent for spectra with anti-coincidence are higher than the spectra without anti-coincidence indicating the importance of intermediate energy neutrons in mixed fields. The quality factor and the corresponding dose equivalent corrected for saturation of lineal energy corresponding to 2 nm of ionization spacing is consistently higher than those derived from the absorbed dose based formulae, the biophysical implications of which are discussed.

Suggestion for future developments for microdosimetry of intermediate energy neutrons in mixed fields are made and discussed.

CONTENTS

Page

CHAPTER 1

INTRODUCTION

1.1 The Requirement of Radiation Protection for Intermediate Energy Neutrons

In recent years the importance of neutrons in the intermediate energy region at about 100 keV has been increasingly recognised in various fields such as in radiobiology and boron neutron capture therapy studies, i.e. $^{10}B(n,\alpha)^{7}Li$, and in the development of neutron sensitive instruments for calibration and radiation protection. However the restricted availability of intermediate energy neutron sources of sufficient intensity has led to slow progress in these fields, thereby giving rise to serious inadequacies in understanding the biological effects of intermediate energy neutrons in tissue and in recognising the performance of existing neutron sensitive instruments at these energies or in developing new ones.

Monoenergetic neutrons in the intermediate energy range from 100 eV to 144 keV can be produced by several methods, details of which have been discussed by Mill and Harvey (1978) and Al-Affan (1985). It is generally known that the filtered neutron beam from high flux reactors is the most appropriate technique of producing intense sources more than 10^7 n cm^{-2} s^{-1}. For example, a filter of scandium gives 2 keV neutrons, iron and aluminium give 24 keV neutrons, sulphur gives 74 keV and silicon gives 144 keV neutrons. Nevertheless, the filtered beam facilities are very limited to this date (Harvey and Mill, 1988).

There are three fundamental principles of the importance of intermediate energy neutrons in radiation protection.

First, the intermediate energy neutrons interact with tissue mainly through elastic scattering to produce secondary charged particles (H, C, N and O) of which protons are the major contribution. The range of protons (<1.2 μm) is less than the cellular dimension, thus protons can cause serious biological damage by depositing their energy in tissue. The relative biological effectiveness (RBE) for mammalian cells is high for intermediate energy neutrons (Key, 1971 and Mill, 1986). This observation can have significant implication in radiobiology and radiation protection.

Second, the charged particles produced by intermediate energy neutrons can lose a significant proportion of energy by non-ionizing interaction through nuclear elastic scattering (Lindhard and Scharff, 1961 and Watt, 1972), the biological implications of which are uncertain. The relevant experiments have been performed but so far including only the use of low-energy charged particles incident directly onto very thin films of dried enzyme samples (Jung and Zimmer, 1966, Sutcliffe and Watt, 1974, Cunningham, 1982, Al-Kazwini, 1983 and Al-Kazwini *et al.*, 1988). The results have shown that a significant damage occurred at these low energies, which suggests the possibility that elastic nuclear collisions play a significant role in determining an increase in RBE at the intermediate neutron energies.

Third, surveys in many different working environments around nuclear reactors and accelerator installations show a significant fraction of neutron dose equivalent is due to intermediate energy neutrons (Harvey and Bending, 1976, Endres and Brackenbush, 1981 and Piesch and Burgkhardt, 1981). Therefore, it is very important to determine the spectra of these neutrons which may vary from site to site depending on the type of reactor, the kind and amount of shielding and location of the plant in order to quantify the dose equivalent of intermediate energy neutrons for radiation protection purposes.

The problem is made more difficult by the coexistence of gamma rays in neutron fields generated from various process such as the result of neutron interactions with the surrounding materials and target volume, and as part of the neutron production process. A

general approach is to separate the dose distribution into components due to neutrons and gamma rays and then multiply each by its appropriate quality to derive the total dose equivalent (ICRU, 1962). Two detector systems of different sensitivity to neutrons and gamma rays are often used to separate the two components (NCRP, 1961). However, there are uncertainties using this technique because of the overall uncertainty in the relative sensitivity of the detectors to neutrons (ICRU, 1977).

The use of dosimeters and survey meters for radiation protection is to measure both the quantity and quality of the neutron fields. A widely used albedo dosimeter, in principle, is sensitive to intermediate energy neutrons but often the readings are adjusted to the basis of instrumental surveys of the environments in which the personnel are exposed (Mill and Harvey, 1978). Multisphere or 'Bonner Sphere' spectrometers which composed of a ^{6}Li I crystal detector placed in turn inside a set of polythene spheres of various sizes to give different amounts of moderation and absorption of the impinging neutrons are often used to study neutron spectra (Hankins, 1963 and Mill and Harvey, 1978). However, the multisphere system is a low resolution system in which the average neutron energy determined is rather uncertain for accurate radiation protection purposes (Endres and Brackenbush, 1981). The use of proton recoil proportional counters, on the other hand, can determine the quantity of neutron fields but are unable to determine the quality of intermediate energy neutrons (Cosack *et al.*, 1972).

1.2 Microdosimetry of Intermediate Energy Neutrons in Mixed Radiation Fields.

The introduction of microdosimetric concepts for the specification of radiation quality based on the stochastic quantities of lineal energy, y, and the specific energy, z, and their frequency distributions has contributed greatly to our understanding of energy deposition distributions in a simulated tissue volume. This has been achieved with the use of tissue-equivalent proportional counters (TEPCs) which comprise of tissue-equivalent (TE) plastic wall and TE gas of low density (Rossi and Rosenweig, 1955a). The employment of

microdosimetric techniques in radiation protection of mixed (n,γ) radiation fields not only offers a new means of explaining the relationship between the actual energy deposition in tissue and possible resulting biological damage, but, the radiation quality of the neutron and gamma-ray components can be separated without recurrence to other instruments or need to make additional measurements (ICRU, 1983 and Booz, 1984a).

Low pressure TEPCs permit, to good approximation, direct determination of microscopic distributions of energy deposition by ionizing radiations within the simulated tissue volumes of several micrometer dimensions (Rossi, 1968 and ICRU, 1983). These TE gas cavity devices enable absorbed dose and dose equivalent to be determined from a single measurement which is of practical value in radiation protection dosimetry and area monitoring (Kawecka *et al.*, 1984, Cowling and Waker, 1985 and Schuhmacher and Krauss, 1986). A notable feature of TEPCs relevant to radiation protection in mixed fields is that pulses produced by fast neutrons are generally larger than those produced by photons, thus a distinction between neutron and photon events is possible by pulse height discrimination (Menzel, 1985). They give excellent dose equivalent response for neutrons above a few hundred keV due to the approximation of LET by y for recoil protons. However, for neutrons below 100 keV their response to secondary charged particles deteriorates rapidly, due to the fact that neutron moderation is governed by the reaction of $^{1}H(n,\gamma)^{2}H$ and $^{14}N(n,p)^{14}C$ (Booz, 1984a). The response of TEPCs to neutrons below 100 keV has been systematically investigated by optmizing the wall thickness, i.e adding a polyethene (PE) cap to the TEPC, in order to provide better response (Kawecka *et al.*, 1984, Schuhmacher *et al.*, 1985, and Schuhmacher and Krauss, 1986). Nevertheless, in their present form, they are incapable of determining separately the components of intermediate energy neutrons in the presence of fast neutrons.

There are at present no methods of assessing separately the quality of the component of intermediate energy neutrons in mixed radiation fields. A TEPC in co-axial double cylindrical form could be designed and manufactured to fulfil this purpose as proposed by Watt (1985)

and was successfully constructed and tested for the first time in its non-TE version by Saion and Watt (1988). The energy deposition spectra of neutrons in the energy region of interest can be measured by an appropriate choice for thickness of the common TE dividing wall separating the inner and outer counters, and by appropriate use of coincidence/anti-coincidence pulse arrangements. Events due to fast neutron generated recoils which interact with both the counters can be removed by the anti-coincidence technique leaving behind the events due to recoils of energy equivalent to the thickness of the dividing wall and those with less energies.

1.3 The Scope of This Work

The present project is aimed at solving the radiation quality problem of intermediate energy neutrons in mixed fields by attempting to explore the possibility of developing a coaxial double cylindrical TEPC, capable of separating the components of neutrons in the intermediate energy region from those of fast neutrons. Ability to do so would be of value for interpretive purposes in radiation protection in the vicinity of reactors etc. where a significant fraction of neutron dose equivalent is due to intermediate energy neutrons. An attempt to develop this new microdosimeter and to explore its operational characteristics in the laboratory and to carry out field trails will be described in this thesis.

In Chapter 2, the fundamental aspects of radiation interactions in tissue, the macroscopic quantity of absorbed dose and its limitation, the microscopic quantities and their distributions and details of microdosimetric techniques in radiation protection based on TEPCs will be reviewed and discussed. The operational principles of TEPC will be discussed in terms of the principles of an ordinary proportional counter to provide technical information for the design and construction for a new microdosimeter.

Chapter 3 is concerned with the theoretical calculations of microdosimetric spectra expected to be detected by the dosimeter operated with coincidence/anti-coincidence arrangements.The effective stopping powers and projected ranges of heavy charged particles

and kerma and kerma factor for intermediate energy neutrons will also be calculated as a prerequisite for the calculation of microdosimetric spectra.

The design and construction of the new microdosimeter will be presented in Chapter 4. Also described are the method of preparation of A-150 plastic film for the common dividing wall of the counter and the electronic system for data acquisition.

The method of energy calibration and the measurements of the gas gain and resolution characteristics will be presented in Chapter 5.

Chapter 6 is concerned with the microdosimetric experiments with photon and neutron sources. Results of the microdosimetric spectra will be presented and discussed. The uncertainties involved and all parameters influencing the results will be discussed.

Conclusions which can be drawn from this work and proposals for future work related to this study will be discussed in Chapter 7.

CHAPTER 2

REVIEW :

Microdosimetric Concepts in Radiation Protection

2.1 Introduction

Since the discovery of X-rays by Roentgen in January, 1896 and the discovery of radioactivity from uranium by Becquerel in November, 1896, the exposure of man to ionizing radiation has increased significantly above the average level of natural background radiation exposure. This additional exposure has resulted from the diagnostic and therapeutic uses of man-made sources of ionizing radiation including that from nuclear accidents and atomic weapon tests. The history of damage and protection from ionizing radiation has been reported elsewhere (e.g. Morgan, 1973). A better understanding of radiation effects is necessary to enable damage from excessive and low-level radiation exposure to be anticipated and quantified. In radiation protection, we are generally concerned with the risk to the population, the late effects to be anticipated and prevented, the control and treatment of potential radiation damage to the general public, radiation workers and the environment. However, some fundamental problems of radiation protection require adequate solution in order to achieve the forgoing objectives. These may be divided into several categories i) an understanding of the biophysical mechanism of radiation damage, ii) the establishment of ways of expressing or measuring radiation quantity and quality to allow the permissible levels of protection from all types of ionizing radiation to be specified and iii) the intelligent enforcement of levels defined to be an acceptable risk.

When ionizing radiations traverse biological systems, charged particles are produced which then deposit their energy in tissue to cause biological and chemical effects. The damage arises when the secondary charged particles transfer their energy primarily in collisions with the orbital electrons of the matter to produce ionization or excitation of atoms

and molecules or leads to dissociation of molecules. Various concepts and quantities have been defined and used to predict the biological mechanism of radiation damage in tissue. The main objective of the quantities used is to provide a better understanding of the fundamental mechanisms of radiation action which can induce, among others, cell killing, mutation, chromosome aberration and carcinogenesis in tissue. Most quantities have been found to be insufficient alone to predict the specified biological effects for a given radiation field. The difference in the types and interaction mechanisms of radiation and in the stochastic nature of energy transferred give rise to the differences in the quality of radiations. A universal combination of quantities which could predict biological effects irrespective of the type or quality of radiations would indeed be very useful. To date, fundamental concepts regarding these quantities are being studied by Watt (Watt *et al.*, 1985, Watt, 1988, Watt, 1989).

In this chapter the fundamental concepts of radiation interaction in tissue are discussed in order to understand the concepts of energy deposition in microscopic and macroscopic volumes. The definition of microdosimetric parameters and their distributions are given for both spherical and cylindrical volumes. The development of the quality parameters based on microdosimetric principles is reviewed with emphasis on the application of TEPC for the determination of dose and dose equivalent in tissue for radiation protection. The principles of TEPC which will provide the fundamental understanding in the design and operation of a new microdosemeter are given.

2.2 Fundamental Aspects of Radiation Interaction in Tissue

2.2.1 Energy Loss by Indirectly Ionizing Radiations

When indirectly ionizing radiations, such as neutrons and photons, interact with matter the energy is lost by interaction with the atomic electrons and nuclei of the target material. Fast neutrons are moderated in tissue to intermediate energy neutrons which then slow down to thermal neutrons and may acquire a Maxwellian velocity distribution with an average velocity of 220 ms^{-1} corresponding to an energy of 0.025 eV. Neutrons interact with nuclei of the tissue constituents in one or more of the following processes.

Spallation is the process by which a nucleus is fragmented by a neutron of energy greater then 20 MeV to eject several particles and nuclear fragments. Neutrons of energy between 5 MeV and 20 MeV can interact by nonelastic scattering to emit particles, other than a single neutron, accompanied by de-excitation gamma rays. At neutron energies from 2.5 MeV to 10 MeV, inelastic scattering can take place in which the neutron is promptly reemitted with a change in direction and a reduction in energy. De-excitation of gamma rays accompany this (n,n') reaction. Neutrons can interact with tissue by elastic scattering in which the neutron collides with a nucleus and transfers part of its kinetic energy to secondary charged particles: mainly protons, C, N, and O ions. In tissue, protons comprise more than 85% of the recoil particles produced by neutrons of energy below 14 MeV and up to 97% for energies below 10 keV (NCRP, 1961). Capture reaction processes are significant for intermediate energy neutrons and thermal neutrons. Two important neutron capture reactions in tissue are $^{14}N(n,p)^{14}C$ and $^{1}H(n,\gamma)^{2}H$. Details of neutron interaction processes have been discussed e.g.by Auxier *et al.* (1968) and ICRU (1977).

Gamma rays are associated with the production of neutrons and their interactions with tissue, mainly by three processes.

Photoelectric absorption is the resonant transfer of the whole energy of a photon to a bound electron which in turn is emitted as a photoelectron of energy equal to the photon energy minus the electron binding energy. This process is dominant at low photon energies between 30 keV to 150 keV in tissue. When the energy of the photon is much larger than the electron binding energy the incident photon is deflected from its original direction by an unbound electron to produce recoil Compton electrons. In Compton scattering, the energy and momentum are conserved. It is dominant for photon energies between 50 keV to 20 MeV. For photon energies greater than 1.02 MeV gamma rays can lose energy by pair production in which the photon interacts in the electromagnetic field of the nucleus to create

an electron-positron pair. Details of gamma ray interactions have been described by Evans (1968).

Charged particles released by neutron and gamma ray interactions in tissue cause the majority of excitations and ionizations. Because the interaction mean free path of photons and neutrons is larger than the structure of interest in microdosimetry, therefore, it is very important to understand the interactions in tissue by short-range charged particles which are now discussed in the following section.

2.2.2 Energy Loss by Charged Particles

Directly ionizing radiations, such as electrons and heavy charge particles, interact with tissue by three principle processes; i) Coulomb-force interactions with electrons in the atoms and molecules, ii) interaction with nuclei in tissue and iii) interactions with the atoms as a whole. Fast heavy charged particles can lose energy by inelastic collisions with the orbital electrons. The energetic electrons that are produced, i.e δ-rays, can have sufficient energy to produce secondary ionizations in space around the primary tracks. Heavy charged particles which pass near the nuclei can interact by inelastic collisions with the atoms and cause appreciable deflections. This Rutherford scattering leads to the excitation of the atom at nuclear level. Slow heavy charged particles, on the other hand, can interact by elastic collisions with the nuclei of the target as the whole and produce recoil charged particles having zig-zag tracks. For heavy charged particles of small velocities ($\frac{v}{c} < 0.03Z$), the particles interact with the atom as a whole in the process known as Rutherford scattering (Bichsel, 1968).

In a manner similar to that for heavy charged particles, fast electrons can lose energy by ionizations and excitations resulting from collision with the orbital electrons of atoms. However, some basic differences are due to the much larger angle of scattering and relativistic effects for electrons with energies of a few hundred kilo-electron volts. Also, electrons can lose energy by bremsstrahlung by which photons are emitted due to

decelaration of electrons in the Coulomb field of the nuclei of the target. The energy loss in this way increases with the increase of electron energy and higher atomic number of the target. This radiation production process in tissue is usually negligible. For electrons of energy below the excitation energy of the atoms, it interacts with the atom as a whole.

2.3 Macroscopic quantity of Absorbed Dose

The fundamental physically measurable quantity of energy imparted is the absorbed dose, D, which is defined as the quotient of $d\bar{\varepsilon}$ by dm, i.e

$$D = \frac{d\bar{\varepsilon}}{dm} \qquad (2.1)$$

where $d\bar{\varepsilon}$ is the mean energy imparted by ionizing radiation in the volume element of mass, dm. Absorbed dose is a macroscopic quantity of ionizing radiation which describes the mean energy imparted at the point of interest within the homogeneous material irradiated by a spatially uniform radiation field.

The statistical fluctuation of energy deposition are greatest for very small volumes, for very small dose and for densely ionizing particles due to the discrete nature of energy transferred in microscopic mass (Rossi, 1968). Thus, the relevant microscopic quantity of energy deposition is the specific energy, z, which is the energy imparted per unit mass of cellular or subcellular dimensions. The difference between the energy deposition in microscopic volumes and in macroscopic volumes can be illustrated in **Fig. 2.1.** Thus, the absorbed dose is a limited concept which does not account for the microscopic distribution of energy imparted.

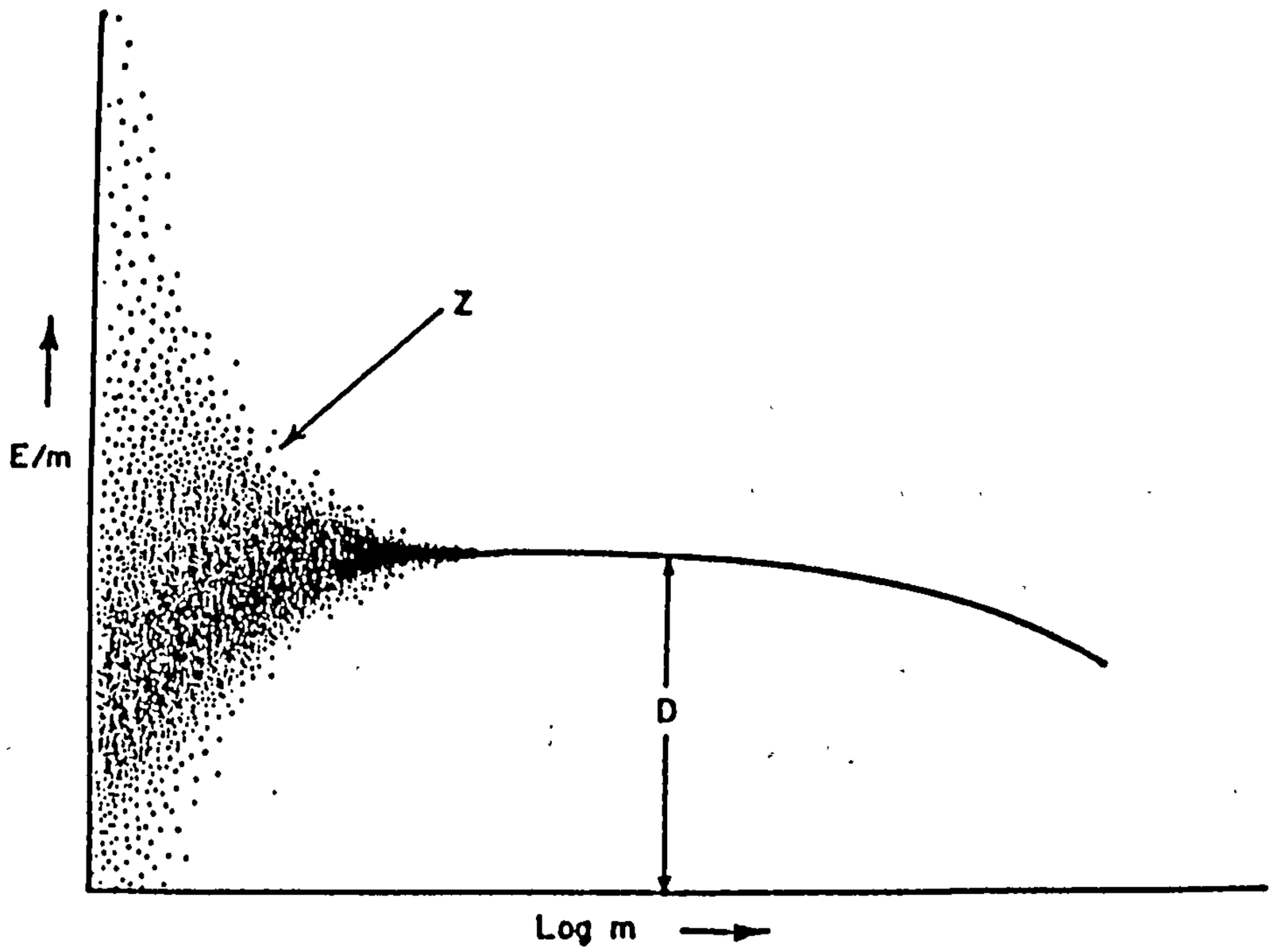

Fig. 2.1 Energy density as a function of mass for which energy density is determined. The horizontal line covers the region in which the absorbed dose can be established in a single measurement. The shaded portion represents the range where statistical fluctuations are important (after Rossi, 1968).

2.4 Microdosimetry

2.4.1 Historical Developments

The concept of microdosimetry has been developed to explain the stochastic nature of energy deposition by ionizing radiations in tissue masses of cellular and subcellular dimensions (Rossi, 1968). The energy deposition spectra in a microscopic volume are measured with a TEPC filled with tissue-equivalent gas. The initial aim of developing TEPC was to measured the absorbed dose distribution in LET, d(L), for radiation protection against high LET radiations (Rossi and Rosenzweig, 1955a). However, an important factor has been the recognition of limitations of LET as a radiation quality specification. Consequently, two stochastic quantities namely the lineal energy, y, (Rossi, 1959) and the specific energy,

z, (Rossi *et al.*, 1961) have been introduced as an alternative to the specification of non-stochastic quantities in terms of LET and absorbed dose respectively. Such quantities and their distributions are the central concepts of microdosimetry based on the TEPC technique. Some other quantities have been derived from or based upon them over the past three decades.

Since the first measurement of energy deposition spectra (Rossi and Rosenzweig, 1955b), the experimental work using TEPC has increased when transistorized circuitry become generally available for data collection (Srdoc, 1970, Rodgers and Gross, 1974 and Hogeweg, 1978). The experimental technique first employed muscle TE wall material developed by Rossi and Failla (1956). Later standard A-150 Shonka plastic TE wall material developed by Shonka and collaborators (Shonka *et al.*, 1958 and Smathers *et al.*, 1970) was used. At about the same time methane based TE gas (Rossi and Failla, 1956) and propane based TE gas (Srdoc, 1970) had been used for counting gases. Spherical TEPCs have been commonly used in microdosimetric measurements because of the isotropic response and also simpler chord length distribution. A cylindrical TEPC has several advantages over a spherical TEPC due to simple counter construction and more uniform gas multiplication within the sensitive volume. However, the chord length distribution in a cylindrical TEPC is not as simple. This leads to further investigations (Wilson and Emery, 1968, Birkhoff *et al.*, 1970 and Kellerer, 1971). Energy deposition spectra in tissue volume depends on chordlength distribution, neutron kerma, stopping power and ranges of the secondary recoils and can be predicted by calculation. The first theoretical calculation of the microdose spectra was developed by Caswell (1966).

ICRU has introduced microdosimetric concepts in several of its reports (ICRU, 1977, 1983 and 1986). There is a wide variety of theoretical techniques and applications of microdosimetry principles based on TEPC technique which are given in ICRU Report No. 36 (ICRU, 1983). Perhaps, the best potential application of the TEPC technique is for measurement of dose equivalent in radiation protection. Recently, ICRU has recommended

that quality factor be based on the lineal energy instead of LET, as previously, because of severe limitations in the concept of the latter (ICRU, 1986).

2.4.2 Microdosimetric Quantities

The lineal energy, y, is defined as the quotient of the energy imparted, ε, to the matter in the volume due to a single energy-deposition event, by the mean chord length, $\bar{l}$, through that volume (ICRU, 1983), i.e

$$y = \frac{\varepsilon}{\bar{l}} \tag{2.2}$$

y is a stochastic quantity and has S.I unit Jm^{-1}, but is commonly expressed in $keV\mu m^{-1}$. The specific energy, z, is defined as the quotient of the energy imparted, ε, to the matter in the volume due to a single energy-deposition event, by the mass, m, of that volume, i.e

$$z_1 = \frac{\varepsilon}{m} \tag{2.3}$$

The specific energy for a multiple energy-deposition event can be expressed by equation (2.4)

$$z = \sum \frac{\varepsilon}{m} \tag{2.4}$$

where $\sum \varepsilon$ is the total energy imparted by the events in the same volume. The unit of the specific energy is the gray (1 Gy = 100 rad = 1 Jkg^{-1}).

Assuming, the energy imparted ε is the same in equation (2.2) and (2.3), then

$$z_1 = \frac{\bar{l}}{m}\, y \tag{2.5}$$

For a given volume, V, and surface area, S, the mean chord length for any convex body can be expressed by the Cauchy relation as $\bar{l} = \frac{4V}{S}$. Then, the relation between z_1 and y for a convex body is given by equation (2.6), i.e.

$$z_1 = \frac{0.1602 \times 4y}{\rho\ S} \tag{2.6}$$

where the quantities are given in their respective units, i.e, z_1 in Gy, y in keVμm^{-1}, S in μm^2, and ρ in gcm^{-3}. For spherical and cylindrical volumes of tissue substitute (ρ=1 gcm^{-3}) the above relationships are given by equations (2.7) and (2.8) respectively.

$$z_1 = \frac{0.204\ y}{d^2} \tag{2.7}$$

$$z_1 = \frac{0.102\ y}{r(r+h)} \tag{2.8}$$

where d is the diameter of the sphere in μm, r and h are the radius and the height of the cylinder in μm respectively.

2.4.3 Microdosimetric Distributions

The probability density or the differential distribution of the number of events in y and the differential distribution of the absorbed dose in y are defined by equations (2.9) and (2.10) respectively (ICRU, 1983).

$$f(y) = \frac{dF(y)}{dy} \tag{2.9}$$

$$d(y) = \frac{dD(y)}{dy} \tag{2.10}$$

where F(y) and D(y) are the distribution functions or the sum distributions for the fraction of events and the fraction of absorbed dose respectively, having values of the lineal energy up to y. The probability densities must be normalized to a unit area. Similarly, the differential distributions for a single event can be written for the specific energy by

$$f_1(z) = \frac{dF_1(z)}{dz} \tag{2.11}$$

$$d_1(z) = \frac{dD_1(z)}{dz} \tag{2.12}$$

The single-event distributions of y are equivalent to the single-event distributions of z, i.e

$$F(y) = F_1(z) \tag{2.13}$$

$$D(y) = D_1(z) \tag{2.14}$$

The single-event differential distributions of z are related to the differential distributions of y by

$$f_1(z) = \frac{m}{\bar{l}}\, f(y) \tag{2.15}$$

$$d_1(z) = \frac{m}{\bar{l}}\, d(y) \tag{2.16}$$

The above relations of equations (2.15) and (2.16) can be simplified for a spherical volume by

$$f_1(z) = \frac{4}{\pi d^2}\, f(y) \tag{2.17}$$

$$d_1(z) = \frac{4}{\pi d^2}\, d(y) \tag{2.18}$$

and for a cylindrical volume by

$$f_1(z) = \frac{2}{\pi r(r+h)}\, f(y) \tag{2.19}$$

$$d_1(z) = \frac{2}{\pi r(r+h)}\, d(y) \tag{2.20}$$

2.4.4 Non-Stochastic Quantities of Mean Values

$\bar{y}_F$ and $\bar{y}_D$ are the mean values of the frequency and absorbed dose distributions of the lineal energy respectively. They were defined by ICRU (1983) as

$$\bar{y}_F = \int_0^\infty y\, f(y)\, dy \tag{2.21}$$

$$\bar{y}_D = \int_0^\infty y\, d(y)\, dy \tag{2.22}$$

Since $d(y) = y\, f(y)/\bar{y}_F$, equation (2.22) can be written as

$$\bar{y}_D = \int_0^\infty y^2\, f(y)\, dy \;/\; \bar{y}_F \tag{2.23}$$

Similarly, the frequency-mean, $\bar{z}_F$, and the dose-mean, $\bar{z}_D$, of the specific energy z are given by

$$\bar{z}_F = \int_0^\infty z\, f_1(z)\, dz \tag{2.24}$$

$$\bar{z}_D = \int_0^\infty z\, d_1(z)\, dz \tag{2.25}$$

or

$$\bar{z}_D = \int_0^\infty z^2\, f_1(z)\, dz \;/\; \bar{z}_F \tag{2.26}$$

Note that, for single event $\bar{z}_F$ and $\bar{z}_D$are normally written as $\bar{z}_1$ and ζ respectively. The changes are not significant other than writing in a consistent set of symbols.

The relations equivalent to equation (2.7) and (2.8) can be written for non-stochastic quantities in their respective units for a spherical volume by equations (2.27) and (2.28) respectively

$$\bar{z}_F = \frac{0.204\, \bar{y}_F}{d^2} \tag{2.27}$$

$$\bar{z}_D = \frac{0.204\, \bar{y}_D}{d^2} \tag{2.28}$$

and for a cylindrical volume by equation (2.29) and (2.30) respectively

$$\bar{z}_F = \frac{0.102\, \bar{y}_F}{r(r+h)} \tag{2.29}$$

$$\bar{z}_D = \frac{0.102\, \bar{y}_D}{r(r+h)} \tag{2.30}$$

2.5 Microdosimetric Methods in Radiation Protection

2.5.1 Characterization of Low Doses

A variety of biological effects in tissue is caused by energy deposition from charged particles released when ionizing radiations interact with the human body. Non-stochastic effects are induced above a dose threshold beyond which there is a progressive increase in

severity. Stochastic effects have no threshold and are determined by the law of probability. However, the general assumption in radiation protection is that the probability of the biological effects in a specified organ is proportional to the absorbed dose, D, and independent of the magnitude of previous doses and of the time they were received (ICRU, 1986). Thus, the general principle of radiation protection is to keep doses as low as reasonably achievable (the ALARA concept), i.e. low doses and low dose rate.

Low doses, conventionally, represent the exposure below the maximum permissible limit of absorbed dose, D_L, which has been assigned to the individual organs depending on their radiosensitivity and on the types of radiation. The annual dose limits for non-stochastic effects for X- or γ - radiation doses is 500 mGy in a year in all organs for occupational exposure, except the lens of the eye for which the limit is 150 mGy in a year (ICRP, 1977). However, for stochastic effects, the annual limit is reduced to 50 mGy in a year for occupational exposure based on uniform whole-body exposure (ICRU, 1986).

When this conservative approach is expressed in terms of microdosimetric characterization, low doses represent the region where critical targets experience only single events of energy deposition and most targets do not experience any energy deposition at all (Kellerer, 1976 and Booz, 1984b). High and low absorbed dose can be characterized by microdosimetric quantities of the specific energy, z, its frequency mean, $\bar{z}_F$, and its dose mean, $\bar{z}_D$. The mean specific energy in affected volumes, $\bar{z}^+$, and its standard deviation were given by ICRU (1983) by equations (2.31) and (2.32) respectively and are dependent on the diameter of the sensitive volume.

$$\bar{z}^+ = \frac{D}{(1- \exp(-\frac{D}{\bar{z}_F}))} \tag{3.31}$$

$$\sigma_{\bar{z}^+} = \bar{z}^+ \left\{ \frac{\bar{z}_D}{D} - (\frac{\bar{z}_D}{D} + 1) \exp(-\frac{D}{\bar{z}_F}) \right\}^{0.5} \tag{3.32}$$

Fig. 2.2 shows the mean specific energy in the critical volume of 8 μm and the region of fluctuation within one standard deviation as a function of absorbed dose and of mean number of energy deposition events for 14 MeV neutrons and ^{60}Co gamma rays (Booz and Feinendegen, 1988). In low-dose region where the absorbed dose, D, is less than 0.2 $\bar{z}_F$, the value of the specific energy is independent of the absorbed dose, i.e. $\bar{z}^+ = \bar{z}_F$. This indicates that in this region the stochastic effect is independent of the absorbed dose which is shown by the fluctuation in $\bar{z}^+$ and a constant absorbed dose on the graph. Clearly, characterization of radiation quality by absorbed dose at low doses and low dose rate does not give much information about the nature of energy deposition. For example the low dose region of 14 MeV neutrons, i.e. less than 10^{-2} Gy, is higher than the low dose region of ^{60}Co gamma rays, i.e. less than 2.5×10^{-4} Gy, which is in contrary with their radiation quality if the number of events is not taken into account. However, in this region where the difference of neutron and gamma-ray events is significant in terms of the mean specific energy in affected volume but not in terms of the absorbed dose, microdosimetric method can be used to resolve the specification of low doses and low dose rate for neutron and gamma-ray exposure. In the high-dose region, however, where the absorbed dose is greater than 25 $\bar{z}_D$, the statistical fluctuation of energy deposition is insignificant, i.e. $\bar{z}^+ = D$, and the conservative approach is still applied. In between the two regions there is a transition from microdosimetry to macrodosimetry.

2.5.2 Separation of Neutron- and Gamma-Dose Fractions

A notable feature of TEPC used in microdosimetry is that pulses produced by fast neutron events are in general larger than those produced by photon events. This enable the separation of radiation quality of neutron and gamma ray components in mixed (n,γ) radiation fields by a pulse height discriminator. Consequently, neutron- and gamma-dose fractions in tissue can be evaluated using this method because the chamber materials are made up from tissue equivalent materials.

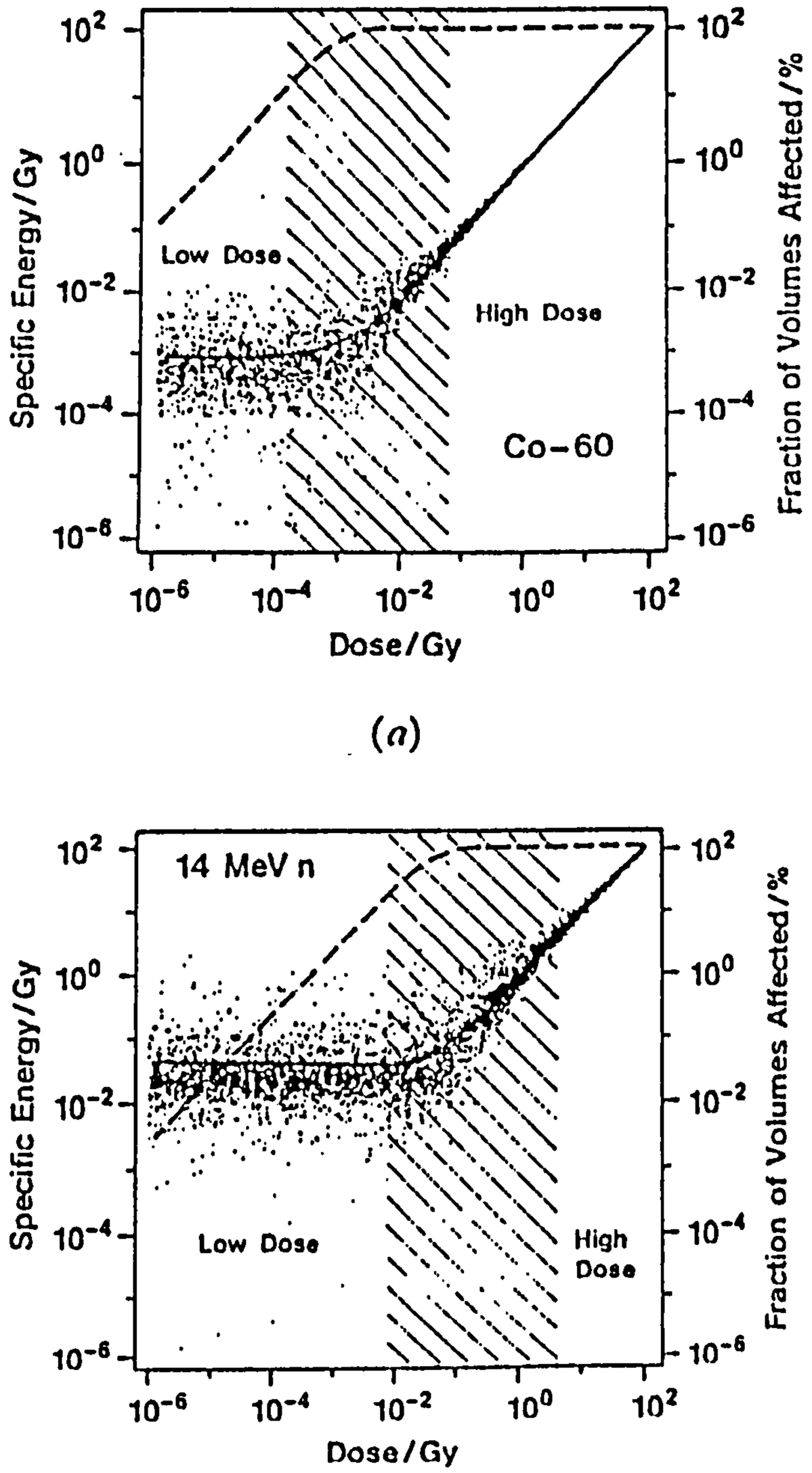

(a)

(b)

Fig. 2.2 Mean specific energy for a critical volume (solid lines) and the percentage of volumes affected (broken lines) as a function of absorbed dose in tissue 8 μm in diameter for (a) ^{60}Co gamma rays and (b) 14 MeV neutrons. The dotted area indicates the corresponding region of fluctuation of $\bar{z}^{+}$ within one standard deviation. The hatched area is the transitional region between low and high doses (after Booz and Feinendegn, 1988).

The distribution of energy deposition measured in TEPC depends on several factors including simulated chord length, gamma ray to neutron absorbed dose ratio and spectral fluence of neutrons and photons. In general, the characteristic distribution of microdosimetric spectra in mixed fields consists of three overlapping regions

1) a low-y region up to about 10-15 keVμm^{-1} due to gamma rays

2) an intermediate-y region up to about 150 keVμm^{-1} due to proton recoils from elastic scattering interactions.

3) a high-y region greater than 150 keVμm^{-1} due to heavy recoils, mainly carbon and oxygen ions.

In practice, the gamma-dose fraction can be determined by fitting the dose distributions from ^{60}Co and ^{24}Na gamma-rays to the measured spectra of mixed fields (Bichsel, 1975, Maier *et al.*, 1975, Menzel and Waker, 1976). However, a better method was introduced by Fidorra and Booz (1978) who fitted the gamma-ray component using gamma rays from fast-neutron interaction in water. Most gamma rays from fast neutron interactions in biological tissue and shielding materials have energies from 2 to 4 MeV. However there is no significant change in the shape of the dose distribution in this energy range because the stopping power of primary electrons of 0.5-6 MeV does not change significantly (Booz, 1984a). Thus, this method could produce a good approximation to the gamma-ray component in mixed fields.

Simple separation of neutron- and gamma-dose fractions for mixed fields is shown in **Fig. 2.3.** Equal areas under the curves represent equal dose fractions. The gamma-dose fraction is mainly due to Compton scattering effects which produce events around y = 3 keVμm^{-1}. Photons from capture reaction, H(n,γ)D, of low-energy neutrons cannot be separated from the primary photons. On the other hand, the neutron-dose fraction is mainly due to recoil protons which produce the most frequent events at 70-90 keVμm^{-1}. Low-energy neutrons are not separable from the gamma-dose fraction if the proton events fall

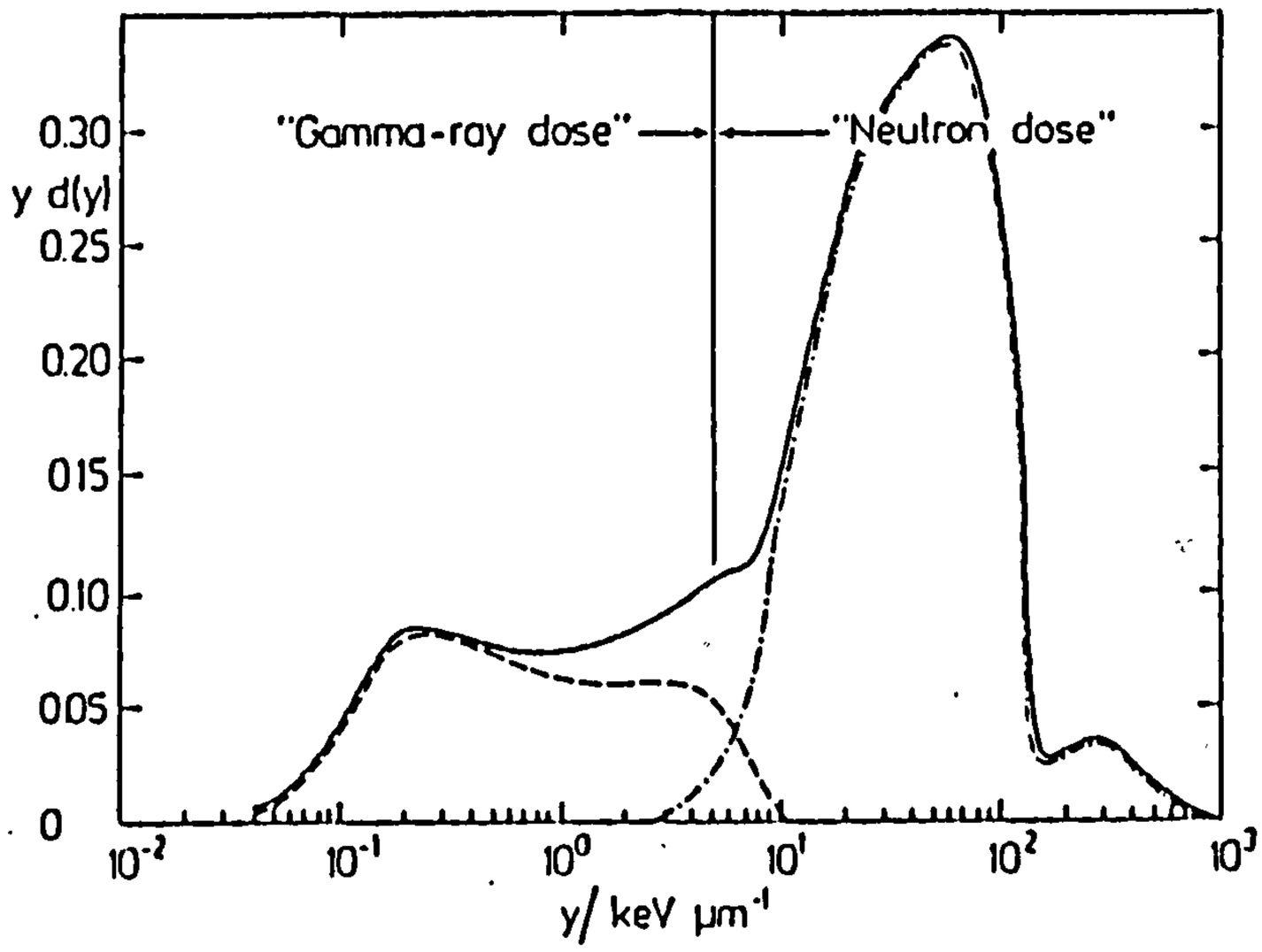

Fig. 2.3 Simple separation of neutron- and gamma-dose fractions from a mixed (n,γ) field into two radiation components: gamma-ray (dashed line) and neutrons (dashed dotted line). Equal areas under the curve represent equal dose fractions (after Booz, 1984a).

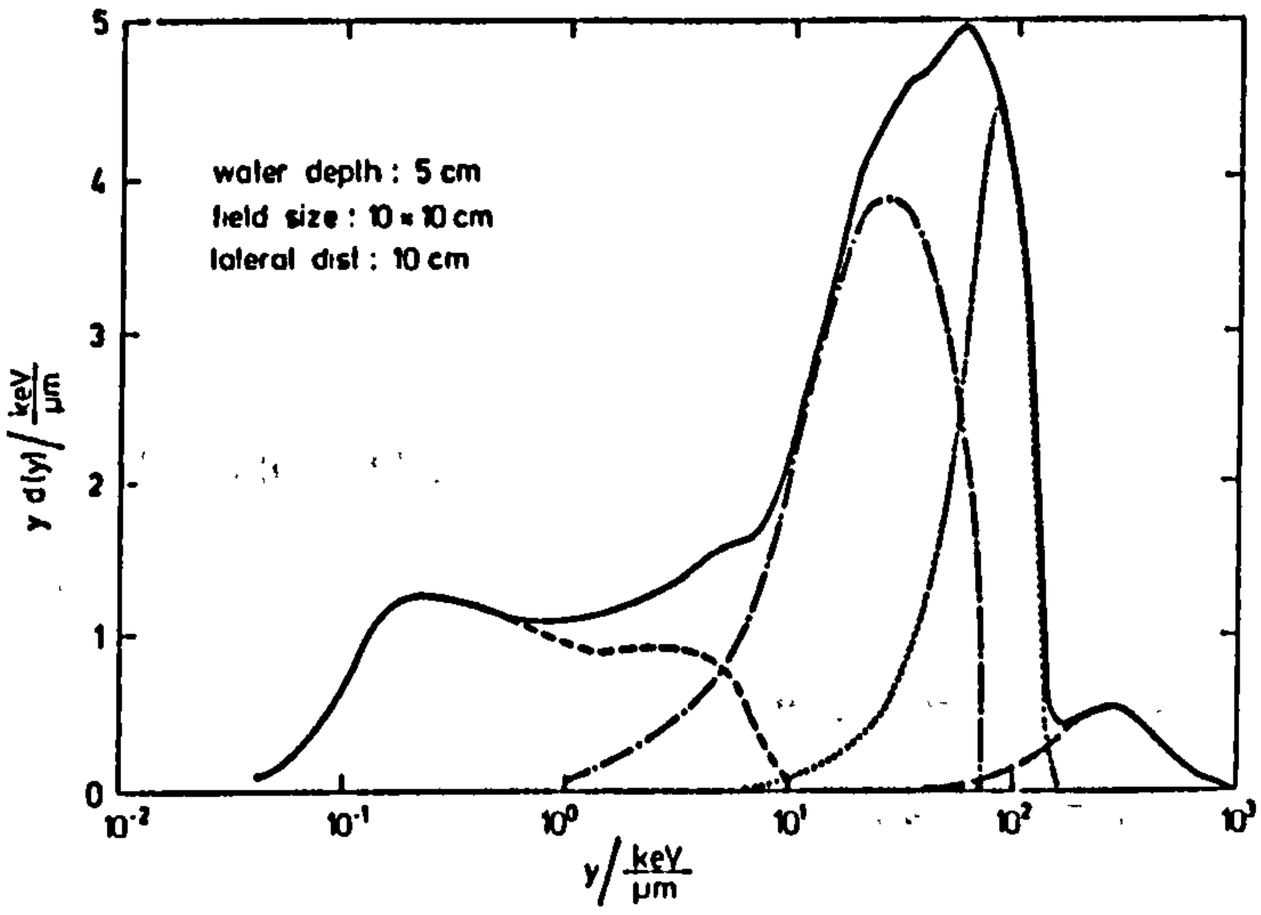

Fig. 2.4 Separation of the y spectrum from a mixed (n,γ) field into four radiation components: gamma-ray (short dashed line), fast recoil protons (dashed dotted line), slow recoil protons (dotted line) and heavy recoil ions (long dashed line). Equal areas under the curve represent equal dose fractions (after Fidorra *et al.*, 1981).

below 7 keVμm^{-1}. The small peak about 300 keVμm^{-1} is due to heavy recoils mainly carbon and oxygen ions.

A more complex method of separation is required to resolve the distributions of gamma rays, fast recoil protons, slow recoil protons and heavy recoil ions as shown in **Fig. 2.4** (Fidorra *et al.*, 1981 and Booz and Poli, 1981). At intermediate neutron energies of less than 100 keV, the dose is almost entirely delivered at lineal energies between 10 and 150 keVμm^{-1} (Rodgers and Gross, 1974). Intermediate energy neutrons are not separable from fast neutrons in mixed fields and require further investigation as is proposed in the present work.

2.5.3 Evaluation of Absorbed Dose in TEPC

The determination of absorbed dose, D, in a low-pressure TEPC is based on gas cavity chamber principles, i.e The Bragg-Gray principle, using the relation in equation (2.33)

$$D_g = \frac{Q\,\bar{w}}{m\,e} \qquad (2.33)$$

where **Q** is the charged produced by ionizing radiation in the cavity, $\bar{w}$ is the mean energy to produce an ion pair in the gas, m is the mass of the TE gas in the counter and e is the electronic charge. For the determination of the absorbed dose in ICRU muscle tissue, correction factors must be applied due to differences of TE materials and muscle tissue (DeLuca *et al.*, 1981).

$$D_t = D_g \; S_g^w \; K_w^t \qquad (2.34)$$

where S_g^w is the ratio of the mass stopping powers for A-150 TE plastic to TE gas, and K_w^t is the ratio of kerma for tissue to A-150 TE plastic.

Two types of single-event calibration, using alpha-particles and soft X-rays, can be used in principle to evaluate absorbed dose in the counter cavity. However, there is uncertainty in the knowledge of cavity volume, gas density and the initial energy of the alpha particles. Alternatively, multiple event calibration with photon source, such as ^{60}Co and ^{24}Na gamma rays can be used which reduces the uncertainty in the determination of the mass of the gas in the cavity.

The absorbed dose in ICRU muscle tissue, D_t, can be estimated from the microdosimetric spectrum using relations (2.27) and (2.29), or by (2.35) and (2.36) for spherical and cylindrical counters respectively.

$$D_t = \frac{0.204}{\rho \; d_g^{\,2}} \int_{y_{min}}^{y_{max}} y \, N(y) \, dy \qquad (2.35)$$

$$D_t = \frac{0.102}{\rho \; r_g (r_g + h_g)} \int_{y_{min}}^{y_{max}} y \, N(y) \, dy \qquad (2.36)$$

where ρ is the density of the gas d_g is the diameter of the spherical counter r_g and h_g are the radius and height of the cylindrical counter respectively. N(y) is the number of counts at the lineal energy, y, determined in the microdosimetric measurement.

The photon and neutron absorbed dose in ICRU muscle tissue can then be deduced from equation (2.37) when an external radiation source is used in the multiple event calibration method.

$$D_t = D_{\gamma,t} + D_{n,t} \qquad (2.37)$$

$$D_t = D_{\gamma,g} + D_{n,g} \, S_g^w \, K_w^t \qquad (2.38)$$

where $D_{\gamma,g}$ and $D_{n,g}$ are given in equations (2.39) and (2.40) respectively (Dietze *et al.*, 1988).

$$D_{\gamma,g} = D_t \, R \, \frac{\bar{w}_\gamma}{\bar{w}_\alpha} \qquad (2.39)$$

$$D_{n,g} = D_t \, (1\text{-}R) \, \frac{\bar{w}_n}{\bar{w}_\alpha} \qquad (2.40)$$

where D_t is given by equation (2.35) or (2.36), R is the ratio of the yield due to electrons to the total ion yield, determined in the multiple event calibration method. $\bar{w}_\gamma$, $\bar{w}_n$ and $\bar{w}_\alpha$ are the mean energies required to produce an ion pair in TE gas for photons, neutrons and alpha particles respectively.

2.5.4 Quality Factor by Microdosimetry

The quality factor, Q, is the principal quality parameter of radiation protection. Q is a Committee designed quantity to represent approximately the ratio between measured biological effectiveness of the radiation in question and the effectiveness of a standard radiation (X- or γ -rays) for a given dose and valid, with an inbuilt safety factor, for relevant biological endpoints. Initially it has been expressed empirically as a function of the linear energy transfer (LET) (ICRU, 1962 and Auxier *et al.*, 1968). However, LET is a concept of limited value in radiation biology simply because the quality is not related to the energy deposition in a given volume as discussed elsewhere (e.g. Rossi, 1968, Kellerer and Chmelevsky, 1975, ICRU, 1983 and Goodhead, 1986). A simple relation between quality factor and LET is given by ICRU / ICRP RBE Committee in 1963 as

$$Q = 0.8 + k L_\infty \qquad (2.41)$$

where k = 0.16 μm/keV. For a dose distributed in LET, the mean quality factor, $\bar{Q}$, can be calculated from equation (2.41) by replacing L_∞ with $\bar{L}_D$ (ICRU, 1970).

It has been shown that for a spherical counter $\bar{y}_F = \bar{L}_\infty$ and $\bar{y}_D = \frac{9}{8}\bar{L}_D$ (Kellerer and Rossi, 1972). Thus, $\bar{Q}$ can be expressed in terms of the microdosimetric quantity $\bar{y}_D$ (Lindblom and Samuelson, 1981) by.

$$\bar{Q} = 0.8 + k' \bar{y}_D \qquad (2.42)$$

where k' = 0.14 μm/keV. Different mathematical methods to approximate $\bar{Q}$ values from microdosimetric spectra have shown that all methods yield about the same mean quality factor for radiation fields composed of gamma rays and fast neutrons above 100 keV (Hartmann *et al.* 1981 and Booz and Poli, 1981). Thus, the difference between $\bar{y}_F = \bar{L}_\infty$ and $\bar{y}_D = \frac{9}{8}\bar{L}_D$ are insignificant in radiation protection. Earlier Kellerer (1970) has shown that there is good correlation between Q and $\bar{y}_D$ as a function of LET as shown in **Fig. 2.5.** For low and medium LET-values the quality factor correlates well with $\bar{y}_D$ but for high LET-values there is no correlation between $\bar{y}_D$ and $\bar{Q}$. ICRU (1983) has introduced an empirical saturation function, equation (2.43), to correlate Q with this function.

$$y_Q = y_0 \{1 - \exp(-\frac{y_D}{y_0})\} \qquad (2.43)$$

where $y_0 = 125\ \text{keV}\mu\text{m}^{-1}$ (Kellerer and Rossi, 1972). A fair agreement was obtained when Q is expressed by equation (2.44) for a spherical diameter of 0.2 μm as shown in **Fig. 2.6.**

$$Q^* = 0.19\, y_Q \qquad (2.44)$$

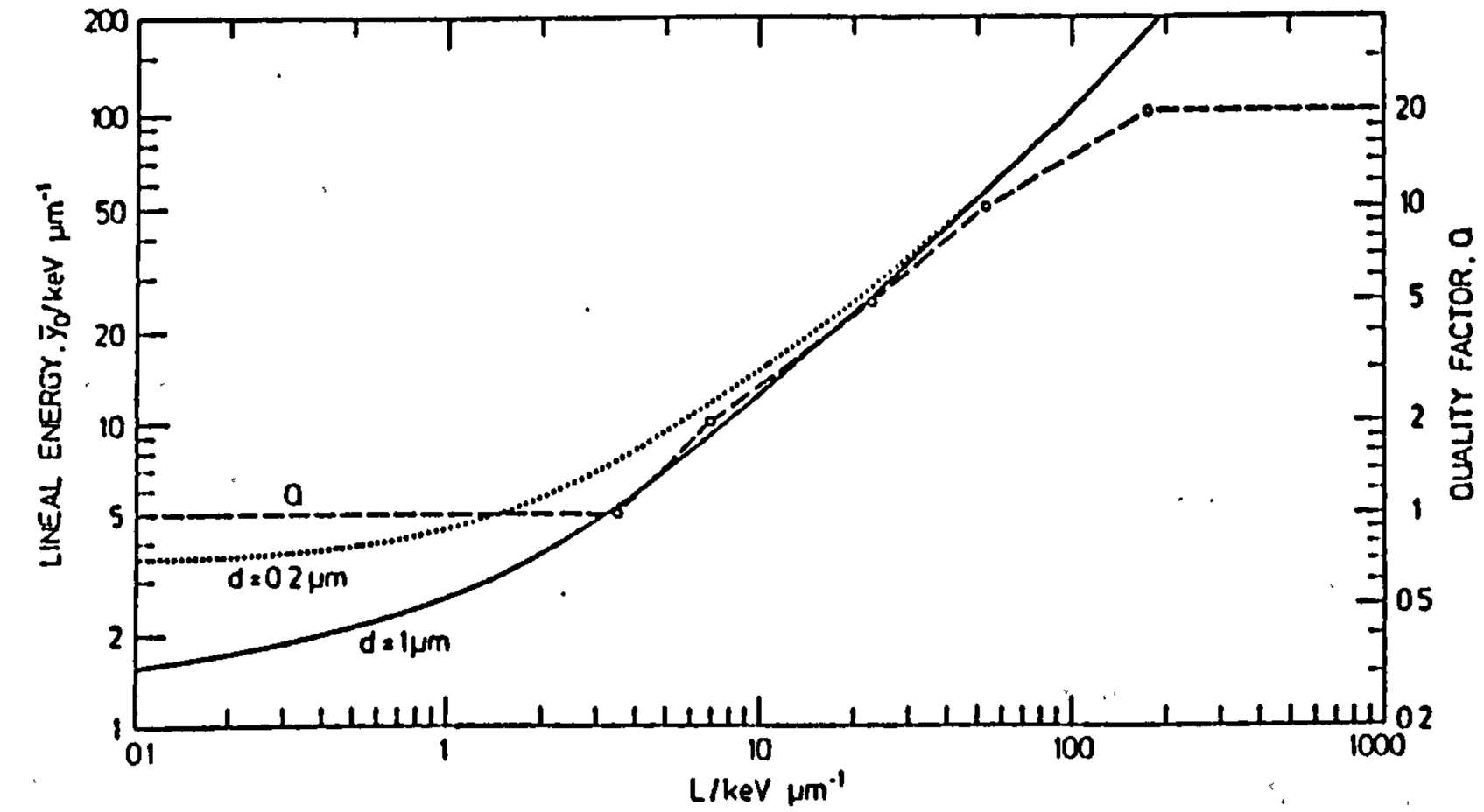

Fig. 2.5 Comparison of the dose-mean lineal energy, $\bar{y}_D$, with the quality factor, Q, plotted as a function of LET (after Kellerer, 1970).

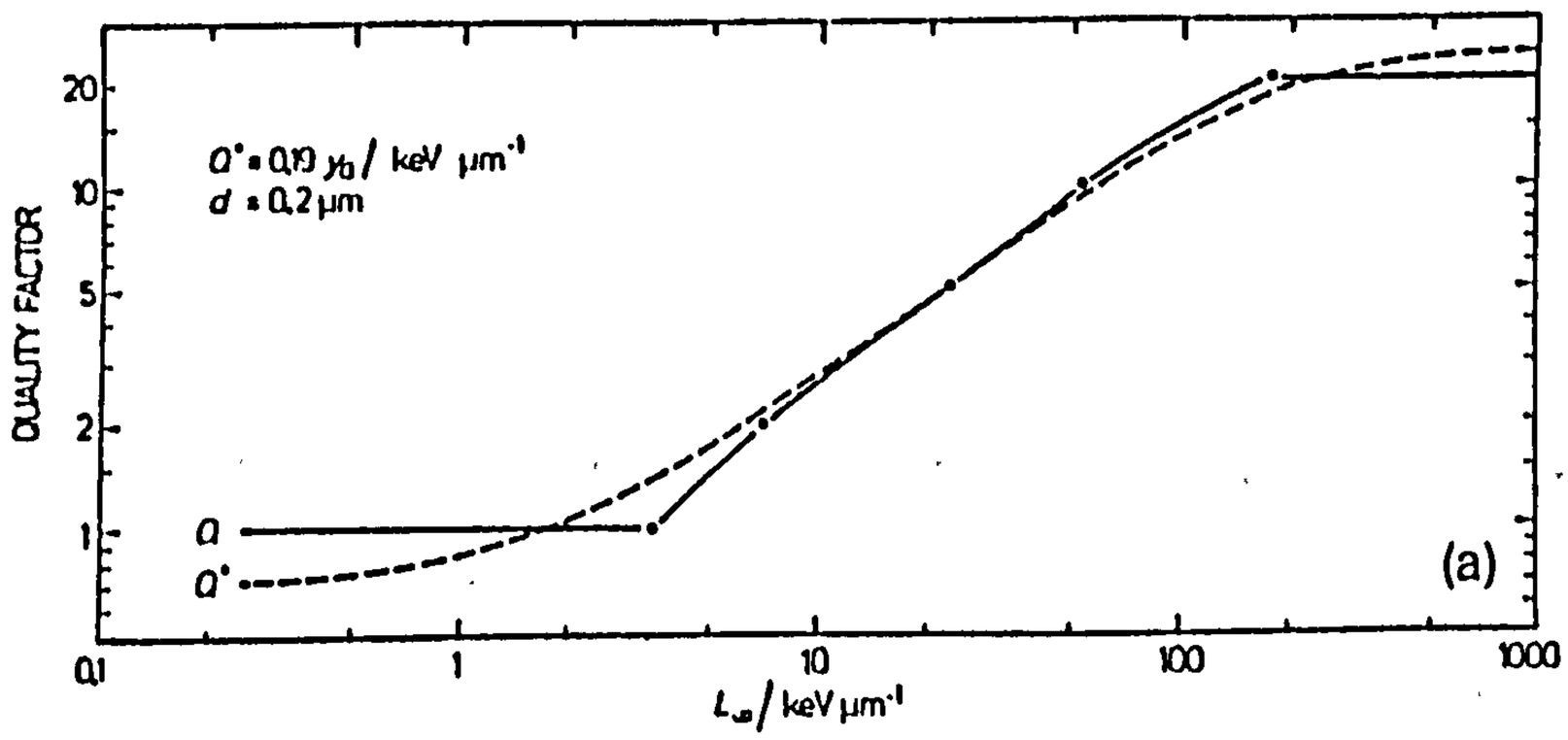

Fig. 2.6 Comparison of the quality factor, Q, as a function of LET with the quality factor, Q^*, as a function of y_Q (after ICRU, 1986).

Although equation (2.44) provides a good approximation value for Q, it is not an alternative definition of the quality factor. Moreover, for electrons, larger values of diameter should be used as the curled electron tracks cause a large difference between y and LET.

A direct definition of Q in terms of y could be very useful from a practical point of view because microdosimetric quantities can be measured experimentally. Earlier, Rossi (1977) has used $\bar{y}_D$ corrected for saturation in an attempt to define Q directly from microdosimetric measurements. He has introduced Q in terms of y^*, the lineal energy corrected for saturation, based on the evidence that RBE of neutrons at low doses can exceed values higher than the value of the conventional Q.

$$\bar{Q} = \int_0^\infty y^{*1.5} \; d(y) \; dy \qquad (2.45)$$

y^* was defined by Kellerer and Rossi (1972) as an empirical correction of lineal energy given by

$$y^* = \frac{y_0^2}{y}\{1-\exp(-\left(\frac{y}{y_0}\right)^2)\} \qquad (2.46)$$

However, the value of Q obtained by equation (2.45) overestimates the risk. Moreover, y_0 = 125 keVμm^{-1} was derived from alpha particles and used for all types of radiation. There is evidence that y_0 varies with particle type (Al-Affan and Watt, 1985). Alternatively, the quality factor can be expressed by equations (2.47) and (2.48) for RBE $\leq$ 100 and RBE > 100 respectively (Al-Affan and Watt, 1987).

$$\bar{Q} = 1.33 \int_0^\infty y^* \; d(y) \; dy \qquad (2.47)$$

$$\bar{Q} = \int_0^{\infty} (0.35 + y^{*1.45}) \; d(y) \; dy \qquad (2.48)$$

The values of y_0 for different types of radiation are given in **Table 2.2.**

Table 2.2 The values of y_0 for different types of radiations (after Al-Affan and Watt, 1985)

Type of radiation	electrons	protons	alpha	Li	C	Ne	Ar
LET=L_0 (keV μm^{-1})	24	64	108	132	185	215	250
y_0 (keV μm^{-1})	3.6*	72	121.5	148.5	208	242	293

* note: electrons produce saturation damage at energies around 50 - 250 eV. As their ranges are only a few nanometers the saturation value cannot be observed in a 1 μm diameter sphere. The saturation value of 3.6 keV/μm for y_0 is based on that for minimum energy electron which has a range = 0.67 μm.

Ricourt *et al.* (1981) have measured microdosimetric spectra in terms of y and used the approximation of $y = \frac{9}{8} L_{\infty}$ to replace the consecutive weighting of Q(L) by Q(y). When the quality can be expressed in terms of y, Q value can be determined by microdosimetric spectrum of the radiation folded with the evaluation function Q(y). The formulation of the concept by microdosimetric method has been described by Zaider and Brenner (1985) who had defined the specific quality function, SQF, for different relevant endpoints in order to make an assessment of the overall quality factor, Q(y). ICRU (1986) has used the procedure similar to that of Zaider and Brenner to define the relation between Q and y in 1 μm diameter of spherical ICRU tissue volume, given by

$$Q(y) = \frac{a_1}{y} \{ 1 - \exp (-a_2 y^2 - a_3 y^3) \} \qquad (2.49)$$

where a_1= 5510 keVμm^{-1}, a_2= 5.0 x 10^{-5} $\mu m^2 keV^{-2}$ and a_3= 2.0 x 10^{-7} $\mu m^3 keV^{-3}$. The relation of equation (2.49) was determined based on general observations and theoretical considerations in radiobiology which indicate that the RBE is maximal at a lineal energy of about 140 keVμm^{-1} as shown in **Fig. 2.7.** A special consideration was also given to observations of chromosome aberrations in human lympohcyte. The effective quality factor, $\bar{Q}$, for any radiation within the range of lineal energy, y, can be written as

$$\bar{Q} = \frac{1}{D} \int_0^\infty Q(y)\, D(y)\, dy \qquad (2.50)$$

where D(y) dy is the absorbed dose in the interval from y to y+dy, D(y) is the distribution of absorbed dose in y and D is the absorbed dose given by equation (2.51).

$$D = \int_0^\infty D(y)\, dy \qquad (2.51)$$

The effective quality factor , $\bar{Q}$, for photons and neutrons of various energies are shown in **Fig. 2.8** (a) and **2.8** (b) respectively. The radiation for which the quality factor is 1.0 is termed the reference radiation which are photons of energy near 100 keV. For photons or electrons of energy greater than 500 keV the quality factor can be 0.5. For high-LET radiation which energy at the point of interest is not known, $\bar{Q}$, value can be taken as 25 which overestimates the risk, in particular, for neutrons due to the fact that there is a number of neutron studies where the maximum RBE values are larger than the recommended $\bar{Q}$ values (Dennis and Dunster, 1985).

2.5.5 Evaluation of Dose Equivalent for Radiation Protection

The quality factor, Q, is a dose weighting factor introduced by ICRP (1966) for radiation protection purposes to account for the difference in biological effectiveness derived from ionizing radiations. The weighted dose which can bring about the same risk for any

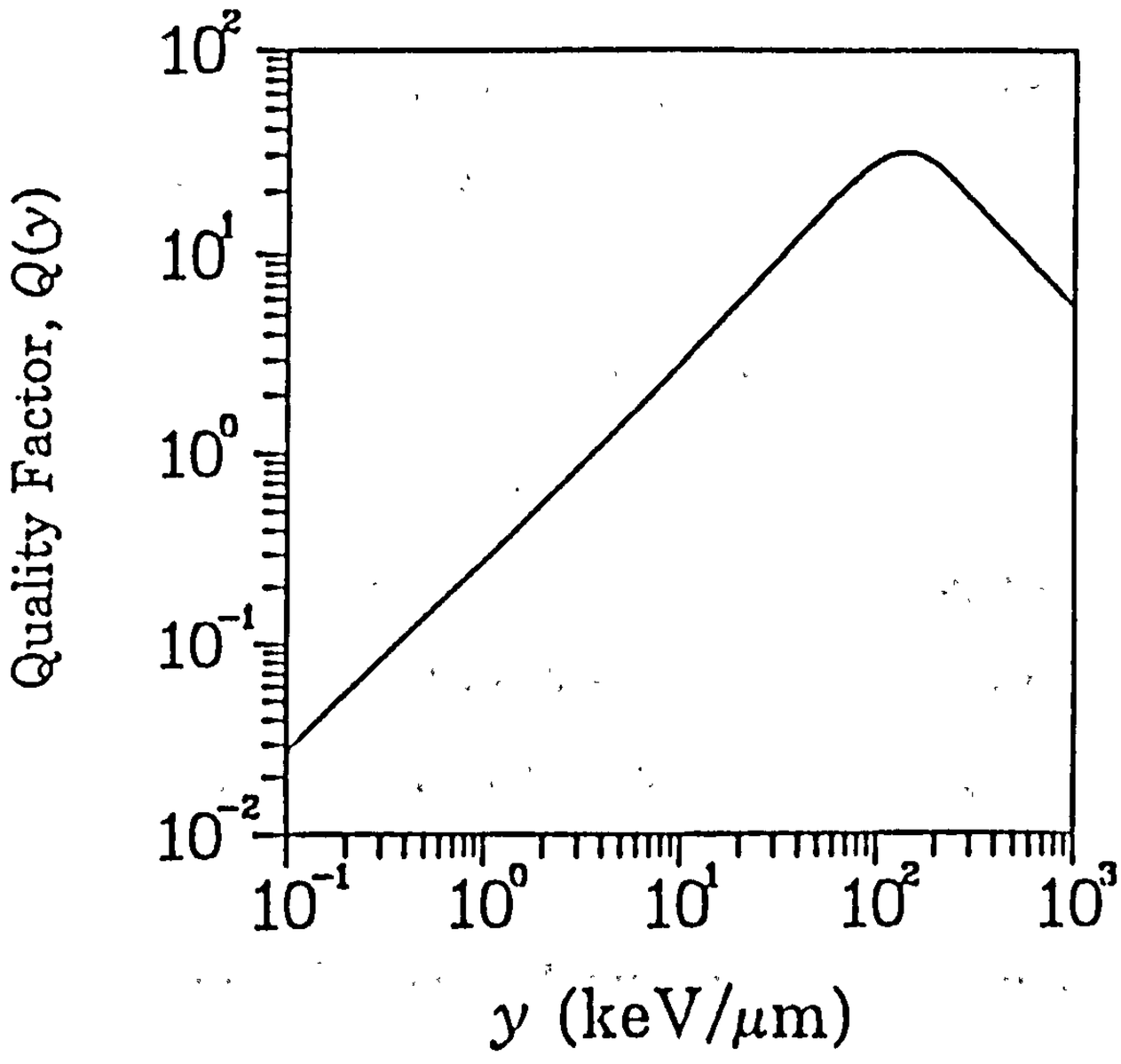

Fig. 2.7 The defining relation between quality factor, Q, and the lineal energy, y, in 1 μm diameter sphere of ICRU tissue (after ICRU, 1986).

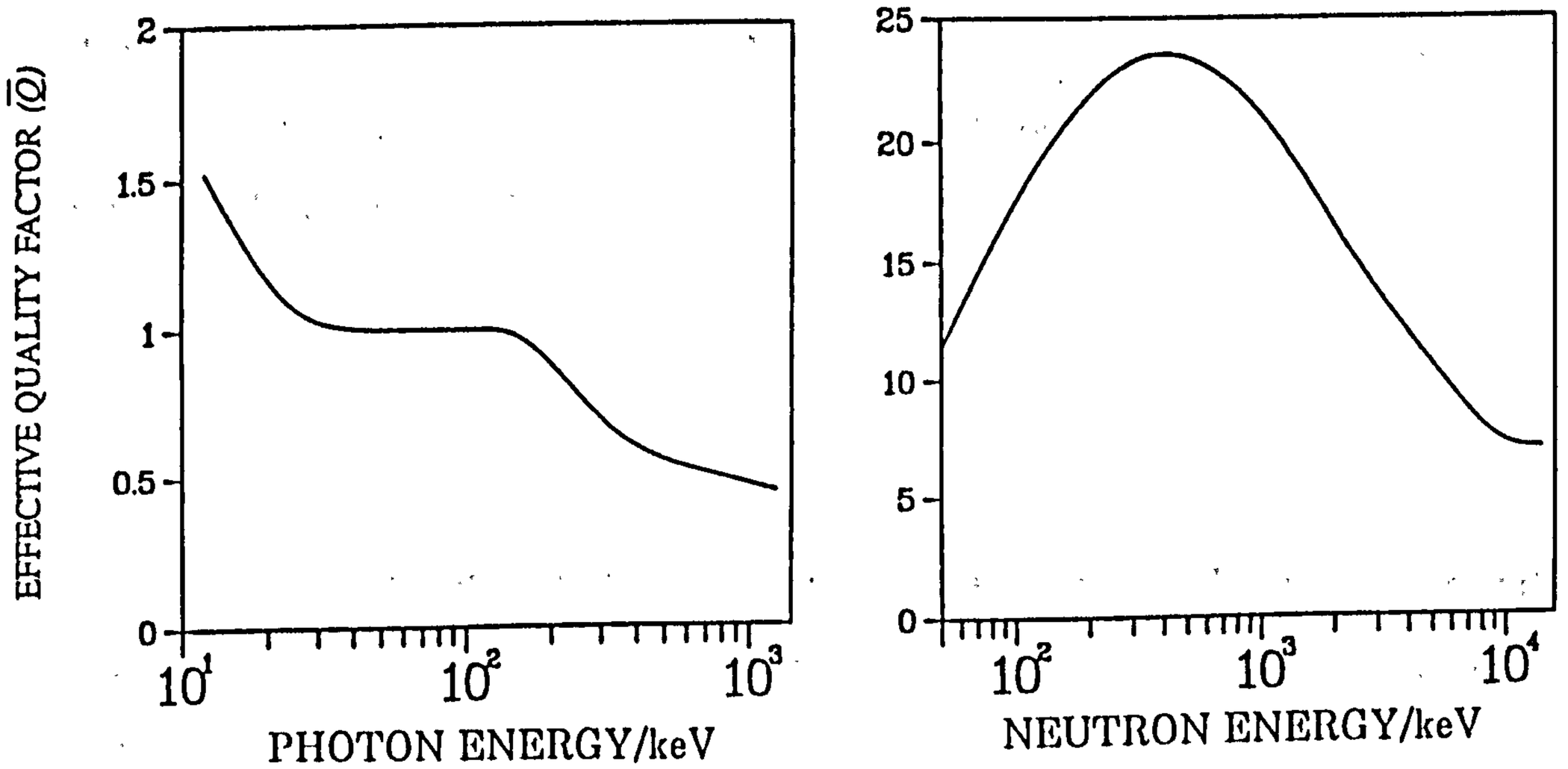

(a) (b)

Fig. 2.8 (a) The effective quality factor, $\bar{Q}$, of photons as a function of photon energy under conditions of CPE, (b) the effective quality factor, $\bar{Q}$, of neutrons as a function of neutron energy under conditions of CPE (after ICRU, 1986).

radiation is known as the dose equivalent, H, which is the product of the quality factor and the absorbed dose, D (ICRU, 1986).

$$H = Q D \tag{2.52}$$

These quantities are specified in the same point of interest. A modifying factor, N, which has been included in the previous definition of dose equivalent (ICRU, 1973) is no longer part of the definition. The unit of dose equivalent is the sievert (Sv), i.e $1\ Sv = 1\ Jkg^{-1}$.

For a complex radiation field with the mean quality factor, $\bar{Q}$, the average dose equivalent is determined from the pulse height spectrum according to equation (2.53).

$$H = D \int_0^\infty d(y)\, Q(y)\, dy \tag{2.53}$$

where Q(y) is the quality factor given by equation (2.49) and d(y) is the normalized dose distribution of absorbed dose in y. The distribution of dose equivalent can be expressed in terms of y by equation (2.54)

$$h(y) = \frac{d(y)\, Q(y)}{\bar{Q}} \tag{2.54}$$

Low-pressure TEPCs, in principle, can be employed as dose equivalent meters for working areas environmental monitoring, personal monitoring and as calibration instruments (Booz, 1984a).

2.6 The Principles of Tissue Equivalent Proportional Counter

2.6.1 The Operation of TEPC

One of the methods which provides information on deposition of energy by ionizing radiations in tissue volumes is by means of a TEPC. The concepts applied is that the energy deposition in the simulated volume is proportional to the number of ion pairs formed in the gas chamber by traversing ionizing radiations. The concepts of TEPC was originated by Rossi (Rossi and Rosenzweig, 1955a). Other than the wall and the counting gas which are tissue equivalent, a requirement for secondary charged particle equilibrium and homogeneity i.e. Fano's theorem, a TEPC, in principle, follows the concepts of an ordinary proportional counter. Details of the operation of proportional counters have been described elsewhere (e.g. Curran and Craggs, 1949, Rossi and Staub, 1949, Wilkinson, 1950, Watt and Ramsden, 1964 and Knoll, 1979).

The proportional counter is a type of gas-filled ionization chamber which consists of a thin axial wire serving as the anode and a cylindrical shell for the cathode. The chamber is filled with a non-electronegative gas which provides an interacting medium surrounding the wire. A high logarithmic increasing electric field is applied between the cathode and the anode to accelerate electrons in the chamber. A single ionizing event in the gas produces an electrical output pulse which has been multiplied 10^2-10^5 times due to gas multiplication in the high field region immediately surrounding the anode. The electric field strength X at any radial distance r from the centre of the wire is given by

$$X = \frac{V}{r \ln (b/a)} \qquad (2.55)$$

where V is the anode voltage, a is the radius of the anode and b is the radius of the cathode (b>>a). The dependence of the electric field on radial distance implies that the gas multiplication region is within a few diameters of the anode from the centre. At the region of low field strength the electrons and ions created by ionizing radiation simply drift to their respective collecting electrodes and in the process these charged particles collide with gas

molecules during their migration. When the electric field strength is sufficiently high, free electrons which have higher mobility than the positive ions, are accelerated and gain enough energy between collisions to produce additional ionizations. The electrons liberated from the secondary ionizations experience the same phenomenon to produce more ionizations.

The gas multiplication process, therefore, takes the form of a cascade known as a Townshend avalanche. The Townshend ionization coefficient, α, is defined as the mean number of secondary electrons produced by an electron per centimeter path (Curran and Craggs, 1949)

$$\frac{\alpha}{P} = A \exp\left(-\frac{BP}{X}\right) \qquad (2.56)$$

where P is the gas pressure, A and B are the constants for a given gas provided that X at the anode is within the range for which the above expression is valid. $\frac{\alpha}{P}$ was found to be a function of reduced field strength, $\frac{X}{P}$, and can have various expressions (Charles, 1972) depending on the probability of ionizations, the electron energy distribution and the electron mobility.

The output pulse is made up from the sum of all avalanches produced at the same time by one ionizing radiation and is therefore proportional to the energy deposited in the creation of the primary ion pairs, N.

$$N = \frac{E_D}{\bar{w}} \qquad (2.57)$$

where E_D is the energy deposited in the counter by ionizing radiation and $\bar{w}$ is the mean energy expanded per ion pair which depends on the types and energy of radiation. It is also important to note that the avalanches arising from the individual electrons are of the same size within statistical limitations and independent of one another.

2.6.2 Rise Time and Pulse Shape

The output signal of a proportional counter depends on the rise time of the pulse generated in the counter and on the pulse shaping network of the electronic circuit. The observed output pulse at the anode is caused by the drift of the positive ions away from the centre wire rather than the drift of the electrons. The positive ions traverse almost all the potential difference toward the cathode while the electrons which are created in the avalanche very close to the anode wire traverse only a small fraction of the potential difference. In the high field region near the centre, positive ions move rapidly which produce a fast-rising pulse height, and in the low field region towards the cathode, their drift velocity decreases leading to a slowly-rising pulse height. This time response of the proportional counter output pulse, V(t), has been studied by Ramsey (1940) and Wilkinson (1950) and is given by

$$V(t) = \frac{N\ G\ e}{2\ C\ \ln\ (b/a)}\ \ln\ (1 + t/t_0) \qquad (2.58)$$

where

$$t_0 = \frac{P\ a^2\ \ln\ (b/a)}{2\ \mu_+\ V_0} \qquad (2.59)$$

G is the gas gain i.e. the number of avalanche electrons divided by the number of the primary electrons, e is the charge of an electron, C is the capacitance of the counter, V_0 is the anode applied voltage and μ_+ is the positive ion mobility. The collection time of ions may take hundreds of microsecond as compared to less than a microsecond for the electrons. The positive ions finally reach the cathode and are collected in time $t = [\ (b/a)^2 - 1\ ]\ t_0$. Then the pulse height of the proportional counter in equation (2.58) is reduced to

$$V_g = \frac{N\ G\ e}{C} \qquad (2.60)$$

Hence, the final height of the pulse, V_g, is proportional to the energy deposited E_D by ionizing radiations.

The pulse shaping time constant of a RC differentiating circuit at the amplifier input are typically chosen around one microsecond. Thus, the slow drift of the positive ions is no longer contributing to the final pulse height. Although the amplitude of the pulse is reduced by the RC network, the shape and the ballistic deficit would always remain the same due to a constant factor of attenuation. Also, the mean pulse length has been reduced by the network, thus, improving the resolution time of the proportional counter. The ballistic deficit for shaping the pulses has been investigated using a wide range of pulse shaping networks in order to find the best network to optimise signal to noise ratio (Mathieson and Charles, 1969, Gott and Charles, 1969 and Breyer and Cimerman, 1970).

2.6.3 Simulation of Tissue Volume

The measurement of the stochastic quantities of lineal energy and specific energy and their distributions is achieved by the simulation of a microscopic volume of biological tissue in a much larger gas cavity of TEPC filled with TE gas of much lower density. If the atomic composition of tissue and TE gas are identical then the mean energy loss of charged particles is identical in both tissue and gas volumes (ICRU, 1983).

$$S_t \rho_t l_t = S_g \rho_g l_g \qquad (2.61)$$

where S is the mass stopping power, ρ is the density and l is the cavity chord length. t and g are subscripts for tissue and gas respectively. If the stopping powers are independent of density, i.e. $S_g = S_t$, then

$$\left(\frac{\rho_t}{\rho_g}\right) = \left(\frac{l_g}{l_t}\right) \qquad (2.62)$$

The simulated chord length of tissue volume of density 1 gcm^{-3} in a gas cavity of pressure P_g torr for a given temperature is therefore

$$l_t = l_g \rho_g \left(\frac{P_g}{760}\right) \tag{2.63}$$

The simulated mean chord lengths for spherical and cylindrical volumes can be determined from equations (2.64) and (2.65) respectively

$$\bar{l}_s = \frac{2}{3} d_g \rho_g \left(\frac{P_g}{760}\right) \tag{2.64}$$

$$\bar{l}_c = \frac{2 r_g h_g}{(r_g + h_g)} \rho_g \left(\frac{P_g}{760}\right) \tag{2.65}$$

where d_g is the diameter of spherical counter and r_g and h_g are the radius and length of cylindrical counter respectively. From equations (2.64) and (2.65) we can easily deduce that a cylindrical cavity of equal height and diameter can be considered as essentially equivalent to a spherical cavity of equal mean chord length.

At very low gas pressure the gas multiplication volume in a TEPC is comparable to that of the total counter volume. The pulse height depends on the position of the charged particle trajectory in the counter and the proportionality to energy deposition at very low pressure is difficult to maintain, thus, limiting the size of the simulated chord length that can be achieved in experiment. The minimum size recommended by ICRU (1983) is 0.3 μm for spherical volume. However, recently there has been reported that microdosimetric spectra have been measured for a spherical volume of 0.14 μm diameter using a well-designed TEPC (Colautti *et al.*, 1985).

CHAPTER 3

THEORETICAL :

Calculation of Stopping Power and Projected Ranges of Projectiles, Neutron Kerma and Kerma Factor and Microdosimetric Spectra of Intermediate Energy Neutrons in a Co-Axial Double Cylindrical TEPC

3.1 Introduction

The objective of assessing separately the energy deposition in tissue due to intermediate energy neutrons below 100 keV from that of fast neutrons is to characterise the radiation quality of these neutrons, since radiation exposure due to intermediate energy neutrons is not fully investigated for protection purposes. Intermediate energy neutrons slow down in tissue matter to generate heavy charged particle recoils which have ranges equal to, or rather less than, the cellular dimensions of most mammalian cells, thereby causing biological damage. If the wall thickness of a TEPC can be made equal to the maximum proton range of intermediate energy neutrons, the energy deposition by these neutrons in mixed radiation field of fast neutrons can be measured in a co-axial double cylindrical TEPC. The object of this chapter is to present the theoretical analysis of this counter, in particular to the counter response to neutron irradiation prior to the counter design.

Knowledge of the stopping power and projected ranges of secondary charged particles and neutron kerma in tissues are very important for accurate prediction of energy deposition of intermediate energy neutron in tissue. This chapter first deals with the calculation of stopping powers and projected ranges of heavy particles generated by neutrons in 4-element tissue constituents, tissue and TE materials for particle energies from 0.1 keV to 1.0 MeV. At low particle energies quasi-elastic scattering can cause the penetration depths , and the corresponding effective stopping power, to differ significantly from CSDA values. The

calculation is based on Ziegler's universal screening function which is better agreement with experiment than that of Lindhard's screening function for low energy projectiles, where the measured stopping power data are scarce. It will be followed by the calculation of kerma and kerma factor of intermediate energy neutrons in tissue and TE materials. The forgoing quantities are required in the subsequent calculation of energy deposition spectra.

3.2 Effective and CSDA Stopping Powers and Projected Ranges of Ions in Tissue Constituents, Tissue and TE materials

The penetration of charged particles through matter is a complex phenomenon which can be measured in terms of stopping power and projected ranges. In the region where projectile velocities are greater than the electronic orbital velocity, v_0 ($v_0 = \frac{e^2}{\hbar} \sim 25$ keV/amu), the pathlength of ions in the matter is a straight line. However, in the low energy region, i.e. $v < v_0$, the pathlength is no longer a straight line but a complex range. This resulted from various interaction processes which could play important role in the stopping of charged particles in the matter, such as an elastic collision with the target atoms, an inelastic collision with the electrons, the charged exchange and the chemical binding effects. In general, there is a competition between the loss of energy of charged particles to electrons and to the recoil particles (Lindhard and Scharff, 1961). The particles undergo successive small angle scattering known as multiple scattering which may produce recoils deflected in the direction inside the cavity, increasing the stopping cross section per atom. The scattering angle becomes larger as the particle energy decreases. The particles will travel in a zig-zag path which partly explains the difference between the projected range and the pathlength of ions at low energies. The difference is very significant at energies where quasi-elastic scattering becomes dominant (Watt, 1972).

Projected range is an average thickness of material traversed by a number of particles directed perpendicular to the material. The effective stopping power is the energy loss per unit length along this projected range. The effective stopping power values will be greater than that of the CSDA values for low-energy ions because of the significant importance of elastic scattering of particles with nuclei of the target material, and range of straggling.

However, the effective stopping power will be the same with the CSDA stopping power for ions at high energies because the loss of energy is mainly by collisions with the atomic electrons and not by nuclear interactions.

3.2.1 Stopping Power of Low-Energy Projectiles

Recently, Ziegler *et al.* (1985) have introduced a new universal screening length, a_z, from which the corresponding screening function produces a tighter grouping, with the standard deviation of 18%, better than the one derived from Lindhard's screening length, a_L, which has the standard deviation of 40%. The two screening lengths are given by equations

$$a_z = \frac{0.8854\ a_0}{(Z_i^{0.23} + Z_j^{0.23})} \tag{3.1}$$

$$a_L = \frac{0.8854\ a_0}{(Z_i^{2/3} + Z_j^{2/3})^{1/2}} \tag{3.2}$$

where a_0 is Bohr radius (0.529 A^o) and Z_i and Z_j are the atomic number of recoil ion i and target atom j respectively. Ziegler *et al.* have found that the atomic screening function vs. a_L is too strong Z dependence (hidden in $a_L \sim Z^{-1/3}$) and they concluded that small exponential factor (i.e. $a_z \sim Z^{-0.23}$) consistently lower the light atomic screening functions than those of the heavy atom pairs. They found that their fitted universal screening function is in a good agreement with the experimental data within 5% of the standard deviation. The reduced energy, ε_z, for ions of energy E (keV), in terms of Ziegler's screening length is given by

$$\varepsilon_z = \frac{32.53\ m_i\ E}{Z_i Z_j\ (m_i+m_j)\ (Z_i^{0.23}+Z_j^{0.23})} \tag{3.3}$$

where m_i and m_j are the masses of particle i and target j respectively.

The total stopping power, ${}^iS_j(E)$, is the sum of the nuclear stopping power, ${}^iS_j^n(E)$, and the electronic stopping power, ${}^iS_j^e(E)$, given by Lindhard *et al.* (1963), but expressed in terms of Ziegler's reduced energy by

$$^{i}S_j(E) = \frac{8.462 \times 10^{-15} Z_i Z_j m_i}{(m_i + m_j)(Z_i^{0.23} + Z_j^{0.23})}[Sn(\varepsilon_z)+Se(\varepsilon_z)] \qquad (3.4)$$

where Sn and Se are the reduced nuclear and electronic stopping powers respectively.

The reduced nuclear stopping power, $Sn(\varepsilon_z)$, is given by Ziegler by equation (3.5) and (3.6) for low and high energy ions respectively.

$$Sn(\varepsilon_z) = \frac{\ln(1+1.1383\,\varepsilon_z)}{2[\varepsilon_z + 0.01321\,\varepsilon_z^{0.21226} + 0.19593\,\varepsilon_z^{0.5}]} \quad \text{for } \varepsilon_z \leq 30 \qquad (3.5)$$

$$\frac{\ln(\varepsilon_z)}{2\,\varepsilon_z} \quad \text{for } \varepsilon_z > 30 \qquad (3.6)$$

The reduced electronic stopping, $Se(\varepsilon_z)$, can be expressed according to Watt and Sutcliffe (1972), but now in terms of Ziegler's screening length, i.e. the dependence on $a_L \sim Z^{-1/3}$ has been replaced by $a_z \sim Z^{-0.23}$.

$$Se(\varepsilon_z) = \frac{7.93 \times 10^{-2} Z_i^{2/3} Z_j^{1/2} (m_i + m_j)^{3/2}}{m_i^{3/2} m_j^{1/2} (Z_i^{0.23} + Z_j^{0.23})^{3/2}}\ \varepsilon_z^{1/2} \qquad (3.7)$$

3.2.2 Stopping Power of High-Energy Projectiles

In the high energy region, the contribution from nuclear stopping power is very small and can be neglected. Therefore, one can consider the electronic stopping power alone to describe the stopping of particles in the matter. The electronic stopping power can be calculated according to the Bethe formula or by Ziegler's code. The latter has been adopted in this work. Ziegler *et al.* (1985) apply the standard Bohr rule known as the heavy-ion scaling rule, which states that the electronic stopping power for heavy ions, S_{HI}, at two velocities is directly proportional to the stopping of protons, S_H, at the same velocities and in the same material given by

$$\frac{S_H(v_i,Z_j)}{S_H(v_j,Z_j)} = \frac{S_{HI}(v_i,Z_j)}{S_{HI}(v_j,Z_j)} \qquad (3.8)$$

where v_i and v_j are velocities of recoil i and target j respectively. S_H is the stopping power of protons per unit charge and has relationship with the stopping power S_{HI} by equation (3.9).

$$S_{HI} = S_H (Z_{HI}\,\beta)^2 \qquad (3.9)$$

Here Z_{HI} is the atomic number of heavy ions and β is its fractional effective charge given by Ziegler as

$$\beta = q + 0.5\,(1-q)\,(v_0/v_F)^2 \ln[1+ (2\Lambda v_F/a_0 v_0)^2] \qquad (3.10)$$

where v_0 and v_F are the Bohr velocity (2.2×10^8 cm s^{-1}) and the Fermi velocity of the target respectively. Λ is the ion screening length and q is the degree of ionization of the ion. Details of the mathematical treatments are given in the original report (Ziegler *et al*, 1985).

The stopping power of protons is taken from the proton coefficients using the following formula (Andersen and Ziegler , 1977).

$$\frac{1}{S_H} = \frac{1}{S_{Low}} + \frac{1}{S_{High}} \qquad (3.11)$$

where S_{Low} and S_{High} are defined as (Ziegler *et al.*, 1985)

$$S_{Low} = C_1(E)^{C_2} + C_3\,(E)^{C_4} \qquad (3.12)$$

$$S_{High} = C_5 \ln (C_7/E + C_8\,E)/\,(E)^{C_6} \qquad (3.13)$$

where C_1, C_2, C_3, C_4, C_5, C_6, C_7, C_8 are the proton stopping coefficients which is the fitting parameters given in **Table 3.1.** The energy E is in keV/amu.

Table 3.1 Proton stopping coefficients used in the calculation of stopping power of ions in solid materials for energies greater than 40 keV/amu (after Ziegler *et al.*, 1985)

Z	1	6	7	8
C_1	0.0091827	3.2579	0.59674	0.75253
C_2	0.0053496	0.0049148	0.0050837	0.0050314
C_3	0.69741	2.7156	4.2073	4.0824
C_4	0.48493	0.36473	0.30612	0.30067
C_5	316.07	2092.2	2394.2	2455.8
C_6	1.0143	1.0291	1.0255	1.0181
C_7	9329.3	2643.6	4.892.1	5069.7
C_8	0.053989	0.018237	0.016006	0.01742

3.2.3 Effective Stopping Power and Projected Ranges

The effective stopping power, ${}^iS_j^{eff}(E)$, and the projected range, ${}^iR_j^P(E)$, can be determined according to Watt and Sutcliffe (1972) in the manner similar to that adopted by Al-Affan *et al.* (1984).

$$ {}^iS_j^{eff}(E) = \frac{{}^iS_j^n(E)}{2\,\gamma\,f(x)} + {}^iS_j^e(E) \qquad (3.14) $$

$$ \frac{1}{{}^iR_j^P(E)} = \frac{1}{2\,\gamma\,f(x)\,{}^iR_j^n(E)} + \frac{1}{{}^iR_j^e(E)} \qquad (3.15) $$

where E is the energy of the recoil i, ${}^iS_j^n(E)$ is the nuclear stopping power of recoil i in atom j, ${}^iS_j^e(E)$ is the electronic stopping power of recoil i in atom j, ${}^iR_j^n(E)$ is the pathlength for nuclear stopping, ${}^iR_j^e(E)$ is the pathlength for electronic stopping and $\gamma^2 = 4m_im_j/(m_i+m_j)^2$. f(x) is the function which converts the effective stopping power and projected range of the nuclear stopping and is represented to better than 10% by Watt and Sutcliffe (1972) as

$$f(x) = 0.021[\ln(\frac{m_i}{m_j})]^2 - 0.1434\,[\ln(\frac{m_i}{m_j})] + 0.3642 \qquad (3.16)$$

However, equation (3.15) was not used directly in this work, instead the projected ranges were calculated according to equation (3.17).

$$^{i}R_j^P(E) = R_1 + \int_{E_1}^{E_{max}} \frac{dE}{^{i}S_j^{eff}(E)} \qquad (3.17)$$

where R_1 is an estimated residual range for charged particles of energy E_1 which is added to the range calculated over energy from E_1 to incident energy E_{max}. R_1 was arbitrary set equal to zero at an E_1 = 10 eV, according to Janni (1982).

3.2.4 Methods of Calculation

The effective stopping powers and projected ranges of heavy recoil ions in tissue constituents (i.e. hydrogen, carbon, nitrogen and oxygen) were calculated as follows. Except for recoil protons, the CSDA nuclear stopping powers for C, N and O ions were calculated according to equations (3.5) and (3.6), and the first term of equation (3.4). The electronic stopping powers for ions in the high energy region were calculated according to Ziegler's code (Ziegler *et al.*, 1985). However, we found that for ions at low energies, Ziegler's code gives values which underestimate the experimental results. Instead, the electronic stopping powers of energy less than 40 keV/amu were calculated according to equation (3.7) and the second term of equation (3.4). The choice of the energy cut off of 40 keV/amu, corresponds to the ion velocity of about 3.0×10^8 cm s^{-1}, was based on the earlier work (Oldenburg and Booz, 1972). Normalization was performed to connect smoothly the stopping power values below 40 keV/amu to Ziegler's electronic stopping powers for every recoil ion interacting on each target.

We have detected the discrepancy of Ziegler's code for protons in all four target tested. Ziegler's code gives values which are lower than experimental results. Therefore, the CSDA

stopping powers of the protons in four-element tissue constituents were obtained by fitting the ICRU Stopping Committee data (Burger, 1986) at energies from 1 keV to 20 MeV. For protons of energy less than 1 keV the values were taken from Oldenburg and Booz (1972), but for protons in hydrogen where Oldenburg and Booz data are higher than the ICRU data, ICRU data were extrapolated down to 0.1 keV. The fitting results produced the deviation of less than 1%.

Consequently, the effective stopping power and projected ranges of the protons and carbon, nitrogen and oxygen ions were calculated according to equations (3.14) and (3.17) respectively. Only the first generation of particle interactions was considered which represents more than 90% of the stopping processes in tissue (Watt, 1972). The effective stopping power and projected ranges in tissue and TE materials were calculated according to the Bragg's additive rule, given by equations (3.18) and (3.19) respectively.

$$ {}^{i}S^{eff}_{mix}(E) = \sum \omega_j \; {}^{i}S^{eff}_{j}(E) \qquad (3.18) $$

$$ \frac{1}{{}^{i}R^{p}_{mix}(E)} = \sum \frac{\omega_j}{{}^{i}R^{p}_{j}(E)} \qquad (3.19) $$

where ω_j is the percentage by weight of the target atom type j in the tissue or in TE materials. The element compositions of ICRU tissue and TE materials were taken from ICRU Report 26 (ICRU, 1977) as shown in **Table 4.1**, but the minor elements were treated as oxygen. The CSDA components of stopping power and projected range were treated in the same manner.

It has been reported that for projectile energies below 150 keV, the experimental stopping power values in compounds deviate from Bragg's rule (Reynolds *et al.*, 1953 and Sautter and Zimmerman, 1965). The deviation is due the chemical bond effects between atoms in the molecule and also due to the phase effects. Thwaites and Watt (1978) have shown that compounds of different phases have different stopping power values. Al-Affan (1985) has used Bragg's rule with a semi-empirical modification to take into account the

chemical bond and phase effects, for protons and alpha particles in some compounds. In spite of these, the present calculations do not take into account the underlying effects as there are typically only a few percent.

3.2.5 Results and Discussion

The effective and CSDA values of stopping power calculated for recoil ions of energy from 0.1 keV to 1 MeV in hydrogen, carbon, nitrogen and oxygen are shown in **Fig. 3.1 - 3.4**. The results are compared with the published experimental results. The theoretical calculations of Oldenburg and Booz (1972) are also shown. The effective stopping power values, as expected, are higher than the CSDA values due to the range straggling of charged particles at low energies in the medium. The deviation for a given recoil, increases with the target mass and decreases with the projectile energy. In the high energy region, however, the deviation is negligible because the component of the nuclear stopping power is very small in comparison with the component of the electronic stopping power. Also, the deviation for a given target, increases with a decrease in the mass of the projectile ions due to the fact that the effective nuclear stopping power increases as the recoil mass decreases. The deviation is the largest for protons in all the targets.

The experimental stopping power data for recoil ions of low energies, shown on the graphs, are generally lower than the present calculations due to the fact that the measurements were performed for the electronic stopping power. In one case, when the calculated nuclear components were added to the experimental data of Arkhipov and Gott (1969), the results are consistent with the effective stopping powers as shown in **Fig. 3.2** for protons in carbon. It shows the significant importance of elastic scattering of protons at low energies in carbon. The experimental data for heavy ions in the low-energy region are scarce and are not sufficient to test the theoretical calculations. However, the present calculation is in better agreement with the experiment results than that of Ziegler's code. Theoretical calculations of Oldenburg and Booz (1972) for CSDA values of C, N and O ions are higher than the present calculations, in particular for ions in hydrogen.

Fig. 3.5 - 3.8 show the stopping powers of ions in the tissue and in TE materials. The results are compared with the measurements by Fakuda (1980 and 1981) for protons and nitrogen ions in methane based TE-gas, as shown in **Fig. 3.7.**

Fig. 3.9 - 3.16 show the projected ranges of recoil particles in the tissue constituents, ICRU tissue and TE materials. The calculated results are compared with the available experimental data. Also shown are the calculated values from Oldenburg and Booz (1972). The effective projected ranges are lower than the CSDA projected ranges due to range straggling of charged particles at low energies where nuclear collisions and multiple scattering become dominant. The results agree with the experiments for protons of energy greater than 10 keV in hydrogen and oxygen, as shown in **Fig. 3.9** and **Fig. 3.12** respectively, and for nitrogen ions in carbon, **Fig. 3.10. Fig. 3.11** shows a deviation between the calculations and experiments, for protons in nitrogen, which could be due to the triple bond effect of nitrogen molecules which was not taken into account. For protons of energy less than 10 keV in carbon, nitrogen and oxygen the experimental data of Borgesen (1985) are lower than the calculations. This may be due to nuclear straggling (Ziegler *et al.*, 1985) which was not included in the present calculation. The experimental data for protons in carbon was extracted for protons in CO and O_2 by applying the Bragg's rule. Nevertheless, the calculated results are in good agreement with experiments (Waibel and Willems, 1985) for protons of energy greater than 1 keV in methane based TE gas, as shown in **Fig.3.15.**

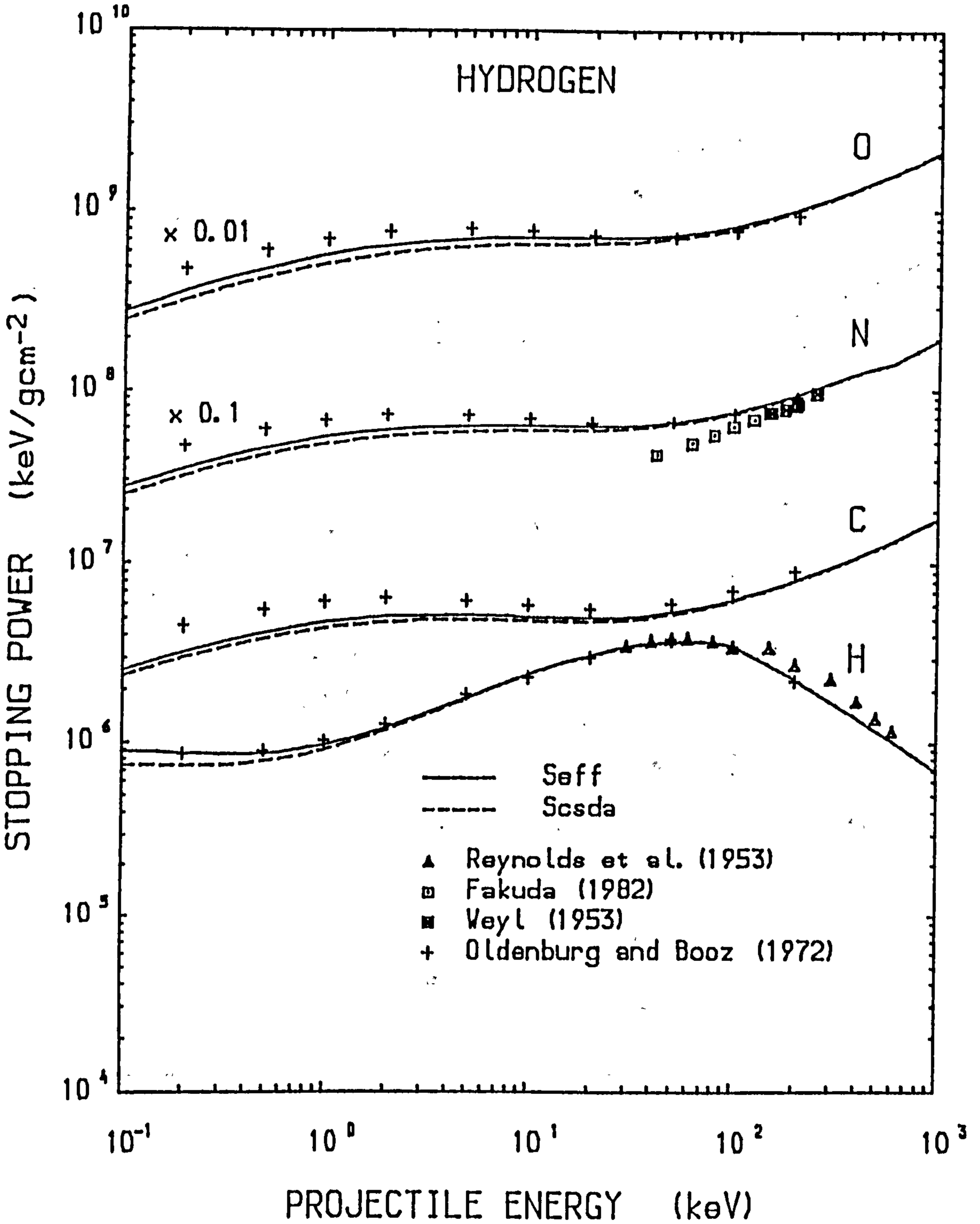

Fig. 3.1 The calculated effective and CSDA values of stopping powers for heavy ions (proton, C, N and O) in hydrogen.

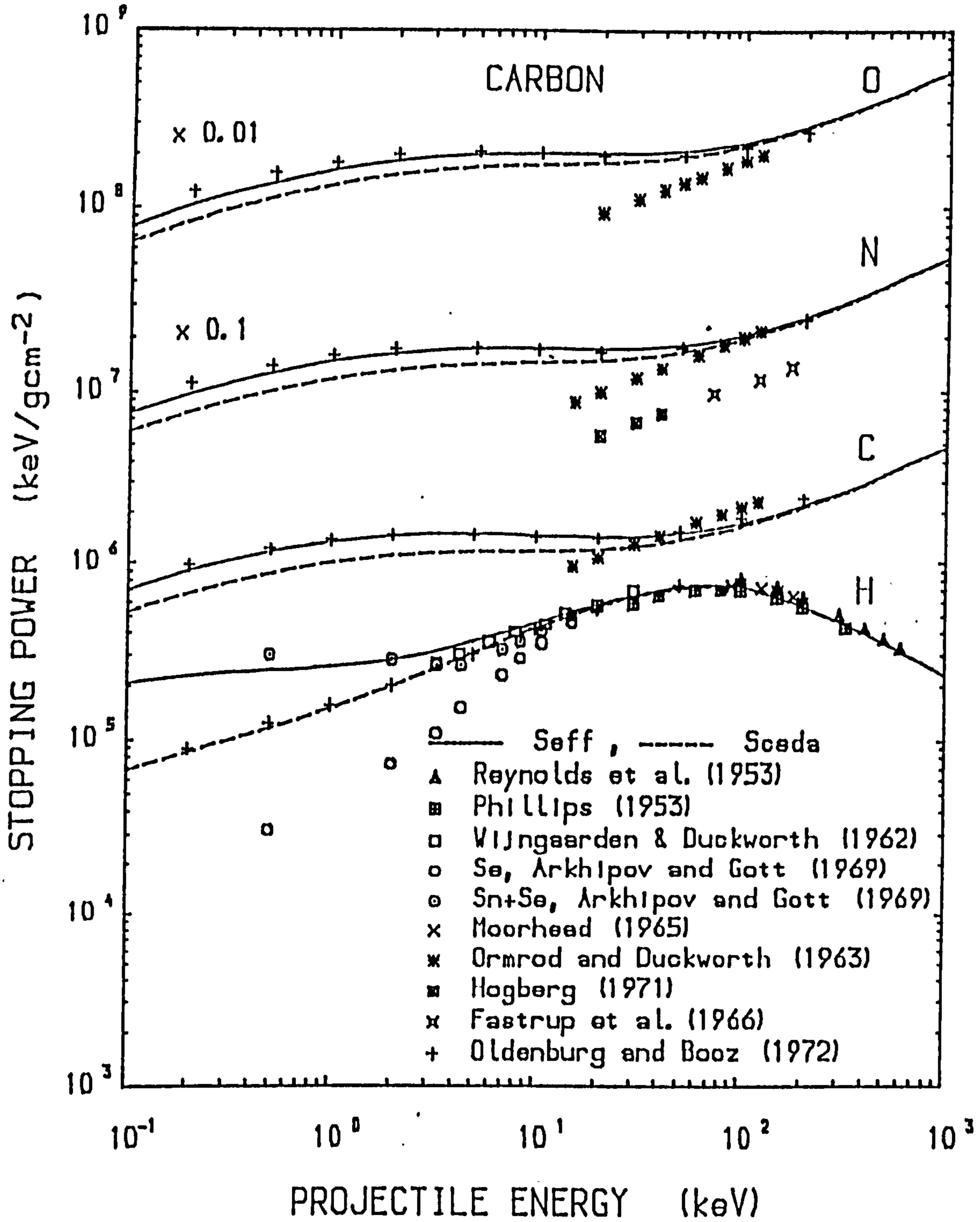

Fig. 3.2 The calculated effective and CSDA values of stopping powers for heavy ions (proton, C, N and O) in carbon.

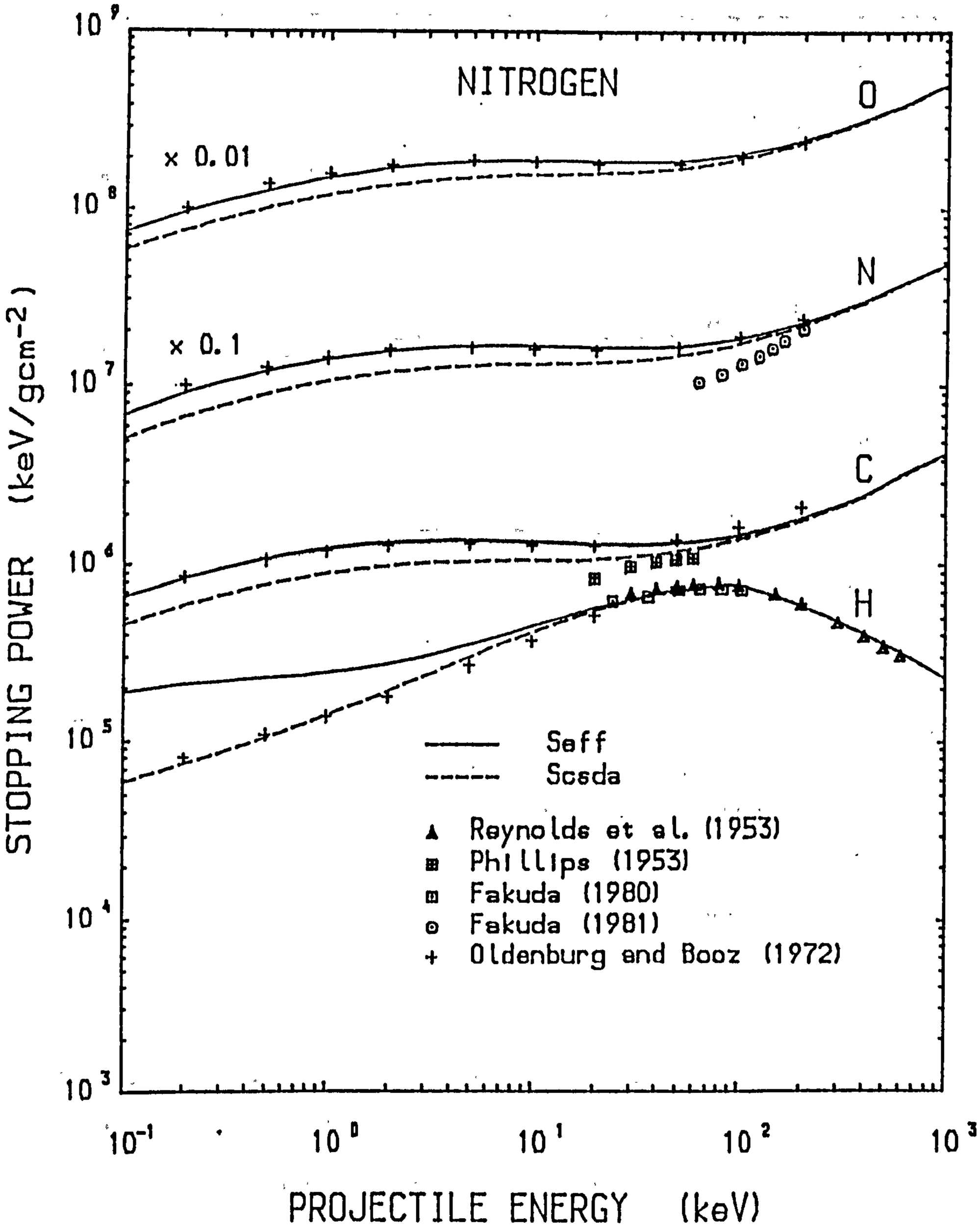

Fig. 3.3 The calculated effective and CSDA values of stopping powers for heavy ions (proton, C, N and O) in nitrogen.

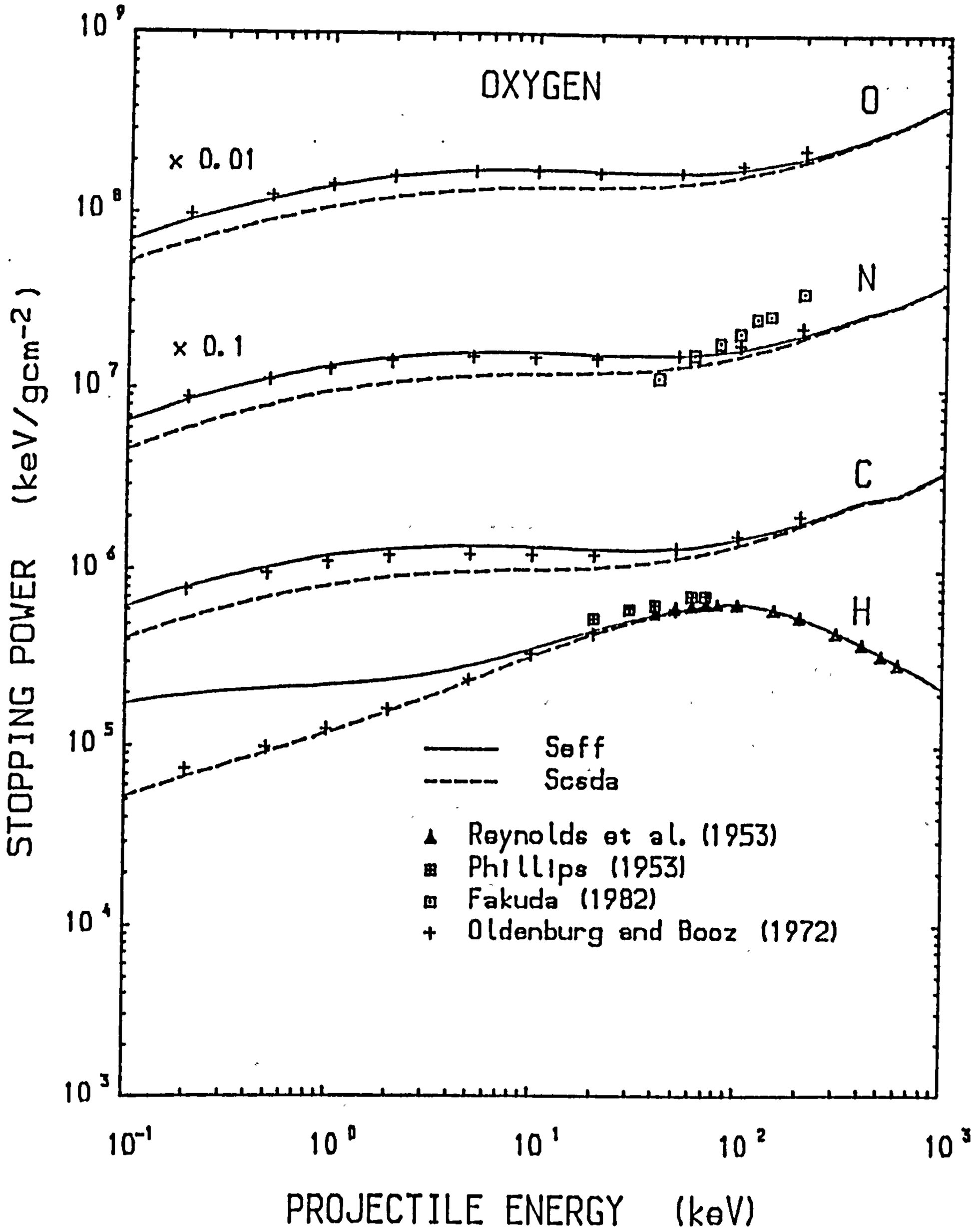

Fig. 3.4 The calculated effective and CSDA values of stopping powers for heavy ions (proton, C, N and O) in oxygen.

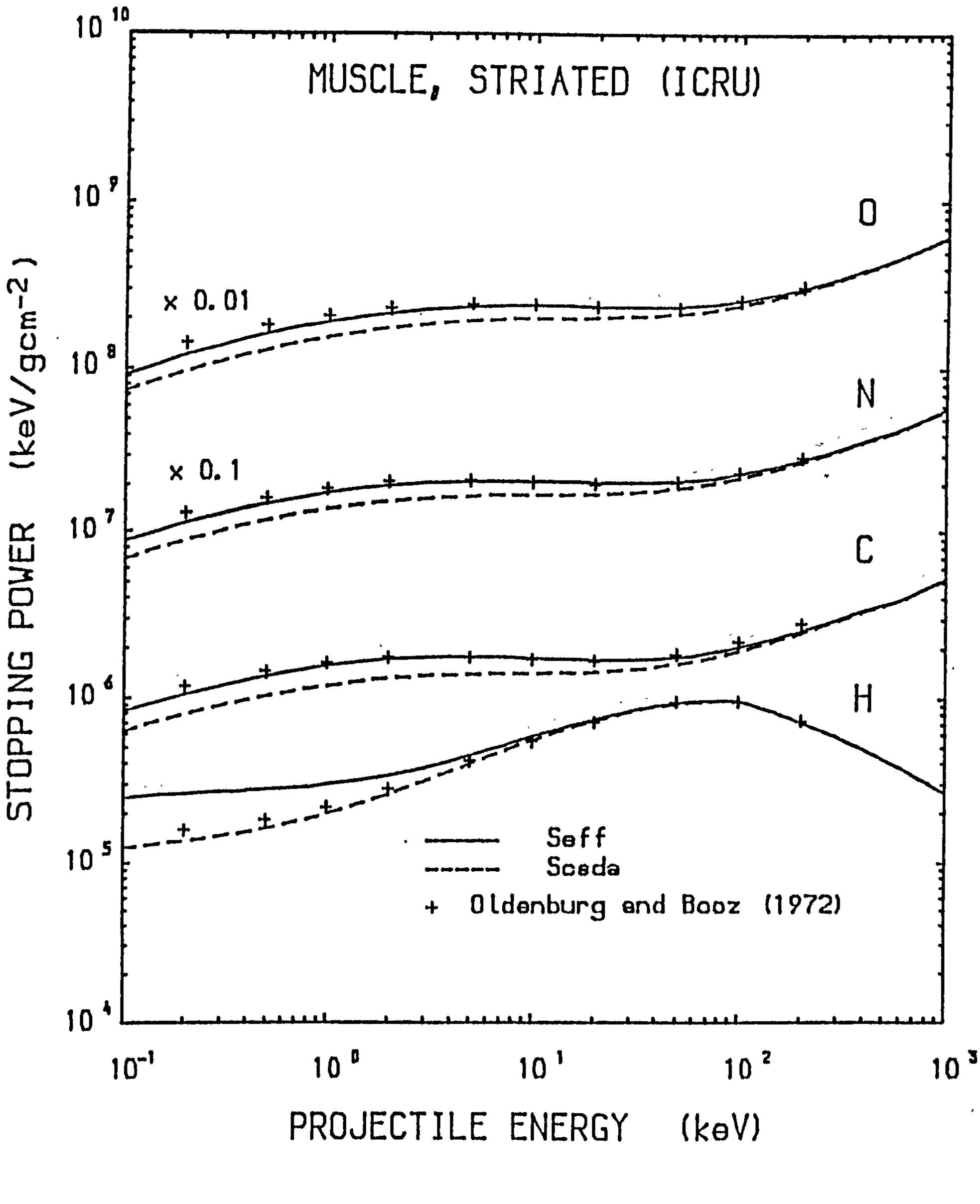

Fig. 3.5 The calculated effective and CSDA values of stopping powers for heavy ions (proton, C, N and O) in ICRU tissue.

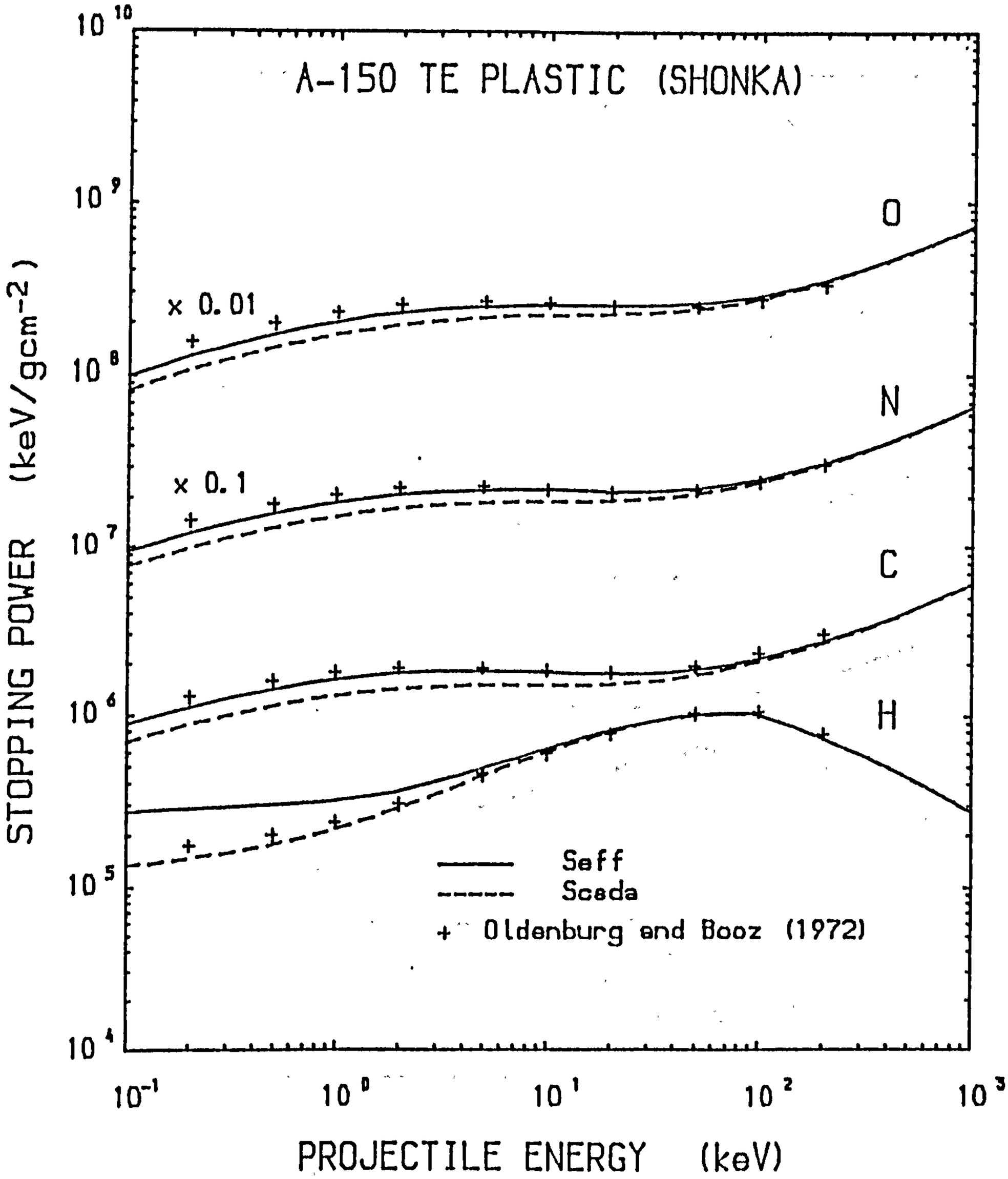

Fig. 3.6 The calculated effective and CSDA values of stopping powers for heavy ions (proton, C, N and O) in A-150 plastic.

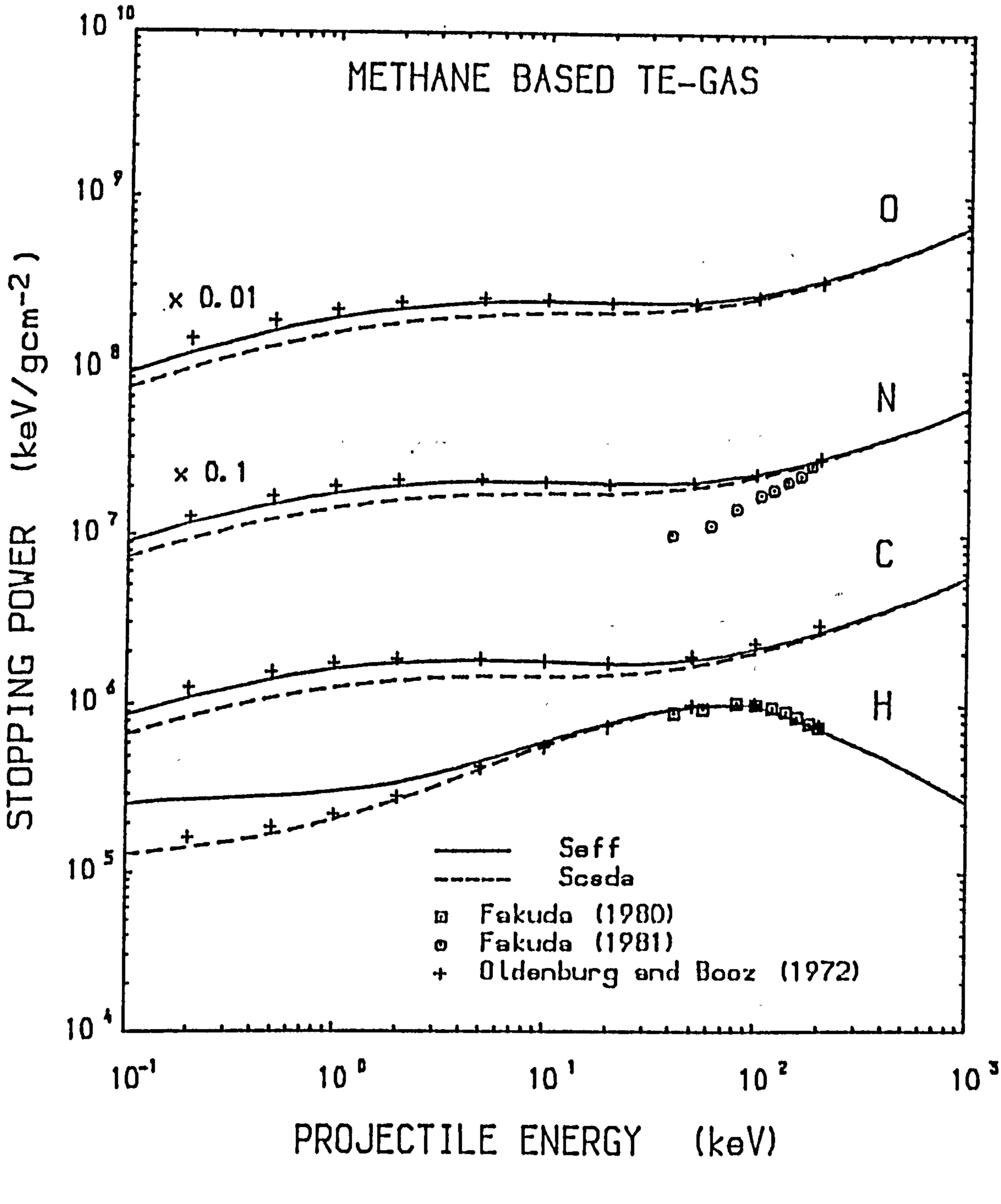

Fig. 3.7 The calculated effective and CSDA values of stopping powers for heavy ions (proton, C, N and O) in methane based TE gas.

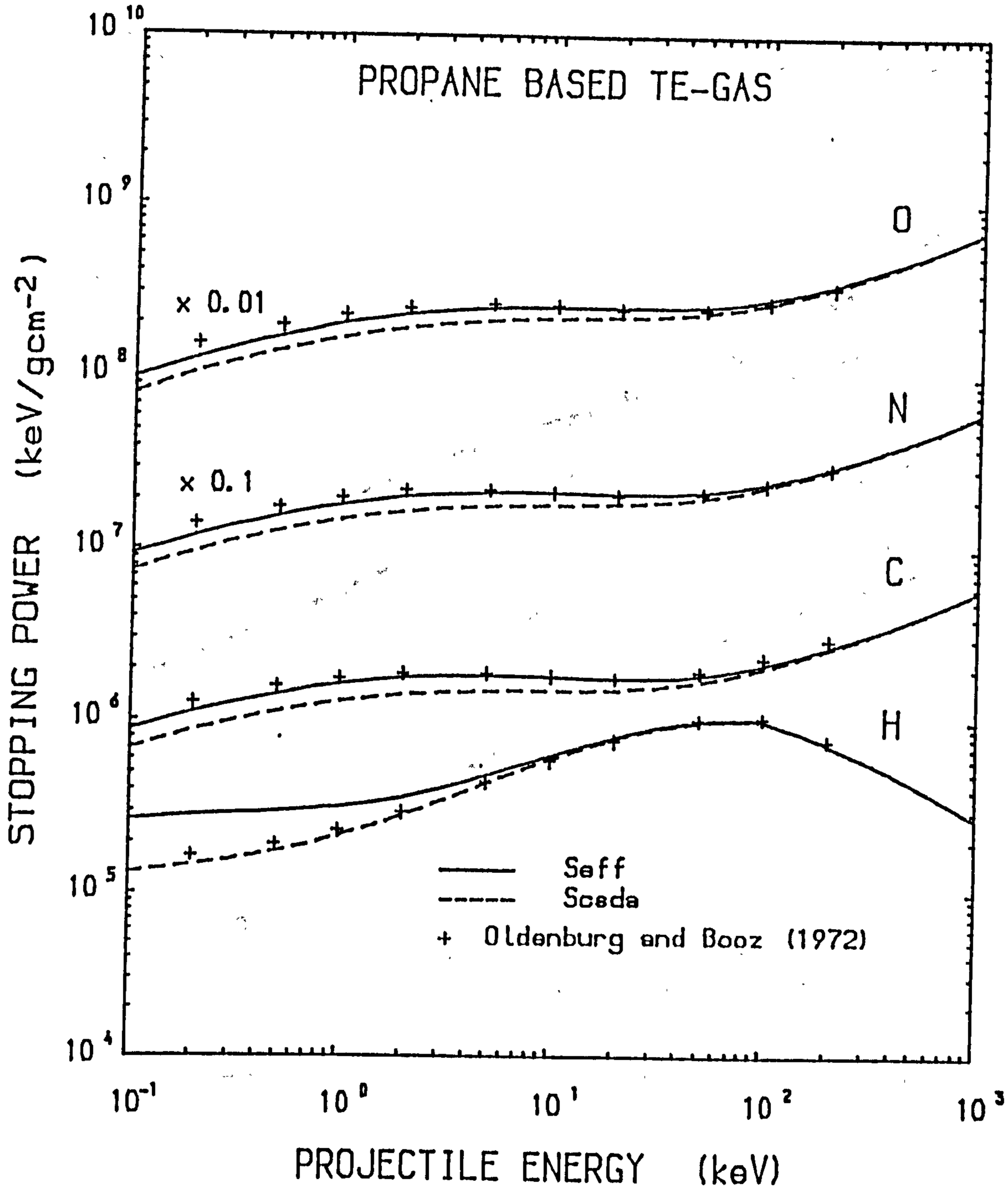

Fig. 3.8 The calculated effective and CSDA values of stopping powers for heavy ions (proton, C, N and O) in propane based TE gas.

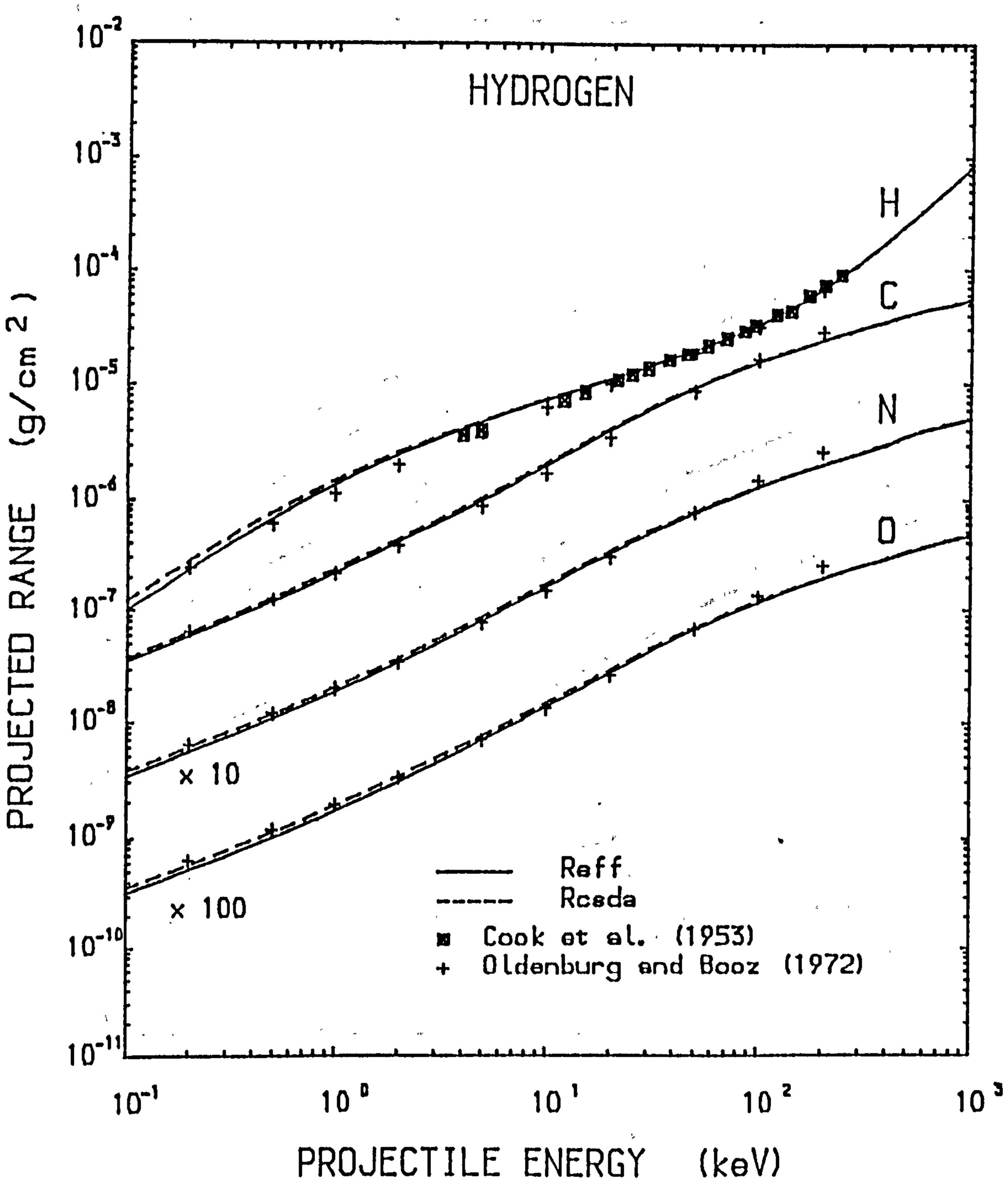

Fig. 3.9 The calculated effective and CSDA values of projected ranges for heavy ions (proton, C, N and O) in hydrogen.

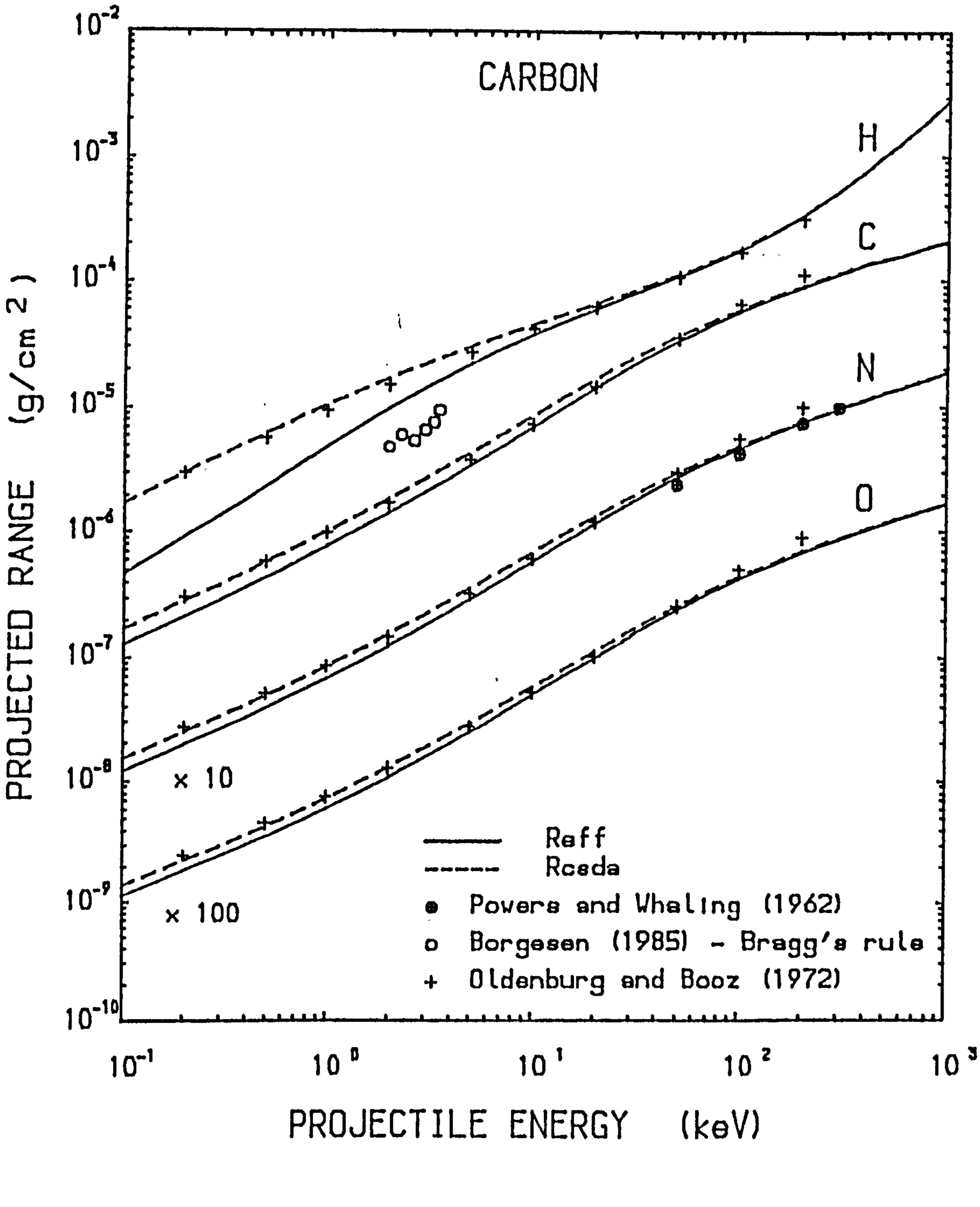

Fig. 3.10 The calculated effective and CSDA values of projected ranges for heavy ions (proton, C, N and O) in carbon.

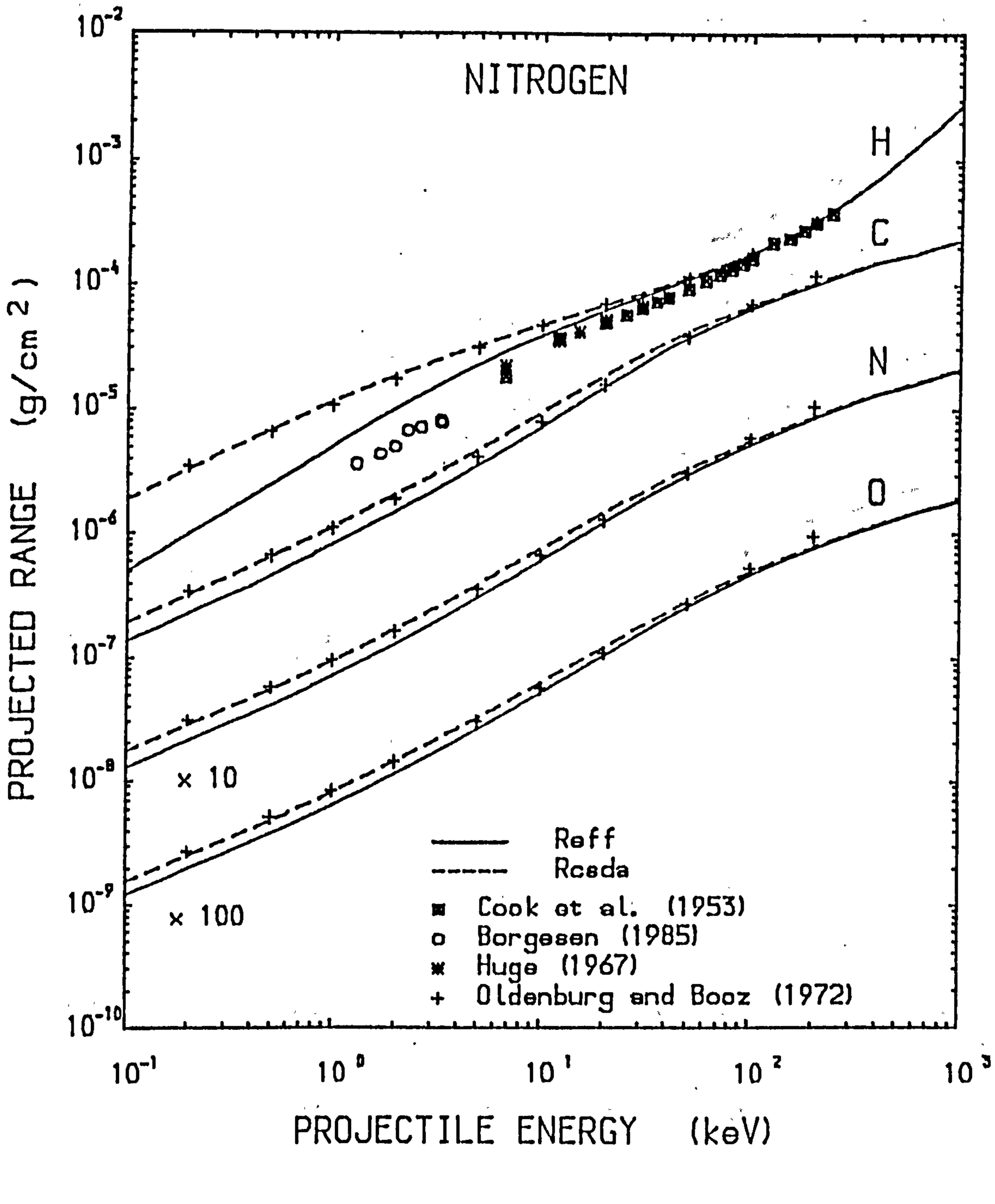

Fig. 3.11 The calculated effective and CSDA values of projected ranges for heavy ions (proton, C, N and O) in nitrogen.

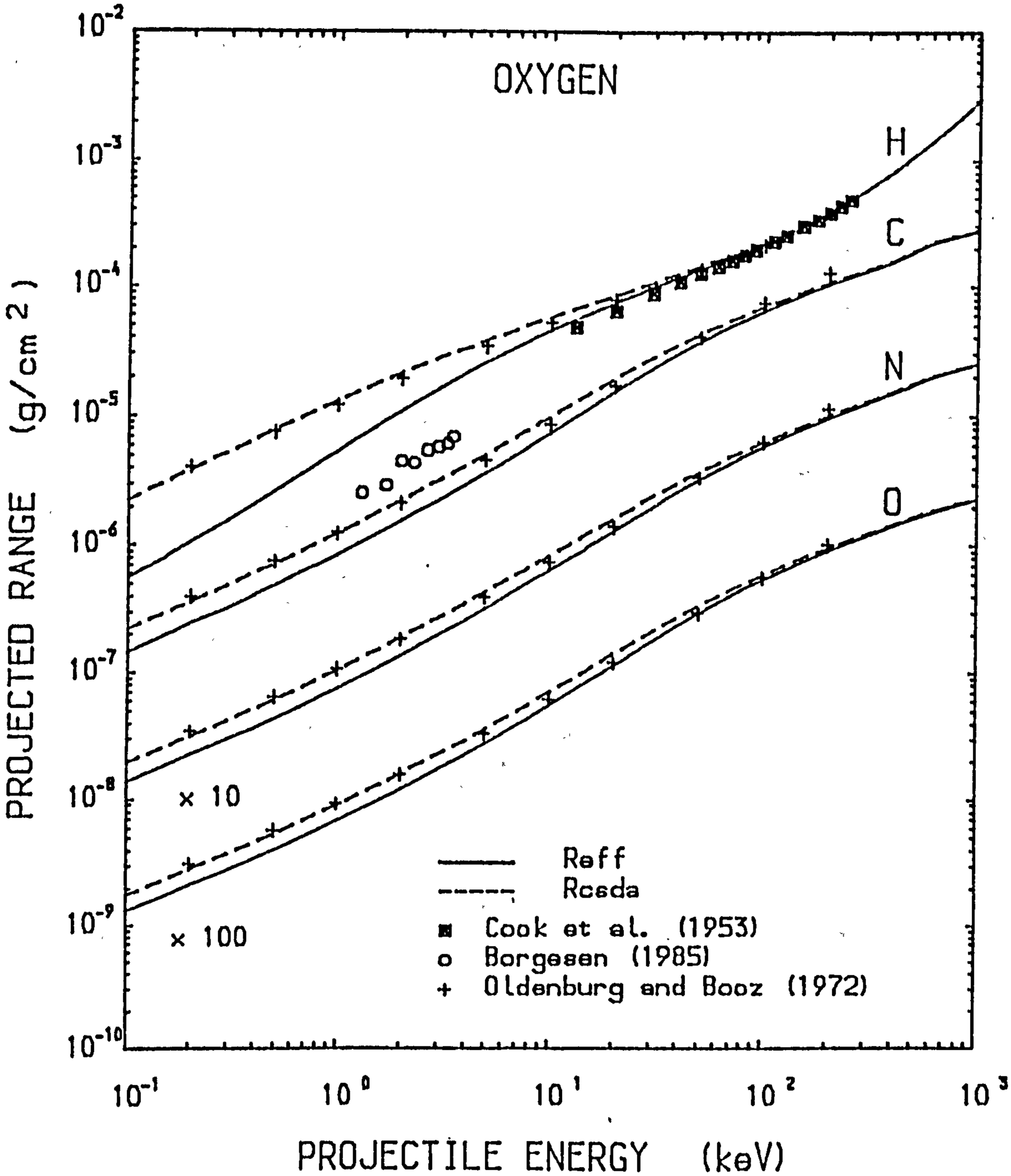

Fig. 3.12 The calculated effective and CSDA values of projected ranges for heavy ions (proton, C, N and O) in oxygen.

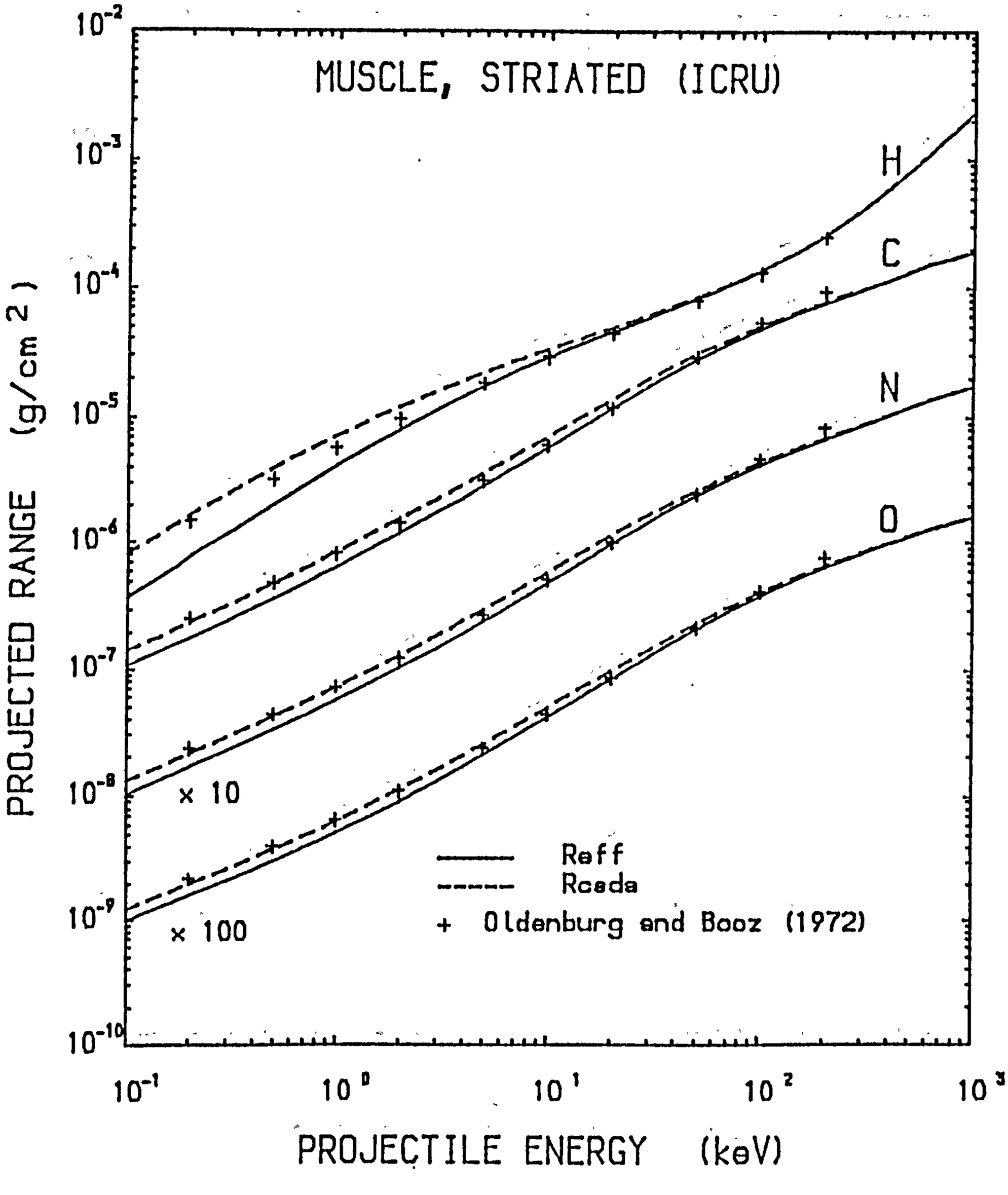

Fig. 3.13 The calculated effective and CSDA values of projected ranges for heavy ions (proton, C, N and O) in ICRU tissue.

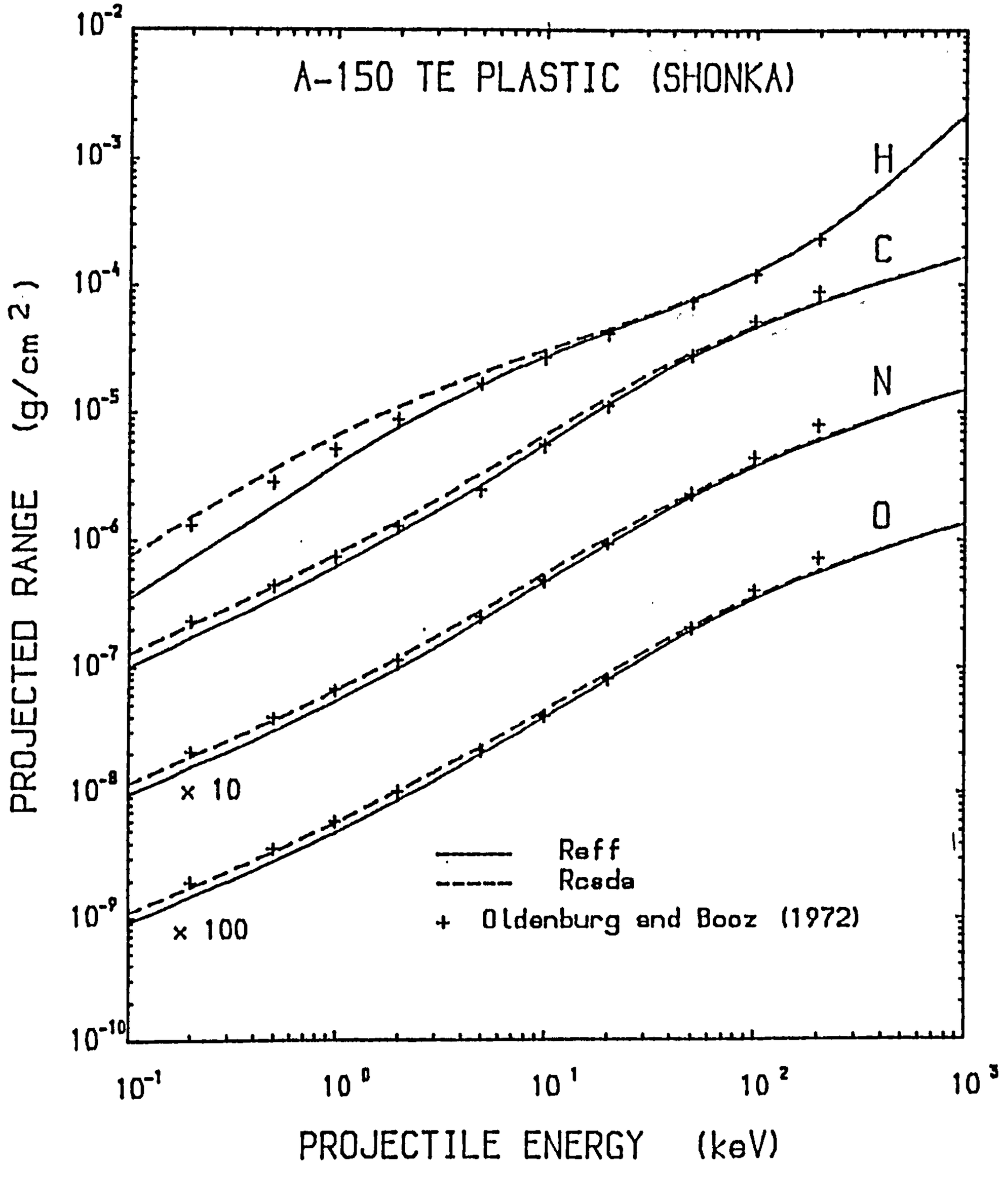

Fig. 3.14 The calculated effective and CSDA values of projected ranges for heavy ions (proton, C, N and O) in A-150 plastic.

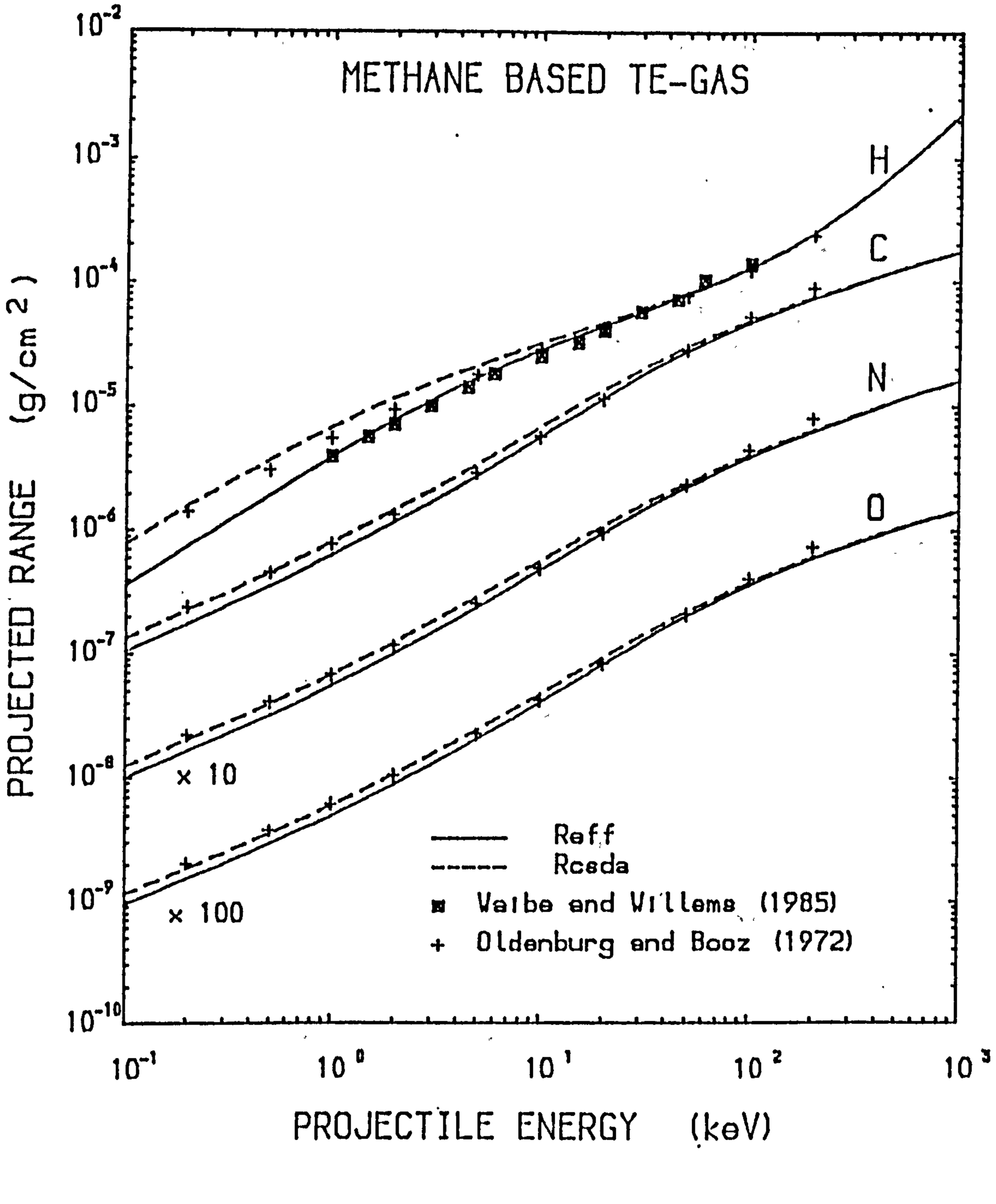

Fig. 3.15 The calculated effective and CSDA values of projected ranges for heavy ions (proton, C, N and O) in methane based TE gas.

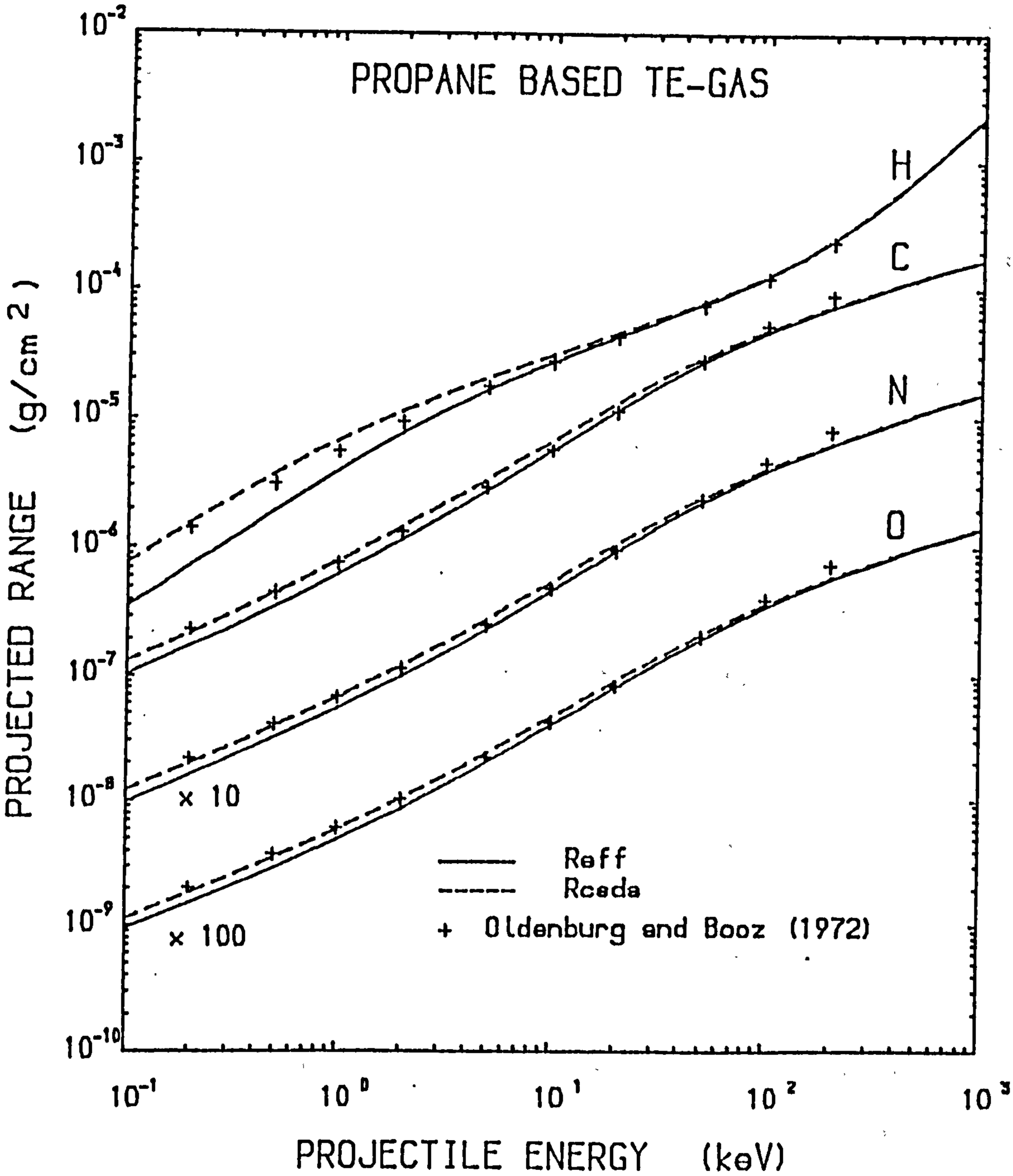

Fig. 3.16 The calculated effective and CSDA values of projected ranges for heavy ions (proton, C, N and O) in propane based TE gas.

3.3 Kerma and Kerma Factor for Intermediate Energy Neutrons

3.3.1 Kerma and Absorbed Dose Relationship in Tissue

The non-stochastic quantities of kerma, K, and absorbed dose, D, are useful for describing the interactions of ionizing radiation in matter. Kerma is defined by ICRU (1977) by

$$K = \frac{d\varepsilon_{tr}}{dm} \tag{3.20}$$

where ε_{tr} is the sum of the initial kinetic energies of all the charged particles liberated by indirectly ionizing particles in the finite volume V of mass m at the point inside the matter. Kerma is expressed in gray (Gy).

At a certain depth in tissue it is possible for charged particle equilibrium (CPE) to exist by which each charged particle of a given type and energy leaving the volume will be replaced by an identical particle of the same energy entering the volume. The conditions for CPE to exist are

1) the atomic composition and the density of the medium are homogeneous

2) the neutron field is uniform throughout the medium

3) there is no electric and magnetic fields present in the volume

When these conditions are met, the number of the secondary charged particles produced per unit volume in each energy interval and element of solid angle will be uniform everywhere in the volume (ICRU, 1977). Then, the kerma is equal to absorbed dose

$$K = D \tag{3.21}$$

For a parallel beam of neutrons incident at normal on the tissue, **Fig. 3.17**, the kerma decreases slowly with increasing depth due to absorption and scattering of neutrons. On the other hand the absorbed dose rises with increasing depth near the surface due to build up ionizing particle interactions and then decreases slowly due to attenuation of neutrons. There

is a small difference between kerma and absorbed dose values at a certain depth in tissue which is attributed to the anistropic transport of radiation energy by charged particles in the forward direction and which deposit their kinetic energy as absorbed dose.

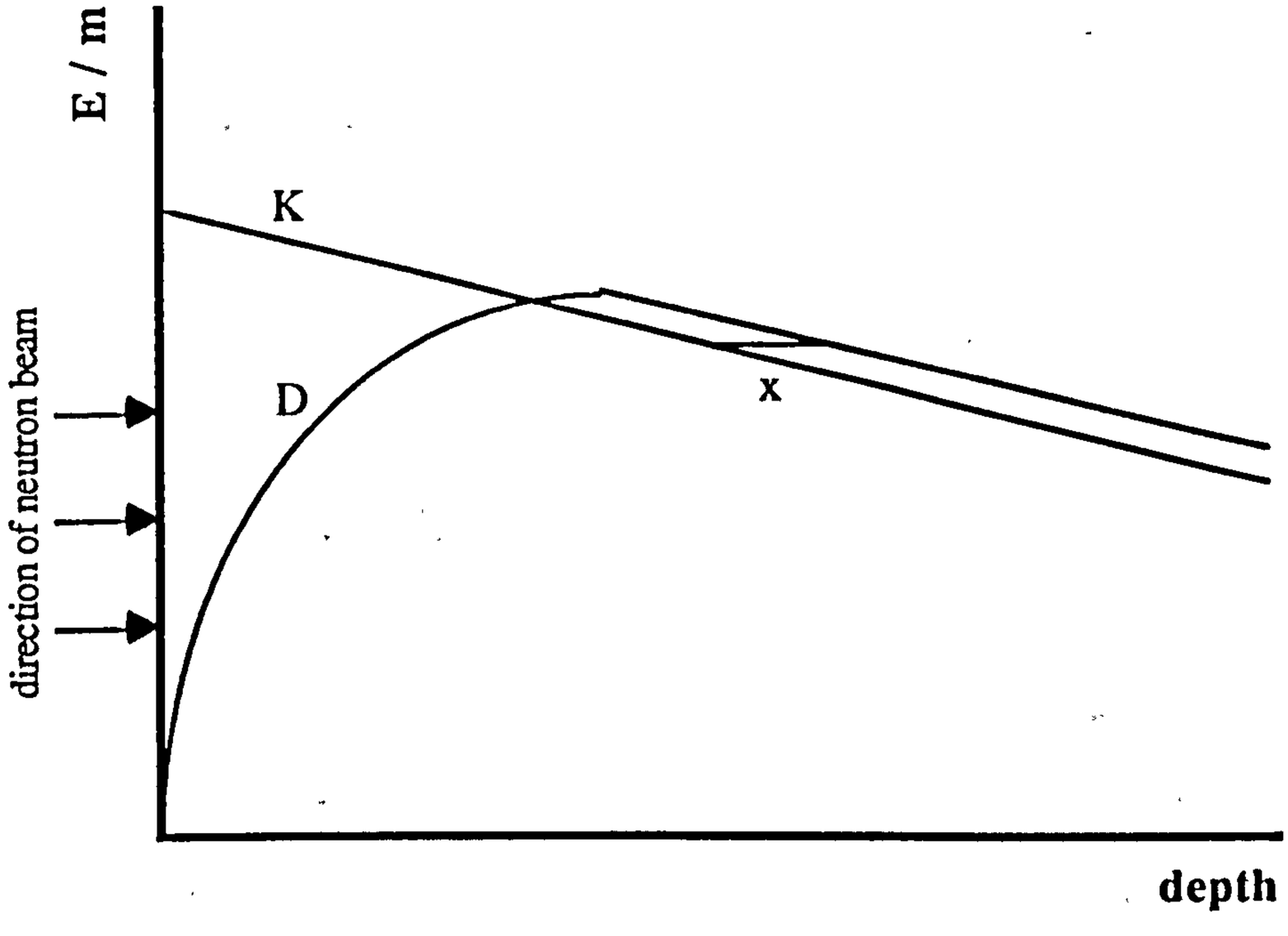

Fig. 3.17 Kerma in the ambient medium and absorbed dose for parallel beam of neutron normally incident on layer of tissue.

3.3.2 Calculation of Kerma and Kerma Factor

For monoenergetic neutrons of fluence, Φ, interacting with a medium, the neutron kerma can be calculated according to equation (3.20). The sum of kinetic energies of charged particles liberated by neutrons is given by equation (3.22).

$$d\varepsilon_{tr} = \Phi(E_n)\, dm \left(\frac{\mu_{tr}}{\rho}\right) \bar{E}_{tr} \qquad (3.22)$$

where $\bar{E}_{tr}$ is the average kinetic energy of the charged particle released per interaction for the element and $\frac{\mu_{tr}}{\rho}$ is the mass energy transfer coefficient given by

$$\frac{\mu_{tr}}{\rho} = \frac{N_t}{m_t}\,\sigma(E_n) \qquad (2.23)$$

where $\sigma(E_n)$ is the interaction cross section of neutrons of energy E_n with the target atom, m_t is mass of the target atom and N_t is the number of target atoms which is equal to $\frac{N_0\, m_t}{W_t}$. N_0 is Avogadro's constant (6.022×10^{23} atoms mole^{-1}) and W_t is the atomic weight of the target. Equation (3.20) can be written as

$$K = 1.602 \times 10^{-17} \frac{N_0}{W_t}\,\sigma(E_n)\,\Phi(E_n)\,\bar{E}_{tr} \qquad (3.24)$$

where E_n is given in keV, $\Phi(E_n)$ in m^{-2}, $\sigma(E_n)$ cm^2 per atom.

For intermediate energy neutrons interacting with tissue, the interactions by elastic scattering and neutron capture are very important. In elastic scattering the neutron transfers its energy to a nucleus which is then ejected as a secondary charged particle with the kinetic energy given by

$$E_{tr}(\theta_{cm}, E_n) = \frac{4\, m_t\, m_n}{(m_t+m_n)^2}\, E_n\,(1-\theta_{cm}) \qquad (3.25)$$

where θ_{cm} is the angle from which the neutron is deflected in the centre-of-mass system, m_n is the mass of the neutron. The average recoil energy, $\bar{E}_{tr}$, can be calculated according to Caswell and Coyne (1980) by

$$\bar{E}_{tr} = \frac{2\, m_t\, m_n}{(m_t+m_n)^2}\, E_n\,(1-f_1) \qquad (3.26)$$

where f_1 is the coefficient of the term of the Legendre polynomial expansion for angular momentum. f_1=0 for intermediate energy neutrons. In the capture reaction of neutron by nitrogen, i.e. $^{14}N(n,p)^{14}C$, the recoil proton and carbon ion are ejected as secondary charged particles in tissue. The average kinetic energy in this reaction is given by

$$\bar{E}_{tr} = E_n + Q \qquad (3.27)$$

where Q=0.657 MeV is the energy liberated from this exothermic reaction.

Neutron kerma in tissue and TE materials can be calculated by taking the sum of kerma for individual element weighted by the mass fraction of the element in tissue according to equation (3.28)

$$K_{jk} = 1.602 \times 10^{-17} \Sigma \frac{N_0}{W_j} \omega_j \Phi(E_n) \Sigma \sigma_{jk}(E_n) [\bar{E}_{tr}(E_n)]_{jk} \qquad (3.28)$$

where j refers to a constituent element in tissue, k refers to the nuclear reaction type, $\sigma_{jk}(E_n)$ is the cross-section of nuclear reaction type k with element type j, ω_j is the fraction by weight of element j in tissue, and $[\bar{E}_{tr}(E_n)]_{jk}$ is the average kinetic energy of secondary charged particle type j from interaction type k. The kerma factor is defined as a quotient of kerma, K, by fluence, Φ, i.e.

$$KF_{jk} = 1.602 \times 10^{-17} \Sigma \frac{N_0}{W_j} \omega_j \Sigma \sigma_{jk}(E_n) [\bar{E}_{tr}(E_n)]_{jk} \qquad (3.29)$$

The fraction of neutron kerma in tissue and the kerma factor for four elements of greatest abundance in tissue (H, C, N, and O), ICRU tissue and TE materials were calculated for neutrons of energy from 0.1 keV to 200 keV. The neutron cross sections were taken from JEF library (the Joint Evaluated File). The elemental compositions of tissue and TE materials were taken from ICRU (1977) with the minor elements treated as oxygen.

3.3.3 Results and Discussion

Fig. 3.18 shows the fraction of neutron kerma in tissue for hydrogen, carbon, nitrogen and oxygen. The results are compared with the kerma extracted from kerma factor data of ICRU (1977) assuming unit neutron fluence. The agreement is very good. The

contribution from recoil protons via elastic scattering is the largest which indicates that the energy deposition in various biological materials is determined mainly by the hydrogen content. A 1% deviation in the total hydrogen content in tissue materials will change the kerma by approximately 10 % (ICRU, 1977). Neutron kerma in tissue varies with energy. Below 1 keV the nitrogen content in tissue cannot be ignored due to the increasing importance of the neutron capture reaction, which contributes to more than 25% of kerma for 0.1 keV neutrons and less than 2% for energies greater than 1 keV.

The kerma factor for hydrogen is the largest compared with those of carbon, nitrogen and oxygen as shown in **Fig. 3.19.** The results are in good agreement with the published data of Ritts *et al.* (1969) and ICRU (1977). This enables us to calculate with good accuracy the kerma factor for tissue and TE materials using equation (3.29) as shown in **Fig. 3.20.** The results show that for these materials the kerma factor can be considered equal with the deviation of less than 2% in the intermediate energy region. The fact is that kerma for hydrogen contributes between 70% to 97% at energies from 0.1 keV to 200 keV and for nitrogen it is between 2% at 1 keV and 30% at 0.1 keV of the total kerma factor. Moreover, tissue and TE materials have nearly the same amount of hydrogen and nitrogen contents. Thus, any difference between the carbon and oxygen contents in these materials will not produce a significant change in the total kerma factor. The calculated values for tissue in this work are in an agreement with the published data from ICRU (1977).

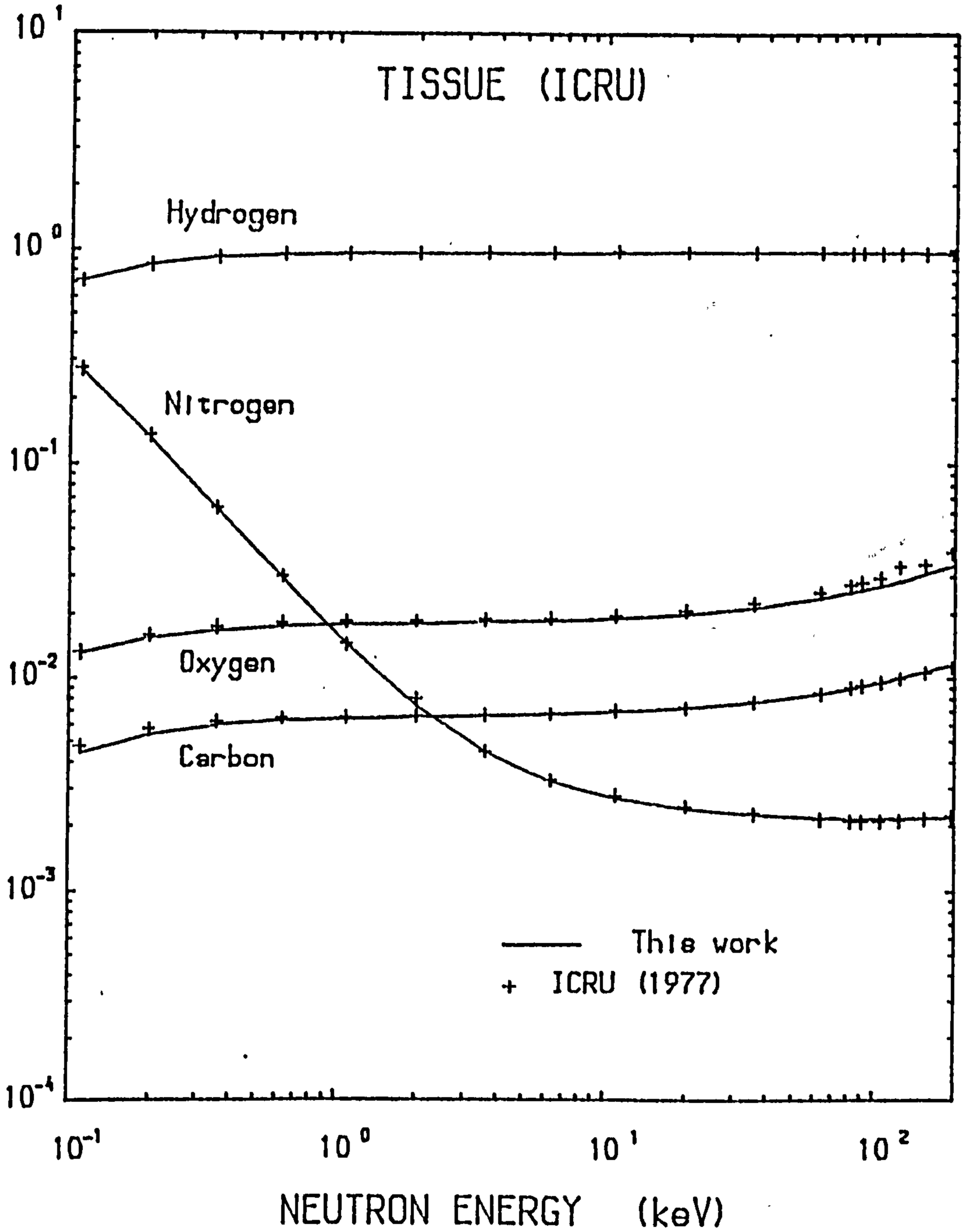

Fig. 3.18 The fraction of neutron kerma of intermediate energy neutrons ≤ 200 keV in tissue for hydrogen, carbon, nitrogen and oxygen. The ICRU data were extracted from kerma factor data assuming unit neutron fluence.

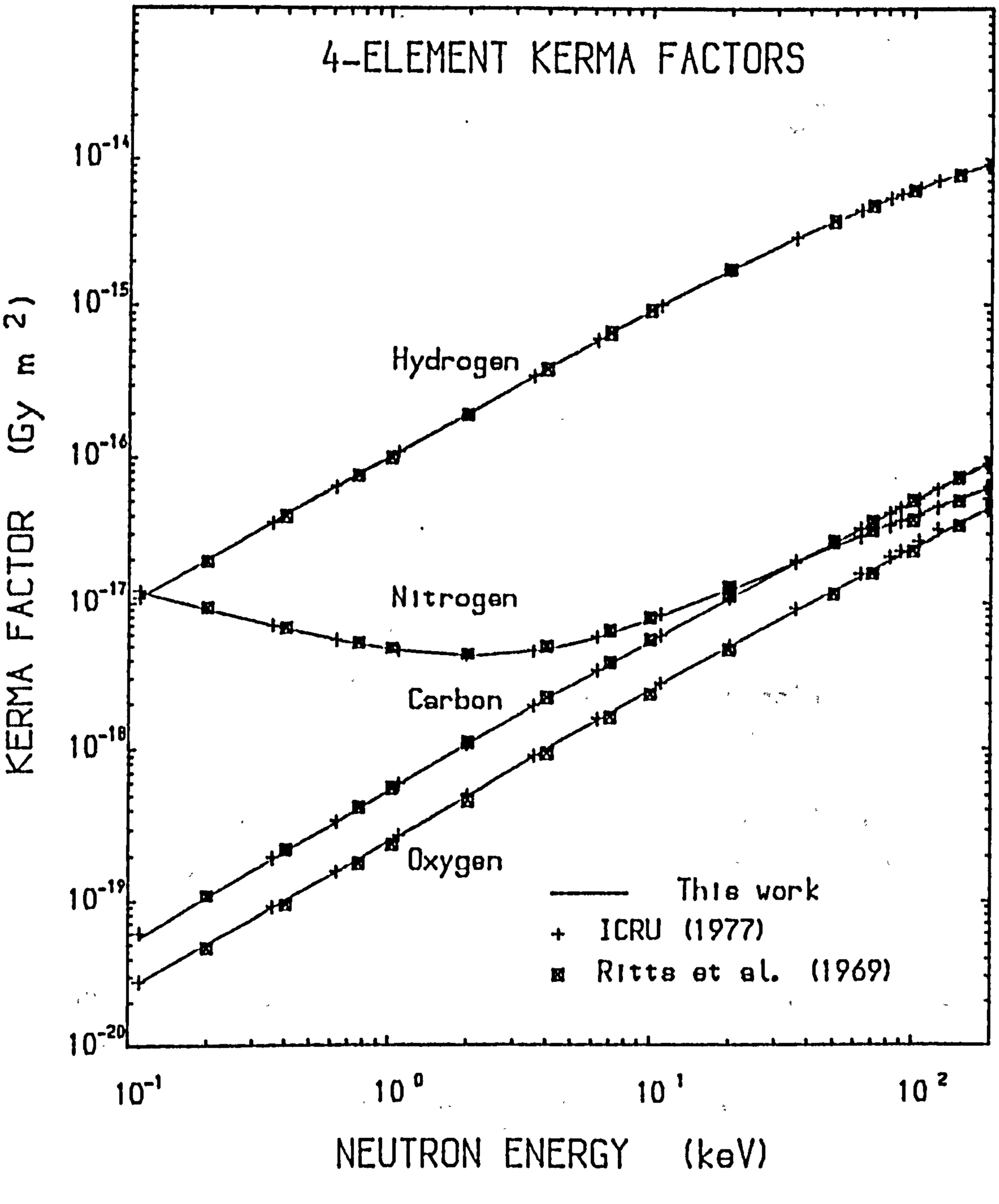

Fig. 3.19 The kerma factor of intermediate energy neutrons ≤ 200 keV in hydrogen, carbon, nitrogen and oxygen. The data of Ritts *et al.* (1969) are for a standard man.

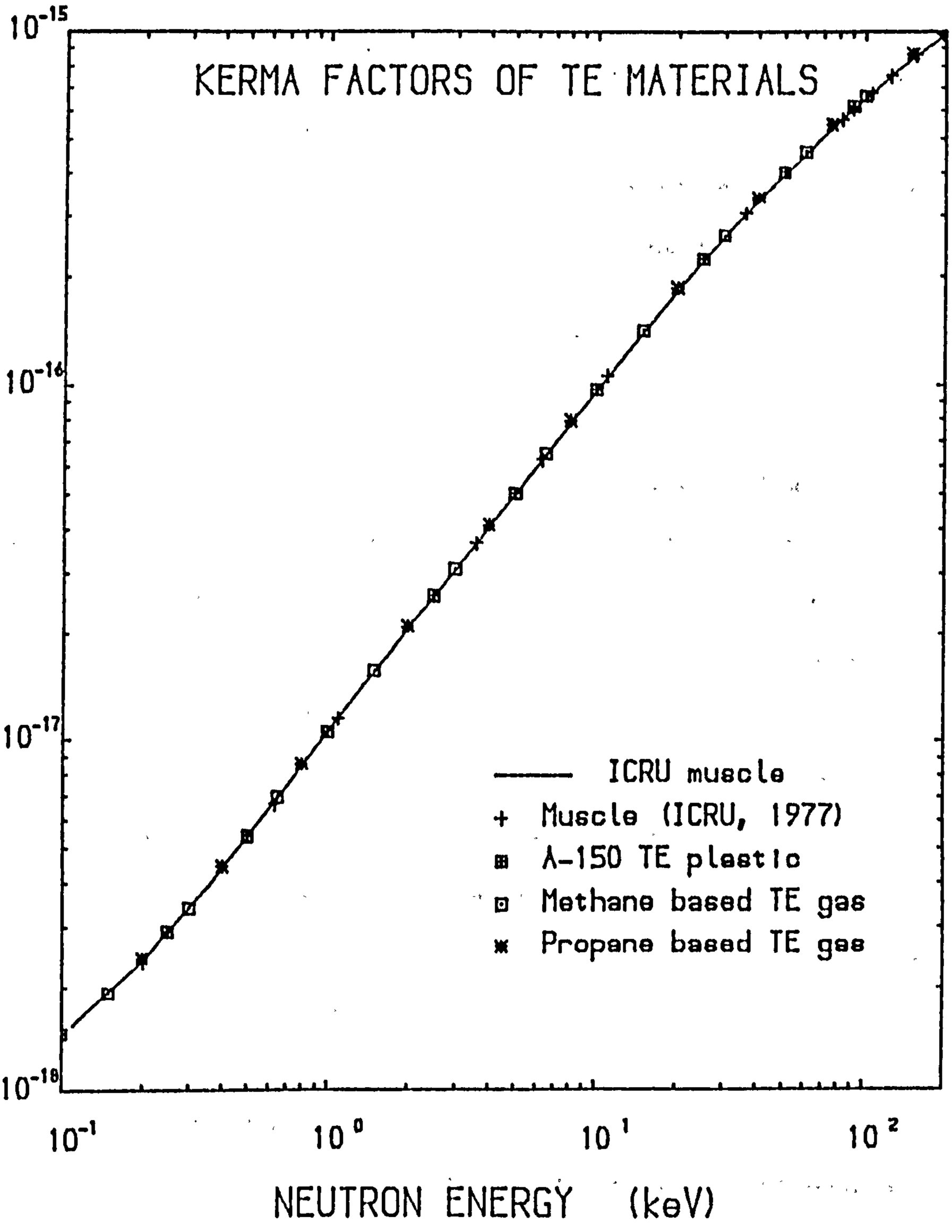

Fig. 3.20 The kerma factor of intermediate energy neutrons ≤ 200 keV in tissue and tissue-equivalent materials. The value is about equal for TE materials with less than 2% deviation between A-150 TE plastic and tissue.

3.4 Fundamental Analytical Calculations of Microdosimetric Spectra

3.4.1 Theoretical Models

The calculation of microdosimetric spectra and their averages have been carried out by two different theoretical models, namely the Monte-Carlo method and analytical method. The objective of the theoretical calculations is not only to test the accuracy of the measurement but also to find the degree of agreement between experiment and theory.

i) Monte-Carlo Method

Application of the Monte-Carlo method to calculation of energy deposition spectra has been developed by Booz and Collaborators (Oldenburg and Booz, 1971 and Booz and Coppola, 1974). In this method, the life history of a neutron and all its secondaries are followed in their ways through the cavity until all of the neutron energy is dissipated or further interaction can be neglected. The program decides all random events of the interaction by the application of random numbers which determine the the point of origin, the type, direction and energy of the primary particle, the point of interaction, the type of the atom and the type of interaction. The statistical weighting factor and interaction cross sections are given in the computation to evaluate energy deposition in the volume of interest. The advantage of this method are that some parameters such as energy loss straggling and delta ray production can be included much easier than that of the analytical method.

ii) Analytical Method

The first analytical model was developed by Caswell (1966) who had performed the calculation of energy deposition by neutrons in spherical cavities. Some improvements have been made in later publications by using new interaction cross section data and incorporating energy loss straggling and delta ray production (Caswell and Coyne, 1972, 1976 and 1978). Independently, other analytical calculations have been developed by Dvorak (1969) and by Edward and Dennis (1975). Al-Affan *et al.* (1984) had performed the calculation for intermediate energy neutrons (1keV - 100 keV) using principles similar to those of Caswell's. However, the CSDA value of stopping power and projected ranges used in Caswell's method has been replaced by the effective stopping power and projected ranges

from Watt and Sutcliffe (1972). This allows for enhanced energy deposition event at low energies due to the increased importance of elastic scattering of neutron interaction in tissue.

The advantages of the analytical calculation are that results can be interpreted in terms of basic physics, are simple to use and involve less CPU time than the Monte-Carlo method which requires large generation of random numbers and thus of the CPU time.

3.4.2 Basic Assumptions and Classes of Particle Track

Most calculations involve some simplifying assumptions which may not represent the actual response of TEPC in the practical situation. However, this approach enables a wide range of parameters to be incorporated in the calculation.

Caswell has simplified his model by using a spherical cavity, taking advantage of the response which is independent of direction and angular distribution of the incident neutrons so that the secondary charged particles that are generated in the interaction of neutrons with tissue will be isotropic. There are other assumptions which must be made in the analytical calculation, namely that

1) secondary charged particle equilibrium (CPE) has been established throughout the volume, i.e. secondary charged particles are produced uniformly throughout the volume, not necessarily isotropically but with the same directional and energy distribution everywhere in the volume.

2) the cavity and wall are made of the same material so that under the condition of a constant atomic composition, Fano's theorem (Fano, 1954) can be applied.

3) the heavy charged particles released by neutron interactions are assumed to travel in straight path.

4) the incident neutrons are isotropic in direction and therefore the secondary charged particle recoils must also be isotropic.

The present calculation also adopts four classes of particle tracks of energy deposition events in the cavity which are listed by Caswell (1966).

1) "Insiders" which are recoil particles originating in the gas cavity and which lose their entire energy in the cavity.
2) "Starters" which are recoil particles originating in the gas cavity and which leave the cavity before losing all their energy.
3) "Stoppers" which are recoil particles originating outside the gas cavity and which enter the cavity and stop within the cavity.
4) "Crossers" which are recoil particles originating outside the cavity and which cross the cavity depositing only a part of their energy before being stopped outside the cavity.

The various types of particle track are shown in **Fig. 3.21.** Note that if the wall is thin enough, the secondary charged particles could penetrate the dividing wall from the outside to enter the cavity, or they may start in the cavity and stop in the outside wall.

3.4.3 The Initial and Equilibrium Spectra of Secondary Charged Particles

The basic nuclear data for analytical calculation of microdosimetric spectra and their averages are; (1) the initial spectra of secondary charged particles produced in the neutron interaction with the matter and (2) the equilibrium spectra of secondary charged particles when they slow down at any point in the irradiated volume.

The initial spectra of secondary charged particles can be calculated according to equation (3.30)

$$N_p(E)\,dE = \Sigma\, N_i \sigma_i(E_n)\, \Phi(E_n) \frac{dE_n}{E_n} \qquad (3.30)$$

where E is the energy of the secondary charged particles and others have been defined in section (3.3). $\Phi(E_n)$ is proportional to $\frac{1}{E_n}$ for intermediate energy neutrons (Caswell and Coyne, 1972).

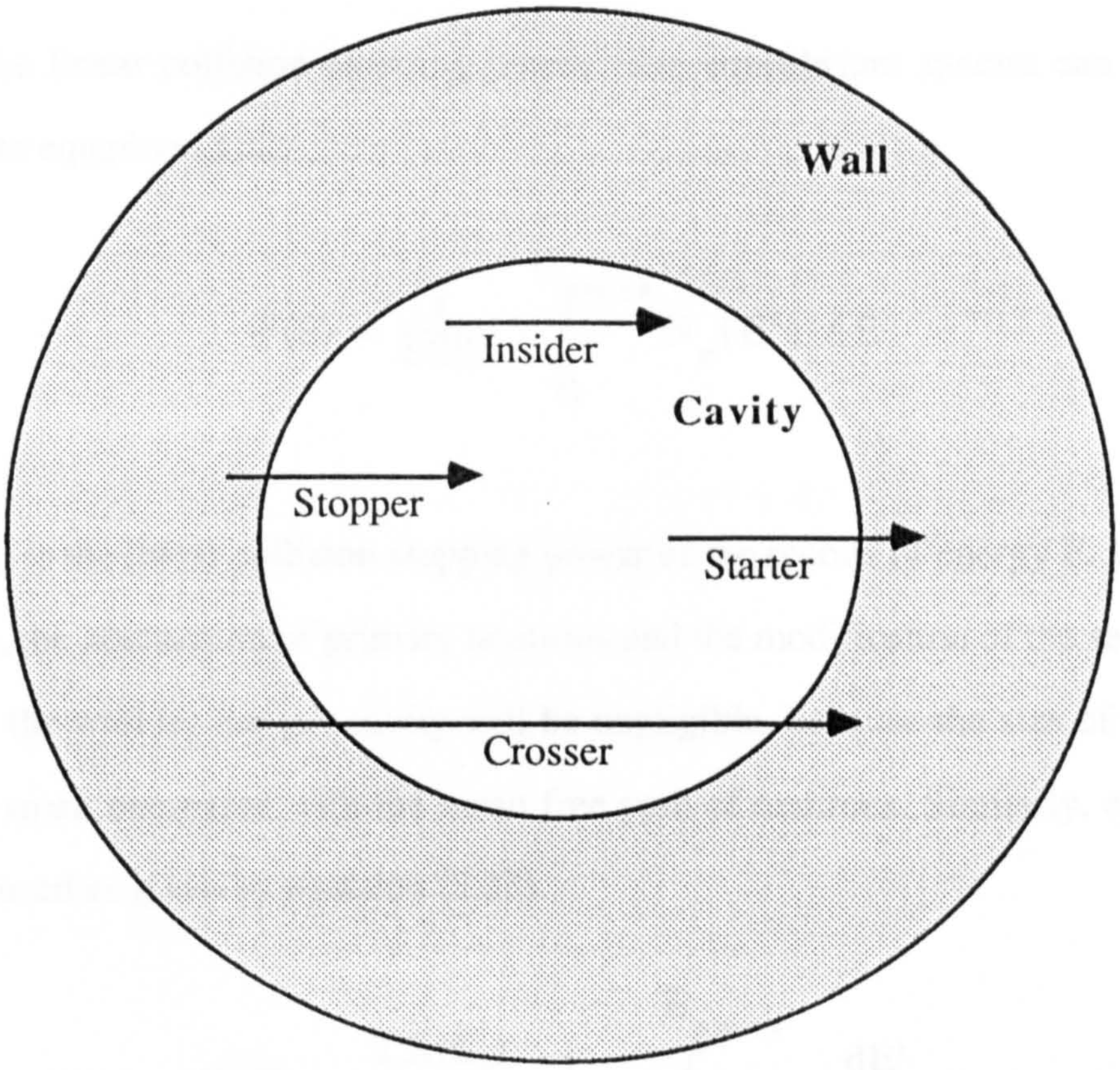

Fig. 3.21 Four classes of track of secondary charged particles in the cavity; insiders, starters, stoppers and crossers (after Caswell, 1966).

From equations (3.24) to (3.26) and (3.30) the initial spectra of secondary recoils due to intermediate energy neutrons can be reduced to

$$N_p(E)\,dE = \frac{2\,K(E_n)}{E_{pmax}}\,\frac{dE}{E_{pmax}} \qquad (3.31)$$

where $K(E_n)$ is the kerma due to charged particles in tissue, and E_{pmax} is the maximum recoil energy of secondary charged particles.

The continuous slowing-down approximation (CSDA) can be used to calculate the equilibrium spectra of the secondary recoils in the cavity. This assumption is valid for neutron interactions because the range of secondary charged particles is much smaller than that of the primary neutrons. Thus, the rate of energy loss by the recoils along the track is

taken as the linear collision stopping power. The equilibrium spectra can be calculated according to equation (3.32)

$$\Psi(E) = \frac{1}{S(E)} \int_{E}^{E_{pmax}} N_p(E')\, dE' \qquad (3.32)$$

where S(E) is the linear collision stopping power of the recoils of energy E. Under the CPE conditions, the attenuation of primary neutrons and the modification of the secondary recoil fluence in the wall by the gas cavity will be negligible, because the size of the volume of interest is small compared with the mean free path of neutrons. Similarly, equation (3.32) can be reduced as given by equation (3.33)

$$\Psi(E) = \frac{2\,K(E_n)}{E_{pmax}} \frac{1}{S(E)} \int_{E}^{E_{pmax}} \frac{dE'}{E_{pmax}} \qquad (3.33)$$

3.4.4 Chord Length Distributions in Cavities

Chord length distributions of the random intersection of convex bodies by straight lines are required for the evaluation of energy deposition spectra in cavity devices such as proportional counters. Caswell (1966) and Rossi (1968) have used the chord length distributions to determine microdosimetric spectra in spherical volumes. In the calculation it is assumed that the recoils produced by neutron interactions in tissue travel in straight lines and that CPE has been established throughout the cavity which meet the conditions for chord length distribution. Two kinds of chord length distribution relevant to the present study have been discussed elsewhere (e.g. Kellerer, 1971 and ICRU, 1983). They are

1) Mean free path randomness (μ-randomness); it is the chord length distribution that result from a convex body being exposed to a uniform isotropic field of straight finite tracks. The chord is defined by a point in Euclidian space and a direction. The point and the direction are from independent uniform distribution.

2) Internal source randomness (i-randomness); it is the segment length distribution that results from a convex body being exposed to a uniform internal source of straight

particle tracks. The segment is defined by a point in the interior of the convex body and a direction. The point and the direction are from independent uniform distributions.

The probability densities for μ-randomness, $f_\mu(l)$, and for i-randomness, $f_i(l)$, are related by

$$f_i(l) = \frac{1}{\bar{l}_\mu} \int_0^\infty f_\mu(l)\, dl \qquad (3.34)$$

where l is the length of chord or segment and $\bar{l}_\mu$ is the mean chord length for μ-randomness which can be determined by Cauchy theorem, i.e. $\bar{l}_\mu = \frac{4V}{S}$. V is the volume of the cavity and S is its surface area.

For a chord length l passing through a sphere of diameter d, the probability densities for the μ-randomness and the i-randomness are well known and are given by $\frac{2l}{d^2}$ and $\frac{3}{2d}(1-\frac{l^2}{d^2})$ respectively for $l \leq d$.The mean values are given as $\bar{l}_\mu = \frac{2d}{3}$ and $\bar{l}_\mu = \frac{3d}{8}$.

Chord length distributions for circular cylinders, however, are more complicated than the spherical volumes and several methods have been used to determined the distribution. For cylinders of infinite length the distribution of μ-randomness could be calculated analytically according to Case (1953). Schwed and Ray (1960), Kellerer (1971) and Mader (1980) have attempted analytical solutions for cylinders of finite length. Birkhoff *et al.* (1970) have given a useful survey of various methods used and have pointed out that the results between various methods are not in agreements. They also used Monte Carlo method to compare their results with other methods. Their results do not agree with the Monte Carlo calculations of Wilson and Emery (1968) and Belonogii *et al.* (1971). A similar attempt was made to generate the distribution using Monte Carlo technique as shown in Appendix A. All the calculations show similar distribution patterns in which there is a sharp increase in the probability when the chord length reaches the diameter and height of the cylinder. However, the methods of calculation need further refirement.

3.5 Calculation of Event Spectra in Co-Axial Double Cylindrical TEPC

3.5.1 Classification of Events

Consider a co-axial double cylindrical TEPC consisting of an inner counter and an outer annular counter at which both are separated by a self-supporting dividing wall of thickness equivalent of the range of 100 keV protons in tissue. The presence of TE dividing wall is to ensure the secondary charged particle equilibrium for intermediate energy neutrons and to prevent recoil particles of energy less than 100 keV originated from fast neutrons interactions in the outer counter from reaching the inner counter. **Fig. 3.22** shows the cross-section of such a counter which illustrates various types of event detected in the counter.

Assuming the conditions discussed in section (3.4.2) are valid and also that there is no wall effect due to the differences in density between the wall and cavity, the energy deposition events of intermediate energy neutrons, in principle, can be detected in the inner counter. The number of events detected in the inner counter consists of the following classes of event.

(1) Energy deposition events due to intermediate energy neutrons. All types of event, i.e. insiders, starters, stoppers and crossers are present as shown in **Fig. 3.21.**

(2) Energy deposition events due to fast neutrons interact in both counters. These recoils are those of starters, stoppers and crossers which can be removed from the inner counter by anti-coincidence arrangement with the outer counter as shown in **Fig. 3.22.** However, the insiders due to fast neutrons must be removed by calculation. Also, there will be some events due to fast neutrons which deposit energy ≤ 100 keV in the inner counter and cannot be removed by anti-coincidence arrangements. These events of starters, stoppers and crossers must be removed by calculation.

(3) There will be some events due to fast neutrons associated with the dividing wall which deposit energy ≤ 100 keV. These recoils are those of starters, stoppers and crossers. Except for crossers which originated in the dividing wall and detected in the outer counter in which they can be removed by anti-coincidence arrangement, others must be removed by calculation.

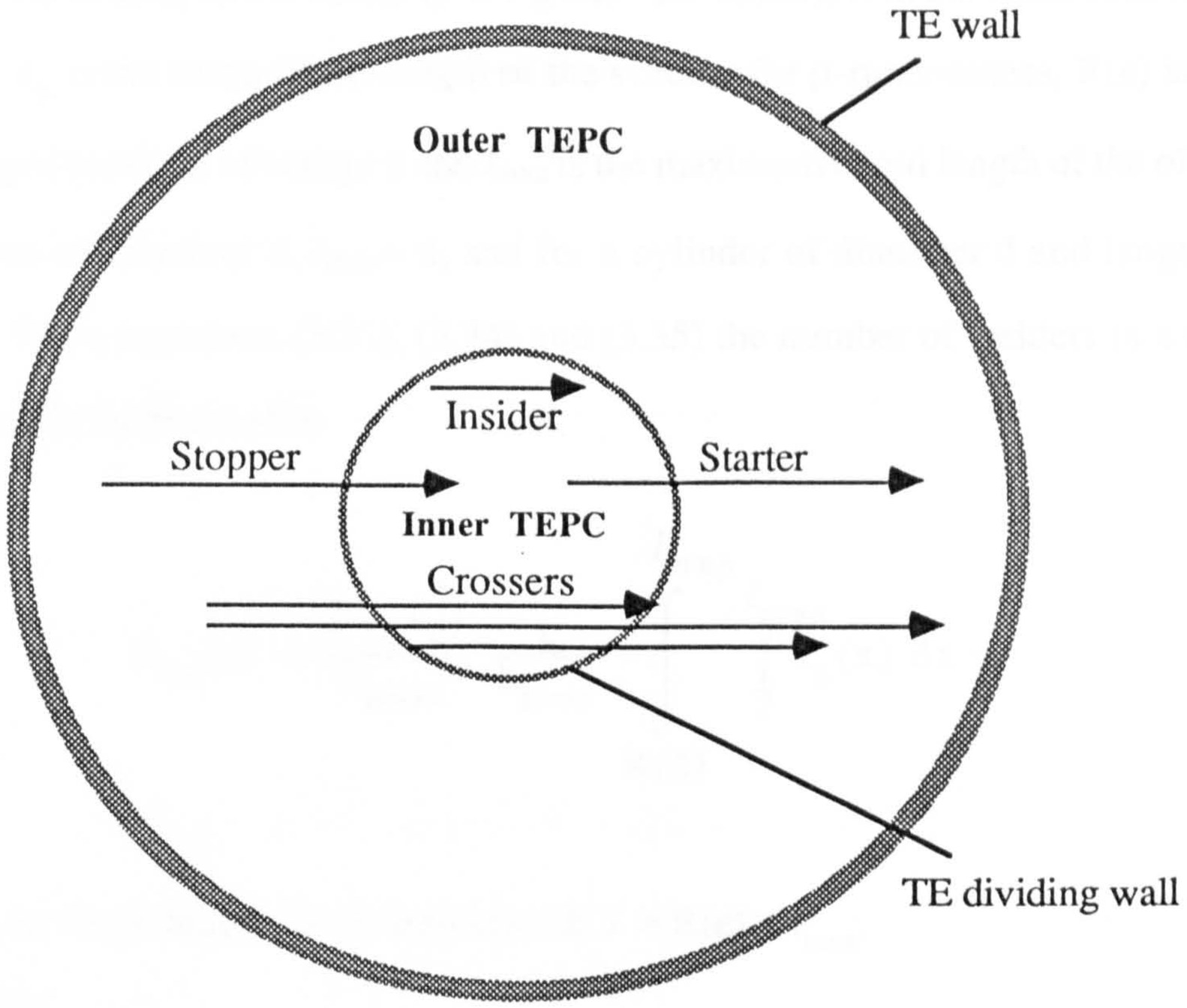

Fig. 3.22 Cross section of a co-axial double cylindrical tissue-equivalent proportional showing three particle tracks, the starters, stoppers and crossers due to fast neutrons which can be removed from the inner counter by anti-coincidence arrangement with the outer counter.

3.5.2 Microdosimetric Spectra of Intermediate Energy Neutrons Detected in the Inner Counter

The number of insiders and starters can be determined by the initial spectrum of the secondary charged particles produced in the cavity, $N_p(\varepsilon)$, and the chord length distribution of i-randomness, $f_i(l)$, as follows

1) Insiders

The number of insiders with energy imparted between ε and $\varepsilon+d\varepsilon$ is given by

$$N_{ins}(\varepsilon)\, d\varepsilon = \rho A \left\{ N_p(\varepsilon)\ \bar{l}_{\mu} \int_{R(\varepsilon)}^{l_{max}} f_i(l)\, dl \right\} d\varepsilon \qquad (3.35)$$

where ρ is the density of the cavity (ρ = 1 g cm^{-3} for tissue), A is the cross-sectional area of the cavity, $\bar{l}_\mu$ is the mean chord length of the volume for μ-randomness, R(ε) is the range of the charged particles of energy ε and l_{max} is the maximum chord length of the of the cavity (for a sphere of diameter d, l_{max}= d, and for a cylinder of diameter d and length h, l_{max}= $\sqrt{(d^2+h^2)}$). From equations (3.31), (3.34) and (3.35) the number of insiders in a unit cross-section area can be deduced to

$$N_{ins}(\varepsilon) = \frac{2\,K(E_n)}{E_{pmax}} \frac{1}{E_{pmax}} \int_{R(\varepsilon)}^{l_{max}} \int_{l}^{l_{max}} f_\mu(x)\,dx\,dl \qquad (3.36)$$

where l is the chord length of the insiders, i.e. $l = R(\varepsilon) \le l_{max}$.

2) Starters

The number of starters with energy imparted between ε and dε is given by

$$N_{str}(\varepsilon)\,d\varepsilon = \rho A \left\{ \bar{l}_\mu \int_{\varepsilon}^{E_{pmax}} N_p(\varepsilon)\, f_i(l)\, \frac{dl}{dE_p}\, dE_p \right\} d\varepsilon \qquad (3.37)$$

where E_p is the energy of the secondary recoil particles. Using the procedure similar to that of the insiders, equation (3.37) can be written as equation (3.38) for the number of starters in a unit cross-sectional area

$$N_{str}(\varepsilon) = \frac{2\,K(E_n)}{E_{pmax}} \frac{1}{E_{pmax}} \int_{\varepsilon}^{E_{pmax}} \int_{l}^{l_{max}} f_\mu(x)\,dx\, \frac{dE_p}{S(E_p-\varepsilon)} \qquad (3.38)$$

where l is the chord length of the starters, i.e. $l = R(E_p) - R(E_p-\varepsilon)$ and $\frac{dl}{dE_p} = \frac{1}{S(E_p-\varepsilon)}$ is the inverse of the stopping power of secondary charged particles. The integrand become zero when $R(E_p) - R(E_p-\varepsilon) > l_{max}$.

The number of stoppers and crossers can be determined by the equilibrium spectrum of secondary charged particles at the surface of the cavity, $\Psi(\varepsilon)$, and the chord length distribution of μ-randomness, $f_\mu(l)$, as follows.

3) Stoppers

The number of stoppers giving energy imparted, ε, between E and E+dE is given by

$$N_{stp}(\varepsilon)\, d\varepsilon = A \left\{ \Psi(\varepsilon) \int_{R(\varepsilon)}^{l_{max}} f_\mu(l)\, dl \right\} d\varepsilon \qquad (3.39)$$

where $R(\varepsilon)$ is the range of the stoppers of energy ε, i.e. $R(E)=R(\varepsilon)$ by definition. From equations (3.33), (3.34) and (3.39), the number of stoppers in a unit cross-section area can be determined by equation (3.40)

$$N_{stp}(\varepsilon) = \frac{2\, K(E_n)}{E_{pmax}} \frac{1}{S(\varepsilon)} \int_{\varepsilon}^{E_{pmax}} \int_{R(\varepsilon)}^{l_{max}} f_\mu(l)\, dl \; \frac{dE_p}{E_{pmax}} \qquad (3.40)$$

where $l = R(\varepsilon) \le l_{max}$ and E_p is the initial energy of the stoppers entering the cavity.

4) Crossers

The number of crossers giving energy imparted between ε and ε+dε, is given by

$$N_{crs}(\varepsilon)\, d\varepsilon = \left\{ A \int_{\varepsilon}^{E_{max}} \Psi(E_p)\, f_\mu(l)\, \frac{dl}{dE_p}\, dE_p \right\} d\varepsilon \qquad (3.41)$$

where E_p is the initial energy of the crossers entering the cavity, l is the range of the crossers, i.e. $l = R(E_p) - R(E_p - \varepsilon)$ and $\frac{dl}{dE_p} = \frac{1}{S(E_p - \varepsilon)}$ is the inverse of the stopping power of the crossers leaving the cavity. Equation (3.41) can be reduced to equation (3.42).

$$N_{crs}(\varepsilon) = \frac{2\,K(E_n)}{E_{pmax}} \int_{\varepsilon}^{E_{pmax}} \frac{1}{S(E_p)} \int_{E_p}^{E_{max}} f_{\mu}(l\,)\,\frac{dE'}{E_{pmax}}\,\frac{dE_p}{S(E_p-\varepsilon)} \qquad (3.42)$$

The total of energy deposition events of intermediate energy neutrons for one type of recoil particles is simply the total event due to insiders, starters, stoppers and crossers. The total number of events for all types of recoil particles is the sum of all recoil type i for protons, carbon, nitrogen and oxygen ions and is given by

$$N_{tot}(\varepsilon) = \Sigma\ [N_{ins}(\varepsilon) + N_{str}(\varepsilon) + N_{stp}(\varepsilon) + N_{crs}(\varepsilon)]_i \qquad (3.43)$$

3.5.3 Microdosimetric Spectra Due to Fast Neutrons Detected in the Inner Counter and which can be Removed by Anti-Coincidence

To calculate the number of events due to fast neutrons detected in the inner counter and which can be removed by anti-coincidence with the outer counter, we require the equivalent energy of the wall thickness, E_{eq}, and the threshold energy of the detector, E_{th}. The threshold energy is the minimum energy required to initiate the signal in the counters. Assume the inner and outer counters have the same threshold energy E_{th} and consider a self-supporting dividing wall of thickness equivalent to the range of 100 keV of protons in tissue, i.e. E_{eq} = 100 keV, then, the number of events due to fast neutrons detected by anti-coincidence can be calculated as follows

Starters, stoppers and crossers of fast neutrons are affected by anti-coincidence arrangement, while insiders are not and must be removed by calculation. The range of the recoils must be greater than $R(E_{eq}+ E_{th})$ for starters, stoppers and crossers. For crossers which cross the dividing wall twice, their range must be greater than $R(2E_{eq}+ E_{th})$. Thus, the number of events per unit dose in the inner counter vetoed by the anti-coincidence is given by equations (3.44), (3.45) and (3.46) for starters, stoppers and crossers respectively.

$$N_{str}^{anti}(\varepsilon) = \frac{2\,K(E_n)}{E_{pmax}} \frac{1}{E_{pmax}} \int_{E_{eq}+E_{th}}^{E_{pmax}} \int_{l}^{l_{max}} f_{\mu}(x)\,dx\,\frac{dE_p}{S(E_p-\varepsilon)} \qquad (3.44)$$

$$N_{stp}^{anti}(\varepsilon) = \frac{2\,K(E_n)}{E_{pmax}} \frac{1}{S(\varepsilon)} \int_{E_{eq}+E_{th}}^{E_{pmax}} \int_{R(\varepsilon)}^{l_{max}} f_{\mu}(l)\,dl\,\frac{dE_p}{E_{pmax}} \qquad (3.45)$$

$$N_{crs}^{anti}(\varepsilon) = \frac{2\,K(E_n)}{E_{pmax}} \int_{E_{eq}+E_{th}}^{E_{pmax}} \frac{1}{S(E_p)} \int_{E_p}^{E_{max}} f_{\mu}(l)\,\frac{dE'}{E_{pmax}}\,\frac{dE_p}{S(E_p-\varepsilon)} \qquad (3.46)$$

where $l = R(\varepsilon)$ for stoppers and $l = R(E_p) - R(E_p-\varepsilon)$ for starters and crossers. The total number of event for all types of recoil is the sum of all recoil type i, i.e.

$$N_{tot}^{anti}(\varepsilon) = \Sigma\,[\,N_{str}^{anti}(\varepsilon) + N_{stp}^{anti}(\varepsilon) + N_{crs}^{anti}(\varepsilon)\,]_i \qquad (3.47)$$

However, there will be some recoils of range less than $R(E_{eq}+E_{th})$ due to fast neutrons which are superimposed on the events due to intermediate energy neutrons and cannot be removed by the anti-coincidence arrangement. These residual events of fast neutrons are insiders, starters, stoppers and crossers and must be removed by calculation. The number of event per unit dose in the inner counter which cannot be vetoed by an anti-coincidence can be calculated from equation (3.36) for insiders, and by equations (3.38), (3.40) and (3.42) for starters, stoppers and crossers respectively, but the upper limit of the integration with respect to E_p is changed from E_{pmax} to $E_{eq}+E_{th}$.

3.5.4 Microdosimetric Spectra Due to Fast Neutron Recoils Associated with the Dividing Wall.

Except for insiders, there will be some events due to fast neutrons which originate in the dividing wall for stoppers and crossers or which originate in the inner counter and are stopped in the dividing wall (starters). They deposit energy less than 100 keV in the inner counter. Only crossers which originated in the dividing wall and reach the outer counter can be discarded by anti-coincidence. Other events cannot be removed by an anti-coincidence arrangement but must be removed by calculation. The recoil must have had a minimum energy of E_{eq} to be considered, i.e. $E_p = E_{eq}$.

The number of event due to fast neutrons for a given recoil type i which must be removed from the spectra of the inner counter is given by equation (3.48).

$$N_i^{wall}(\varepsilon) = \frac{1}{E_{pmax}} \int_{E_{eq}}^{E_{pmax}} \{ N_{str}(\varepsilon) + N_{stp}(\varepsilon) + N_{crs}(\varepsilon) \} \, dE_p \qquad (3.48)$$

where, $N_{str}(\varepsilon)$, $N_{stp}(\varepsilon)$ and $N_{crs}(\varepsilon)$ are given by equations (3.38), (3.40) and (3.42) respectively. The total number of event for all types of recoil is the sum of all recoil type i, i.e.

$$N_{tot}^{wall}(\varepsilon) = \Sigma \, N_i^{wall}(\varepsilon) \qquad (3.49)$$

3.6 Methods of Calculation of Event Spectra

The response of the inner counter was calculated in terms of the frequency distributions of energy deposition events due to insiders, starters, stoppers and crossers. The calculation was performed for a spherical volume at various diameters from 0.3 to 3.0 μm. The extension of the calculation to a cylindrical volume is straight forward when the chord length distribution of μ-randomness of the cavity is known.

The co-axial counter is assumed to be irradiated isotropically by monoenergetic neutrons of various energies. Neutron cross-sections for hydrogen, carbon, nitrogen and oxygen were obtained from data file of the JEF-Library (Joint Evaluated File). For interactions of fast neutrons ($E_n \geq 200$ keV) only the elastic scattering component was considered, but for interactions of intermediate energy neutrons ($E_n \leq 200$ keV) the elastic scattering and neutron capture, i.e. $^{14}N(n,p)^{14}C$ reaction, were considered to be significant. The composition of tissue was taken from ICRU (1977), but as before the minor elements (Na, Mg, P, S, K and Ca) were treated as oxygen.

The effective stopping power and projected ranges of secondary charged particles generated by neutrons in tissue (i.e. protons, C, N, and O ions) were calculated according to the previous method described in section (3.2). The program was first incorporated into the main program for calculation of microdosimetric spectra. It was a successful attempt however, but the CPU time was exessive. Therefore, the results of the stopping powers and projected ranges of heavy charged particles in tissue have been fitted with the polynomial expressions which had a deviation of less than 1% for hydrogen and less than 2% for carbon, nitrogen and oxygen in ICRU tissue. It was necessary to divide the results into several energy bands in order to achieve good fits.

The neutron kerma for hydrogen, carbon, nitrogen and oxygen in ICRU tissue was calculated directly according to the method described in section (3.3).

For the response of the counter to intermediate energy neutrons, neutrons of energy 1, 10, 50 and 100 keV are assumed.

For the counter operating in coincidence/anti-coincidence arrangements, it was assumed that the counter is irradiated isotropically with monoenergetic neutrons of energy from 0.5 to 10 MeV. The thickness of the dividing wall was taken as equivalent to the range of 100 keV protons, i.e. $E_{eq} = 100$ keV. The threshold of 5 keV was assumed for the inner and the outer counters.

The spectra due to the presence of the dividing wall were also calculated for fast neutrons of energy from 500 keV to 5 MeV.

3.7 Results and Discussion

3.7.1 Event Spectra of Intermediate Energy Neutrons

Fig. 3.23-3.30 show the energy deposition spectra of intermediate energy neutrons of various energies for tissue diameters of 0.3, 0.5, 1.0 and 3.0 μm. The nature of these distributions has been described elsewhere for example by Caswell (1966) and Al-Affan *et al.* (1984). As the heavy recoils have maximum energies equal to 0.28 E_n (for C), 0.25 E_n (for N) and 0.22 E_n (for O) and have correspondingly small ranges less than 0.2 μm they occur almost entirely as insiders. The energy deposition spectra due to proton recoils dominate the distributions. Their ranges are less than 1.2 μm.

The distribution of the events due to insiders, starters, stoppers and crossers depends on the tissue diameter and neutron energy. Insiders are important at lower neutron energies and for larger diameters. The spectra of 1 keV neutrons are dominated by insiders in all the sphere sizes since their ranges are less than 70 nm. Crossers, on the other hand, are dominated for smaller sphere sizes and at higher neutron energies. For example, for tissue diameter of 0.3 μm crossers due to 50 keV neutrons are important, **Fig. 3.24** (a), but when the tissue diameter is increased to 0.5 μm crossers due to 100 keV neutrons only become important, **Fig. 3.26** (b). Crossers are negligible at tissue sphere of 3.0 μm for all the neutron energies. Al-Affan *et al.* (1984) have suggested that if the sphere diameter d is less than one quarter of the range $\bar{R}$ of the average energy of proton, then crossers dominate the event spectra and if d is greater than four times the range $\bar{R}$ then insiders dominate the event spectra. Starters and stoppers are important at higher neutron energies in all tissue diameters. Also, they are not negligible for 1 keV neutrons.

The results for tissue diameter of 1.0 μm , **Fig. 3.27** and **3.28**, are in agreement with those calculated by Al-Affan *et al.* (1984), as expected, since no significant change has been made in the effective stopping power and projected ranges of protons in tissue

calculated in this work. However, there is an increase in the events for insiders due to carbon recoils for 1 keV neutrons, **Fig. 3.27** (a). This is due to the differences in the stopping power of carbon ions in tissue and consequently the projected ranges used in the present calculation. Nevertheless, the difference is of minor importance in experiment because the pulse induced by 1 keV protons is generally very small to be detected in TEPCs due to the limitation of the TE gas multiplication.

The frequency and dose mean lineal energies for tissue diameters of 1.0 and 0.5 μm are shown in **Table 3.2** calculated for intermediate energy neutrons at various energies.

Table 3.2 The frequency and dose mean lineal energies for neutrons of energy 1keV to 100 keV in tissue of diameter 1.0 and 0.5 μm.

Neutron Energy	$\bar{y}_F$ (keV/μm)		$\bar{y}_D$ (keV/μm)	
(keV)	1.0 μm	0.5 μm	1.0 μm	0.5 μm
1	0.819	1.582	0.929	1.858
10	6.56	10.29	8.78	17.57
50	23.95	27.97	35.46	70.84
100	41.25	43.15	57.85	110

3.7.2 Event Spectra of Fast Neutrons for the Counter Operating Without and with Anti-Coincidence Modes.

Fig.3.31-3.36 show the calculated energy deposition spectra due to fast neutrons of energy from 0.5 to 3.0 MeV for the counter operated without and with anti-coincidence arrangements. The results show that when the counter is operated in anti-coincidence mode, figures (b), a large proportion of the proton events, figures (a), is vetoed resulting in a flat response to intermediate energy neutrons. Events due to crossers make the main contribution at higher neutron energies and for smaller sphere size. While insiders are dominated at lower

neutron energies and for larger sphere size. Starters and stoppers are important at lower neutron energies and are also not negligible at higher energies.

In anti-coincidence spectra, crossers are important at higher energy depositions while insiders, starters and crossers are important at the lower energy depositions and for larger tissue diameters. The crossers fall sharply toward higher energy depositions as the end of their tracks penetrate the dividing wall.

Analysis of the results shows that if co-axial microdosimeters were to be used for measurement of energy deposition spectra due to 50 and 100 keV neutron components in the presence of an equal dose of fast neutrons the spectra must be corrected for events of energy ≤ 100 keV generated by fast neutrons. **Fig. 3.37** shows the percentage of dose needed for correction at various neutron energies from 0.5 to 10 MeV for tissue diameter of 0.5, 1.0 and 3.0 μm. The dose correction factor increases with the decrease in neutron energy and sphere size. There is no significant difference in the correction factor for 50 and 100 keV neutrons at larger diameter because fast neutrons of energy ≥ 2 MeV deposit less energy in the intermediate energy region. However, as the neutron energy decreases the event spectra for larger diameter also increases and thus the dose correction, because the events are now dominated by insiders as shown in **Fig 3.35** (b).

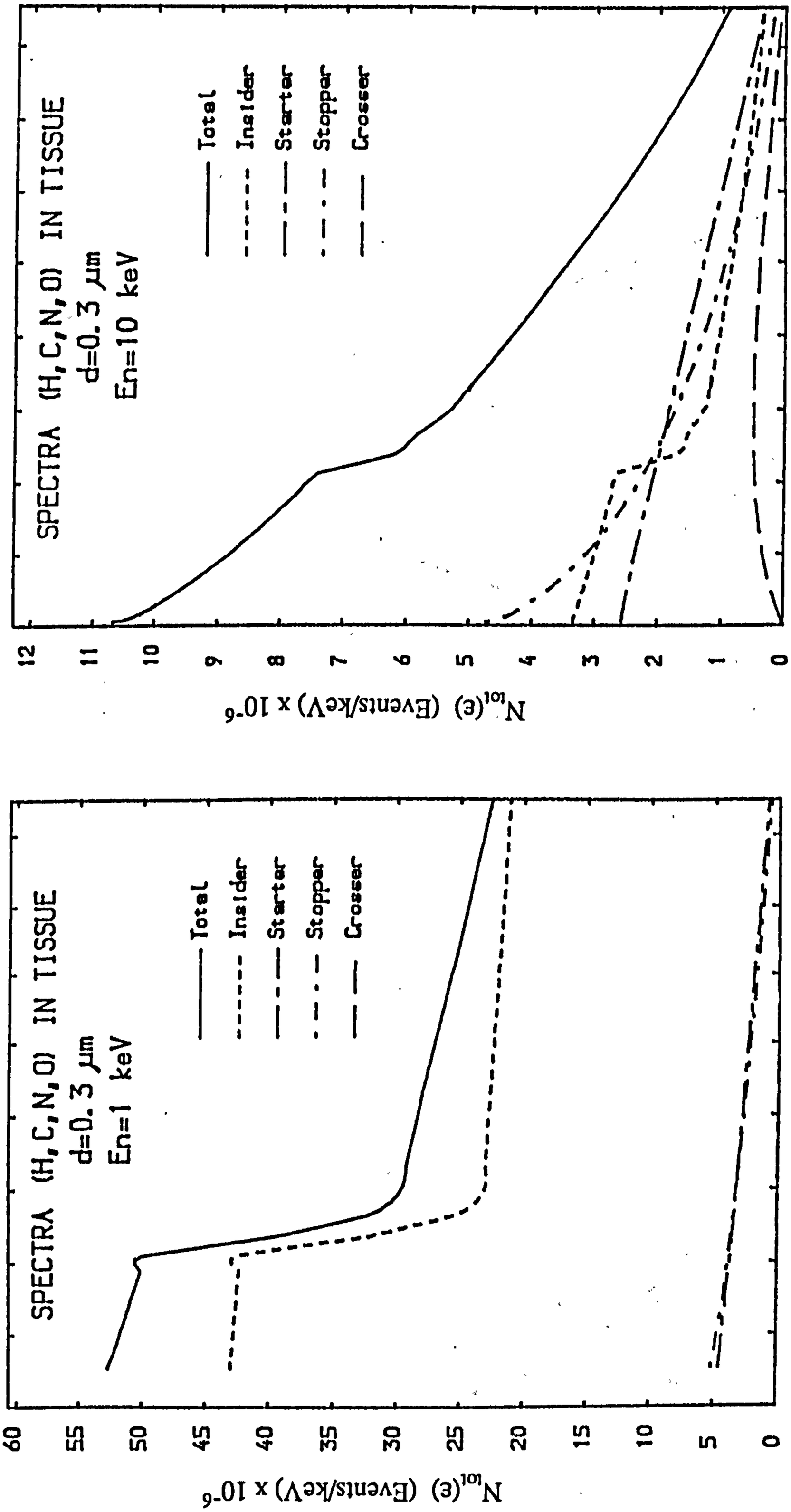

Fig. 3.23 Component of energy deposition spectra in tissue sphere 0.3 μm in diameter for (a) 1 keV and (b) 10 keV neutrons. Insiders dominate the event at 1 keV and crossers begin to appear at 10 keV.

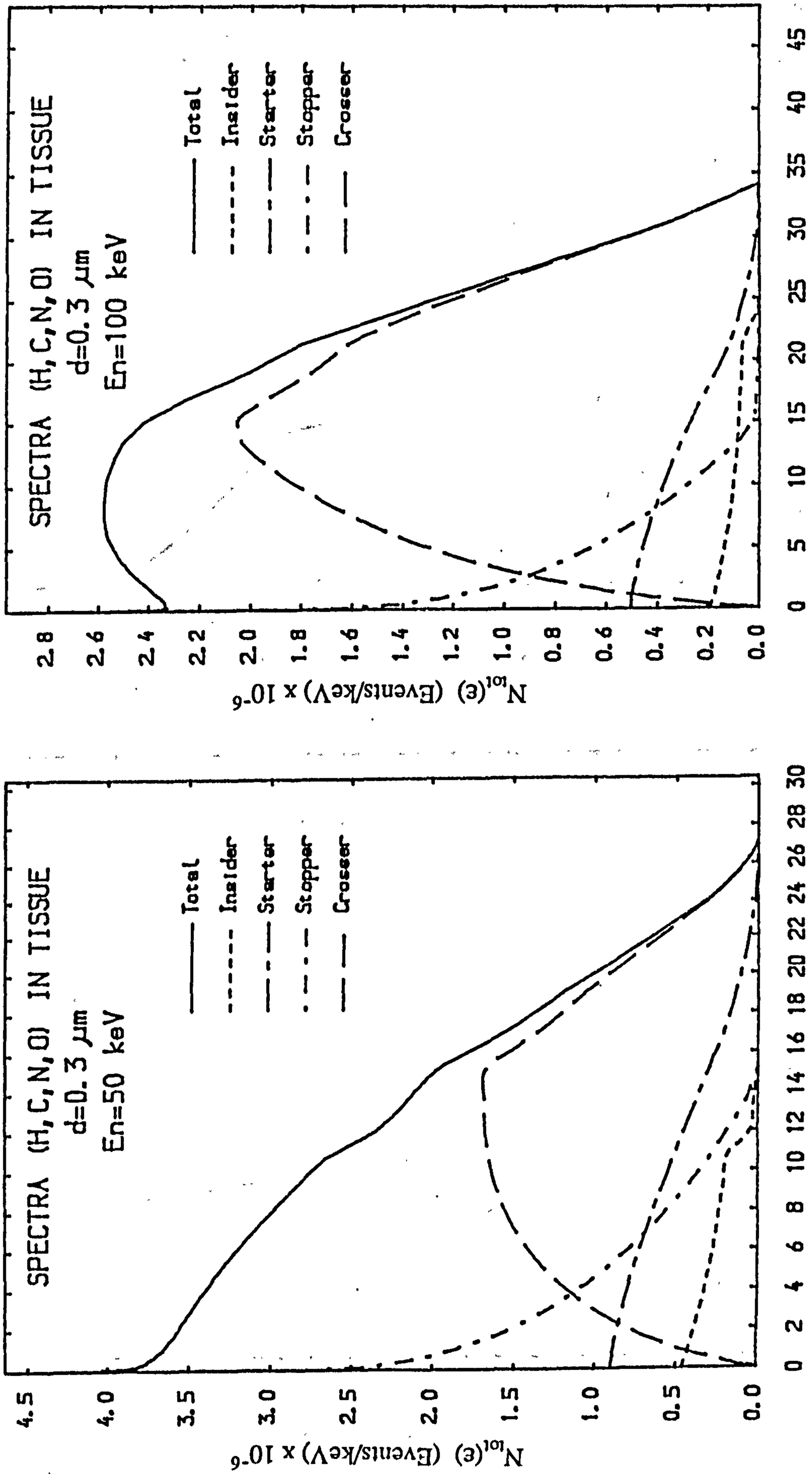

Fig. 3.24 Component of energy deposition spectra in tissue sphere 0.3 μm in diameter for (a) 50 keV and (b) 100 keV neutrons. Crossers dominate the events at 50 keV and 100 keV.

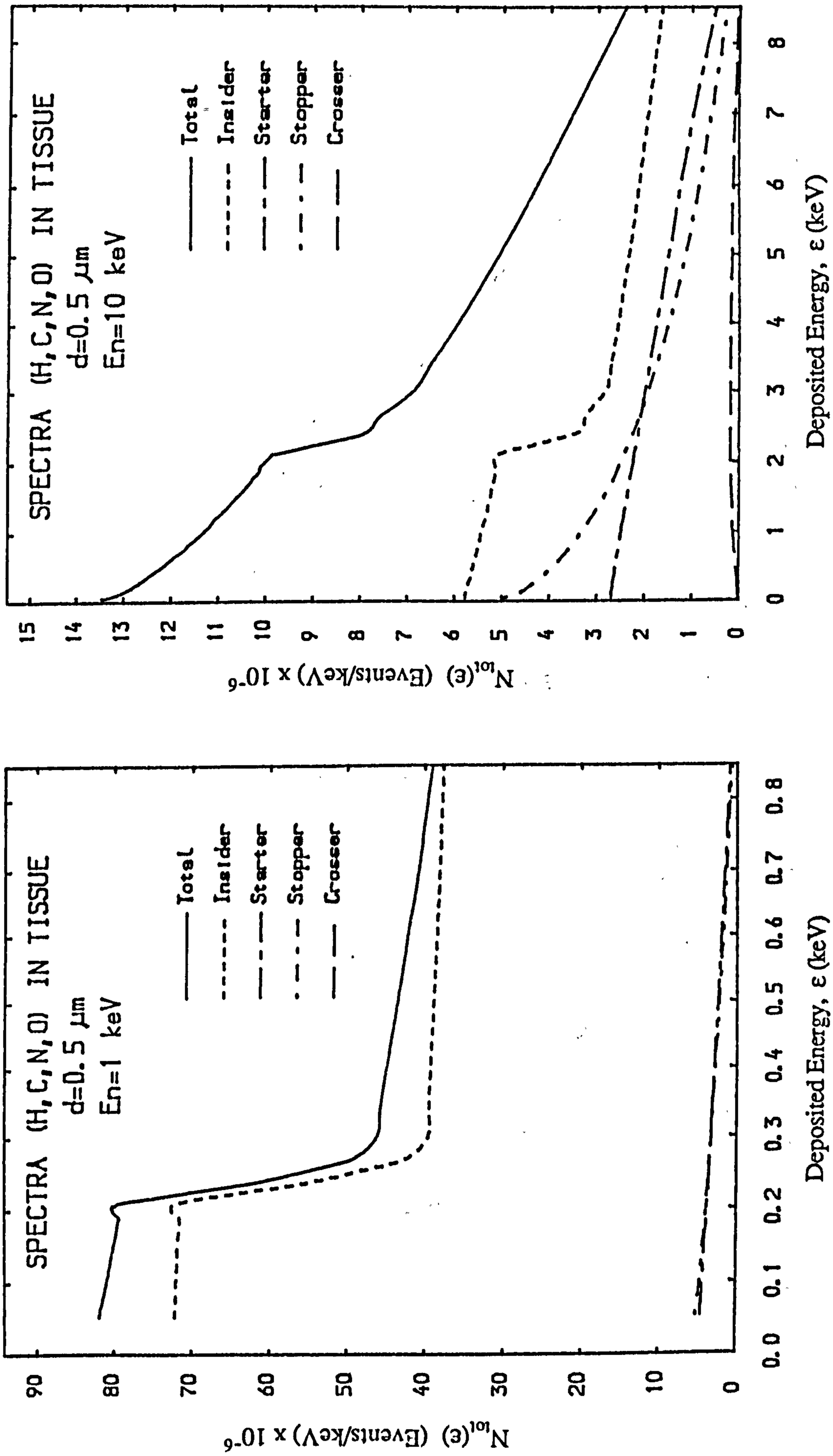

Fig. 3.25 Component of energy deposition spectra in tissue sphere 0.5 μm in diameter for (a) 1 keV and (b) 10 keV neutrons.

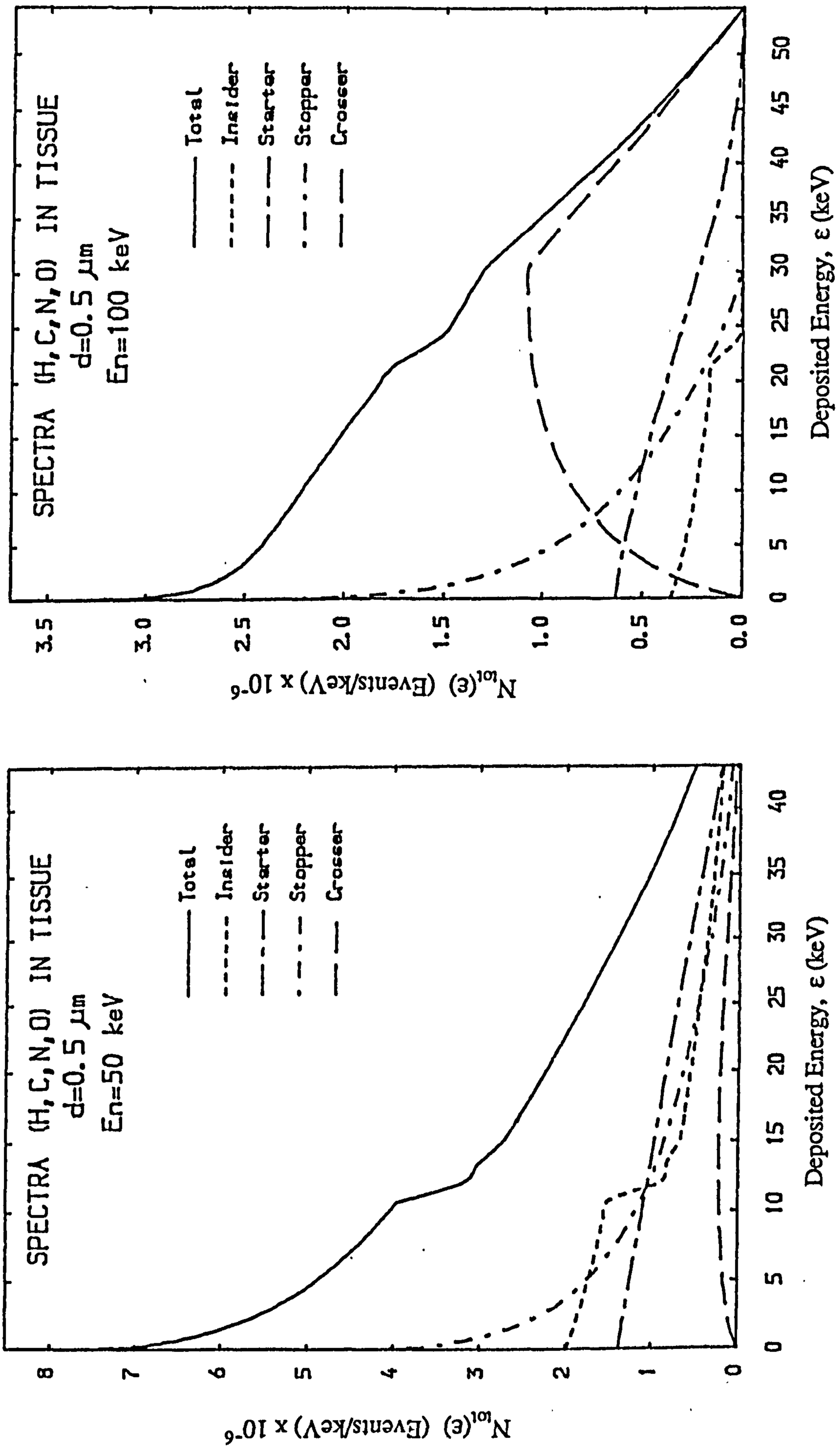

Fig. 3.26 Component of energy deposition spectra in tissue sphere 0.5 μm in diameter for (a) 50 keV and (b) 100 keV neutrons. Crossers dominate the events at 100 keV.

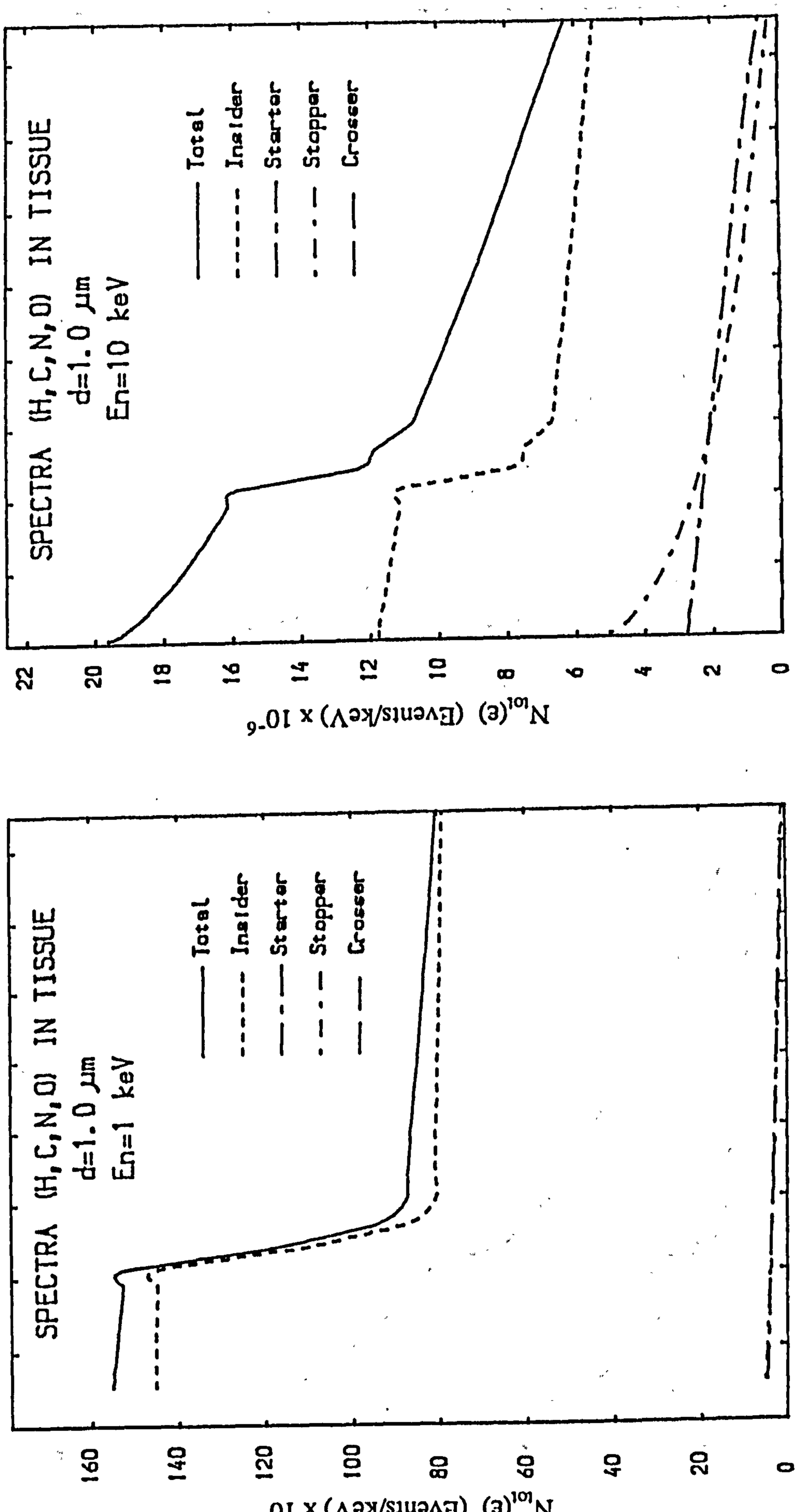

Fig. 3.27 Component of energy deposition spectra in tissue sphere 1.0 μm in diameter for (a) 1 keV and (b) 10 keV neutrons. Insiders dominate the events at 1 keV and 10 keV.

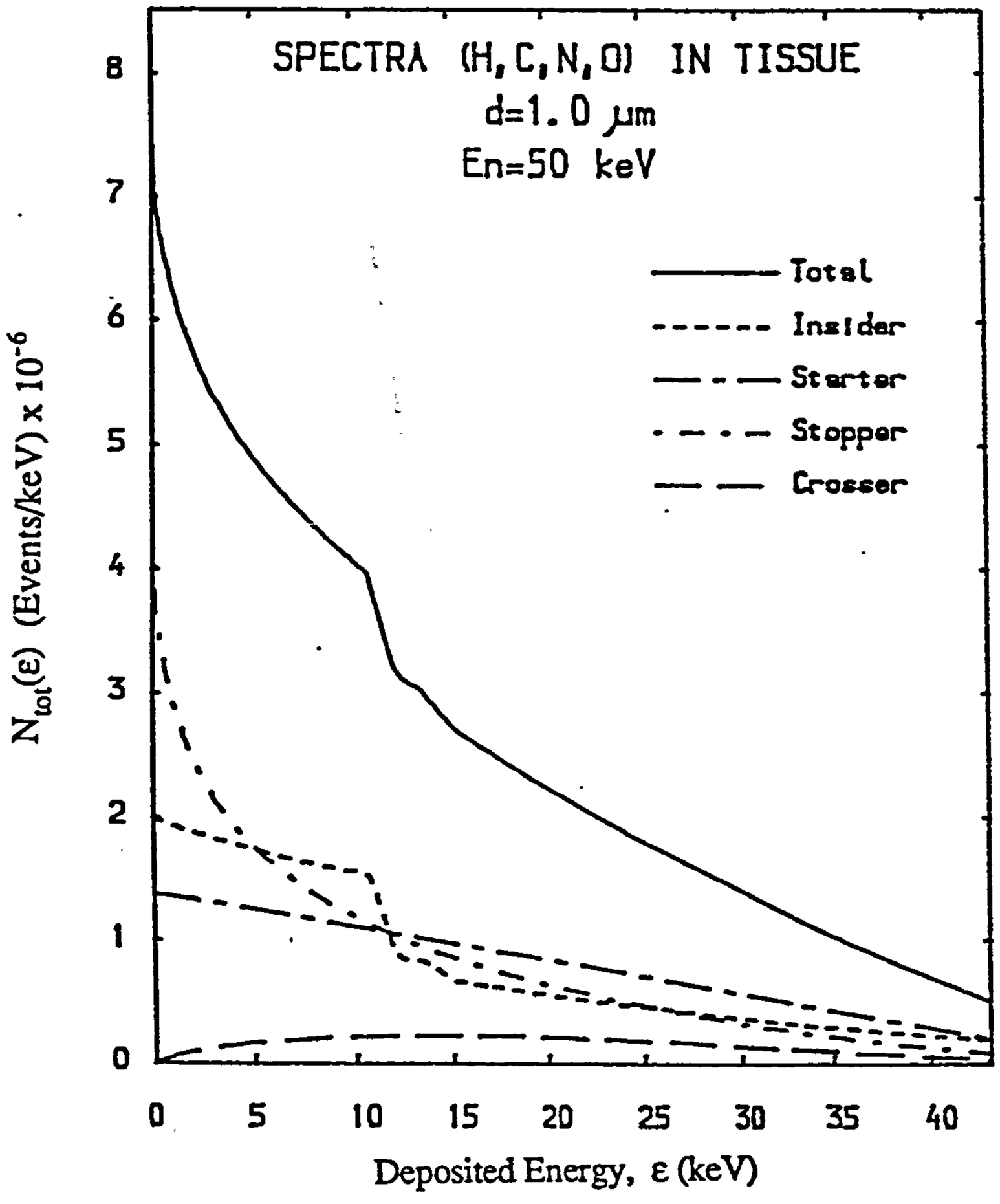

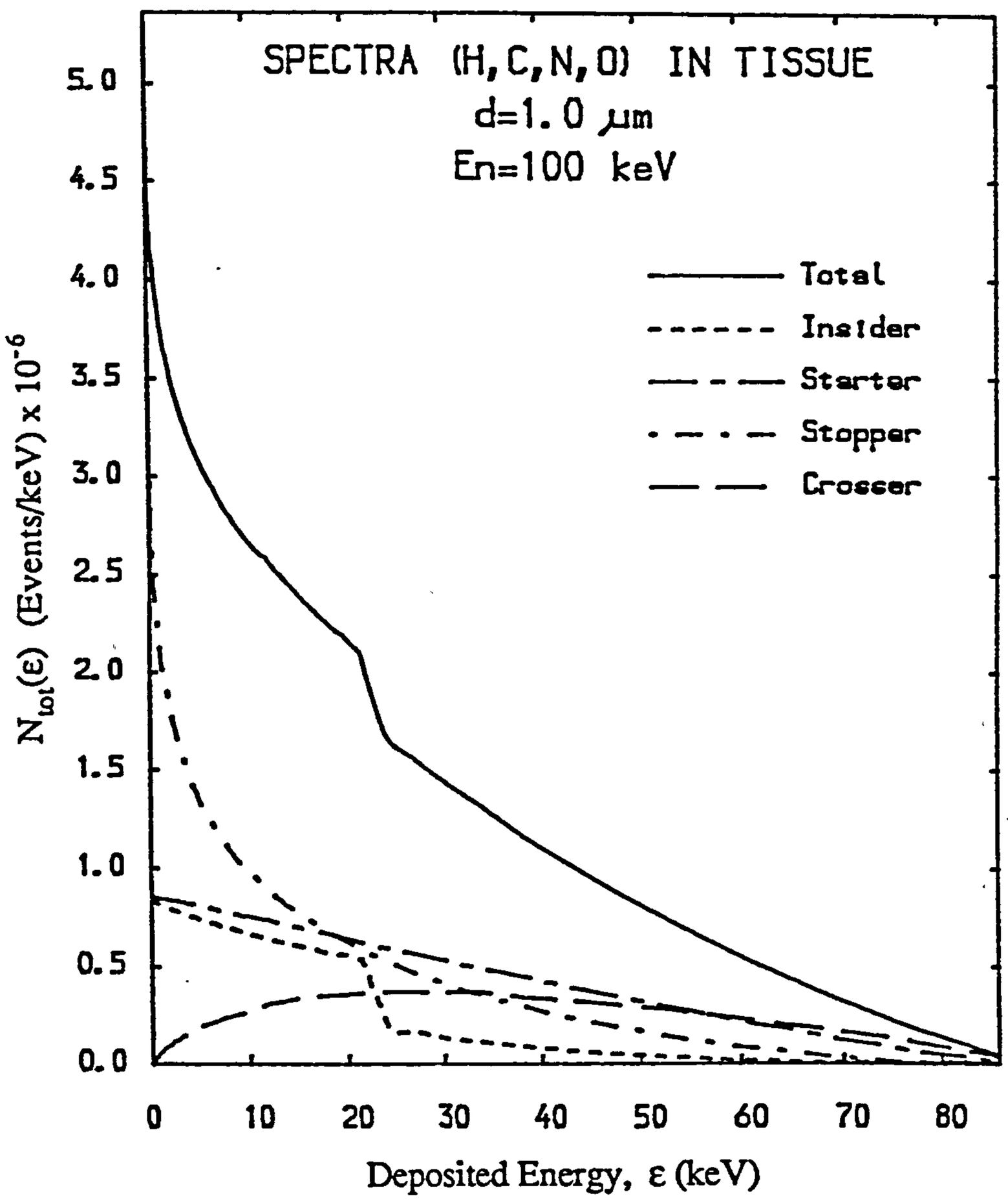

Fig. 3.28 Component of energy deposition spectra in tissue sphere 1.0 μm in diameter for (a) 50 keV and (b) 100 keV neutrons.

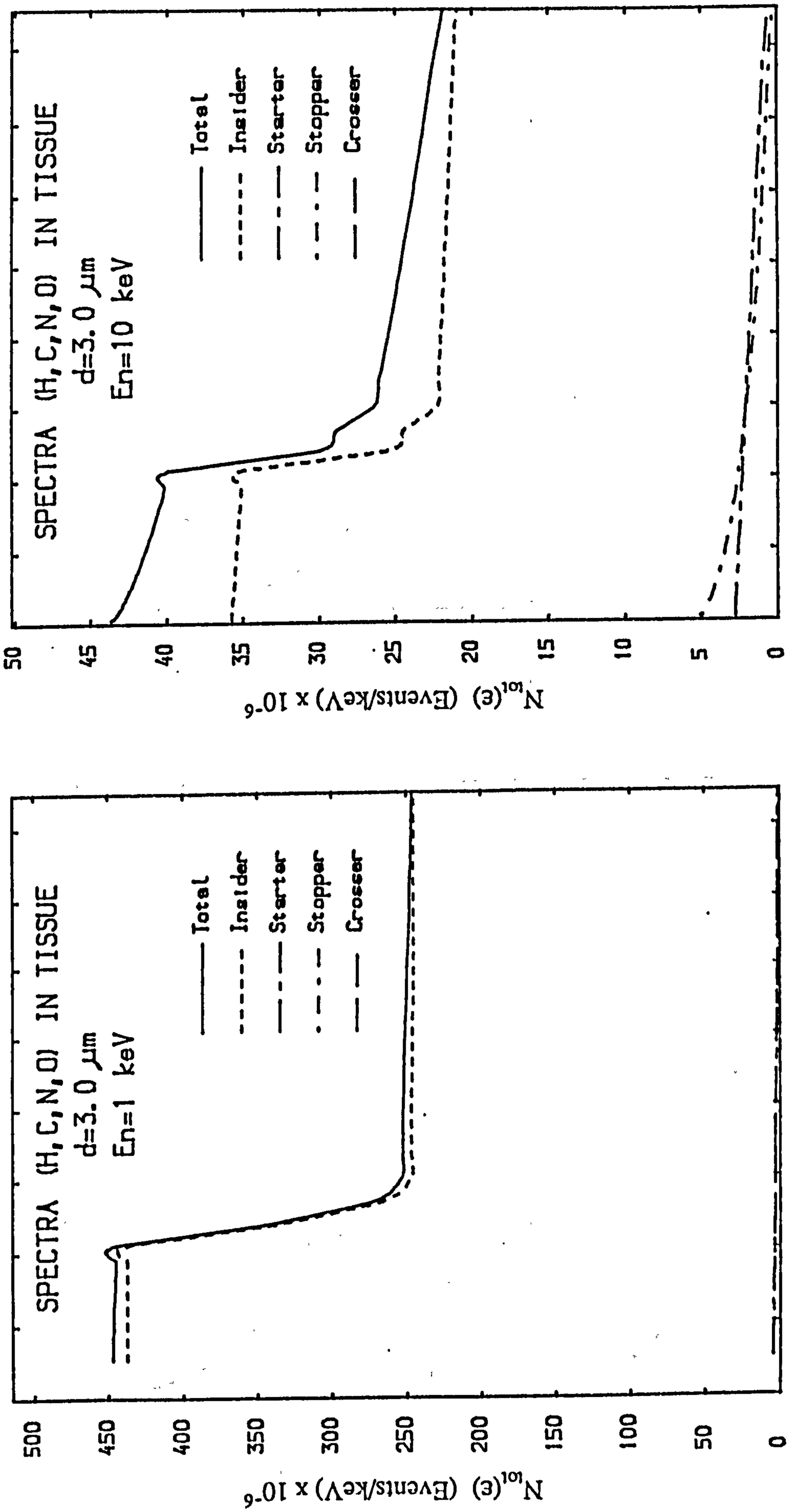

Fig. 3.29 Component of energy deposition spectra in tissue sphere 3.0 μm in diameter for (a) 1 keV and (b) 10 keV neutrons.

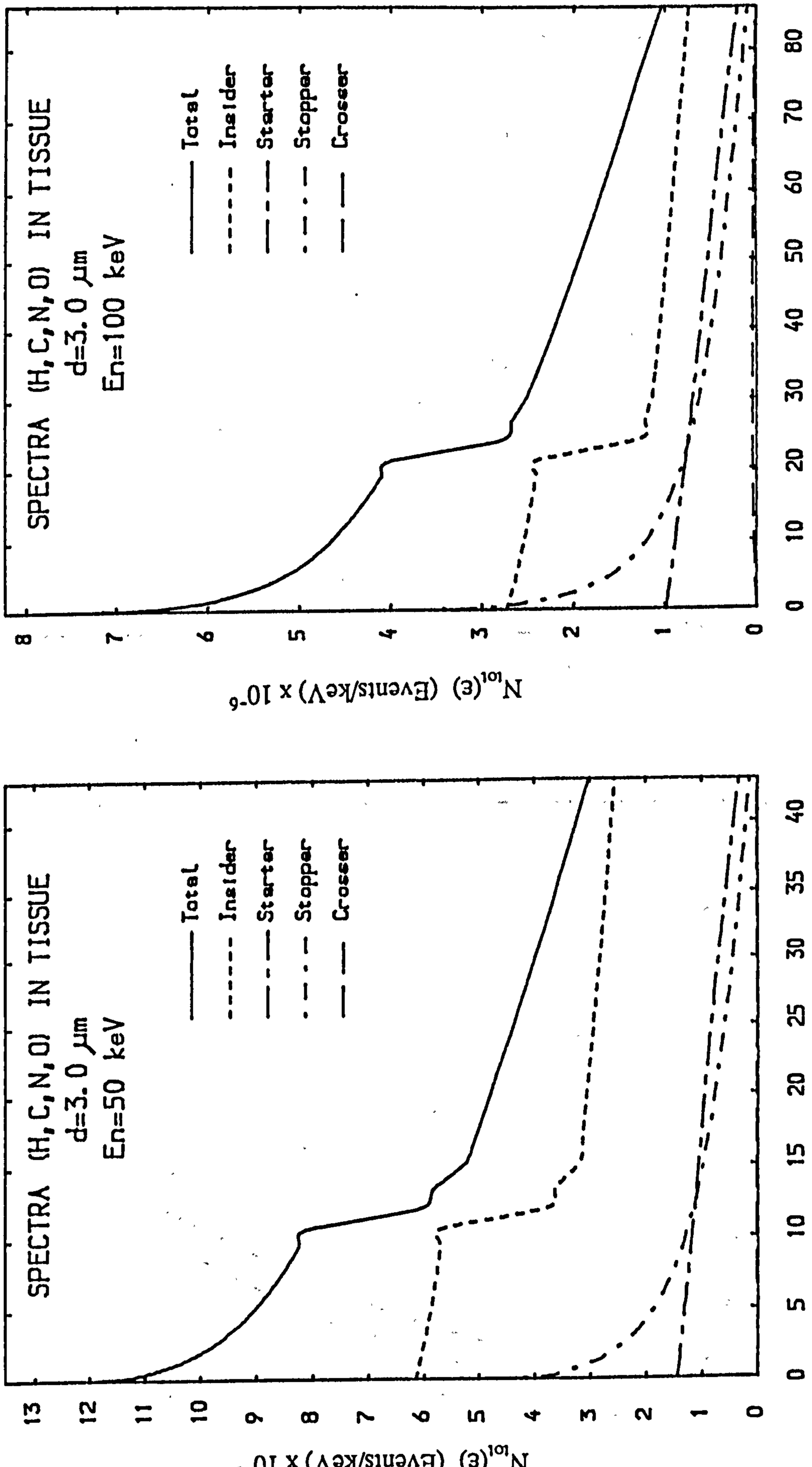

Fig. 3.30 Component of energy deposition spectra in tissue sphere 1.0 μm in diameter for (a) 50 keV and (b) 100 keV neutrons. Note that crossers are negligible at a large diameter while insiders dominate the events.

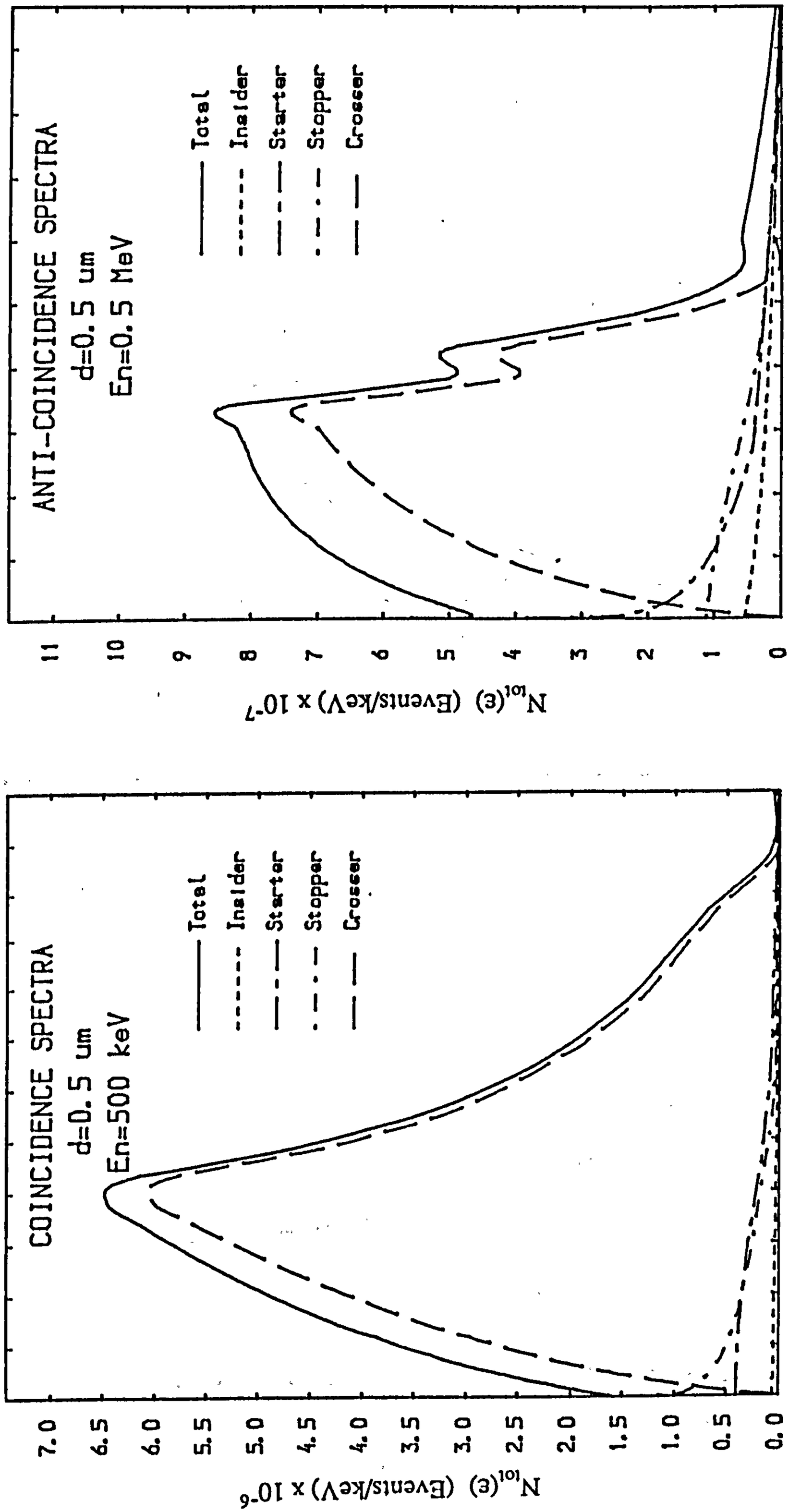

Fig. 3.31 Energy deposition spectra in a tissue sphere 0.5 μm diameter for a co-axial TEPC operated (a) without and (b) with anti-coincience modes for 500 keV neutrons. The thickness of the dividing wall is equivalent to the range of 100 keV protons.

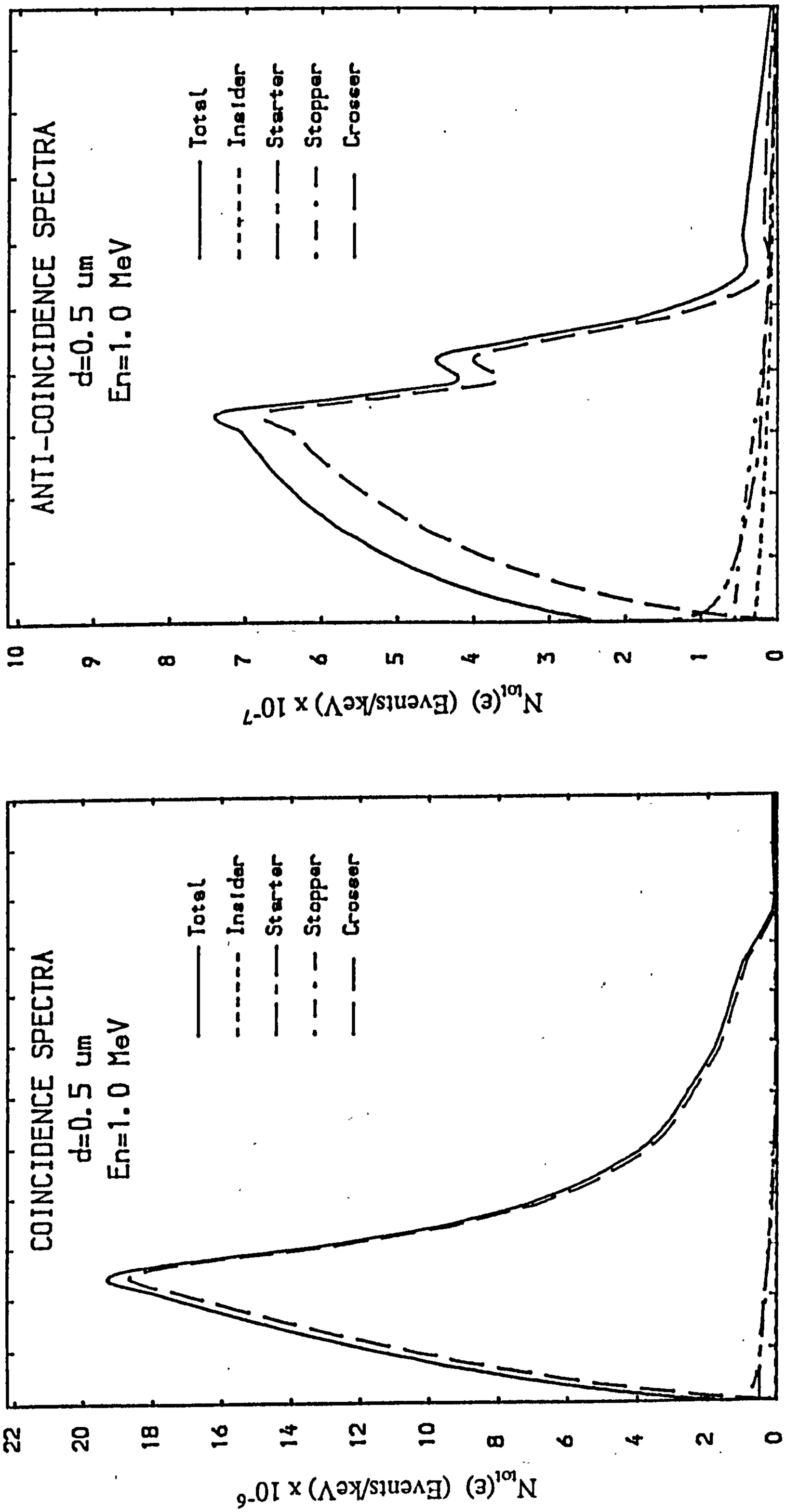

Fig. 3.32 Energy deposition spectra in a tissue sphere 0.5 μm diameter for a coaxial TEPC operated (a) without and (b) with anti-coincinence modes for 1 MeV neutrons. Note that crossers dominate the events in (b) for this diameter of sphere.

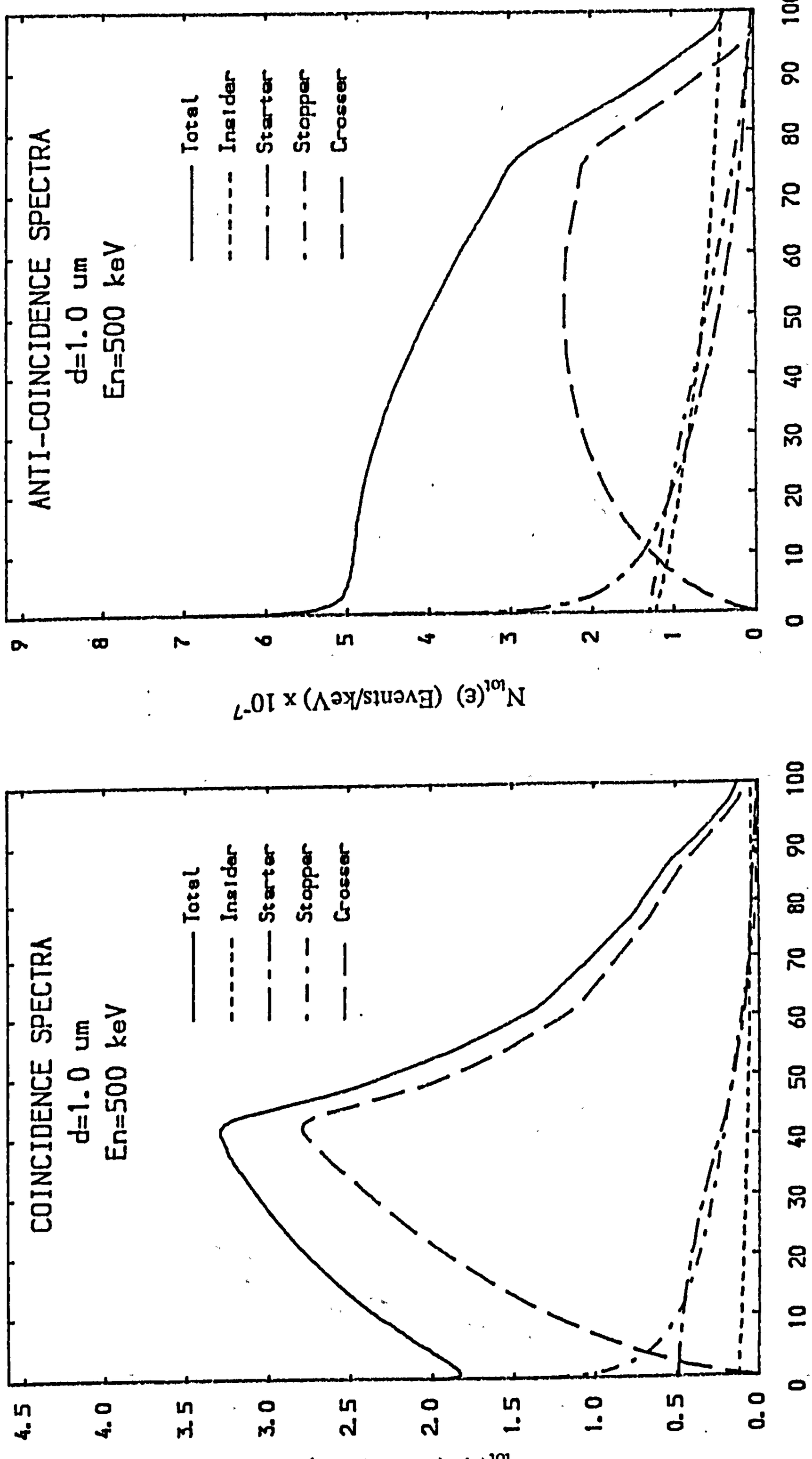

Fig. 3.33 Energy deposition spectra in a tissue sphere 1.0 μm diameter for a cylindrical TEPC operated (a) without and (b) with anti-coincidence modes for 500 keV neutrons. A large proportion of crossers, stoppers and starters is vetoed in anti-coincidence spectrum.

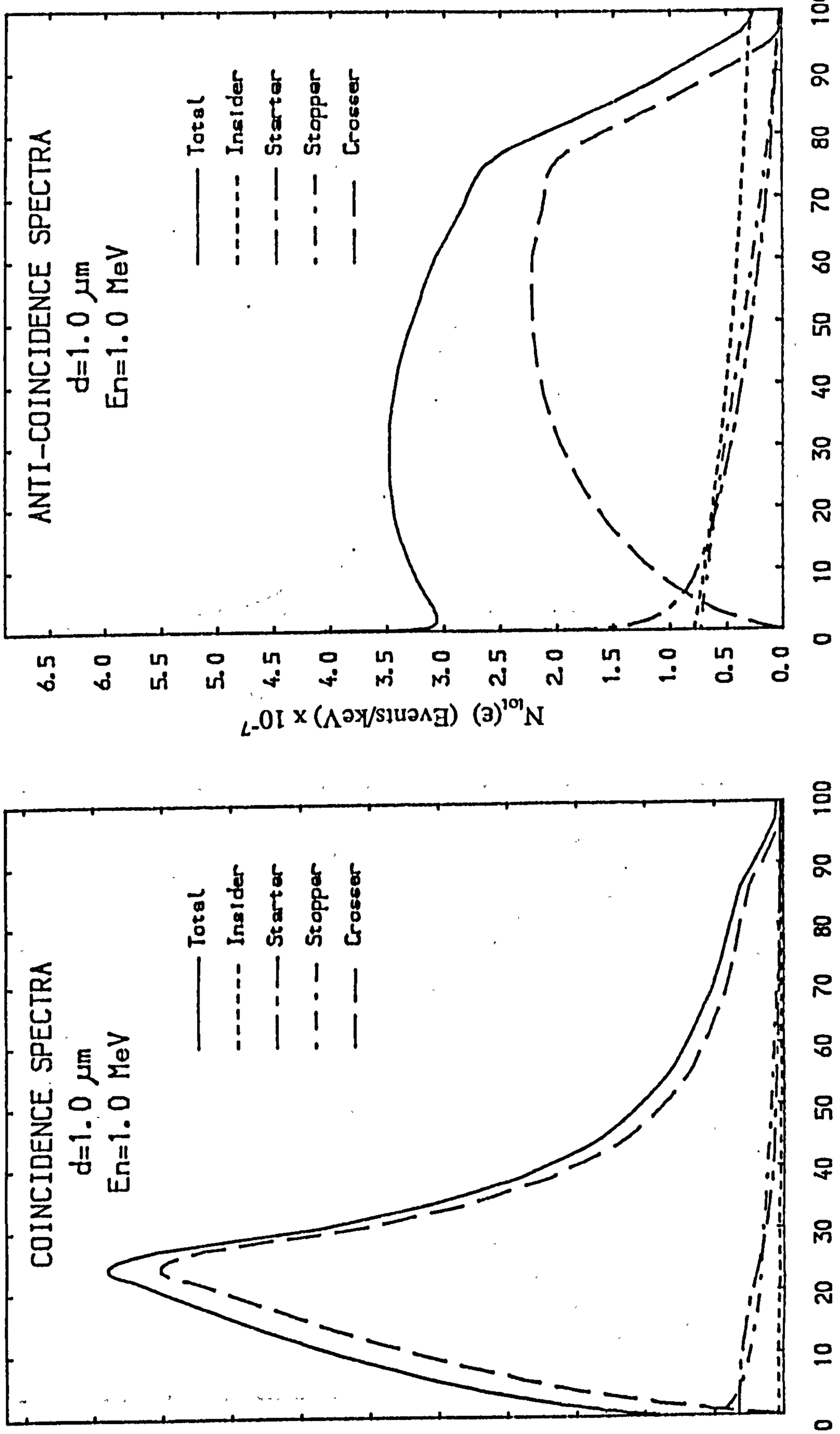

Fig. 3.34 Energy deposition spectra in a tissue sphere 1.0 μm diameter for a TEPC operated (a) without and (b) with anti-coincinence modes for 1 MeV neutrons.

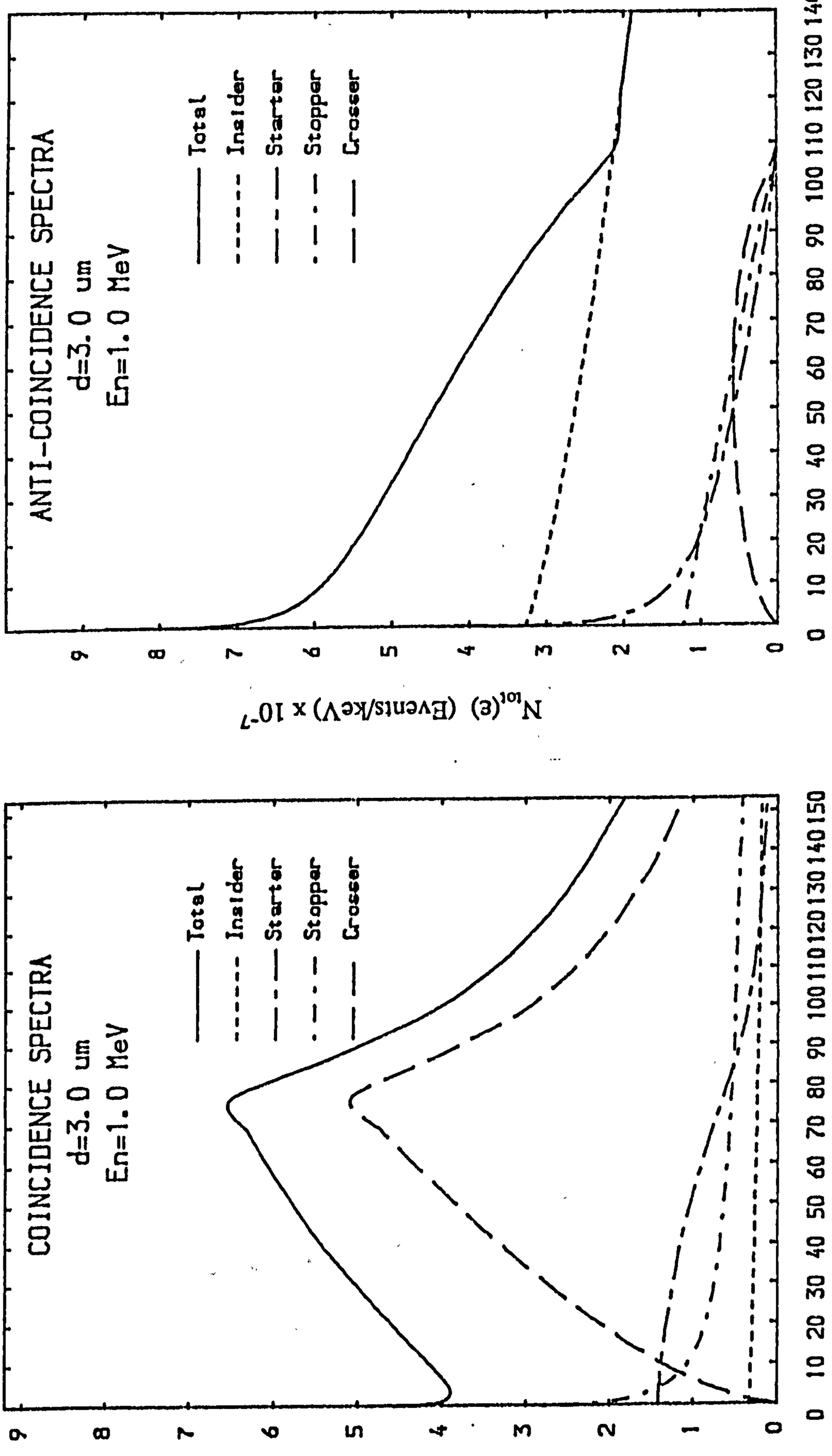

Fig. 3.35 Energy deposition spectra in a tissue sphere 3.0 μm diameter for a co-axial TEPC operated (a) without and (b) with anti-coincience modes for 1 MeV neutrons. Note that insiders dominate the events in (b) for this large diameter of sphere.

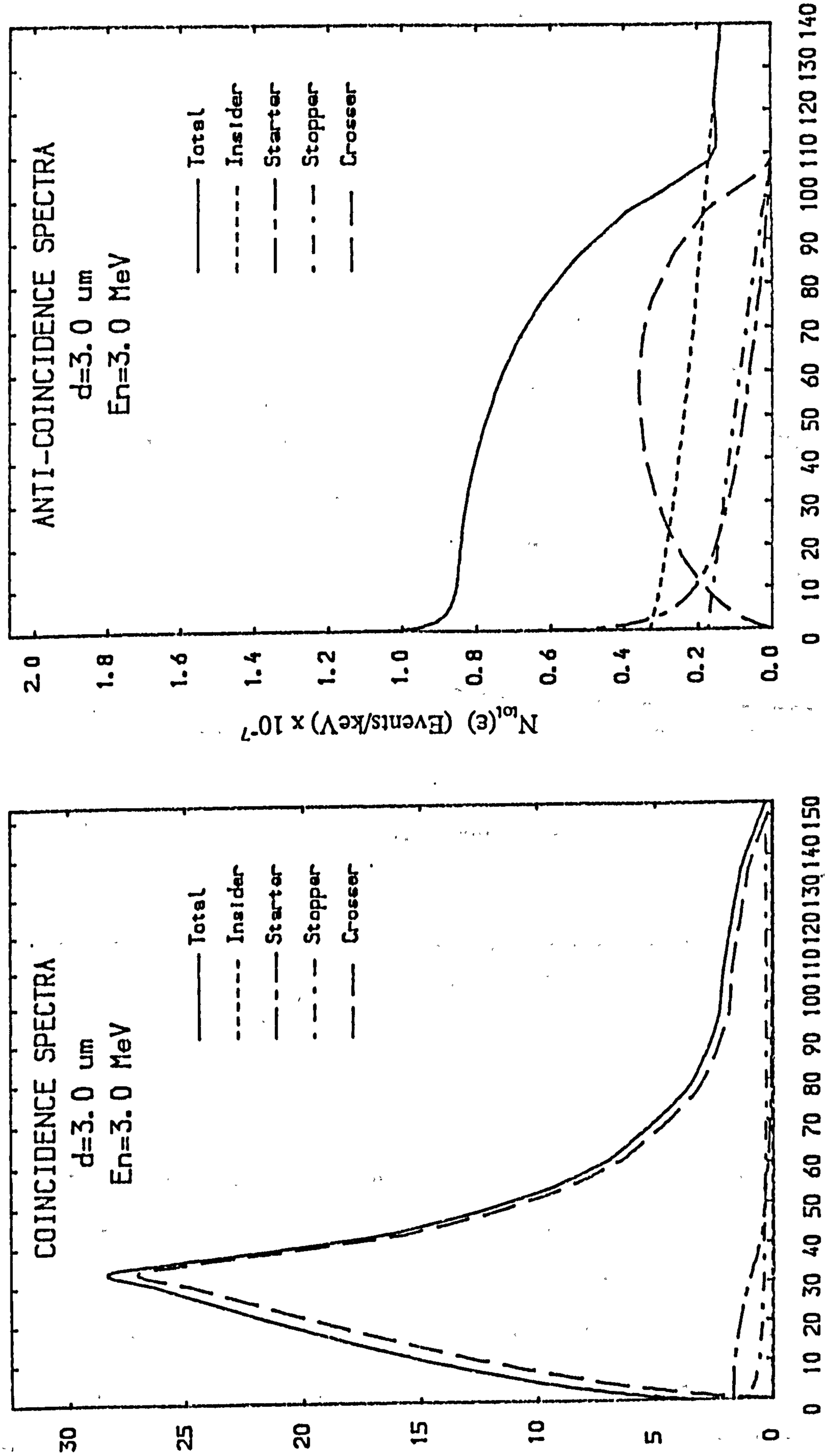

Fig. 3.36 Energy deposition spectra in a tissue sphere 3.0 μm diameter for a co-axial TEPC operated (a) without and (b) with anti-coincinence modes for 3 MeV neutrons. Note that the crossers are begining to dominate at 3 MeV in anti-coincidence spectrum.

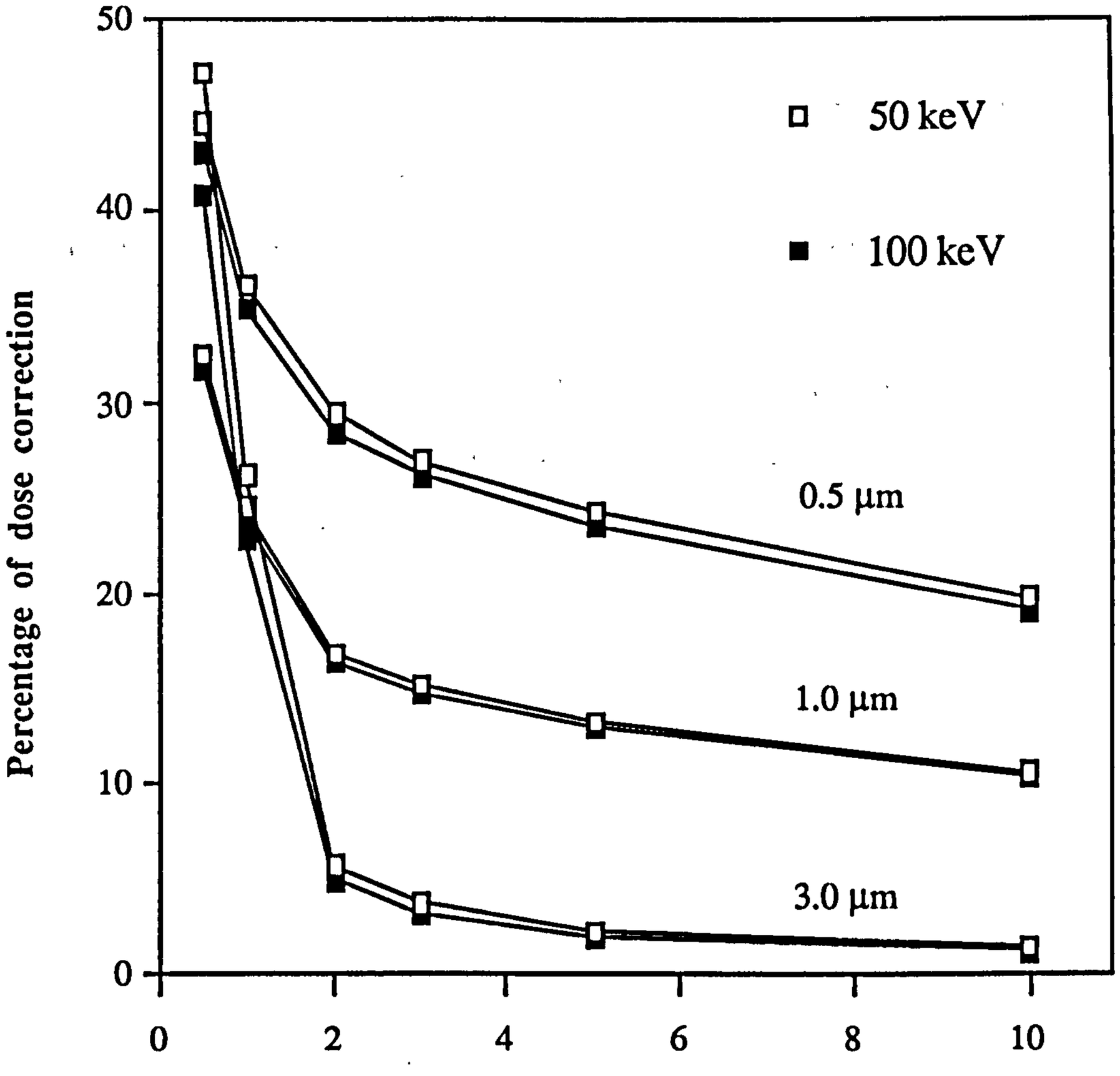

Fig. 3.37. The dose correction for intermediate energy neutrons measured in co-axial TEPC for mixed fields of fast neutrons at various simulated tissue diameters and for equal doses of the neutron components.

3.7.3 Event Spectra of Fast Neutrons in the Presence of the Dividing Wall

There will be additional spectra of fast neutrons inherent in the co-axial dosimeter due to the presence of the dividing wall and must be corrected by calculation. **Fig. 3.38-3.43** show the spectra due to the dividing wall for simulated tissue diameter of 0.5 , 1.0 and 3.0 μm at various neutron energies from 500 keV to 5.0 MeV. The spectra are dominated by starters and stoppers. Crossers become important only at higher neutron energy and for smaller diameter. As expected, starters and stoppers are important at lower energy deposition, while crossers dominate at higher energy deposition.

Analysis of the results show that the correction factor attributed to the dividing wall is less than 12, 10 and 5 % in the presence of an equal dose of 1.0 MeV fast neutrons to intermediate energy neutrons at simulated tissue diameters of 0.5, 1.0 and 3.0 μm respectively. The correction factor for 500 keV neutrons is less than that of 1 MeV neutrons because the events are dominated by starters which increase as the tissue diameter increases. Also, the correction factor for neutrons of energy > 1 MeV is less than that of 1 MeV neutrons since the starters decrease as the neutron energy increases.

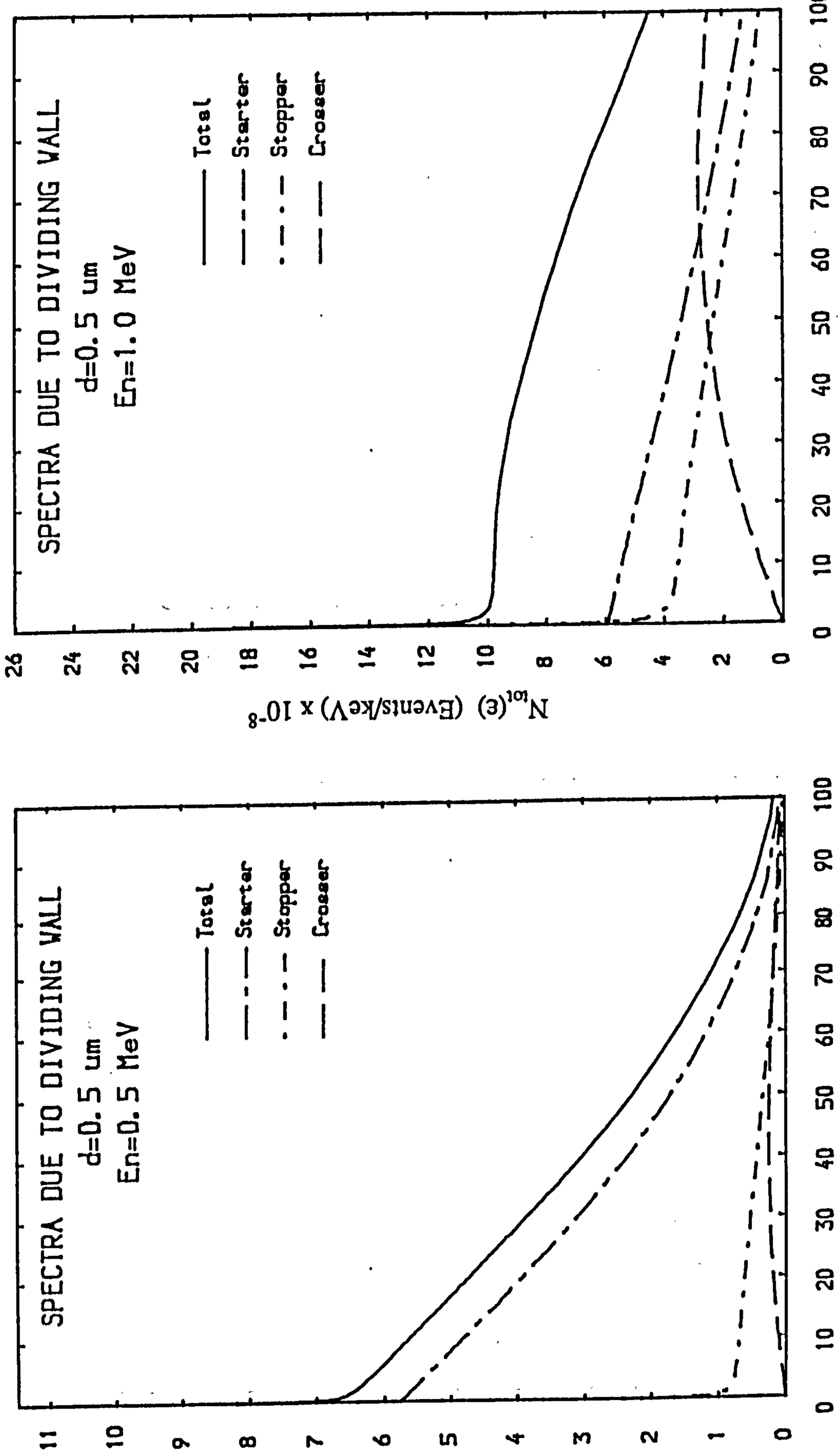

Fig. 3.38 Event spectra in a tissue sphere 0.5 μm diameter corrected due to the presence of dividing wall for (a) 0.5 MeV and (b) 1.0 MeV neutrons.

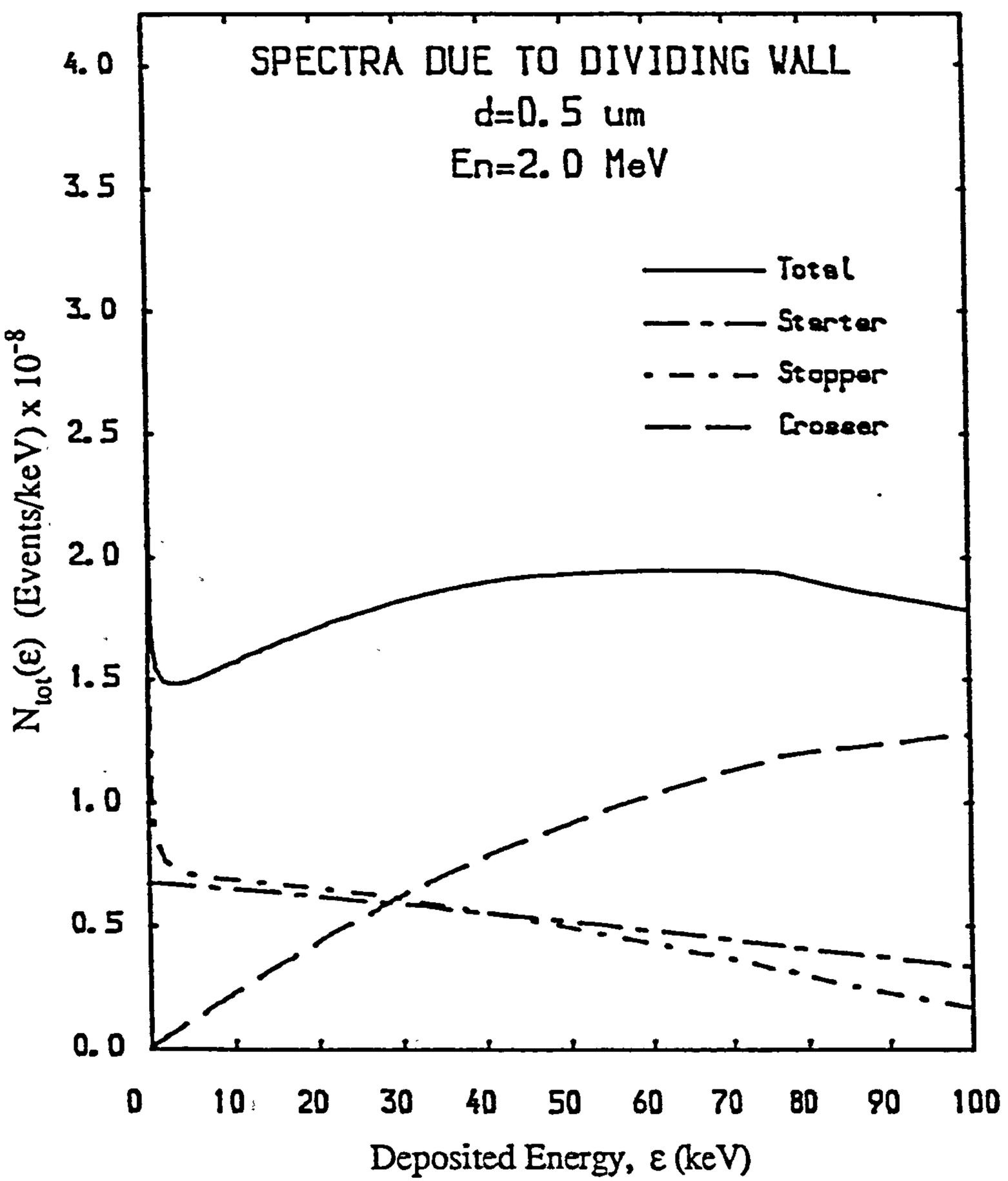

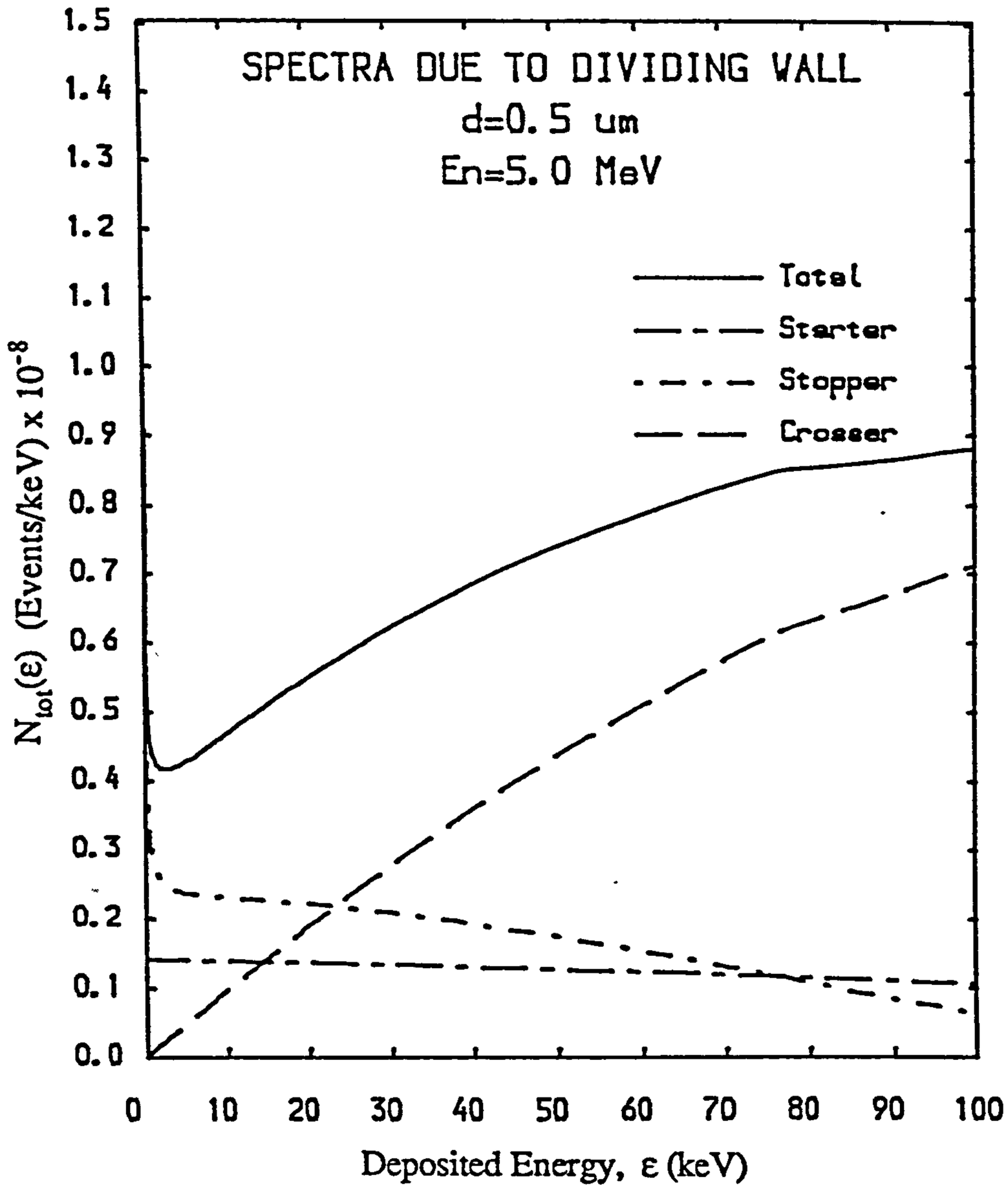

Fig. 3.39 Event spectra in a tissue sphere 0.5 μm diameter corrected due to the presence of dividing wall for (a) 2.0 MeV and (b) 5.0 MeV neutrons.

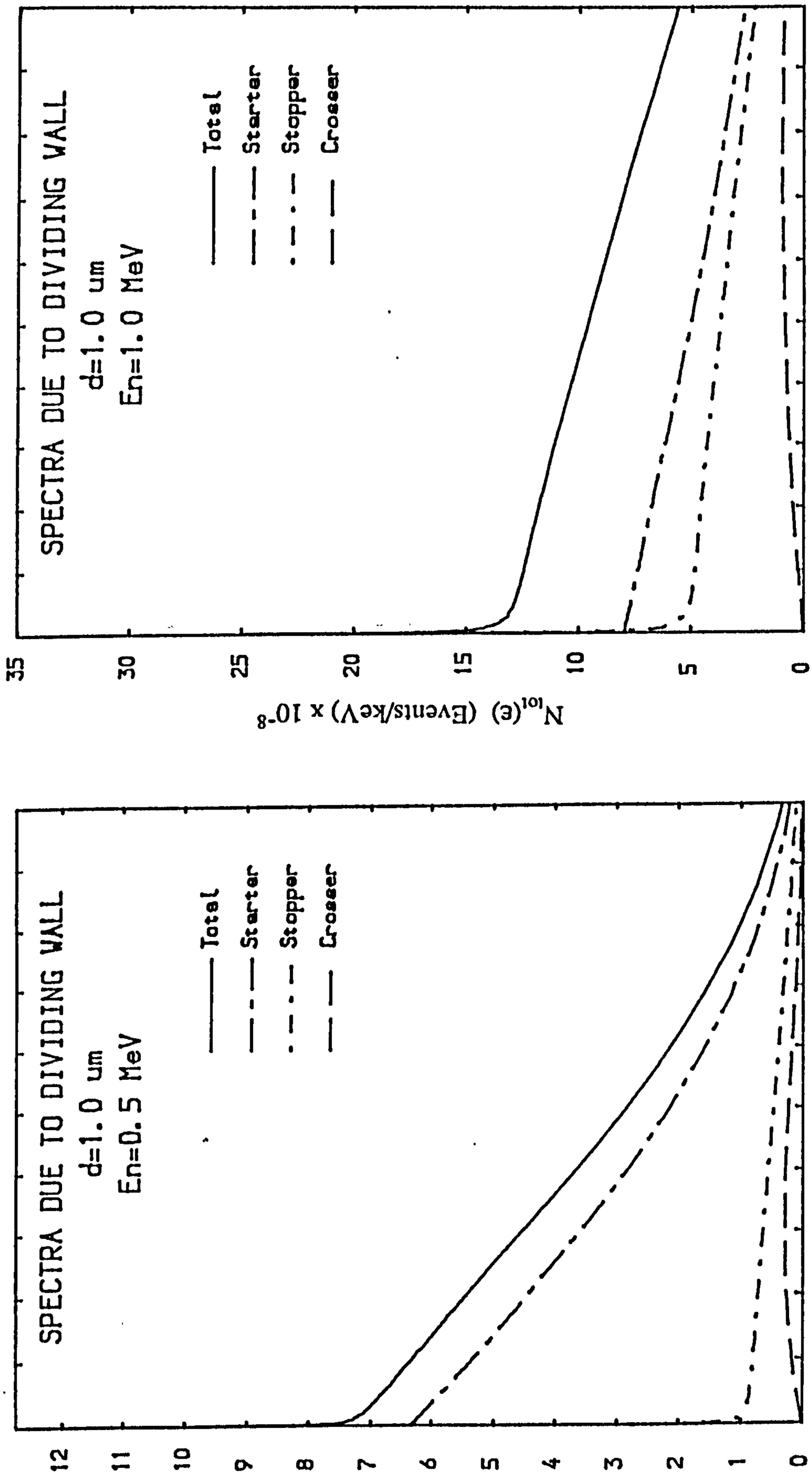

Fig. 3.40 Event spectra in a tissue sphere 1.0 μm diameter corrected due to the presence of dividing wall for (a) 0.5 MeV and (b) 1.0 MeV neutrons.

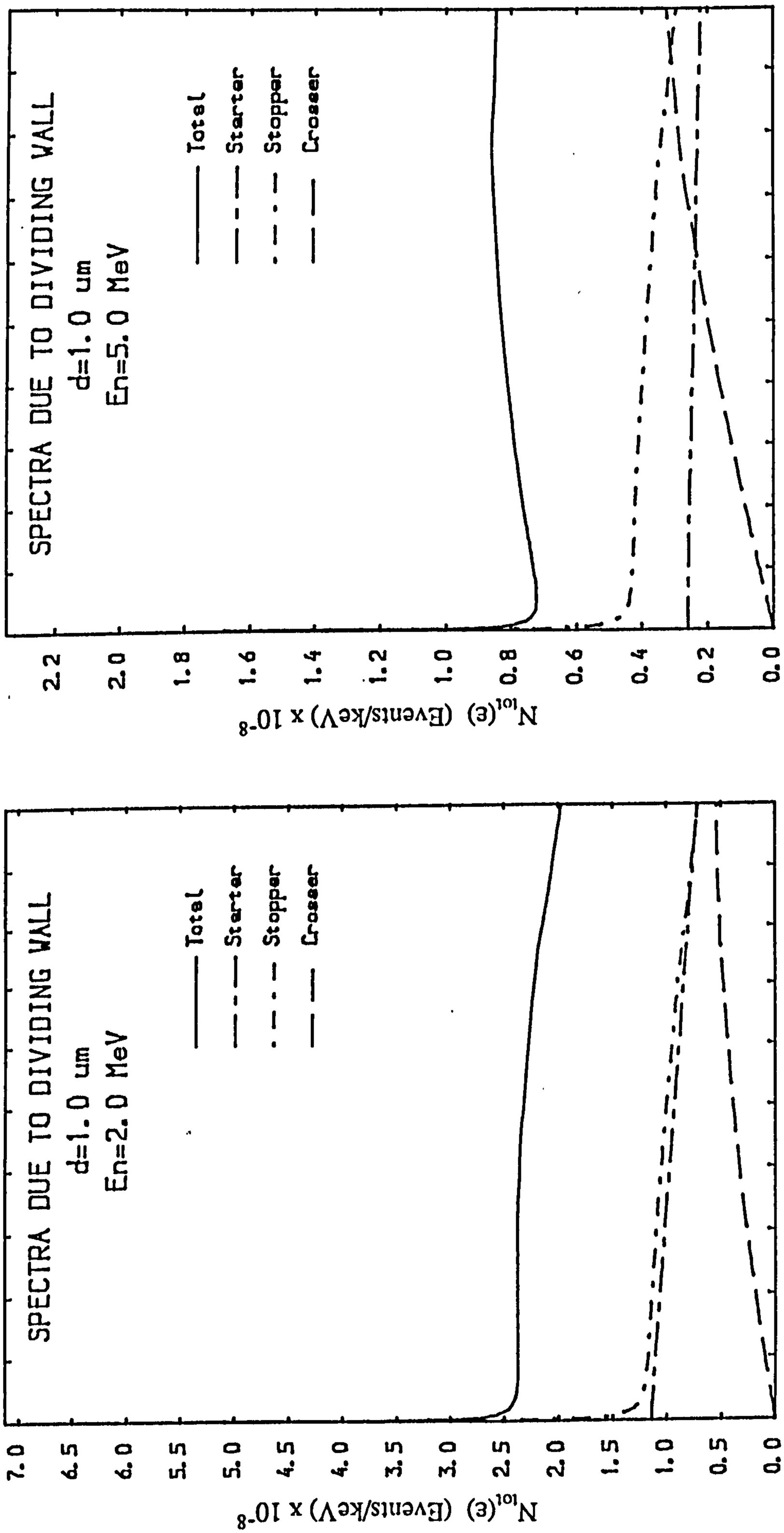

Fig. 3.41 Event spectra in a tissue sphere 1.0 μm diameter corrected due to the presence of dividing wall for (a) 2.0 MeV and (b) 5.0 MeV neutrons.

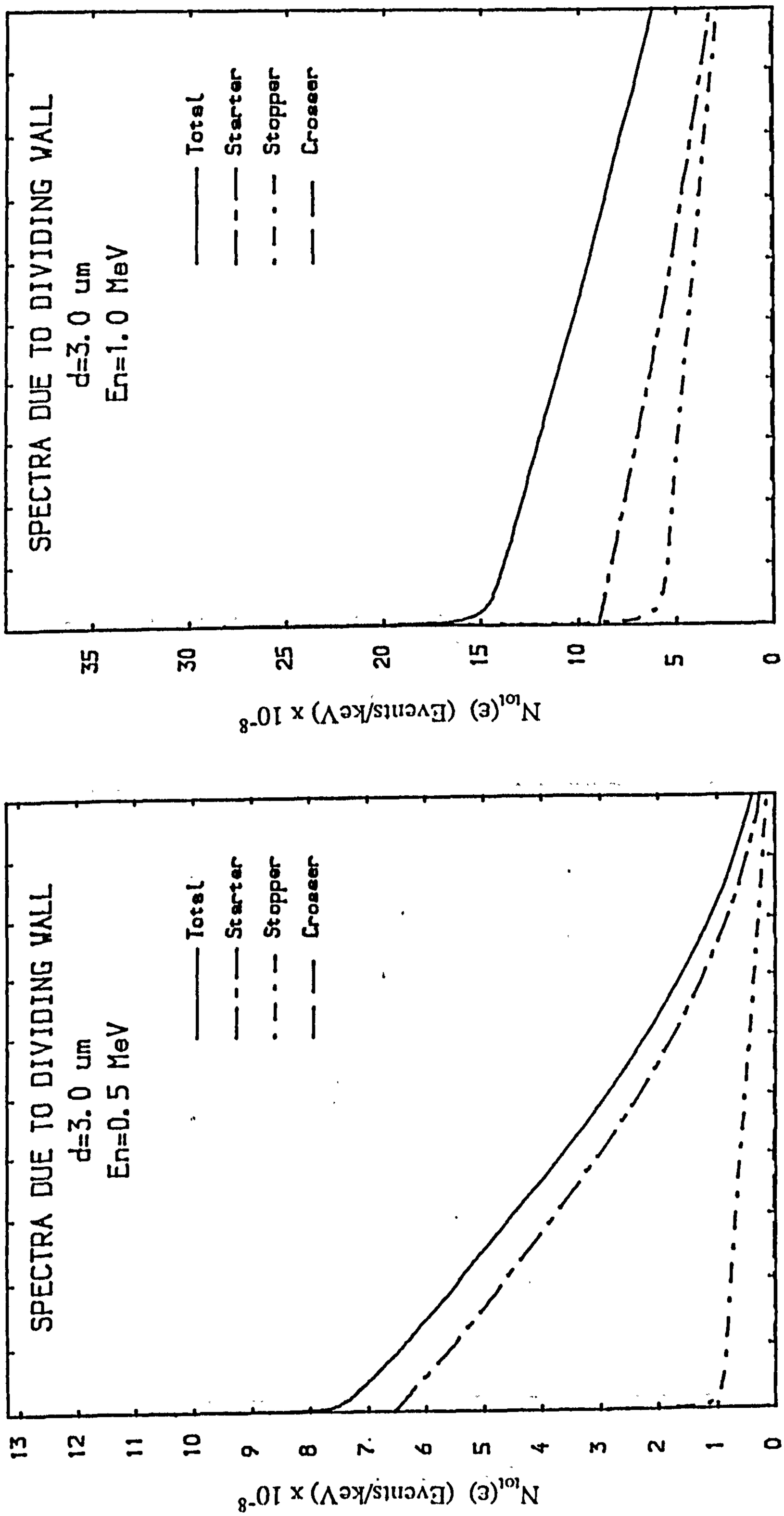

Fig. 3.42 Event spectra in a tissue sphere 3.0 µm diameter corrected due to the presence of dividing wall for (a) 0.5 MeV and (b) 1.0 MeV neutrons.

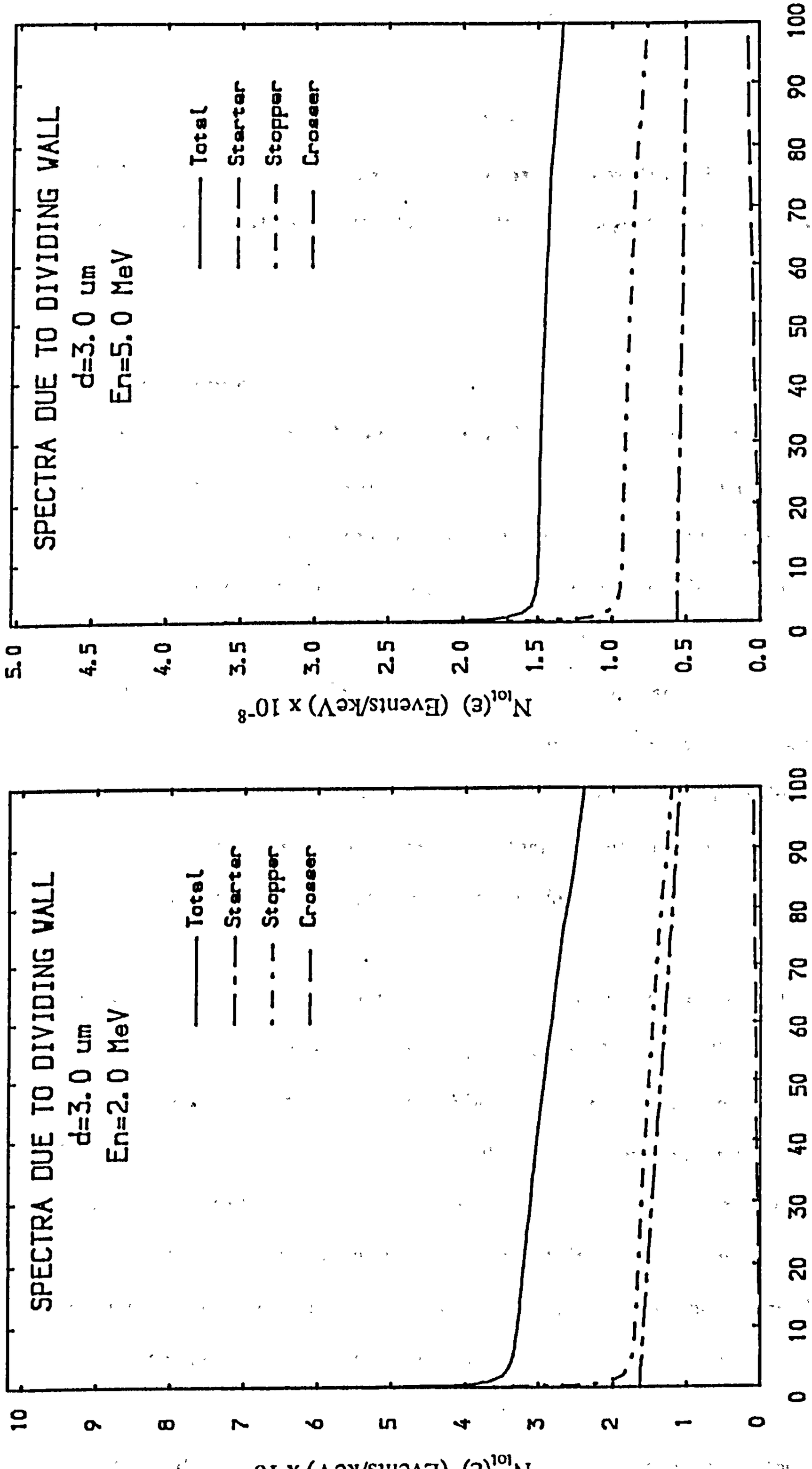

Fig. 3.43 Event spectra in a tissue sphere 3.0 μm diameter corrected due to the presence of dividing wall for (a) 2.0 MeV and (b) 5.0 MeV neutrons.

CHAPTER 4

EXPERIMENTAL:

TE Film Preparation, Design and Construction of the Co-Axial Double Cylindrical TEPC and Instrumentation

4.1 TE Film Preparation

4.1.1 Significance of TE Materials Used in Microdosimetry

For the purpose of tissue simulation it is important that the walls of a proportional counter used in microdosimetry are made from TE material and that the chamber is filled with TE gas so that the interaction cross sections and the mass collision stopping powers of charged particles in the gas cavity will be identical to those of tissue. Moreover, when the walls and the gas cavity have identical atomic composition, Fano's theorem can be applied. The theorem states that the fluence of the secondary charged particles is constant if the fluence of the primary particles is constant and that under this condition the fluence is independent of the density variation provided that the interaction cross sections and the stopping powers of particles are independent of the density (ICRU, 1983).

In the present study, the standard A-150 TE Shonka plastic was used to construct a co-axial double cylindrical proportional counter. The material was supplied in two forms by the Physical Science Laboratory, Illinois Benedictine College, USA, namely (a) in a pre-cast solid block used for the construction of TE walls of the outer counter and (b) in the form of plastic granules for use in the preparation of TE films. A-150 plastic is considered muscle equivalent in terms of hydrogen and nitrogen content (ICRU, 1964), with the substitution of carbon for oxygen to increase the electrical conductivity of the material for practical purposes. It also has a reasonable strength and is easy to shape and smooth.

TE gas used in microdosimetry serves a twofold purpose; as an interacting medium in which the energy deposition of charged particles is being measured, and as a counting gas.

The important criteria for the latter use are good characteristics in terms of large gas gain, linear response to the energy loss and small electronegativity which reduces the possibility of recombination occurring in the counter.

The standard propane TE gas was supplied by Air Product Ltd., UK., with the mixture of 55.09% C_3H_8, 39.5% CO_2 and 5.41% N_2. This gives the molecular weight of 43.17 and the density of 1.785×10^{-3} gcm^{-3} at 20 °C. The important criteria for the TE gas mixtures are the quality of tissue approximation and good homogeneity with the TE walls. Methane based TE gas has its carbon and oxygen content closer to that of standard muscle than to the A-150 plastic. In contrast, the carbon and oxygen content of propane based TE gas is closer to that of the standard A-150 TE plastic than muscle (ICRU, 1983). This difference in composition leads to the difference in stopping powers of charged particles in the gas and wall of the counter.

Awschalom and Attix (1980) and DeLuca (1981) have used other types of TE gas mixture that match the composition of A-150 TE plastic, with argon substituted for calcium. This would simplify the application of Bragg-Gray cavity theory, i.e. that the production of charged particle per unit mass in the gas and in the wall would be the same when both have the same composition. Consequently, the stopping power ratio between the gas and the wall is one. However, there is a deviation between the stopping power in the solid and in the gas phases of the same material for low energy charged particles (Thwaites and Watt, 1978).

The elemental composition of the ICRU tissues and TE materials are shown in Table **4.1.** This table indicates that there is no material which ideally meet the condition of tissue equivalence for all types and energies of radiation, since this equivalence depends on the mean energy expended per ion pair, the stopping power and the interaction cross sections, and also for various types of standard tissues such as muscle, bone, fat and lungs which are different in composition. Even if the wall and the counting gas are of the same composition, wall effects due to scattered tracks of the secondary charged particles can produce an increase in energy deposition in the counter leading to distortion of the measured spectrum. There are

four types of wall effect known as delta-ray effect, re-entry effect, V-effect and scattering effect in which details are given in ICRU (1983).

Table 4.1 The percentage composition of ICRU tissues and TE materials used in microdosimetric study.

Material	H	C	N	O	F	Ar	Ca	Others
Muscle [1]	10.2	12.3	3.5	72.9	-	-	0.007	1.093
CH_4 TE gas [1]	10.2	45.6	3.5	40.7	-	-	-	-
C_3H_8 TE gas [1]	10.3	56.9	3.5	29.3	-	-	-	-
A-150 TE Plastic[1]	10.2	77.6	3.5	5.2	1.7	-	1.8	-
A-150 Mix 4 [2]	10.2	76.8	3.6	5.9	1.7	1.8	-	-
A-150 Mix 5 [3]	10.2	76.8	3.6	9.04	-	0.36	-	-
Bone [1]	6.4	27.8	2.7	41.0	-	-	14.7	7.4
B-100 Plastic [1]	6.6	53.7	2.2	3.2	16.7	-	17.7	-

(1) ICRU (1977)
(2) Awschalom and Attix (1981)
(3) DeLuca (1981)

4.1.2 Method of Preparation of A-150 TE Plastic Films

TE film is a vital component in the construction of the co-axial double cylindrical TEPC, being used as a common dividing wall between the inner and outer counters. The film should have a thickness equivalent to the maximum range of protons generated by neutrons of the energy of interest in tissue. **Fig. 4.1** shows the thickness of A-150 plastic films calculated for neutrons at various energies less than 1.2 MeV. To enable the counter to operate for neutrons of energy 100 keV and 800 keV, thicknesses of 1.25 μm and 14.5 μm respectively are required.

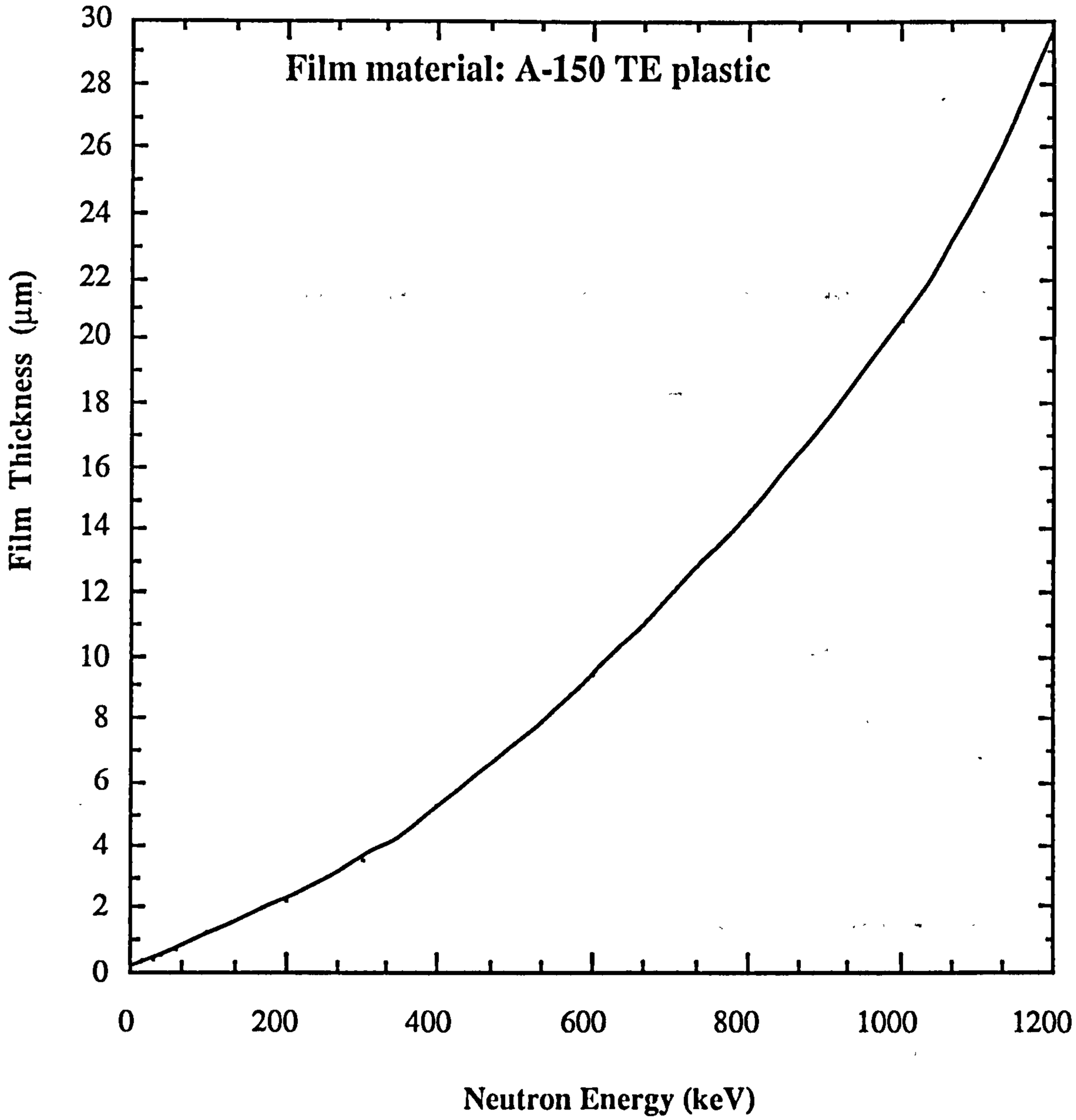

Fig. 4.1 Calculated thicknesses of A-150 TE plastic film corresponding to the penetration depth of the maximum energy proton recoils generated by the neutron energies shown. The film thickness determines the upper energy neutron detection threshold which can be read from the graph

While methods for the preparation of thin organic films are numerous, such as film stretching (Barrus and Blake, 1977) and dissolution and evaporation (Yeung, 1981), no method for the preparation of TE films has been reported. Further investigation is required in this field. The following experiment describes how TE films can be fabricated from a

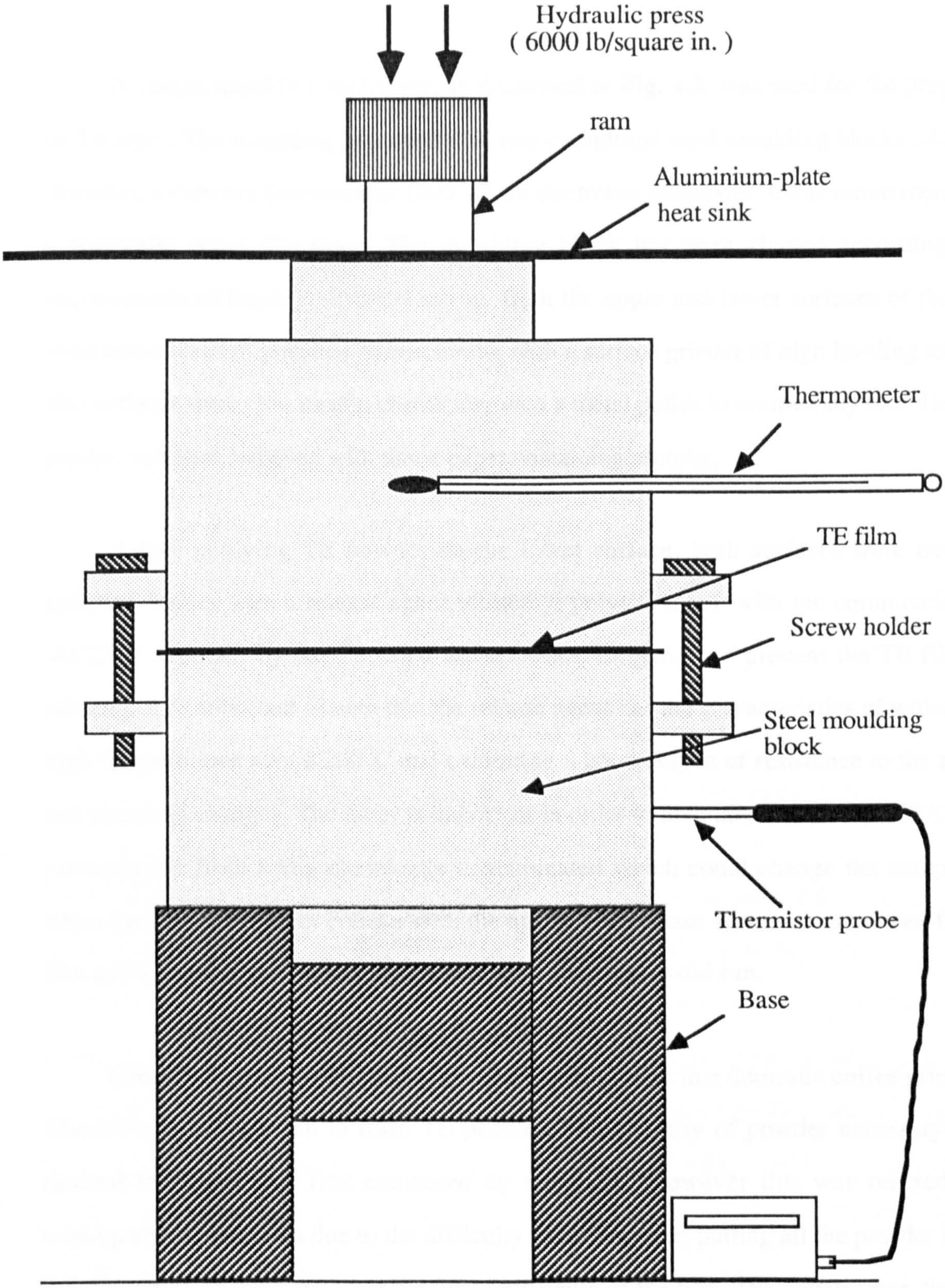

Fig.4.2 Side view of the moulding jig for the preparation of A-150 TE Shonka plastic film

commercial A-150 TE plastic.

A simple moulding technique, as illustrated in **Fig. 4.2**, was used for the preparation of TE film . The moulding jig consists of two cylindrical steel moulding blocks 14.0 cm in diameter, a mercury thermometer (200°C), an electronic-thermistor temperature monitor and a hydraulic press (20 tons). The moulding block has been shaped according to the requirements of the experimental set-up. Both the upper and lower surfaces of the mould were smoothed and polished by machining with a surface grinder of high leveling tolerance. The surfaces were then treated chemically with a metal polish to remove any dirt. The polish residue was then removed with tissue paper containing acetone.

Before applying TE powder on the lower surface, both surfaces were treated by spraying lightly with a release agent (dimethyl polysiloxane), with the commercial name 'ACCEL' supplied by the Certified Laboratories, England, to prevent the TE film from sticking. It is important to note that the release agent has the characteristics of withstanding high temperatures above 200°C and exhibiting a good degree of resistance to the physical and chemical changes. The latter is important in order to maintain the quality of TE film by preventing it from being chemically contaminated which could change the composition, when the film is in direct contact with the agent. The release agent was removed from the film using tissue paper containing acetone after each successful run.

Commercial A-150 TE plastic granules were ground in a domestic coffee grinder and filtered with a silk cloth to form TE powder. The quantity of powder necessary for the desired thickness was first estimated by weighing. However this was relaxed in the subsequent experiments due to the difficulty experienced in putting all the powder onto the mould surface without affecting the final uniformity of the film. The powder was distributed evenly on the lower surface by shaking the filter, the amount required being inspected by visual observation. The upper block was then placed into position guided by three metal rods which were used to prevent the block from tilting over while under high pressure. The mould was then heated up gradually using a flame torch to a temperature of approximately

170°C for about 2 minutes and then compressed to 41.38 MPa (6000 lb./ in^2). The pressure was maintained for about 80 minutes before allowing the temperature dropped to approximately 60°C. The temperature of the mould was monitored by a mercury thermometer and a thermistor probe. The temperature and the pressure applied in the experiment are within the recommended values given by ICRU (1977). It was found that reducing the cooling time by about half improved the quality of the film. This was achieved by blowing cold air directly onto the mould and by using an aluminium plate placed between the mould and the ram as a heat sink.

Three screws were used to jack up the upper moulding block before removing. This became routine procedure because of the formation of a vacuum space between the blocks while under high pressure. The film remained attached to the lower surface and was extracted very gently by hand.

4.1.3 Film Thickness Measurements

There are various methods by which film thickness can be measured. They depend on one or more quantities such as the mass absorption coefficients for X-rays, the stopping power for β- and α-particle absorption methods and the refractive indices of material in laser interferometry. The beta absorption method has the drawback of depositing too low an energy to give a good signal-to-background ratio. Also, the alpha absorption method is a non-absolute method which required calibration with the known thickness of material under investigation. It has been reported that a microbalance weighing method was very accurate with an uncertainty of less than 1% for the measurement of polythene film of thickness 0.1 μm (Yeung, 1981). It is absolute and non-destructive. However it can only be used if the uniformity of the thickness is known.

We adopted the weighing method for measurement of the film thickness for three main reasons: 1) it is simple, relaible and reproducible, 2) the method is non-destructive since the film will be used after weighing and 3) the method yields directly the areal density or film thickness. Several attempts have been made to make good quality TE films of various

thicknesses. The quality was determined by visual inspection of the films for uniform distribution of carbon in the plastic, film size, formation of holes the size of pin tips and tear.

The best TE film was selected from a batch of films prepared in the previous experiment. The film was cut to the required size and measured to 0.5 mm using a venyl clipper. The weight was then determined using two microbalances to an accuracy of less than 0.1%. Both the mechanical and semi-electronic microbalances reproduced the weight to within 0.1 mg. The thickness of the film was determined simply by the ratio of the weight to the area and density. The density of the film was taken as 1.116 g cm^{-3} which is for bulk TE plastic (Waker, 1988). The accuracy of the result was checked using a micrometer gauge. The average thickness was calculated from several measurements at points randomly selected on the film. However the standard error obtained by the micrometer gauge is the minimum scale divided by two, since all the measurements produced about the same results. **Table 4.2** tabulates the results from both measurements for a TE film of area of 8 cm x 9 cm and weighing at 130.3 mg. The standard error obtain from the weighing method was calculated according to the standard error formula. The mass, area and density measurements produced errors as much as 0.1 mg, 0.1 cm^2 and 0.001 g cm^{-3} respectively. The thickness obtained from the weighing method is taken as the actual thickness of the TE plastic film prepared for this project.

Table 4.2 The thickness of A-150 TE plastic film measured by weighing and gauge methods

Method	Thickness (μm)	Error
Weighing	16.20 ± 0.049	± 0.3 %
Micrometer gauge	17.78 ± 1.32	± 7.4 %

It is very important to note that several factors inherent in the moulding technique have the drawback of producing thicker films than required. The quantity of powder used predetermines the thickness achieved. However, when the quantity is very small, thin films of thickness less than 5 μm were formed at various spots, since not enough plastic material was present to flow on the mould surfaces. On the other hand, when the quantity was increased slightly, the plastic film concentrated at the centre, thereby reducing the film size. The size of TE film required was about 8 cm x 7 cm. A compromise must be made between the thickness and the size of the film. Hot stainless steel rollers of temperature 150 - 160 °C have been used to reduce the film thickness from 20 μm to well below 10 μm. Nevertheless, the quality of the films deteriorated due to the formation of pinholes and the uniformity was difficult to maintain because the films became thinner at the edges than at the centre.

4.1.4 Film Thickness Uniformity Measurement

Although the mould surfaces were constructed using a grinding machine of very high leveling tolerance, it is wrong to assume that the thickness uniformity has been satisfied. An alpha particle absorption method has been used to measure the film uniformity with the assumption that the distribution of carbon molecules in the film is uniform. The experimental apparatus is a typical energy loss measurement set-up as shown in **Fig. 4.3.** It is a vacuum chamber 18 cm in diameter and 6 cm in height. Inside are arranged an ^{241}Am alpha source, a silicon surface barrier detector, brass collimators 1.0 mm in diameter and a sample holder. The detector was a ruggedized Neutronics silicon surface barrier detector, 200 mm^2 active area with 100 μm depletion layer depth and 40 $\mu g/cm^2$ aluminium window and having alpha resolution of 18 keV FWHM. The electronic instruments consist of a preamplifier (ORTEC Model 125), a main amplifier (ORTEC Model 472A) and a multichannel analyser. The sample holder can rotate the film across the particle beam at a number of randomly selected points. It is necessary to adjust the position of the film in order to cover the whole area.

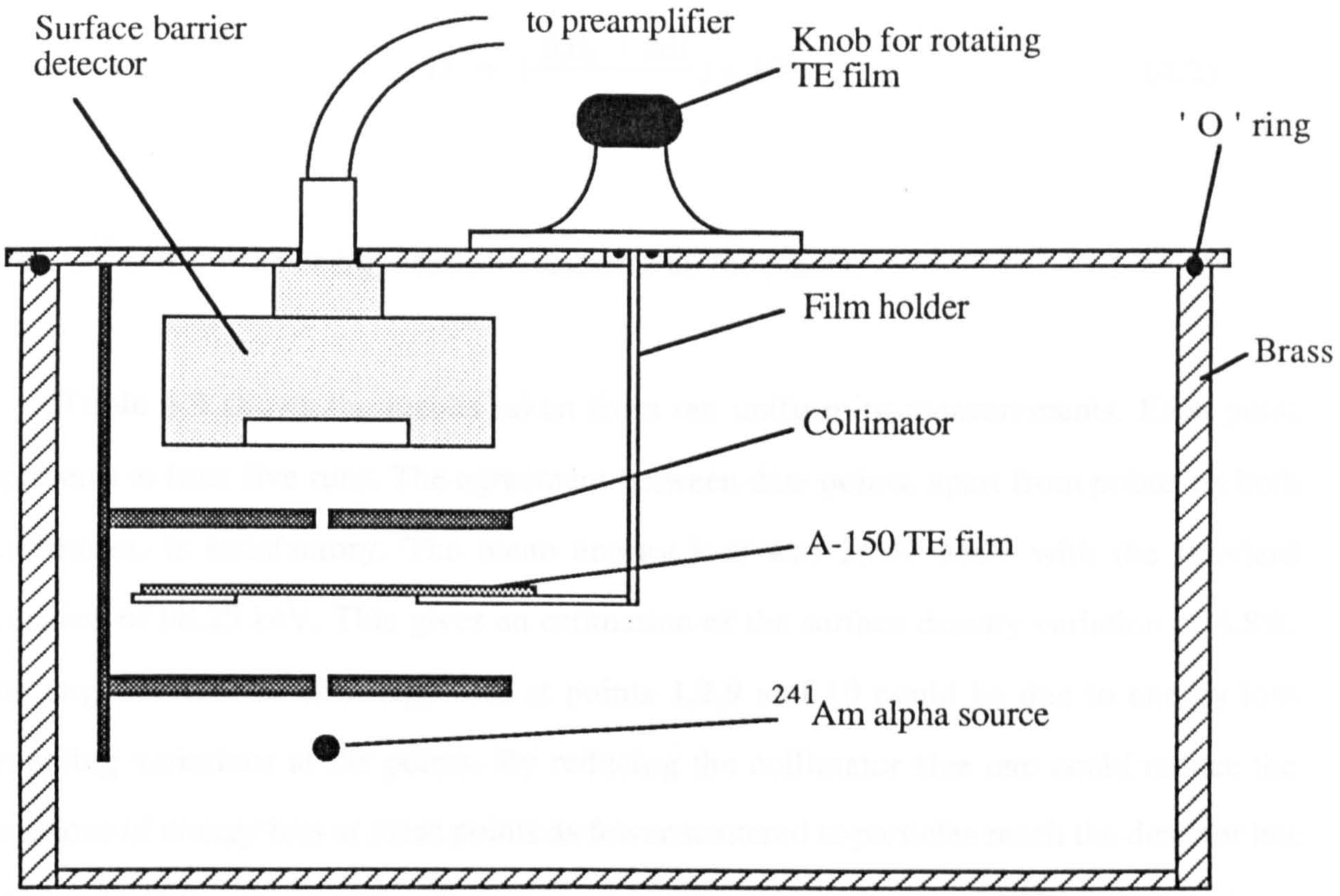

Fig. 4.3 Vacuum chamber used in energy loss measurements of alpha particles for the determination of A-150 TE film thickness uniformity

The uniformity of the film thickness was determined by measuring the energy loss of alpha particles across the film at the selected points. The spectrum of energy loss was displayed on a MCA which was calibrated using a multiple alpha source containing ^{239}Pu (E_α=5.157 MeV), ^{241}Am (E_α=5.486 MeV) and ^{242}Cm (E_α=5.806 MeV). The film thickness uniformity can be expressed quantitatively in terms of the deviations of the energy loss from the mean value at the selected points. The energy loss at any given point, i, is represented by

$$\Delta E_i = (5486 - E_{\alpha i}) \text{ keV} \qquad (4.1)$$

where $E_{\alpha i}$ is the transmitted energy of alpha particles at point i as determined from the calibration curve. The deviation of the individual energy loss is simply given by

$$D = \left(\frac{\Delta E_i - \Delta\bar{E}}{\Delta\bar{E}}\right) \times 100 \qquad (4.2)$$

where $\Delta\bar{E}$ is the mean energy loss calculated for all the points.

Table 4.3 shows the results taken from ten uniformity measurements. Each point represents at least five runs. The agreement between data points, apart from points on both extremities, is satisfactory. The mean energy loss was 2.047 MeV with the standard deviation of 98.25 keV. This gives an estimation of the surface density variation of 4.8%. The large deviations of energy loss at points 1,2,9 and 10 could be due to energy loss straggling variations at the points. By reducing the collimator size one could reduce the variations of energy loss at these points as fewer scattered α-particles reach the detector but only by sacrificing the counting time.

Table 4.3 Energy loss variations in the thickness uniformity measurements of A-150 TE plastic film

Data point	ΔE_i (keV)	$\Delta E_i - \Delta\bar{E}$ (keV)	D %
1	1916	-131	-6.42
2	1920	-127	-6.23
3	1980	-74	-3.64
4	1980	-67	-3.27
5	2057	10	0.46
6	2077	30	1.44
7	2078	31	1.49
8	2110	63	3.05
9	2157	110	5.34
10	2207	160	7.79

4.2 Fundamental Aspects in the Counter Design

The goal of the present study is to design and develop a new microdosemeter, a co-axial double cylindrical TEPC, which can be used to determine the quality factor and dose equivalent of neutrons at a selective energy in mixed radiation fields. There are some aspects that must be satisfied in the design including those of the materials of construction and the counter operation for better performance. The final design in the present work is ultimately a compromise between ease of construction which depends on the technical facilities available and utility.

4.2.1 Materials of Construction

Apart from the dividing wall, other components found in this design are common in the convential TEPCs. The wall must be self supported tissue equivalent material with good electrical conductivity as an electrode. There are several ways in which the dividing wall could be constructed. Al-Affan (1985) has made an attempt to construct this type of counter in which copper micromesh having transmission of 93 % was used to separate the inner and outer counters. This made the inner counter effectively a wall-less counter and forced only the recoil particles due to insiders to be of significance, thereby reducing the sensitivity of the counter. Nevertheless, the onset of electrical breakdown cannot be resolved. An organic film could be mounted on the mesh to form a dividing wall and it should have the strength to be self supporting, since the micromesh apparently is not strong enough to use as a support without affecting it shape. A self-supported aluminised polyester film (thickness ≈ 2.5 μm) has been successfully used for the dividing wall (Saion and Watt, 1988), but the counter is the non-tissue equivalent. The coated aluminium is used to increase the electrical conductivity. TE film made from A-150 plastic has been used for the dividing wall in the final version of the counter because it satisfies the dual requirement of tissue equivalence and electrical conductivity.

A-150 TE plastic is a common material used in TEPC design for the walls where the slowing-down spectrum within the counter primarily originates.The minimum thickness is determined by the maximum range of the secondary charged particles.

Metals are commonly used to enclose the counter to enable electrostatic screening and to ensure a good vacuum. Low atomic number materials such as aluminium should be used to minimise the background counts caused by gamma-rays generated from neutron interactions with the canister. The anode material could be considered a minor perturbation as far as neutron interaction is concerned.

4.2.2 Saturation Factor

The electric field strength at the wall of the counter must be sufficiently high to prevent the loss of intrinsic detection efficiency due to recombination and attachment of ion pairs. The saturation is given in terms of the ratio of electric field strength, X, to the gas pressure, P. When the saturation of ion collection is achieved, the pulse height generated by the counter will be constant for an equal energy deposition. Therefore, the counter will have a linear response to the energy loss. Watt (1967) has determined the saturation factor for alpha particles in various gases. **Table 4.4** shows the saturation factors of some gases and the minimum operating voltages for a counter of radius 1.0 cm, anode radius 0.0125 mm and applied pressure 50 torr, filled with the respective gas.

Table 4.4 The saturation factor of some gases and the minimum voltage applied to a counter of diameter 2.0 cm, anode radius 0.0125mm and gas pressure of 50 torr

Parameter	CO_2	CH_4	P_{10}	CH_4 TE gas
$\frac{X}{P}$ ($Vcm^{-1}torr^{-1}$)(1)	1.0	0.8	0.2	0.85
Voltage (V)	300	240	60	255

(1) Watt (1967)

4.2.3 Sufficient Gas Gain for Counter Operation

The gas gain of TEPC must be sufficiently large so that the pulse produced by a single ion pair will be recorded above the noise level of the associated electronics. The typical noise generated from an ORTEC nuclear electronic system consisting of a preamplifier (Model 142PC) and an amplifier (Model 474A) is 1mV. The preamplifier has a feedback capacitance of 0.15 pF and when connected to the TEPC, assuming the counter capacitance being 1.0 pF, the creation of a single ion pair will produce a pulse of 1.23 μV. Since the amplifier has a minimum gain of 5, then the counter signal becomes 6.15 μV. Therefore a gas gain greater than 163 is required so that the pulse generated from one ion pair can exceed the noise level.

4.2.4 Voltage Screening and Field Shaping

The high voltage insulation required for every TEPC design, can be achieved using PTFE. Also, the anode wire should be screened from all voltage insulators to minimise spurious counts by the application of guard tubes. The guard tube voltage, V(r), at radius r from the centre of the anode is given by

$$V(r) = V_0 \frac{\ln(b/r)}{\ln(b/a)} \qquad (4.3)$$

where V_0 is the anode voltage, a is the radius of the anode and b is the radius of the counter. It is important to maintain the uniformity of the electrical field throughout the sensitive volume so that gas multiplication along the anode is constant. The application of field tubes can improve the field non-uniformity at the ends of the anode.

4.3 Construction of the Counters

Two co-axial double cylindrical proportional counters have been designed and constructed as shown in the photograph of **Fig. 4.4.** The following describes details of the non-tissue and tissue equivalent versions.

4.3.1 Non-Tissue Equivalent Counter

In the first instance a prototype non-tissue equivalent co-axial double cylindrical proportional counter has been designed and constructed. The technical aspects of the design and construction have been studied. A photograph of **Fig. 4.5** shows the internal part of the counter in which the common dividing wall of aluminised polyester of thickness 2.5 μm is clearly shown forming a good cylindrical shape. The inner counter was first assembled and then inserted into the outer counter. After all the insulation and screening problems had been satisfied we found difficulty in overcoming the presence of spurious counts in addition to the pulses generated from ionizing radiations. We had discovered that the major cause of electrical sparking was due to the construction of the self-supporting dividing wall. The sharp edges of the aluminised polyester film have been recognised as the cause of the sparking problem. After folding over the sharp edges the counter worked perfectly.

The technical aspects of the design and the operational characteristics of this counter have been described (Saion and Watt, 1988). **Table 4.6** illustrates the construction features of the prototype non-tissue co-axial double cylindrical proportional counter.

When all the technical aspects of the counter design have been studied and satisfied, including the calibration problem, the next stage is to design and construct a new tissue equivalent version of the counter.

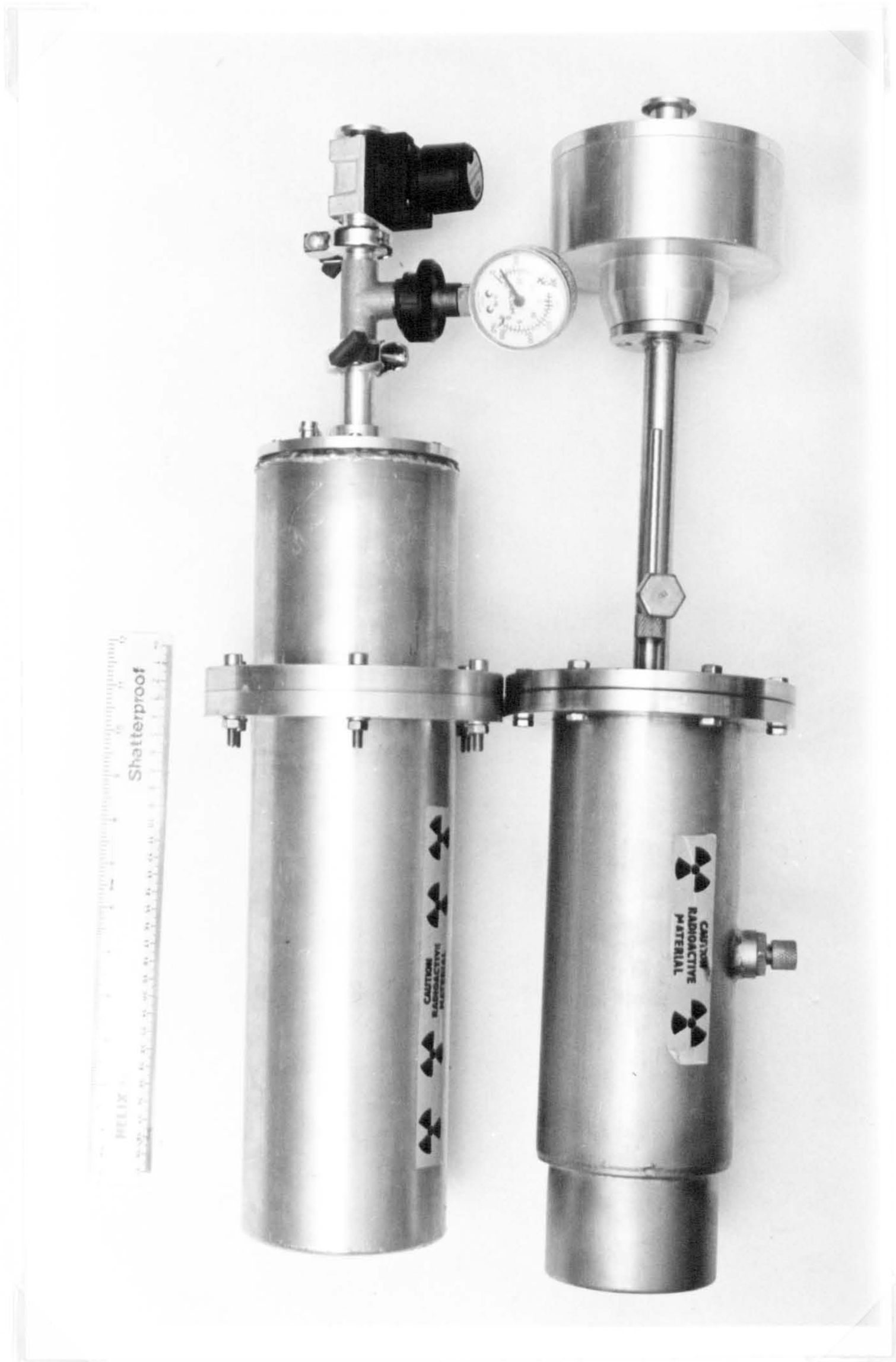

Fig. 4.4 Photograph of tissue equivalent and non-tissue equivalent co-axial double cylindrical proportional counters in their final form. The former is shown with its pressure gauge connected.

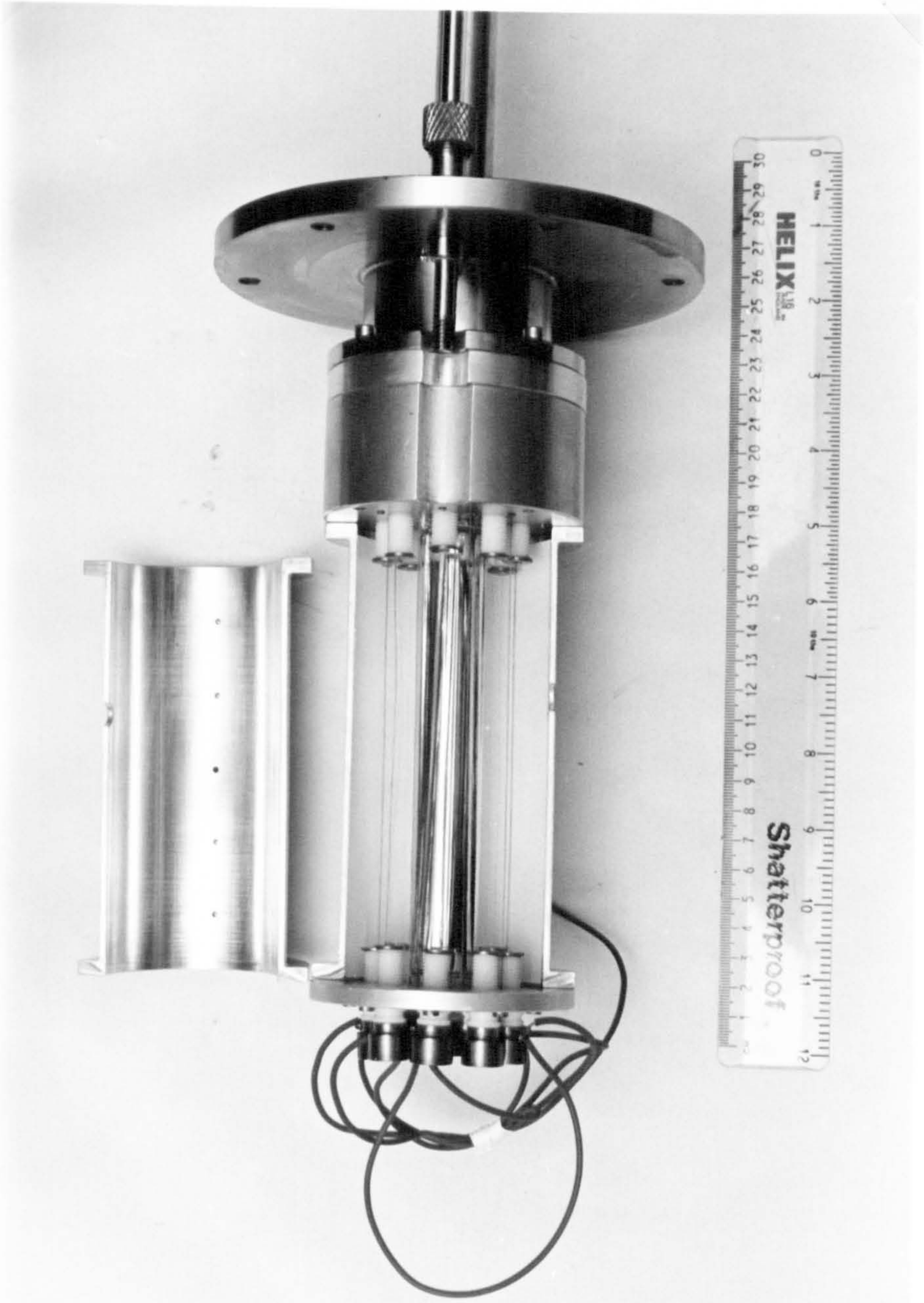

Fig. 4.5 Photohraph of the internal part of the non-tissue equivalent co-axial double cylindrical proportional counter. The wall of the outer counter is split open when the picture was taken to view the 2.5-µm common dividing wall which is clearly shown in the middle.

Table 4.6 Constructional features of the prototype non-tissue equivalent co-axial double cylindrical proportional counter

Feature	Inner Counter	Outer Counter
Diameter, d (cm)	2.0 ± 0.05	2.0 ± 0.05
Length, h (cm)	9.5 ± 0.05	11.8 ± 0.05
Mean chord length, l (cm)	1.81	1.84
Wall material	polyester	aluminium
Wall Thickness	2.5 μm	1.5 mm
Number of anode	1	8
Capacitance	0.87 pF	7.2 pF

4.3.2 General Description of a Co-Axial Double Cylindrical TEPC

The prototype co-axial double cylindrical TEPC has been designed and constructed as shown in the photograph of **Fig. 4.6**.The schematic drawing of the counter is given in **Fig. 4.7.** The new microdosemeter consists of an outer annular eight-anode multiwire TEPC and an inner single-anode TEPC. They are separated by a dividing wall of A-150 TE plastic of thickness 16.2 μm. The thickness of the dividing wall is equivalent to the range of protons of energy 850 keV as deduced from **Fig. 4.1.** The inner and outer TEPCs can be operated in coincidence and anti-coincidence for neutrons of energy greater than 850 keV in which protons of energy greater than 850 keV penetrate the dividing wall and give a response in both the inner and outer counters. Protons of energy less than 850 keV cannot pass through the dividing wall and the event can be detected in the inner counter when operated in anti-coincidence with the outer counter. Alternatively, the counter could be used to operate independently from each other as in ordinary TEPCs for neutrons of energy greater than 100 keV.

The counter is enclosed in an aluminium canister 1.0 mm in thickness to provide electrostatic screening and to form a high vacuum enclosure. The dimension of the microdosemeter was chosen in order to satisfy several basic practical limitations, namely :

Fig. 4.6 Photograph of the co-axial double cylindrical tissue-equivalent proportional counter

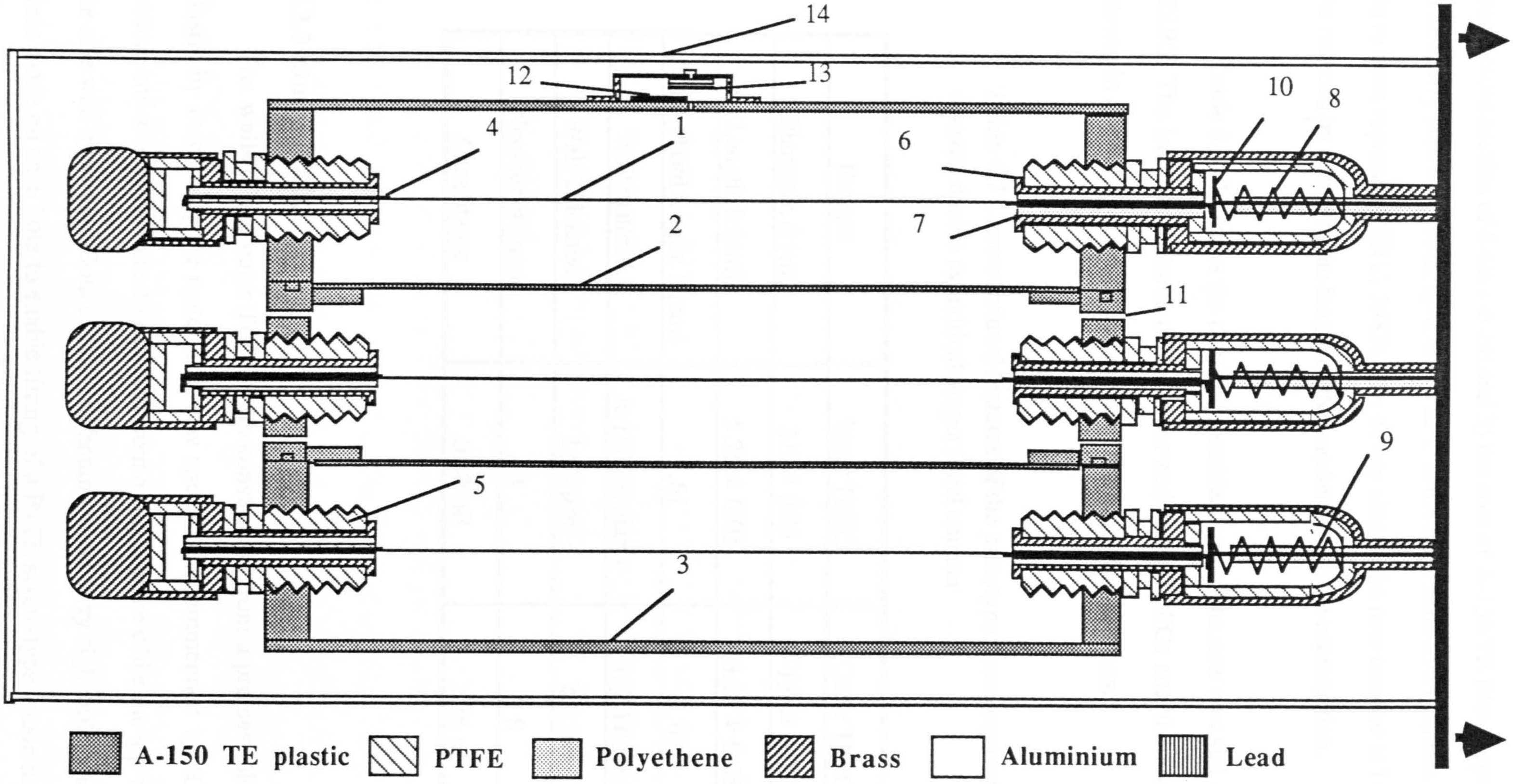

Fig. 4.7 Schematic drawing of the Co-Axial Double Cylindrical TEPC; 1. Anode, 2. Dividing Wall, 3. Outer Wall, 4. Copper Wire, 5. Insulator, 6. Guard Tube, 7. Insulator Tube, 8. Spring, 9. Co-Axial Cable, 10. Contact Plate, 11. Hole for Gas Filling, 12. Lead Shutter, 13. Alpha Internal Source, 14. Electrostatic and Vacuum Canister.

1) the cavity size, 2) the available size of a pre-cast block of A-150 TE plastic which has a cross section of 6 cm x 6 cm and 3) the area of A-150 TE film prepared for this work. The cavity size for 1-inch. spherical TEPC is 6.4 cm^3. Sensitive volumes as low as 0.2 cm^3 have been reported (ICRU, 1983). The cavity size of the new counter is 14.9 cm^3 and could be reduced by reducing the length of the anodes during the construction.

Table 4.7 illustrates the constructional features of the new co-axial double cylindrical TEPC. The internal features of the inner and outer TEPCs and the anode assembly are shown in **Fig 4.7** and details are given in the following sections.

Table 4.7 Constructional features of the prototype tissue equivalent co-axial double cylindrical proportional counter

Feature	Inner TEPC	Outer TEPC
Diameter, d (cm)	1.9 ± 0.05	1.9 ± 0.05
Length, h (cm)	5.25 ± 0.05	5.25 ± 0.05
Mean chord length, *l* (cm)	1.61	1.61
Wall material	A-150 TE plastic	A-150 TE plastic
Wall Thickness	16.2 μm	2.0 mm
Number of anode	1	8
Capacitance	0.49 pF	2.76 pF

4.3.3 Outer TEPC

The walls of the outer TEPC were constructed from a pre-cast block of A-150 TE plastic by machining the material at low speed as recommended by ICRU (1977). The bottom and side walls were constructed from a single piece while the top wall was joined to the side wall by screws. Both the top and bottom walls carry eight holes each. Screw threads were made on each hole to enable fitting of a PTFE screw-type anode assembly. Cathode wire of diameter 0.5 mm was fixed centrally between two anodes on the same circumference

as the anodes and anchored by screws. This arrangement is necessary to improve the electric-field uniformity of the outer counter.

Prior to the anode and cathode assembly, the outer counter was cut equally into two sections along the length which opened up for easy assess to the inner counter during construction and for inspection of the anode tension. This leaves a 1.5 mm gap along the walls in the final assembly which provides an opening for gas filling. All anodes were terminated at a point by co-axial cables and connected to a BNC (SHV type) for an output connection.

4.3.4 Inner TEPC

Two cylindrical discs of diameter 1.9 cm were constructed from A-150 TE plastic to form the top and bottom walls of the inner counter and also to provide supports for the construction of the common TE dividing wall. They were fixed to both ends of the outer counter by super glue. The top and bottom walls have been provided with a hole similar to that of the outer counter and with a ring groove for the termination of the TE dividing wall by a metal coupling. TE film of required size was rolled and suspended on the discs which guide the film to form a cylindrical shape. The edges of the film were folded over so that no sharp edges are exposed since they could generate a high electric field and cause spurious counts due to sparking.

Prior to the construction of the dividing wall the anode of the inner TEPC was assembled and the anode tension adjusted. Gas filling of the inner TEPC was achieved via eight holes of diameter 1.0 mm, drilled on each side of the top and bottom walls.

4.3.5 Anode Assembly

Some important modifications commonly applied to single-anode proportional counters have been made to reduce the complexity of the anode assembly, without affecting the overall performance. Field tubes are absent in the present design which could cause the electrical field non-uniformity due to an abrupt transition from the sensitive region to the

dead regions near the ends. All anode wires were soldered to much thicker copper wires of diameter 0.3 mm at both ends with the objective of terminating the gas multiplication near the ends and also using them as anchors for the anodes. All anodes were made from Cu/Be (98:2) wires of diameter 0.05 mm. This wire has special features in terms of strength and ease of soldering.

To construct the anode assembly the copper wire which carried the anode was inserted into an insulator consisting of PTFE and polyethylene tubes of thickness 0.3 mm and 1.1 mm respectively. The insulator was then placed into a guard tube made from brass. Surrounding the guard tube is PTFE insulation with threads on the outside to form a screw-type anode assembly. The anode assembly can be assembled on the top and bottom ends of the counter like a screw. By turning the anode assembly the tension of the anode can be adjusted. The threads also perform as charge dampers.

4.4 Gas Filling and High Vacuum System

The new microdosemeter requires routine gas filling which has been achieved using a high vacuum system specially assembled for use throughout this work as shown in the photograph of **Fig. 4.8**. A schematic diagram of **Fig. 4.9** shows the gas filling and high vacuum system. A rotary pump which is incorporated with a pirani gauge, P1, was used for rough and backing pumping while the water-cooling diffusion pump was used for high cold pumping monitored by a penning gauge, P2. A pressure gauge P3 (100 torr) which has been calibrated with a mercury manometer was used to measure the pressure of the counter.

The counter was pumped down to 5.0×10^{-6} torr continuously for 24 hours and then flushed several times with TE gas before it is ready for use. Both the flushing and filling of TE gas were done at a slow rate as a safety measure against breaking the TE dividing wall due to a sudden pressure difference between the inner and outer TEPCs. A pressure gauge P4 (760 torr) was used to monitor this process. Gas purity, which is directly affected by gas contamination due to outgassing of the materials in use, gas diffusion through sealing gaskets and molecular dissociation in the avalanche, is a very important factor in TEPC operation in order to ensure gas gain and resolution stabilities. A steady flow of TE gas could be applied to avoid from gas contamination by adjusting valve V6 and a regulator R. But the need for eliminating the use of the gas-flow system is obvious for practical reasons mainly because of the time to obtain a stable pressure was inconveniently very long. Therefore, the counter has been kept at a constant pressure throughout the measurement by the closure of an isolation valve V9. In this case the operation of the counter was restricted to eight hours before filling again with fresh TE gas. The stability of the counter performance is good as the gas gain only dropped by 8-10 % after five days without refilling.

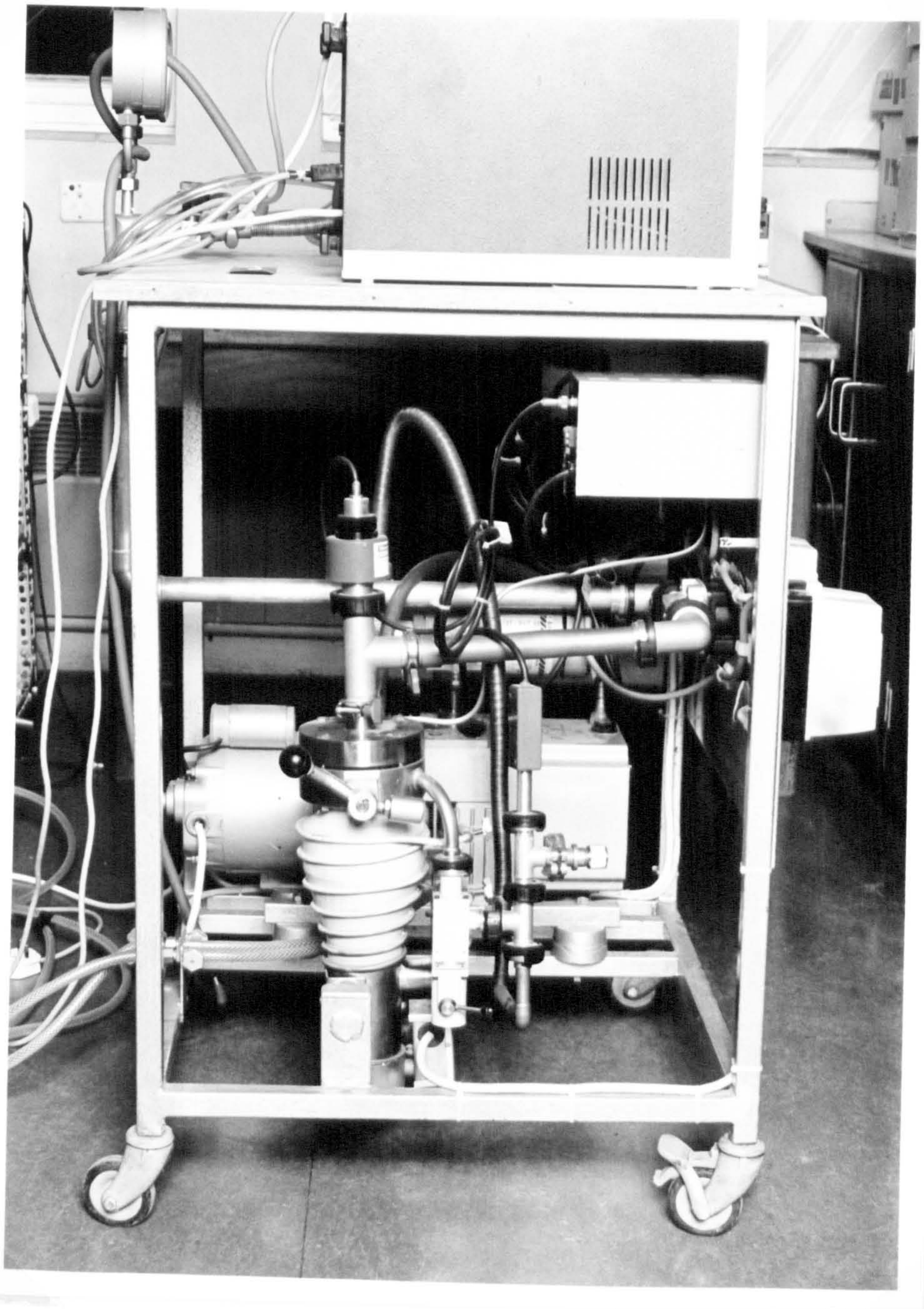

Fig. 4.8 Photograph of the high vacuum system used for gas filling.

Safety measures have been included in the high vacuum assembly to protect the system from damage due to the possibility of water and power interruptions when unattended. The diffusion pump will be switched off automatically during these interruptions and can only be switched on manually to continue pumping. However the rotary pump will resume normally when the electrical power has recovered. A high vacuum electromagnetic air admittance valve has been fitted in the transmission line immediately next to the rotary pump to prevent air and lubricating oil from being sucked into the vacuum chamber when the system is switched off.

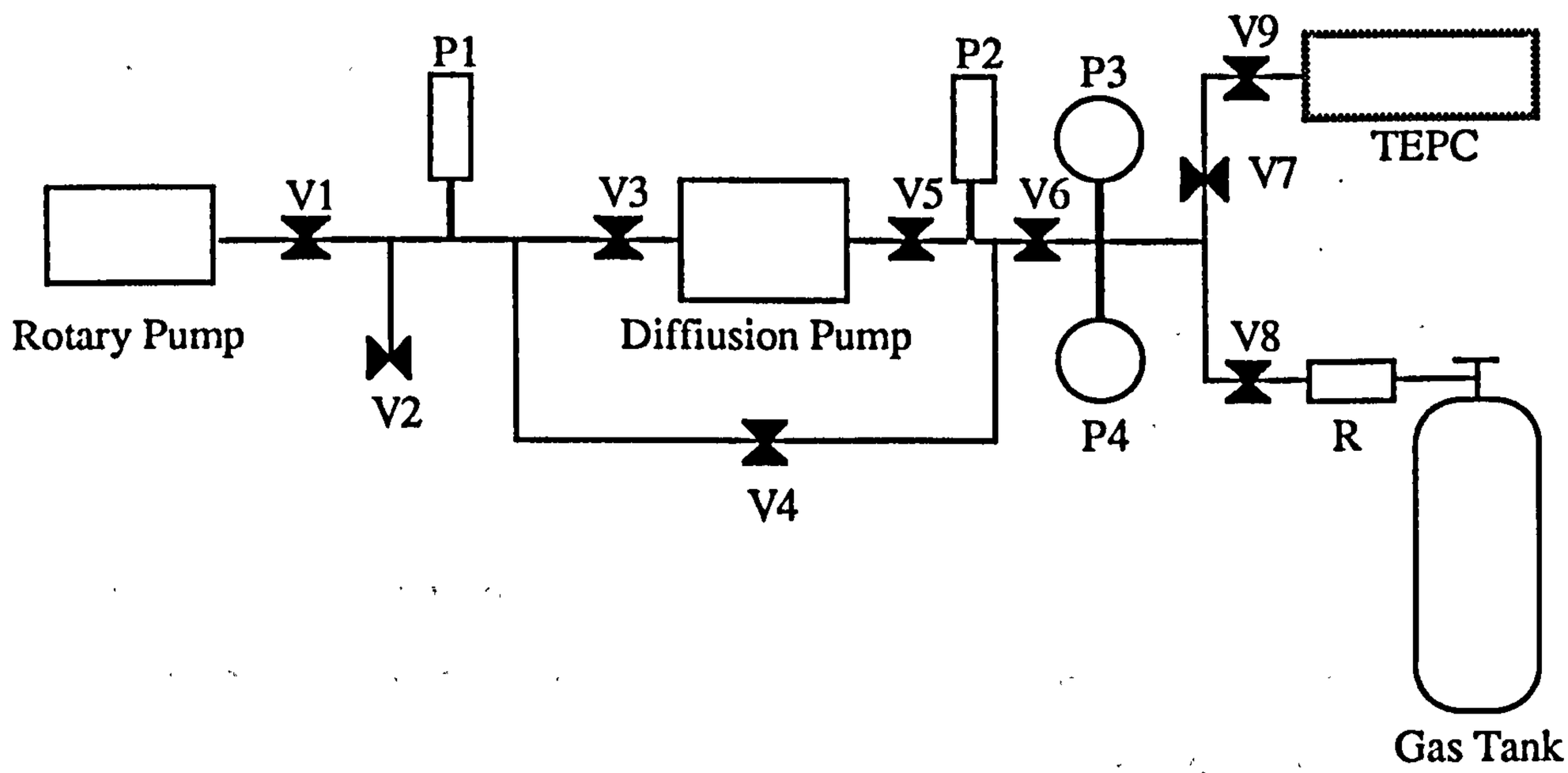

Fig. 4.9 Schematic diagram of the high vacuum system for gas filling. V1 is the magnetic valve, V2 is the admittance valve, V3....V9 are gate valves, P1 is the Pirani gauge, P2 is the Penning gauge, P3 is the pressure gauge (100 torr), P4 is the pressure gauge (760 torr) and R is the gas regulator.

4.5 Electronic Instrumentation

The electronic instrument used for data collection throughout this work is described as follows:

4.5.1 Preamplifiers

Two charge-sensitive preamplifiers (ORTEC, Model 142PC) have been used in this project to provide intermediate amplification of the output signals from the inner and the outer counters. The typical charge sensitivity of the preamplifiers is 2.58 μV/ion pair. These low noise preamplifiers use field effect transistors (FET) which would resolve pulses due to one ion pair from the noise background. The noise level increases as the RC factor of the counter increases. Therefore, short cables of 30 cm in length were used to connect the SHV input of the preamplifiers to the counters.

A positive bias voltage was applied to both the counters via preamplifiers. A series of load resistance, 3MΩ, is supplied in the SHV input of the preamplifier so that any DC signal or leakage current drawn by the connector can flow through these resistors.

4.5.2 Spectroscopy Amplifiers

The preamplifier outputs have been connected to the inputs of amplifiers (ORTEC, Model 472 and 472A) with the shaping constant set at 2 μs for better resolution. A unipolar output was used to analyse the pulses, either directly connected to the Multichannel Buffer (MCB) or to the coincidence and anti-coincidence unit.

4.5.3 Coincidence and Anti-Coincidence Unit

A simple coincidence and anti-coincidence unit has been design and constructed for use in the microdosimetric measurement as shown in **Fig. 4.10.** It is often in microdosimetric measurement that the electronic gain of the linear amplifier is increased to cover 3 to 4 decades of spectra. Consequently, the noise level is also increased and the coincidence/anti-coincidence should be able to remove the effect of low-voltage noise pulses.The unit has an adjustable input offset for the minimum input voltage so that the low-voltage noise pulses

will not give effect to the logic operation. Also, the response of the gate is very fast, thereby, minimise the resolving time. The gate outputs were delayed approximately 0.1 μs from the inputs, thereby a delay unit was used to delay the propagation of the input signals of the MCA.

4.5.4 Delay and Stretcher

A Single Linear Gate and Stretcher (TENNELEC, Model TC 309) was used as a delay amplifier and stretcher. The unit accepts linear signals and generates an output pulse with an amplitude equal to the linear input signal after the shape is optimised for superior performance for the multichannel analyser. It can accept a minimum signal voltage of 20 mV which is very common in the microdosimetric measurements.

4.5.5 Multichannel Analysers

Pulses generated by the counters were analysed in an ADCAM multichannel buffer (ORTEC, Model 918 MCB) linked with a BBC microcomputer via RS-232-C cable with the baud rate setting at 9600 baud. The analyser designed for high performance in real-time data acquisition is programmable by issuing ASCII commands. It consists of 13-bit fast ADC, first-in-first-out (FIFO) buffer memory, an internal Z80 microprocessor, 8K 24-bit words data memory and 8-bit words 16K ROM 8KRAM program memory. This system was used to analyse the characteristics of the counter.

In the microdosimetric measurements a multichannel analyser (NORLAND, Model 5300) was used.

4.5.6 Research pulser

Pulses from a research pulser (ORTEC, Model 448) were fed to the test input of the preamplifiers to check the overall function of the electronic system prior to any measurement and to equate pulses derived from the counters in the gas gain measurements. Also, it has been used to determine the linearity of the multichannel analysers. Typical pulse

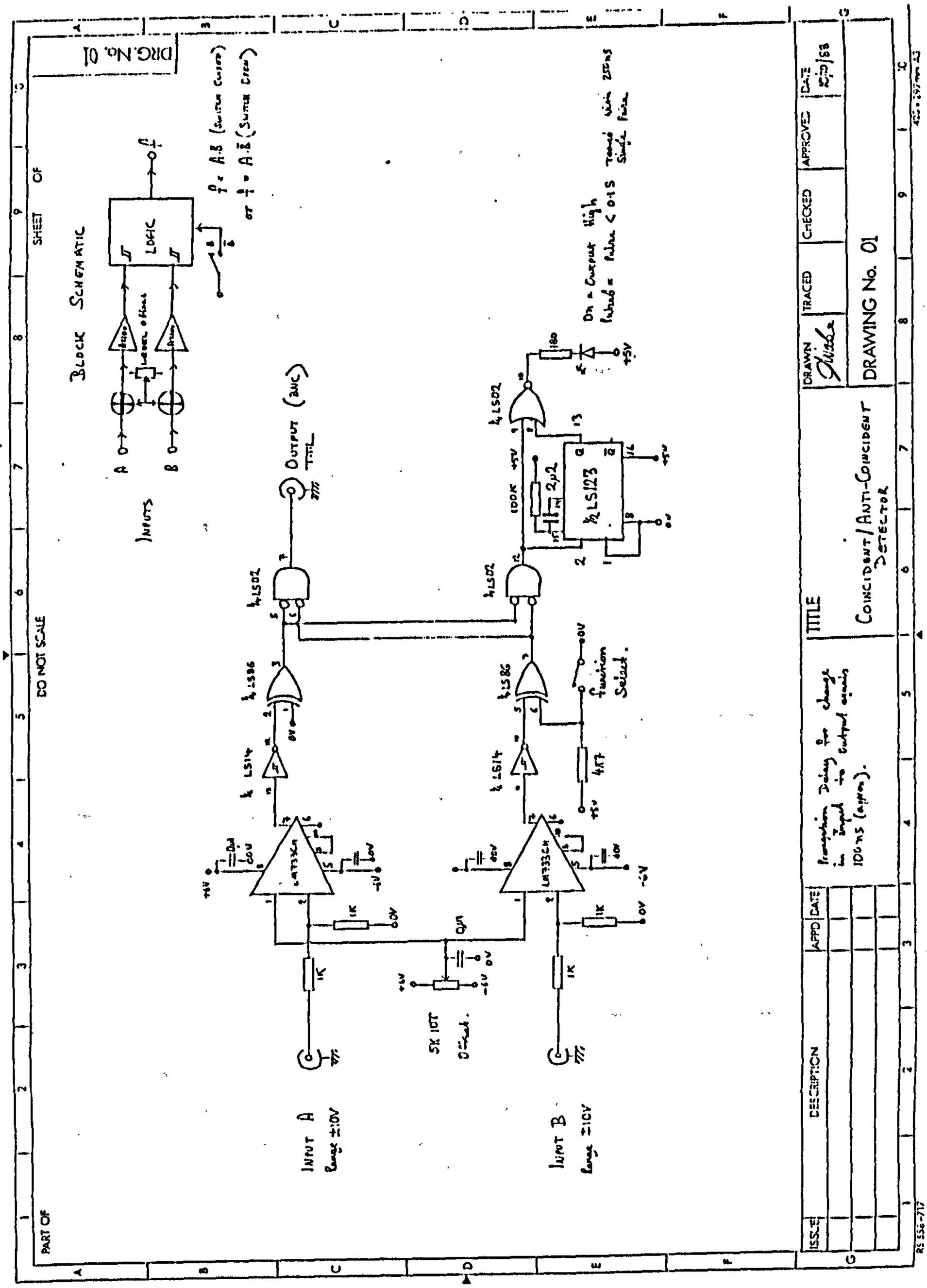

Fig. 4. 10. Electronic circuit of the coincidence and anti-coincidence unit.

characteristics for the rise time was 20 ns and for the decay time was 50 ms, at pulse rate from 10 to 100 pulses per second depending on the applications.

4.5.7 High Voltage Power Supplies

The operating voltages of the counters were supplied by a high voltage power supply (ORTEC, Model 456) with positive potential to the anodes. Both counters operated at the same voltages in the measurement.

The guard tube potentials, supplied by a high voltage power supply (ORTEC, Model 459), were set to a voltage of $0.32V_o$, V_o being the potential of the anode.

The schematic diagram of the electronic system for microdosimetric measurements is shown in **Fig. 4.11**.

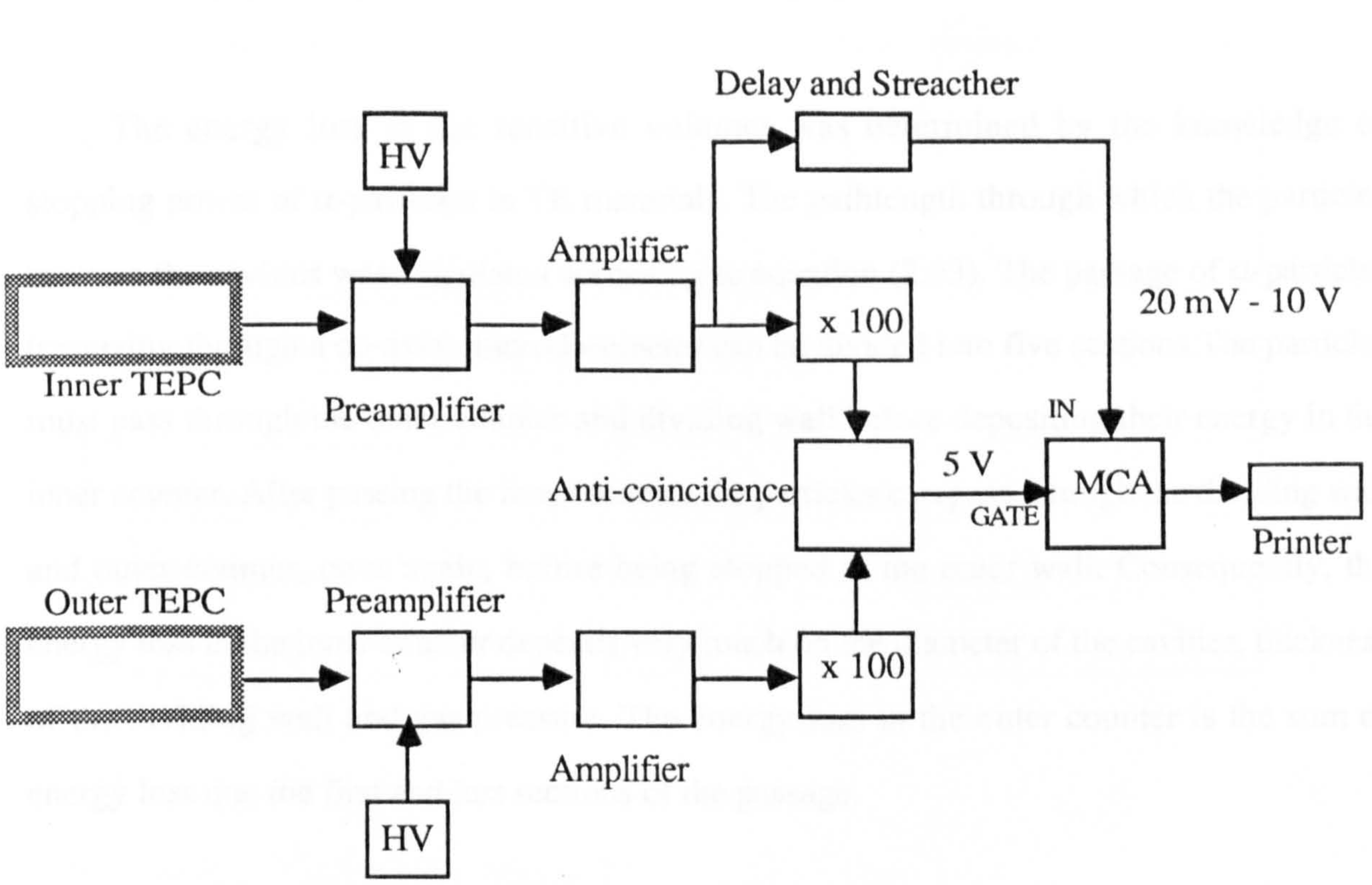

Fig. 4.11 Block diagram of the electronic system for microdosimetric measurements.

CHAPTER 5

CHARACTERISTIC MEASUREMENTS: Experiment for Gas Gain and Resolution of the Co-Axial Double Cylindrical TEPC

5.1 Energy Calibration

5.1.1 Calculation of Energy Loss in the Counter

For the purpose of energy calibration, the counter was equipped with a gravity-operated built-in internal ^{241}Am source which emits 5.486 MeV α-particles. The collimated α-particle beam was admitted to both the inner and outer counters through a small bore-hole of diameter 0.3 mm, drilled centrally on the side wall of the outer counter, thereby allowing the beam to pass through the sensitive volumes and perpendicular to the counter axes.

The energy loss in the sensitive volumes was determined by the knowledge of stopping power of α-particles in TE materials. The pathlength through which the particles traverse the cavities was calculated according to equation (2.63). The passage of α-particles traversing through a co-axial microdosemeter can be divided into five sections.The particles must pass through the outer counter and dividing wall before depositing their energy in the inner counter. After passing the inner counter the particles can pass through the dividing wall and outer counter, once again, before being stopped in the outer wall. Consequently, the energy loss in the inner counter depends very much on the diameter of the cavities, thickness of the dividing wall and gas pressure. The energy loss in the outer counter is the sum of energy loss due the first and last sections of the passage.

The mean energy loss, $\bar{E}_D$, of the α-particles in traversing the pathlength, Δx (gcm^{-2}), in TE materials was calculated by a simple relation given by the equation (5.1)

$$\bar{E}_D = \left(\frac{dE_i}{dx}\right) \Delta x \qquad (5.1)$$

where $\frac{dE_i}{dx}$ is the stopping power of alpha particles in TE materials in keV cm^2 g^{-1} and E_i is the initial energy of the particles. The stopping power data for alpha particles in TE materials were taken from Oldenburg and Booz (1972). The mean energy loss from the passage of 5.486 MeV ^{241}Am α-particles in the counter at pressures equivalent to the mean chord lengths from 0.05 μm to 2.0 μm are tabulated in **Table 5.1** for propane based TE gases. **Fig. 5.1** shows the mean energy loss in the inner and outer counters at various simulated mean chord lengths. The results show that the energy deposited increases with the increase of the mean chord length. More energy is deposited in the inner counter than that of the outer counter. It has been reported recently that Oldenburg and Booz data can overestimate the energy deposition for mean chord lengths below about 1.0 μm in the calibration of TEPCs (Schrewe *et al.*, 1988). However, the deviation is expected to be less than 7%.

Table 5.1 Mean energy loss from the passage of ^{241}Am α-particles in a co-axial double cylindrical TEPC at various applied pressures.

Pressure (torr)	Inner TEPC $\bar{E}_D$ (keV)	Outer TEPC $\bar{E}_D$ (keV)
5.29	27.11	21.02
13.23	68.29	52.58
26.46	138.22	105.16
29.69	209.88	157.73
52.98	283.34	210.31

5.1.2 Energy Calibration Method

The calibration of the counter has been performed using a single-event calibration method by irradiating the counter with ^{241}Am α-particles that produced a known energy deposition in the counter. This method has the advantages of being simple, fast and reliable. Nevertheless, there are uncertainties associated with this method due to the discrepancies in

various published stopping power data around the Bragg peak, the self absorption of the energy of α-particles in the source layer, the uncertainty of path length determination and poor geometrical quality of the beam collimation (ICRU, 1983 and Schrewe *et al.*, 1987).

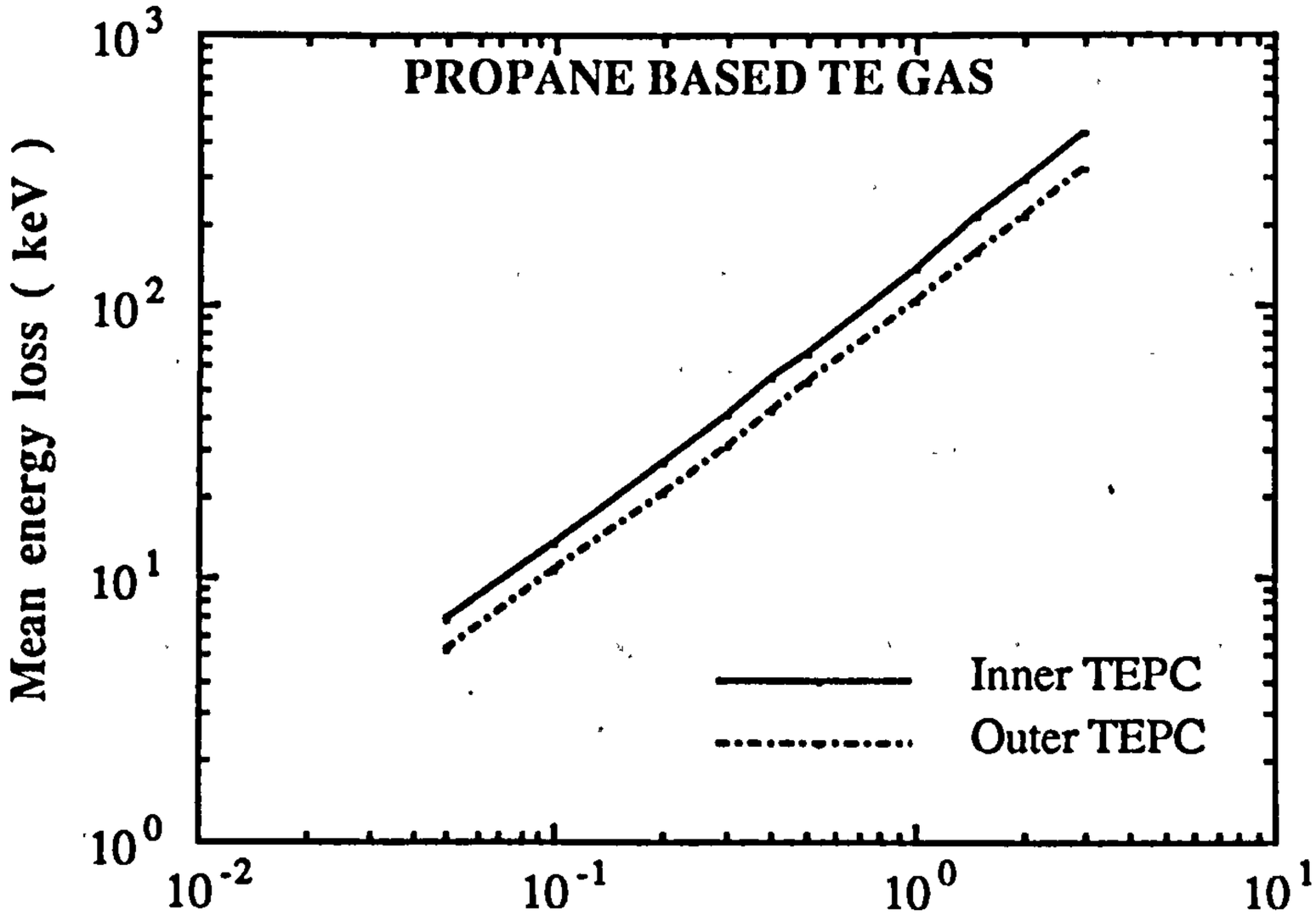

Fig. 5.1 Mean energy loss in the counter as a function of mean chord length for propane based TE gas.

Also, a constant value of $\bar{w}$, the mean energy expanded per ion pair formed, is assumed, despite the fact that the dependence of $\bar{w}$ on the type and energy of ionizing radiations (ICRU, 1979). ICRU (1983) has recommended the use of the α-particles in the calibration of the microdosemeter for fast neutrons, since there is no significant difference between $\bar{w}$ value of 5 MeV alpha particles and that of recoil protons. In the present work $\bar{w}$ was taken as 31 eV, as suggested by ICRU (1979).

A lead shutter was used to shut off the calibration beam when the counter stem is in the upright position or to open when the counter is in the downward position. In this way, the counter can be operated in the horizontal position with or without the beam shut off.

Fig. 5.2 shows the typical energy calibration spectrum of the inner TEPC at the mean chord length of 1.0 μm. At higher mean chord lengths the spectrum shape is non-gaussian, as is typical for the energy loss spectrum of α-particles in a thick absorber. However, the spectrum becomes gaussian in shape at the mean chord lengths less than 0.3 μm. In contrast, the spectrum for the outer TEPC is gaussian in shape at 1.0 μm but has two peaks as shown in **Fig. 5.3** (a). An extra peak at the lower energies indicates that there is some energy loss due to recombination of ions resulting from the non-uniform electric field strength in the outer counter. Nevertheless, the event does not contribute to the measurement of microdosimetric spectra because the peak does not appear when the outer counter is operated in coincidence with the inner counter as shown in **Fig. 5.3** (b).

Also, the coincidence/anti-coincidence unit constructed in this work is a good performance device as indicated in **Fig. 5.3**, by which the gaussian shape of the actual energy loss spectrum is clearly shown with no significant loss in events.

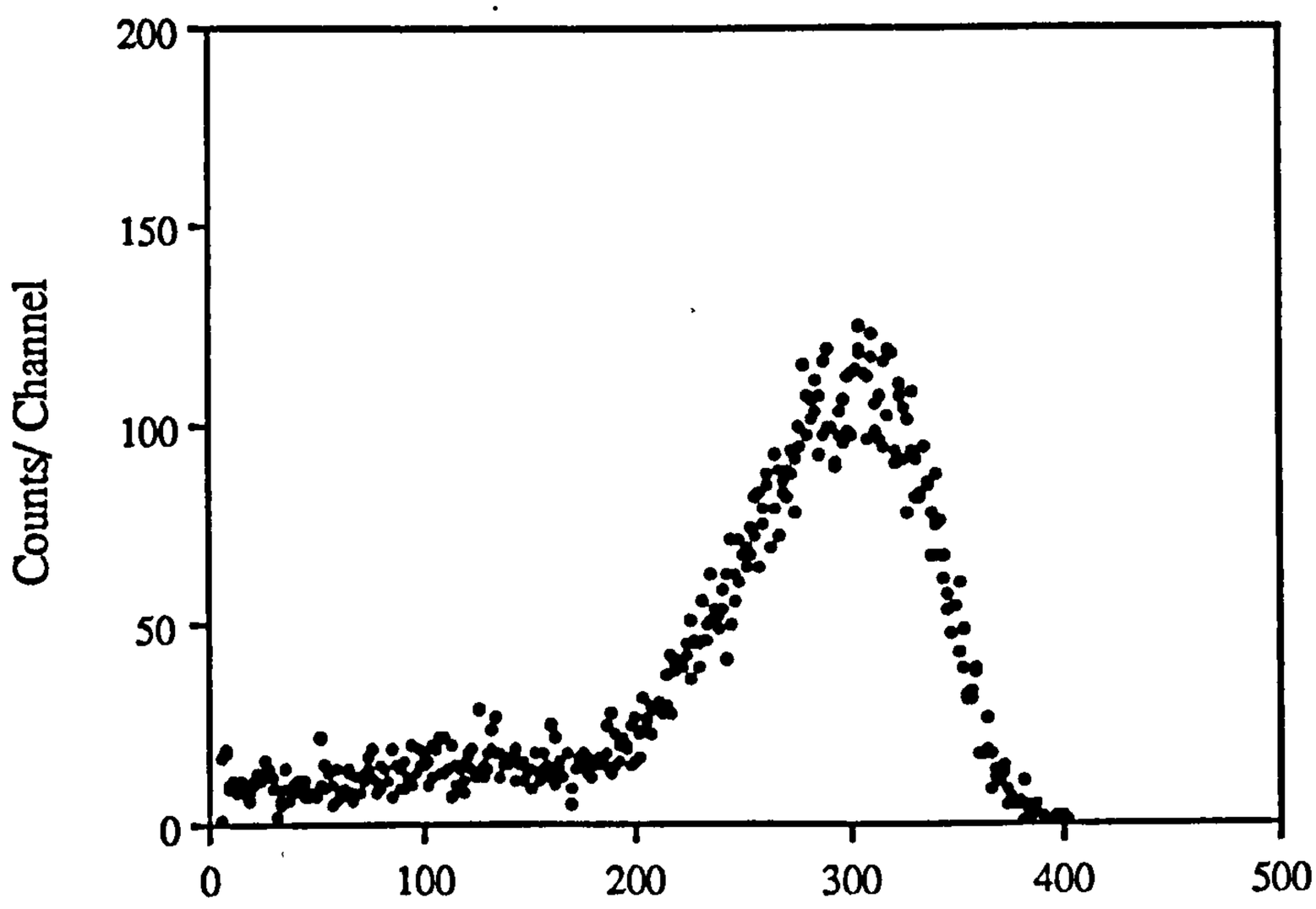

Fig.5.2. Typical energy loss spectrum of 5.486 MeV α-particles in Inner TEPC.

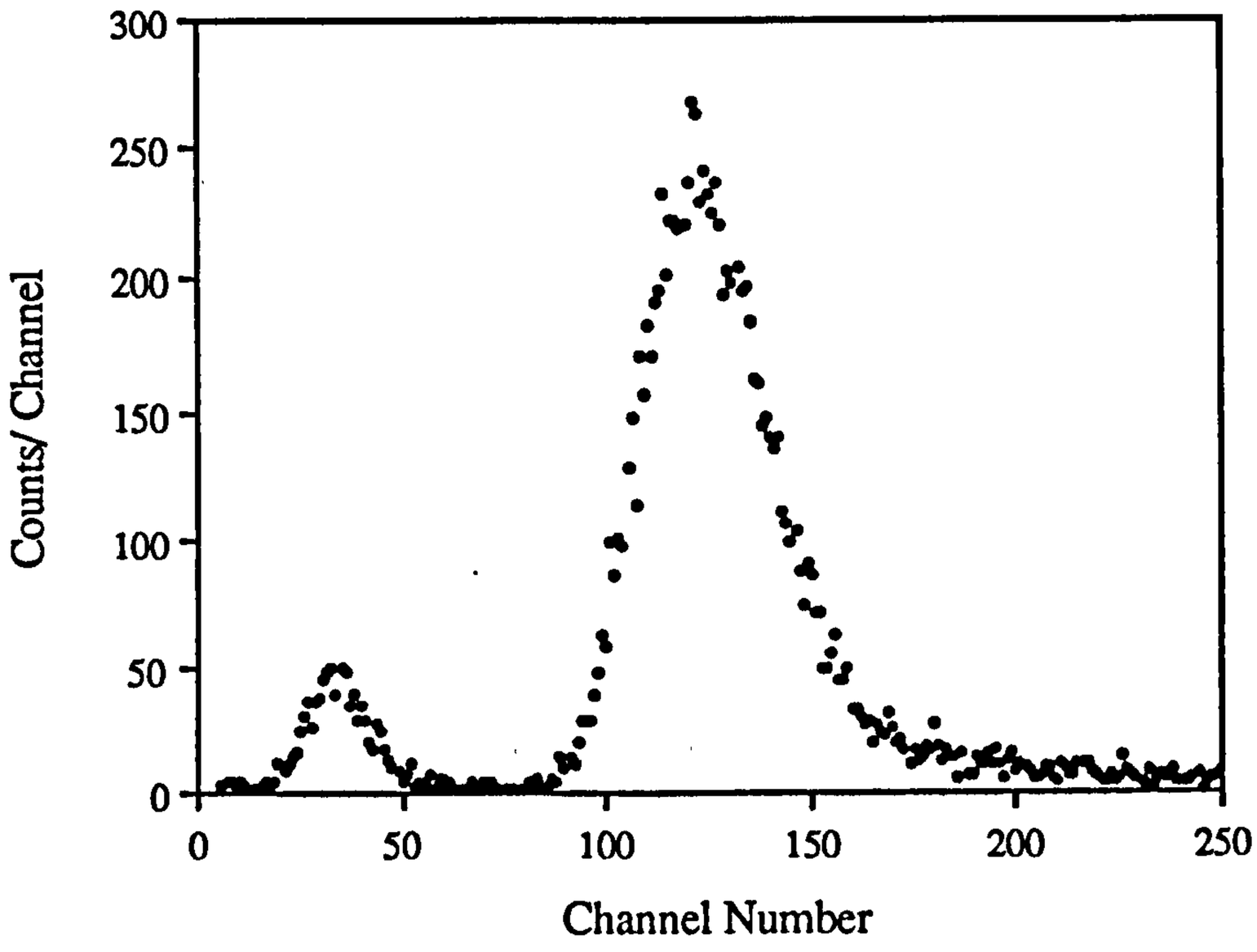

(a)

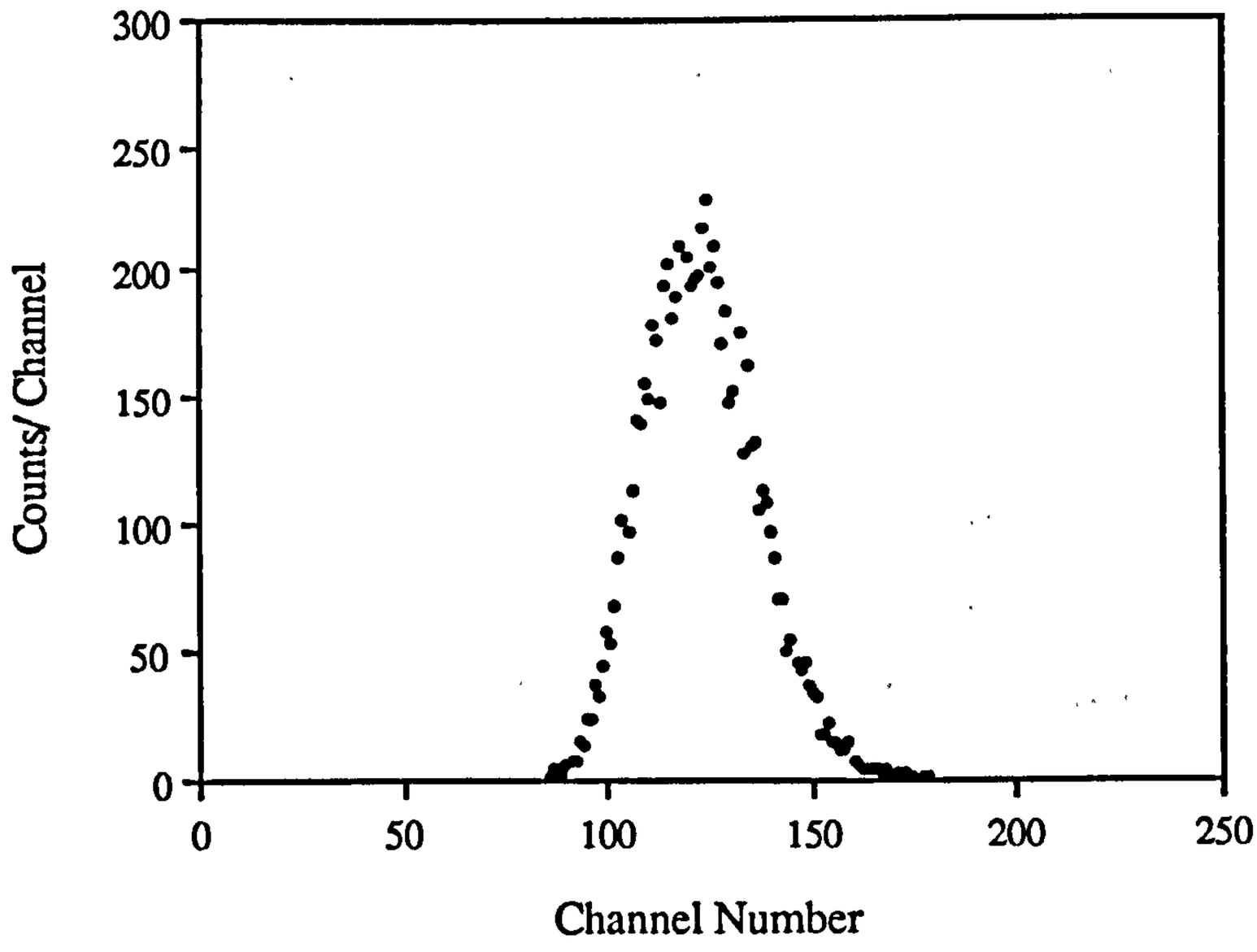

(b)

Fig. 5.3. Typical energy loss spectrum of 5.486 MeV α-particles in (a) Outer TEPC and (b) Outer TEPC in coincidence with the Inner TEPC.

At the simulated mean chord length of 3.0 μm, the peak of the energy loss spectrum in the inner TEPC was almost unrecognizable from those of low energy events without sacrificing a longer counting time. This was taken as the upper limit at which the counter can be operated with the present method of energy calibration.

Due to the limited range of channel number on the MCA it is not possible to cover microdosimetric spectra over 3 to 4 decades. It is necessary therefore to extrapolate the position of the calibration peak at higher electronic gains corresponding to the lower values of lineal energy. This was done by a series of measurement of the calibration peak at lower electronic gain settings. More than five points were required to obtain a calibration curve and the error has been reduced by performing the calibration measurements before and after each microdosimetric measurement.

Alternatively, the counter could be calibrated using monoenergetic photons from K-lines of Mn (^{55}Fe) and Cl (^{37}Ar) that give energy of 5.88 keV and 2.82 keV respectively, in order to increase the counter operation to much higher mean chord lengths. Low energy monoenergetic X-rays from either K-lines of carbon, fluorine or aluminium target that give low energy of 0.277 keV, 0.69 keV and 1.49 keV respectively can also be used at lower chord lengths.

Fig. 5.4 shows the calculated electron ranges in TE gases at various pressures for monoenergetic X-ray sources. They were derived from the experimental results by Cole (1969) who had concluded that the range of low energy electrons in air and plastic materials can be expressed by the empirical formula, equation (5.2). It was then applied to the secondary electrons with energies of those of X-rays when traversing the inner counter filled with TE gases at temperature of 20 °C. It is important to note that, the range of the secondary electrons must be less than the effective diameter of the counter i.e. about $\frac{1}{3}$ of the diameter for a spherical counter (Srdoc, 1970).

$$\text{Range} = \{\ 0.0431(E+0.367)^{1.77} - 0.007\ \} \times 10^{-6}\ \text{g cm}^{-2} \qquad (5.2)$$

where E is the energy of the electrons in keV.

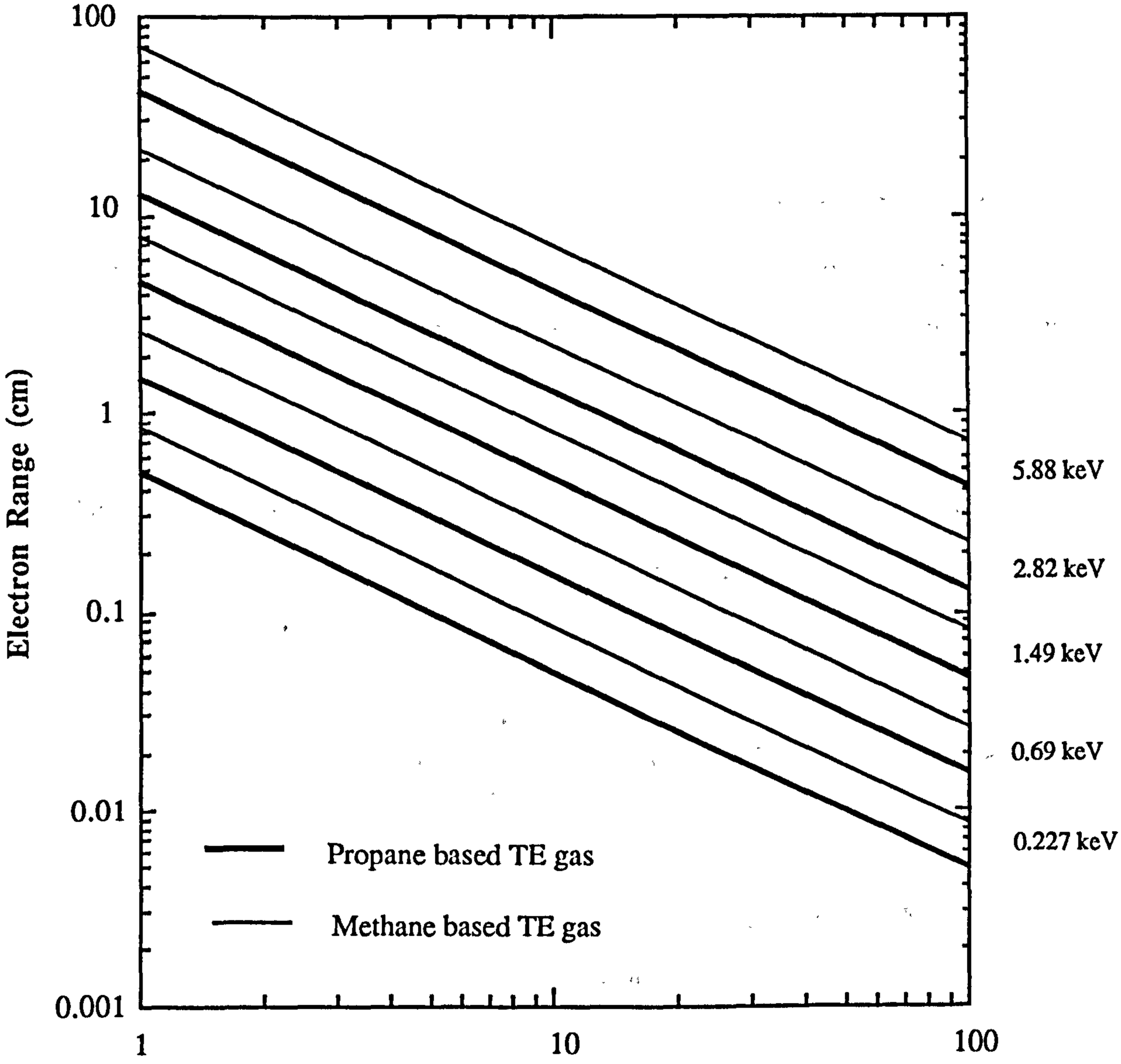

Fig. 5.4 Ranges of 5.88, 2.82, 1.49, 0.69 and 0.227 keV electrons in TE gases at temperature 20 °C.

5.2 Gas Gain Characteristics

5.2.1 Gas Multiplication

The number of electrons produced in the avalanche, dN, at a distance between r and r+dr from the anode is proportional to the number of primary electrons, N, created in the counter by ionizing radiation

$$dN = \alpha_T N \, dr \tag{5.3}$$

where α_T is the first Townshend coefficient which depends on the electric field strength, X, the type and pressure of the gas. For the counter operated in the proportional region where recombination, space charge and photoelectric effect are consider negligible, the output pulse is proportional to the gas multiplication.

Gas multiplication factor, G, can be defined as the ratio of the number of electrons collected at the anode to the number of electrons created, thus by integrating equation (5.3), the gas gain can be expressed by

$$\ln G = \int_a^r \alpha_T(P,X) \, dr \tag{5.4}$$

where a is the anode radius, r is the critical radius from the centre of the anode where avalanche starts to occur and P is the pressure of the gas.

Rossi and Staub (1949) have noted that the gas multiplication process occurs within the cylindrical region very close to the anode and at the voltage higher than the minimum voltage at which the multiplication starts. They have found that the gas gain can be expressed as functions of $\frac{V}{\ln(b/a)}$ and Pa.

$$G = f\left(\frac{V}{\ln(b/a)}, Pa \right) \tag{5.5}$$

where V is the applied voltage and b is the cathode radius. Various expressions have been proposed and tested according to the relation (5.5) for example Rose and Korff (1941), Curran and Craggs (1949), Diethorn (1956), William and Sara (1962), Kocharov and Korolev (1963). Semi-empirical formulae derived from the experiments have found to be restricted to the range of the counter geometry, the pressure and type of gas used. Gold and Bennett (1965) and Zastawny (1966) have expressed the gas gain in terms of the reduced field strength, $\frac{X}{P}$, and obtained a good fit to the experimental results. Shalves and Hopstone (1978) have studied details of the various factors affecting the gas gain using eighteen counters of different dimensions and types of gas. They predicted the gas gain to within 2%. A similar attempt has been made recently by Kowalski (1985) using different mixtures based on innert gases with organic and inorganic quench gases.

The behaviour of the gas gain over the range of gas pressure typically used in microdosimetry, however, can be expressed according to Campion (1971b) by integrating equation (5.4) over the anode and cathode radii of a and b respectively, by

$$\ln G = \frac{AV}{B\ln(b/a)}\left[\exp\left\{-\frac{aBP\ln(b/a)}{V}\right\} - \exp\left\{-\frac{bBP\ln(b/a)}{V}\right\}\right] \qquad (5.6)$$

The first term of equation (5.6) is the typical gas gain expression for conventional proportional counters (Williams and Sara, 1962) when the avalanche region is very close to the anode. However for low-pressure TEPC where the multiplication region spread over the sensitive volume, the second term must be taken into account. The constant values of A and B depend on various experimental conditions such as the type of gas and the reduced field strength as shown in **Table 5.2.**

5.2.2 Gas Gain Measurement

The gas gains for both the inner and outer counters were measured for propane TE gas mixture at various simulated mean chord lengths from 0.05 μm to 2.0 μm and for different anode voltages. The relative gas gains were obtained by comparing the output

Table 5.2 Constant values of A and B for TE gas mixtures

TE gas mixture	A $torr^{-1}\ cm^{-1}$	B $V\ torr^{-1}\ cm^{-1}$	E/P $V\ torr^{-1} cm^{-1}$	Reference
Methane	9.9	212	100-250	Campion (1972)
Methane	18.5	369	1000-4000	Eickel and Booz (1976)
Neon	8.0	139	260-2000	Hogeweg (1978)
Methane	12.3	222	350-3200	DeLuca *et al.* (1982)
Propane	10.8	165	-do-	-do-
A150 Mix 1	19.1	315	-do-	-do-
A150 Mix 2	19.9	307	-do-	-do-

pulse generated in the counter due to ^{241}Am α-particles passing through the sensitive volumes with that delivered from a research pulser fed to the test input of a preamplifier.The pulse height analyser (ORTEC MCB) was used to equate the channel number of the pulser peak with that of the energy deposited by the calibration source. The relative gas gain values were calculated using equation

$$G = \frac{C_T\ \bar{w}\ V_g}{\bar{E}_D\ e} \qquad (5.7)$$

where C_T is the test capacitance, V_g is the pulse height of the pulser and $\bar{E}_D$ is the mean energy loss for a given mean chord length. $\bar{w}$ was taken as 31.0 eV/ion pair for α-particles in TE gas (ICRU, 1979).

Fig. 5.5 and **Fig. 5.6** show the results of the gas gain measurements for the inner and outer counters respectively. The gas gain is expressed as a function of anode bias voltage. The gas gain of the inner counter is twice as high than that of the outer counter for a given simulated mean chord length. This is as expected because the reduced field strength in

the inner counter is higher than that of the outer counter for a given applied voltage. Consequently, the inner counter has the operational voltage lower than that of the outer counter. **Fig. 5.7** shows the gas gain characteristics of the counters when presented in $\frac{\ln G}{P}$ vs. $\frac{V}{P}$ plot. There is no significant difference in the operational characteristics between the two counters for reduced field strength from 670-6700 V $torr^{-1}$. The data at the reduced field strengths greater than 200 V $torr^{-1}$ could be fitted for Campion formula with A=22.5 $torr^{-1}$ cm^{-1} and B=396 V $torr^{-1}$ cm^{-1}. It shows that the gas gain characteristics of the counters agree with the prediction formula, but the constant A and B are considerably higher than those of previous measurements (DeLuca *et al.*, 1982). The difference might be due to the different reduced field strength used in this experiment.

Kemshall *et al.* (1969) and Mathieson and Charles (1969) have shown that the gas gain deduced using a pulse generator could lead to a considerable error due to amplifier shaping networks. The pulse height, V_s, after shaping by RC integrating and differentiating networks of time T is given by an empirical equation (5.8).

$$V_s = \frac{V_0}{2 \ln(b/a)} [\, 0.087 + 0.797 \log_{10} (\frac{4\ V\ \mu_+\ T}{a^2\ 2 \ln(b/a)})] \qquad (5.8)$$

where V_0 is the pulse height before shaping, V is the applied voltage, μ_+ is the positive ion mobility i.e. $\mu_+ = 3.0\ cm^2V^{-1}s^{-1}$ for TE gas (Gott and Charles, 1979) and T is the pulse shaping of the amplifier used. The gas gain could be corrected for shaping time constant by dividing the measured values by V_s / V_0. However, no attempt was made to correct the the measured results. The experimental error was kept minimal by the use of a step pulse generator with fast rise time constant. For the main amplifier, a large decay shaping time constant of 3.0 μs was applied. Reducing the decay time constant to 1 μs lead to the reduction of the gas gain about 1%. Therefore, the shaping time constant 1-3 μs did not change the gas gain considerably.

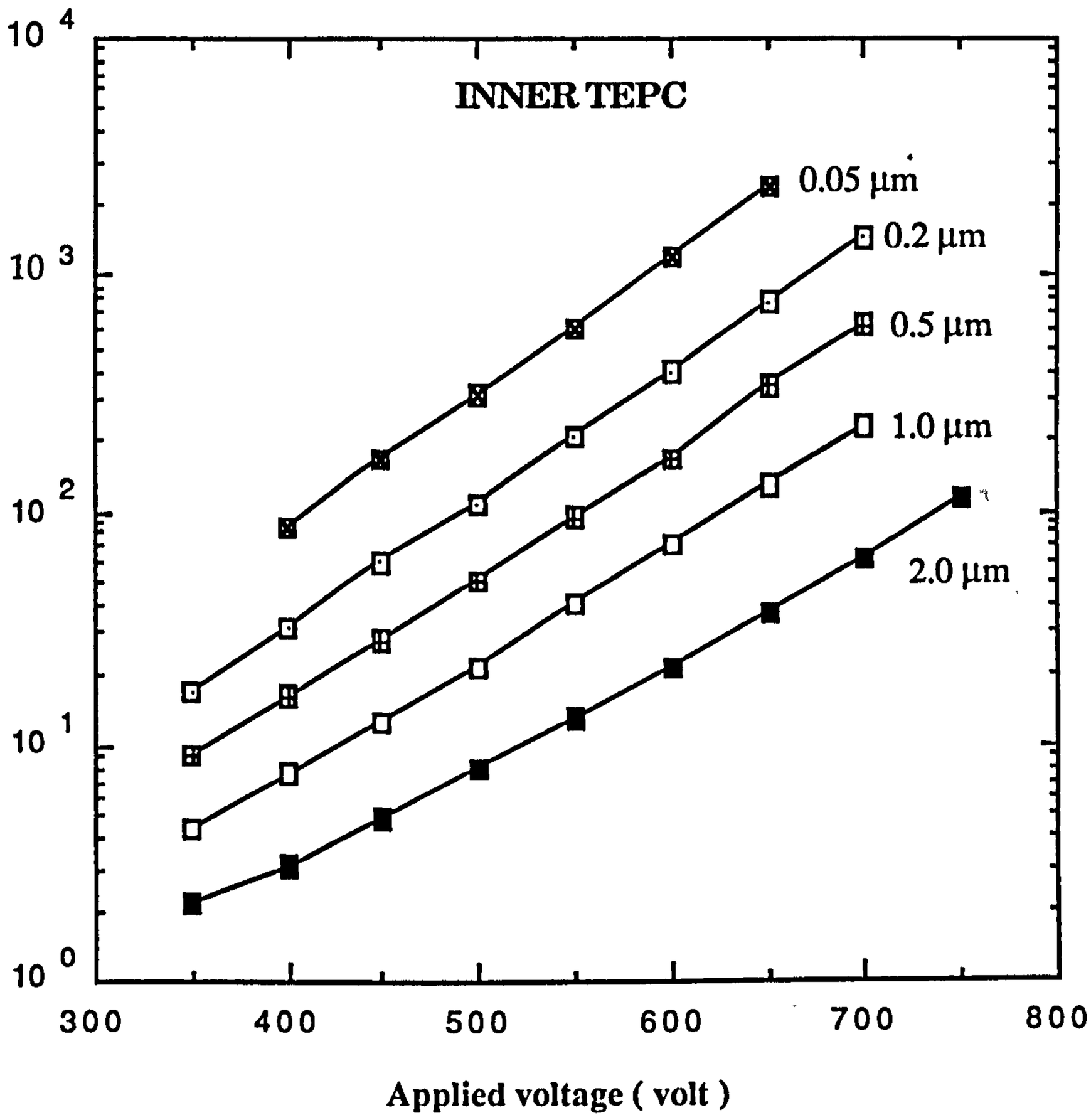

Fig.5.5 Gas gain characteristics of the inner TEPC at various anode voltages.

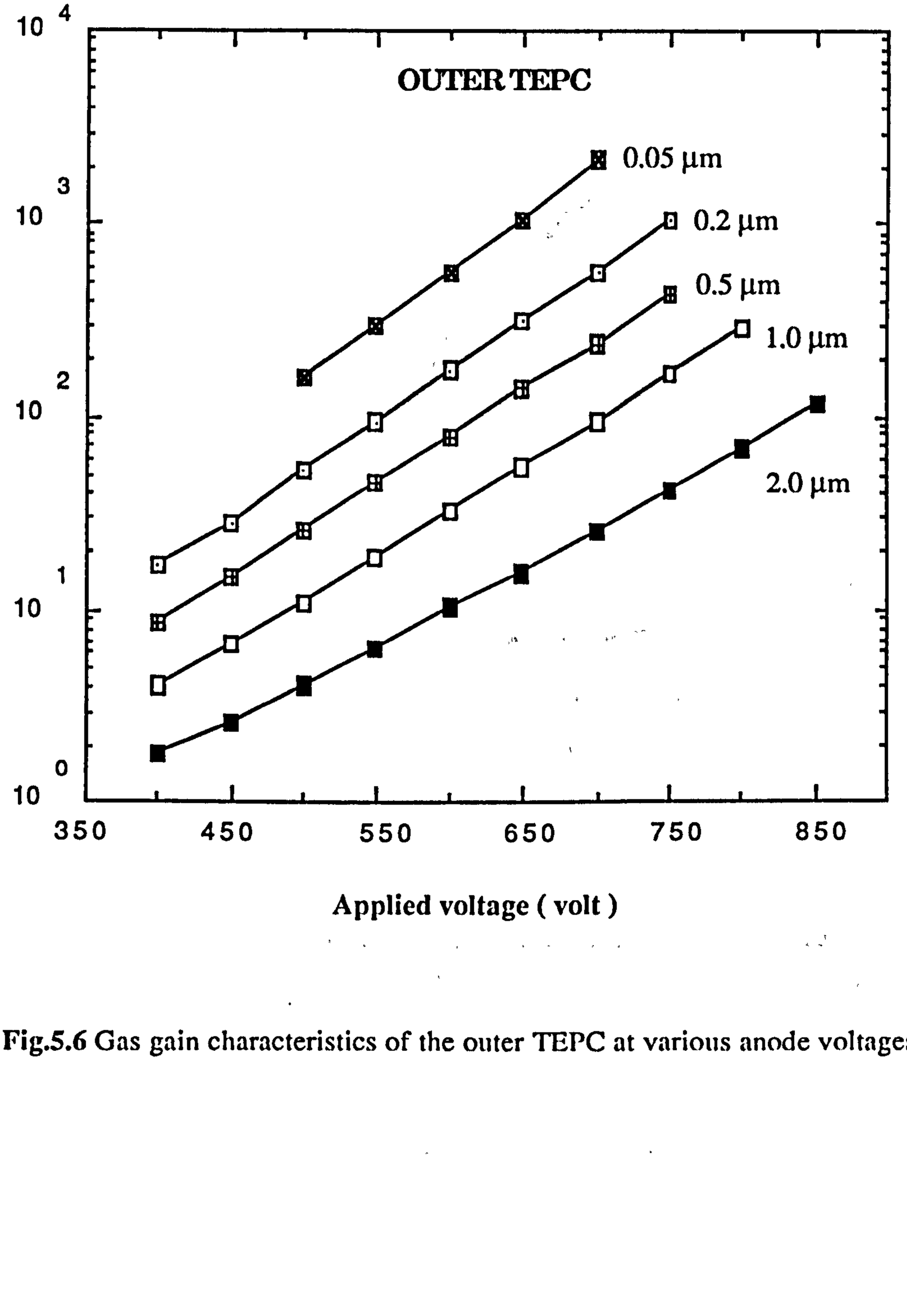

Fig.5.6 Gas gain characteristics of the outer TEPC at various anode voltages.

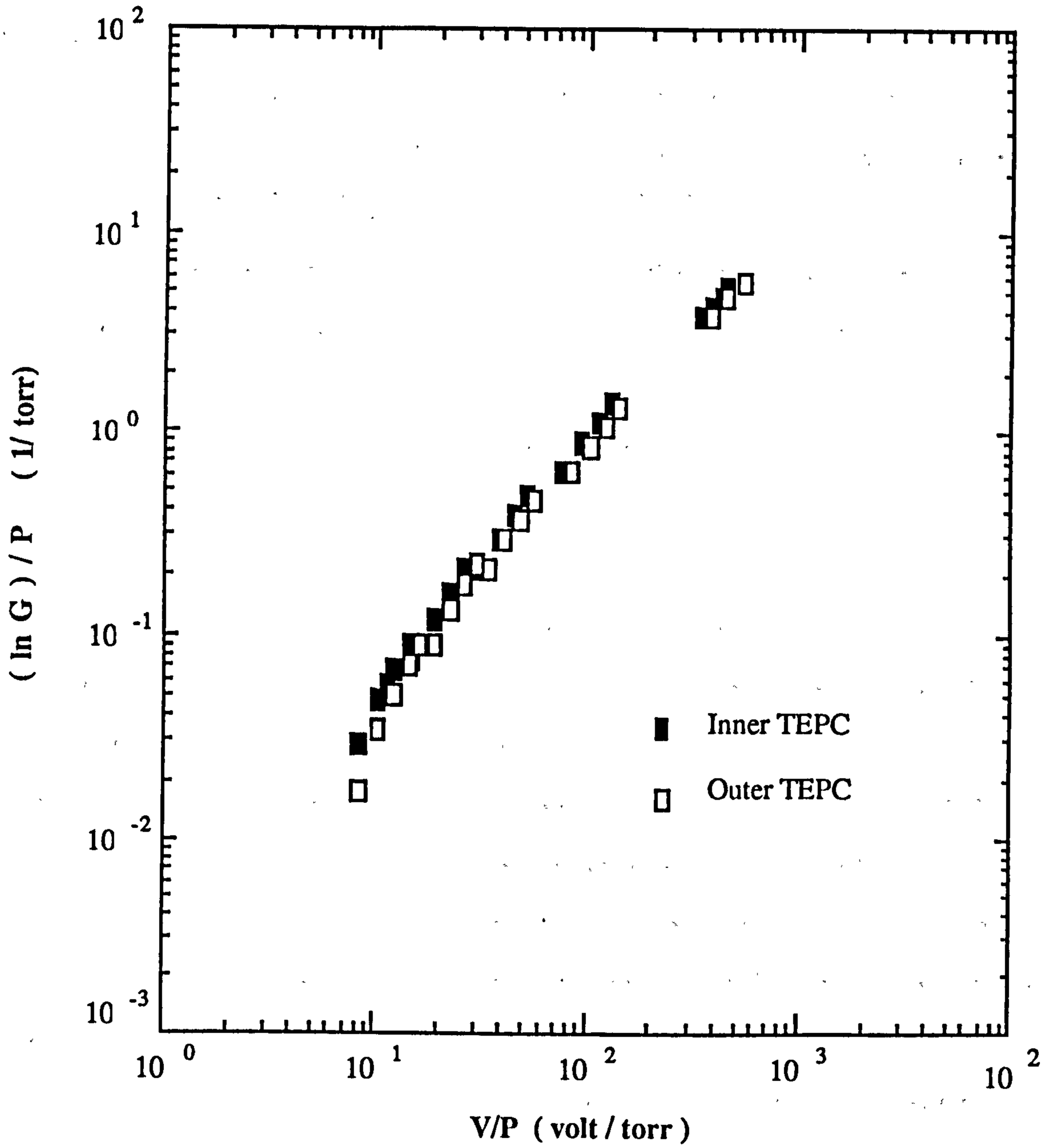

Fig. 5.7 Gas gain characteristics presented in the form of $\frac{\ln G}{P}$ vs. $\frac{V}{P}$ plot.

5.3 Energy Resolution Characteristics

5.3.1 Counter Resolution and Fluctuation Factors

Energy resolution is the quantity which determines the ability of the counter to resolve fine detail of the pulse height distribution due to a monoenergetic radiation source. The response function of a proportional counter is usually a Gaussian shape. The energy resolution, R, is conventionally defined as the ratio of the full width half maximum (FWHM) energy, ΔE, and the full peak energy, E, i.e. $R = \frac{\Delta E}{E}$. For a Gaussian distribution with a standard deviation, σ, the FWHM represents the variance with the relation, FWHM = $2(2 \ln 2)^{0.5} \sigma$. Then the counter's resolution can be determined by equation (5.8).

$$R = 2.354 \sigma \qquad (5.8)$$

There are two potential sources of fluctuation namely the statistical and instrumental fluctuations. The statistical fluctuation is the most important in the counter operation which cannot be avoided and represents inherent noise in the counter. The instrumental fluctuation, on the other hand, is related to the geometrical and operational factors of the counter and the electronic noise of signal processing system, which both can be minimized. The relative variance of the pulse height distribution due to the statistical fluctuation is originated from two main sources of random event. Firstly, charged particles lose energy in the stochastic nature due to variations in the individual interactions or collisions, each of which produces a distribution of possible energy transfers, i.e. energy loss straggling. Secondly, the formation of charge, Q, in the counter depends on each individual avalanche which associated with the initial ion pairs created by passing monoenergetic particles and gas multiplication process.

The sources of fluctuation are independent from one another and the overall energy resolution is the quadrature sum of the FWHM values (Knoll, 1979). The sum of the relative variances of the fluctuations in the counter is then

$$\sigma^2 = \left(\frac{\sigma_\Omega}{\Omega}\right)^2 + \left(\frac{\sigma_n}{n}\right)^2 + \left(\frac{\sigma_M}{M}\right)^2 + \left(\frac{\sigma_I}{I}\right)^2 \qquad (5.9)$$

where the first, second, third and fourth terms are the relative variance for energy loss straggling, ion pair formation, gas multiplication process and instrumental fluctuations respectively.

5.3.2 Energy Loss Straggling

Energy loss straggling is considered the major source of fluctuation of energy deposition in the counter which can contribute more than 90 % of the overall resolution. The variance for energy loss straggling can be calculated according to equation (5.10) for a Gaussian distribution function and is valid for thick absorbers. It is also valid for particles of velocity higher than that the atomic orbital electrons provided that the energy loss should not exceed 10 % of the initial value.

$$\left(\frac{\sigma_\Omega}{\Omega}\right)^2 = 4\pi e^4 Z_1^2 N Z_2 \Delta x / \bar{E}_D^2 \qquad (5.10)$$

where $\bar{E}_D$ is the energy deposited in the sensitive volume of the inner counter $e^4=(r_0mc^2)^2=(2.818 \times 10^{-13}$ cm x 511 keV$)^2$, NZ_2 is the electronic density of tissue, i.e. $NZ_2=3.3229 \times 10^{23}$ electrons/cm^3 (Geary and Haque, 1976) and Z_1 is the atomic number of the heavy charged particles.

5.3.3 Fluctuation in the Number of Ion Pairs

The mean number of ion pairs, n, produced by charged particles in the counter is the quotient of the mean energy loss, $\bar{E}_D$, and the mean energy expended per ion pair, $\bar{w}$. The formation of an ion pair is not a completely independent event but departs from a simple Possion statistics by the Fano factor, F. The relative variance due to the number of ion pairs created in the counter is given by

$$\left(\frac{\sigma_n}{n}\right)^2 = \frac{F}{n} \qquad (5.11)$$

The value of F depends on the relative ionization and excitation cross sections of the filling gas. The typical value is less than one. Measured values of Fano factors for methane and propane based TE gases are 0.37 and 0.31 respectively (Srdoc, 1979).

5.2.4 Fluctuation in the Gas Multiplication

Electrons produced in the gas multiplication process cannot be considered independently of the past history of the electrons. The number of electrons in the avalanche has the probability according to the Polya distribution (Knoll, 1979).

$$P(A) = \left[\frac{A(1+\theta)}{\bar{A}}\right]^{\theta} \exp\left\{-\frac{A(1+\theta)}{\bar{A}}\right\} \qquad (5.12)$$

where A is the number of electrons for any one avalanche, $\bar{A}$ is the mean value of A, and $0<\theta<1$. The relative variance due to single-electron avalanche is then

$$\left(\frac{\sigma_A}{\bar{A}}\right)^2 = \frac{1}{\bar{A}} + b \qquad (5.13)$$

where $b=(1+\theta)^{-1}$. For any value of $\bar{A}$, the relative variance reduces to b. Let M be the average multiplication factor from all the avalanches that produce charge Q=neM, then the relative variance due to gas multiplication from n number of avalanches is

$$\left(\frac{\sigma_M}{M}\right)^2 = \frac{1}{n}\left(\frac{\sigma_A}{\bar{A}}\right)^2 = \frac{b}{n} \qquad (5.14)$$

For TE gases the value of b can be taken as 0.65 (Campbell and Ledingham, 1966 and Srdoc, 1979).

5.3.5 Instrumentation Fluctuation

There are several factors in which the instrumentation fluctuation could be minimized to allow the resolution approaching the statistical fluctuations. In the present work, however,

this fluctuation was not included in the calculation and the following steps have been taken to ensure the instrumental fluctuation is kept at a minimum.

The quality of the anode wire used, i.e. its smoothness, roundness and uniformity, is extremely critical for good resolution (Fink, 1975). The uniformity and smoothness of the anode wire have been checked by visual inspection under a microscope. The observation confirmed the standard tolerance claimed by the manufacturer, i.e. better than ± 5% of the diameter. The nonuniformity of the anode will lead to a nonuniform electric field strength along the anode wire and therefore of the gas multiplication. The observed pulses in the lower field region are smaller than the average pulse height which in turn increases the width of the pulse height spectrum and worsens the resolution. Field strength nonuniformity can be improved by the use of field tubes commonly applied in a single-wire proportional counter (Cockcrof and Curran, 1951 and Watt and Ramsden, 1964) or using helical grids for spherical TEPCs (Rossi and Rosenzweig, 1955a).

Other factors affecting resolution are the operating parameters of the counter such as gas impurities, the gas pressure and applied voltage stabilities (Knoll, 1979). Before filling with the TE gas, the counter has been pumped down to a pressure of about 10^{-6} torr for at least 24 hours and then flushed several times with TE gas until the purity was satisfactory. The chamber was then sealed off by a valve at the required pressure. The resolutions had not changed significantly six hours after the gas filling which indicates that the spectra are expected not to deteriorate due to resolution drift. Prolonged evacuation and flushing certainly improved the gas purity and therefore the resolution.

5.3.6 Resolution Measurement

The resolution of the inner TEPC has been measured using ^{241}Am α-particles at various simulated mean chord lengths. The measurements were performed at the same gas gain to minimise the dependence of this parameter (DeLuca *et al.*,1982). In this experiment, the FWHM of the energy loss spectrum is a weighted mean value for at least five measurements.

The experimental results are plotted as a function the simulated mean chord length and the inverse square root of the energy deposition is shown in **Fig. 5.8** (a) and **Fig. 5.8** (b) respectively. Error bars on the experimental curves represent the standard deviations from at least five measurements. The results are in good agreement with the theoretical calculations which are shown by the solid curves on the graphs.

Table 5.3 Energy resolution calculated for the inner TEPC filled with propane based TE gas for various mean chord lengths.

$\bar{l}$ (μm)	$\bar{E}_D$ (keV)	$(\frac{\sigma_\Omega}{\Omega})^2$ x 10^4	$(\frac{\sigma_n}{n})^2$ x 10^4	$(\frac{\sigma_M}{M})^2$ x 10^4	Resolution %
0.1	13.254	232.84	15.20	7.25	37.62
0.2	27.112	111.19	7.49	3.54	26.03
0.5	68.29	43.85	2.95	1.41	16.35
1.0	138.22	21.41	1.46	0.69	11.43
1.5	209.88	13.93	0.95	0.47	9.23
2.0	283.34	10.19	0.71	0.34	7.89

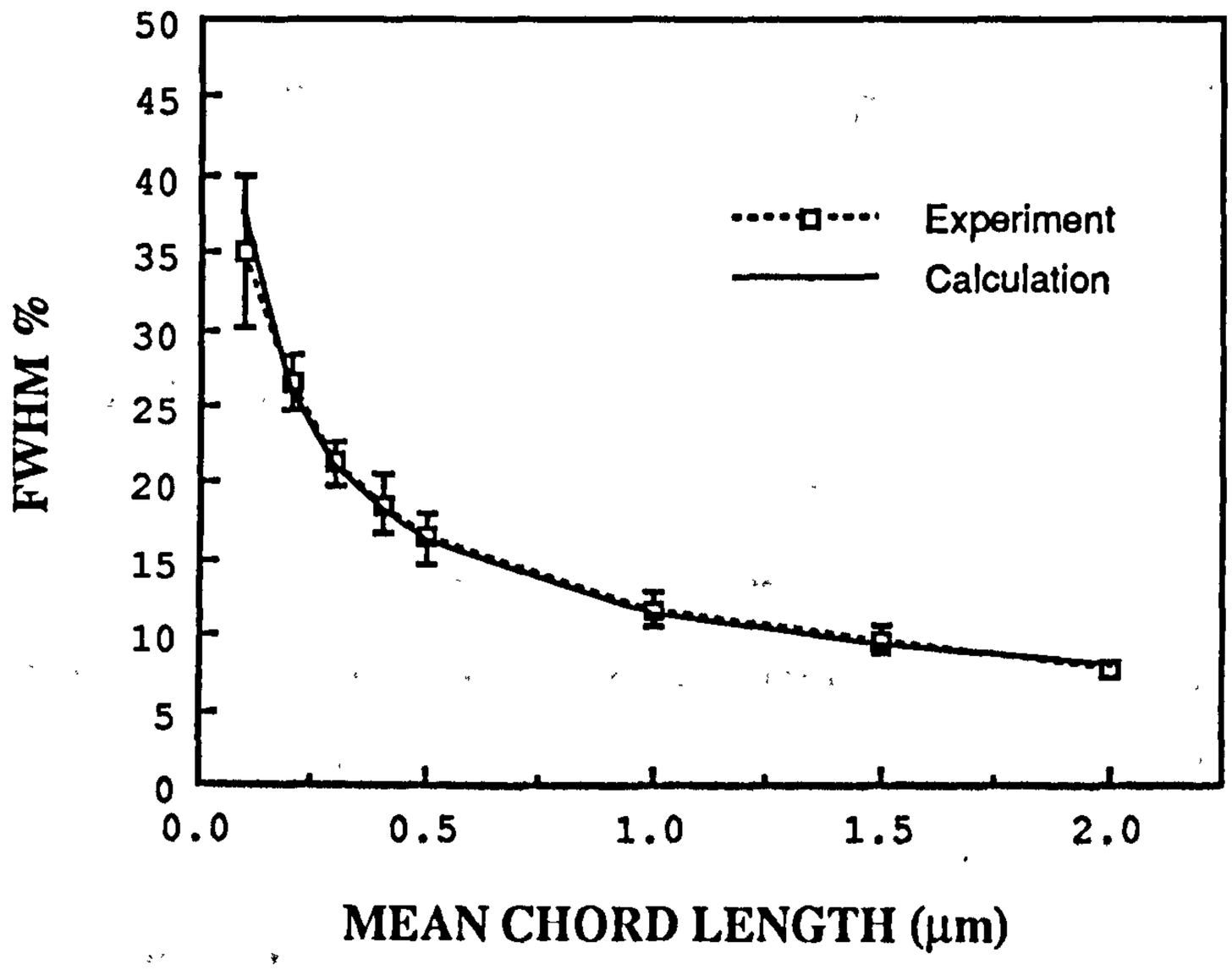

(a)

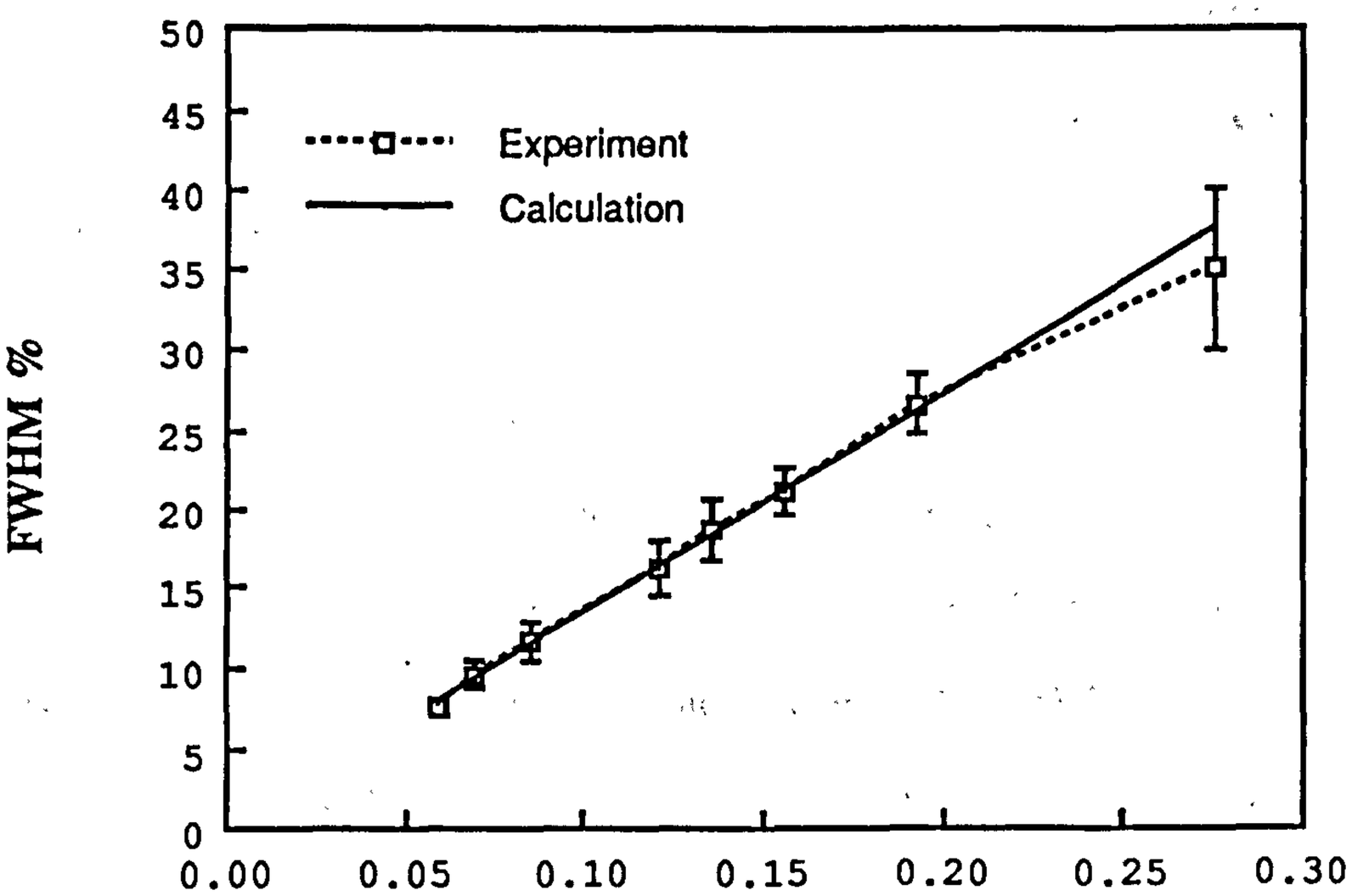

(b)

Fig. 5.8 Resolution characteristic of the inner TEPC (a) FWHM vs. mean chord length (b) FWHM vs. $\sqrt{E}$.

CHAPTER 6

MICRODOSIMETRIC MEASUREMENTS:
Experiment with Photons and Mixed (n,γ) Radiation Fields

6.1 Irradiation Facilities

To determine the operational characteristics of the new co-axial double cylindrical microdosimeter, a series of experiments has been performed with neutron and photon sources. Except for the low-LET irradiation, the measurements were made at the irradiation facilities of the Scottish Universities Research and Reactor Centre, East Kilbride, Scotland.

6.1.1 Low-LET Radiation Source

The cobalt-60 source used in this work was placed very close to the counter without the use of a collimator. The gamma rays emitting from the source are as the result of beta decay from the parent nucleus $^{60}_{27}$Co with the half-life of 5.26 years to the daughter nucleus $^{60}_{28}$Ni . Deexcitation takes place in the excited states of the daughter nucleus to produce gamma rays with energies of 1.173 and 1.332 MeV.

6.1.2 The UTR-300 Nuclear Reactor

The UTR-300 nuclear reactor whose power has been upgraded to 300kW and other facilities in the centre have been discussed by Wilson (1965) and Izatt and Scobie (1967). Light water is used as moderator coolant. The reactor uses 90% enriched uranium-235 as fuel and graphite as neutron reflector and partially as moderator.

The neutron beam was obtained from the central vertical stringer from the top of the reactor. The typical energy spectrum of neutrons emerging from the beam tube at reactor power of 40 kW has been measured using threshold detectors by Boddy *et al.* (1969). The spectrum seems fairly degraded when compared with the neutron spectrum from fission

reaction of ^{252}Cf neutron source and shows a large portion of thermal neutrons. The spectrum has a broad peak at about 1MeV with a tail extending to 10 MeV. This spectrum was taken using a beam collimator with an aperture of 15 cm x 7.5 cm typically used in in-vivo activation analysis for clinical examination at reactor power of 20 kW (Boddy *et al.*, 1972).

In the present work, however, a circular beam collimator with the diameter of 10 cm nearest to the reactor core and 13 cm at the opening was used instead and the reactor power was set at 1 kW. The spectrum was not measured.

6.1.2 Radioactive Neutron sources

Neutrons are produced through (γ,n) and (α,n) nuclear reactions or through spontaneous fission (e.g. ^{252}Cf). ^{252}Cf and ^{241}Am-Be radioactive neutron sources were used to irradiate the counter. Their characteristics are shown in **Table 6.1.** The neutron yield per gram is lower for the ^{241}Am-Be compound source than for the spontaneous fission source of ^{252}Cf.

Table 6.1 General characteristics of radioactive neutron sources of 10^8 $n.s^{-1}$ emission.

Neutron	Half-life	Neutron yield	Dose Equivalent Rate at 1m	
Source	(year)	$n.s^{-1}$/ $3.7x10^{10}$ Bq	neutron (μSv/hr)	γ-ray (mR/hr)
^{252}Cf	2.65	4.3×10^9	840	6.2
^{241}Am-Be	458	2.2×10^6	1100	100

A typical spectrum for ^{252}Cf neutrons shows that it has a broad peak at about 1.6 MeV with the tail extending to 10 MeV Boddy *et al.* (1972). The average neutron energy is about 2.35 MeV (Claros, 1973). The neutrons emerging from ^{241}Am-Be source produced

through the $^{9}Be(\alpha,n)^{12}C$ nuclear reaction has a broad spectrum at about 5.5 MeV with the secondary at about 8.0 MeV and a tail extending to about 12 MeV. The average neutron energy is about 4.39 MeV. The neutron fluences at the beam exit for ^{252}Cf and ^{241}Am-Be neutron sources were calculated to be 4.295×10^{4} and 6.437×10^{3} n cm^{-2} s^{-1} respectively.

6.2 Methods of Microdosimetric Spectra Measurement

6.2.1 Experimental Procedures

The experiment has been divided into two sections as follows

1) In the low-LET spectrum measurements, the microdosimeter was irradiated with ^{60}Co gamma rays at pressure corresponds to the simulated tissue mean chord length of 0.5, 1.0 and 2.0 μm. The uncertainty of the chord length was about 0.01 μm, being only dependent on the smallest readable scale on the pressure gauge meter. The experiment was performed with inner counter TEPC operated without anti-coincidence with the outer TEPC, and then immediately followed by the inner TEPC operated with anti-coincidence with the outer TEPC. Two successive runs have been made using two different electronic gain setting at the relative gain of 1:10. This enables us to cover two decades of y-spectrum from about 0.1 to 20 keV/μm. In each run, background noise was determined for subtraction.

2) In the irradiation with mixed radiation fields, the pressure of the counter was maintained corresponding to the mean chord length of 1.0 μm. In a manner similar to that procedure used for low-LET irradiation, the experiment was performed with the microdosimeter operated without and with anti-coincidence modes. Four successive runs were made with the electronic gain setting at 2.5, 15, 100 and 1000. The assembled spectrum then covers four decades of y-spectrum from about 0.3 to 1000 keV/μm.

The neutron beam from the reactor was obtained by removing the central vertical stringer plug. The microdosimeter was mounted perpendicular to the beam axis at the top of the stringer in which the hole extends 200 cm into the reactor core. Similar procedure has been followed for irradiation with radioactive neutron sources but the counter position was 11 cm and 38 cm from the ^{252}Cf and ^{241}Am-Be sources respectively. However, the middle

of the sensitive volume was about 2.0 - 3.0 cm off the beam axis in irradiation with the ^{241}Am-Be neutron source. Apart from the beam hole, about 2.5 cm in diameter, the sources were enclosed in their polyethylene seals. The counter was covered with cadmium 1.0 mm in thickness to remove thermal neutrons. The irradiation times were 200, 2000 and 10,000 seconds for the UTR-300 reactor, ^{252}Cf and ^{241}Am-Be sources respectively.

6.2.2 Spectrum Analysis

The spectra were collected in terms of counts per channel vs. channel on a linear-linear scale from the MCA. The channel can be easily converted to y values using the relation obtained from the calibration procedure, based on the knowledge of the mean linear energy transfer and mean chord length of the sensitive volume as discussed in section (5.1). The following relation has been used for the conversion to lineal energy y.

$$y_i = k \cdot \frac{N_i}{N_\alpha} \qquad (6.1)$$

where $k = \bar{E}_D / \bar{l}$, $\bar{E}_D$ is the energy deposited in the counter, $\bar{l}$ is the mean chord length of simulated tissue mean chord length, N_i is the i-th channel number and N_α is the channel number of the calibration peak as derived from the calibration curve. Note that the measured calibration peak position and that deduced from the calibration curve was almost the same value, showing that the counter has a linear response to the electronic gain. The energy loss for simulated mean chord length of 0.5, 1.0, and 2.0 μm are 68.3, 138.2 and 283.9 keV respectively.

The sub-spectra after background subtraction were assembled into composite spectrum in log-log scale. The data was not normalized to the dead-time-corrected count since the dead time was usually less than 1% except that at the highest electronic gain where the dead time was about 3-5 %. The combined spectra covers several decades and each decade has been divided into 25 equal logarithmic intervals, B, given by the following relation.

$$y_i = y_0 \times 10^{i/B} \tag{6.2}$$

where y_0 is the initial lineal energy of the decade, i is the interval number and B=25. To obtain the frequency distribution, f(y), the number of count at the lineal energy y, N(y), is normalised to the total count. Thus, the frequency and dose distributions of lineal energy can be written in the linear scale by equations (6.3) and (6.4) respectively, as

$$f(y_i) = \frac{N(y_i)}{\sum N(y_i)} \tag{6.3}$$

$$d(y_i) = \frac{y_i\, f(y_i)}{\bar{y}_F} \tag{6.4}$$

In the logarithmic scale the frequency distribution becomes $y_i\, f(y_i)$. Other quantities which are related to f(y) and d(y) are straight forward. A computer program has been written for the calculation of microdosimetric spectra, the mean values of lineal energy and quality factor derived from various methods for mixed radiation fields are given in Appendix B. For graphical presentation in logarithmic scale, the following relations have been applied (ICRU, 1983).

$$f(y)\, dy = y\, f(y)\, d(\ln y) = \ln 10\; y\, f(y)\, d(\log y) \tag{6.4}$$

and
$$\Delta \log y = \frac{(\log y_n - \log y_0)}{n} = \frac{1}{B} \tag{6.5}$$

Thus,
$$\int_0^\infty f(y)\, dy = \frac{\ln 10}{B} \Sigma y_i\, f(y_i) = 1 \tag{6.7}$$

$$\int_0^\infty d(y)\, dy = \frac{\ln 10}{B} \Sigma y_i\, d(y_i) = 1 \tag{6.8}$$

The ^{60}Co gamma ray spectra were measured as low as 0.15 keV/μm and therefore an extrapolation to the lower y is necessary to evaluate the frequency and dose mean lineal energies. Various procedures have been recommended (Booz, 1976). In the present work, the y f(y) spectrum was extrapolated down to 10 eV with a constant slope. The extrapolation to higher values of y is relatively easy because the slope is approximately constant for all the spectra. On the other hand, the spectra of the mixed fields were measured as low as 0.2-0.4 keV/μm and no extrapolation was made on the spectra below the measured values. Instead, it was simply assumed that the low y events are due entirely to photons. Therefore, ^{60}Co spectra for 1 μm mean chord length were fitted to the measured spectra for both with and without anti-coincidence modes of operation.

For the subtraction of gamma fractions, various methods have been applied for example matching f(y) vs log y (Causins and Rushton, 1984), y^2 f(y) vs log y (Haque and Saqan, 1978), d(y) vs log y (Srdoc *et al.*, 1981) and y d(y) vs log y (Schumaucher *et al.*, 1987). Also, various gamma ray spectra have been used for example ^{226}Ra, ^{137}Cs, ^{60}Co and ^{24}Na. In this work, however, we matched the y^2 N(y) vs log y spectrum for the subtraction of the gamma component. First, the ^{60}Co spectrum was multiplied by a constant factor until it merged to the spectra of the mixed fields. Then N(y) for gamma and neutron components was deduced for further computation. It should be pointed out that the gamma-ray energy depositions in mixed fields are not identical with the ^{60}Co gamma-ray spectrum. Thus the ^{60}Co gamma-ray spectrum was used only for the approximation of photon events in regions of low y-values.

6.3 Results and Discussion

6.3.1 Microdosimetric Spectra of Low-LET Radiation

6.3.1.1 y f(y) vs y distribution

The y f(y) vs y spectra of ^{60}Co gamma rays are shown in **Fig. 6.1** and **Fig. 6.2** for counter operated without and with anti-coincidence modes respectively. The spectra show a positive slope, a peak and a shoulder depending on the mean chord length and the mode of operation.

In the spectra without anti-coincidence, **Fig. 6.1**, the initial slope appears at about 0.2 keV/μm and the peak occupies between 0.2 keV/μm to 0.3 keV/ μm. Both the slope and the peak are nearly independent of the mean chord length. Nevertheless, the peak of the 0.5-μm spectrum is slightly shifted to higher y which may be due to the calibration problem . The general shape of the spectra is that, for large value of y the spectra decreases until a shoulder is formed at about 6.0 keV/μm. The steepness of the negative slope depends on the mean chord length. The spectrum for higher mean chord length steeper than that for lower mean chord length. At the shoulder region, however, the gradient of all the spectra is about equal.

In the spectra with anti-coincidence, **Fig.6.2**, the initial slope appears at about 0.3 keV/μm and the peak occupies between 0.3 to 0.5 keV/μm, both being independent of the mean chord length. They form shoulders at about 5.0 keV/μm which drops with the gradient of about equal value.

The peak of the spectra without anti-coincidence events is due to high energy electrons having ranges that are large in comparison with the simulated volume dimension, i.e crossers. These Compton electrons have energy at about 700 keV for ^{60}Co (Booz, 1976). The spectra with anti-coincidence have less events below about 0.3 keV/μm, and in turn the peak position is shifted to higher value of y. This shows that the crossers which deposit energy at lower y values, have been vetoed. This shift of the peak position indicates that the quality of ^{60}Co has been modified to that contributed from the insiders and those associated to the dividing wall, i.e. crossers, stoppers and starters with the energy corresponds to the thickness of the dividing wall or less. The peak for the anti-coincidence spectra is due to electron crossers confined within the dividing wall, i.e. equivalent to the range of electrons of energy about 600 keV corresponds to the wall thickness of 16 μm (Berger and Seltzer, 1982), and those with less energy.

At the higher value of y, the spectra with anti-coincidence decrease more slowly than the spectra without anti-coincidence.

6.3.1.2 y d(y) vs y distribution

The y d(y) vs y spectra of ^{60}Co gamma rays at the simulated mean chord lengths of 0.5, 1.0 and 2.0 μm are shown in **Fig. 6.3, Fig. 6.4** and **Fig. 6.5** respectively for the counter operated without and with anti-coincidence modes. The spectra are normalised to a unit dose. The general shape of the spectra shows a peak whose width and position are dependent on the mean chord length and mode of operation.

In the spectra without anti-coincidence, a peak appears at about 0.3-0.4 keV/μm, being narrower for the 2.0-μm spectrum than the peaks for the 1.0-μm and 0.5-μm spectra. Booz (1976) stated that the peak is due to electron crossers with the electron energy of about 700 keV produced by ^{60}Co gamma-ray interactions (Booz, 1976) and the width is determined by the avalanche statistics and Fano fluctuation. The peak of 2.0-μm spectrum is higher in magnitude than for the 1.0-μm and 0.5-μm spectra because more events were observed at the higher mean chord length as expected. The peak is shifted slightly to a higher value of y for smaller mean chord length which could be attributed due to the calibration problems since the shifting is consistent with decreasing mean chord length.

Except for the 0.5-μm spectrum, the spectra with anti-coincidence, also show a peak whose position is dependent on the mean chord length, but the peak appears at about 0.4-0.5 keV/μm. The spectrum of anti-coincidence mode is due mainly to insiders and those associated to the dividing wall, i.e. crossers, stoppers and starters, with the energy corresponds to the thickness of the dividing wall or less. No peak is observed for 0.5-μm spectrum as less crossers at the lower y for small volume. As the mean chord length decreases, crossers are becoming more important, therefore, it is quite consistent that small dose at the lower y is observed at the smaller mean chord length because the crossers have been vetoed by the anti-coincidence.

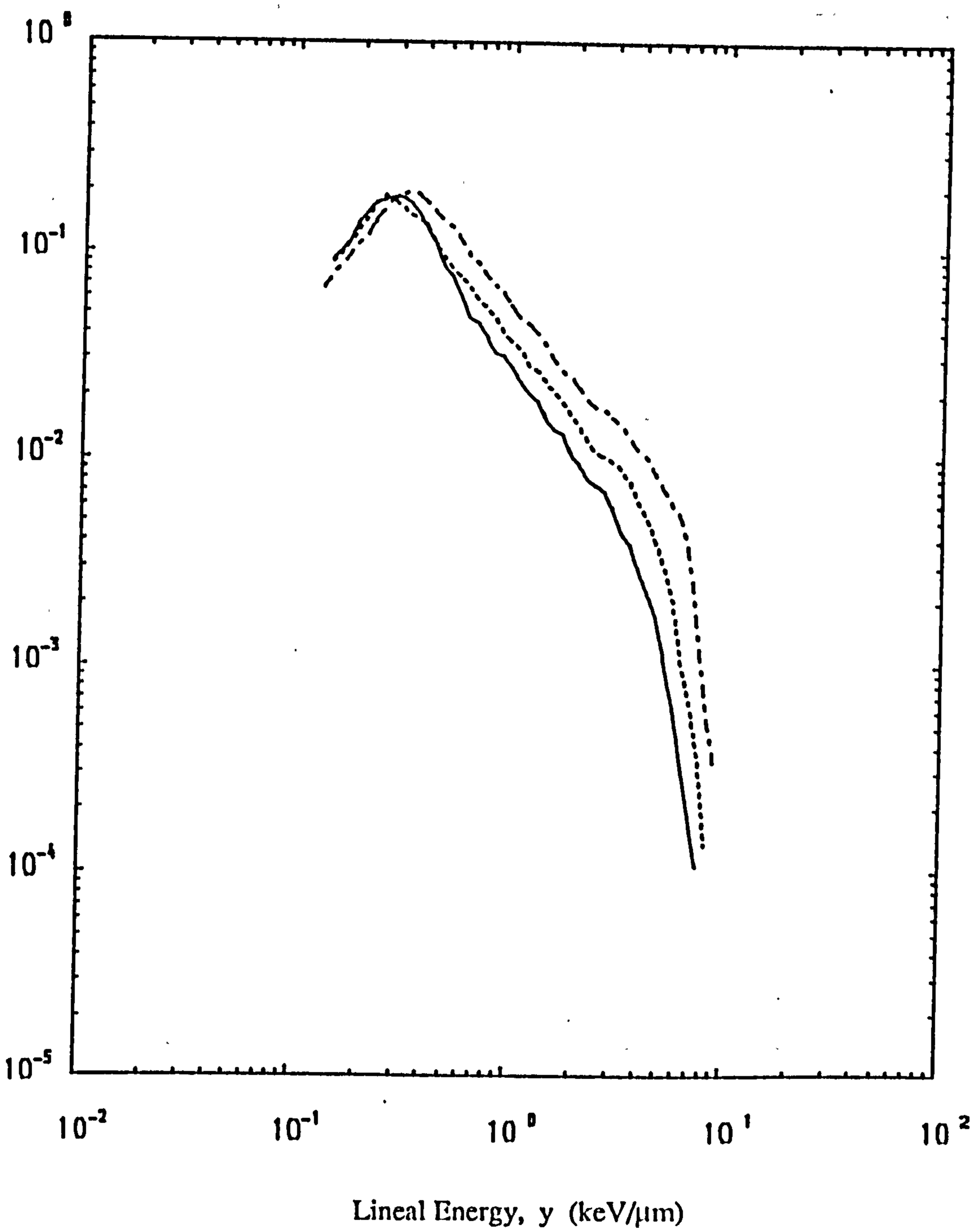

Fig. 6.1 y f(y) spectra of ^{60}Co gamma-rays for co-axial double cylindrical TEPC operated without anti-coincidence at various mean chord lengths.

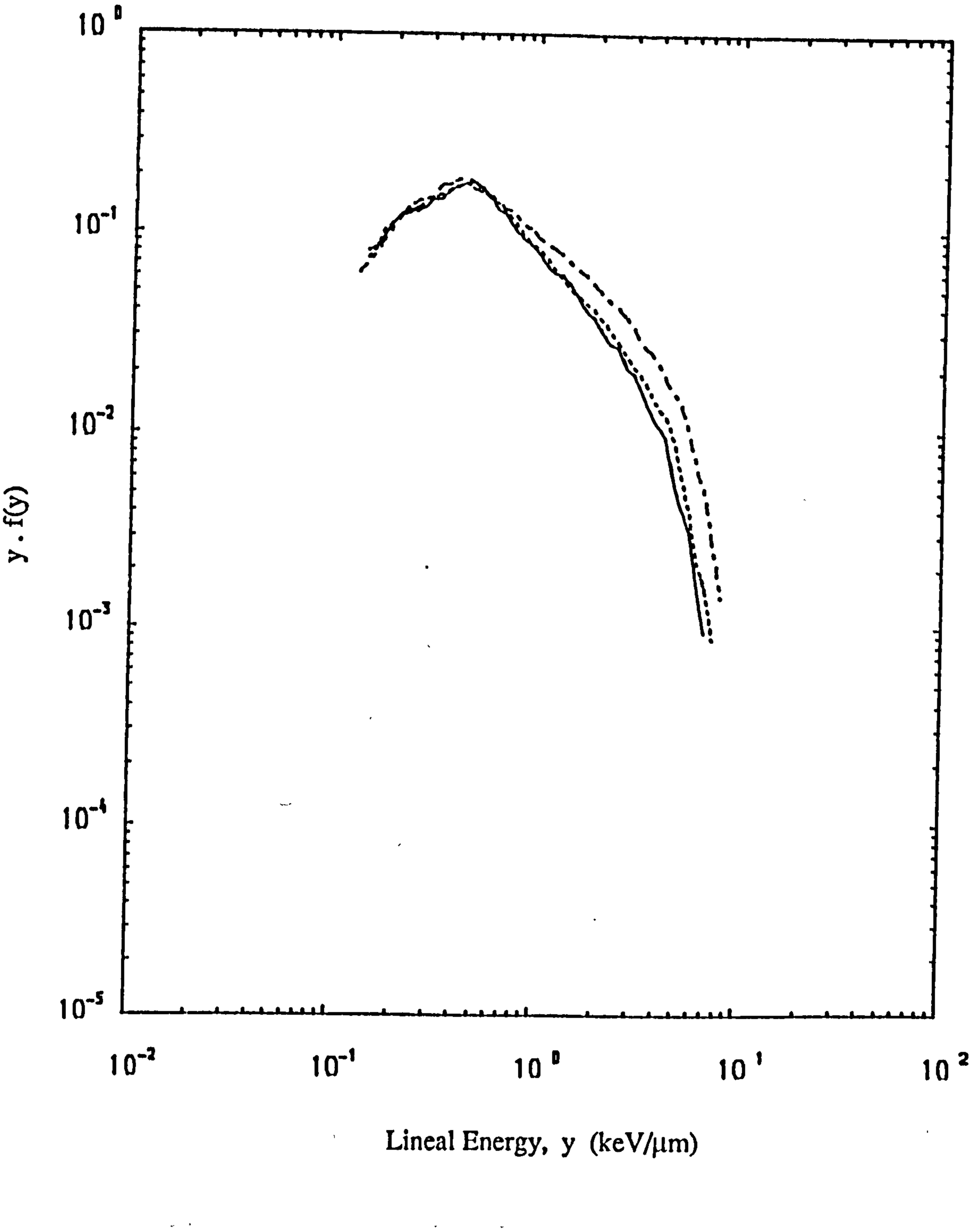

Fig. 6.2 y f(y) spectra of ^{60}Co gamma-rays for co-axial double cylindrical TEPC operated with anti-coincidence at various mean chord lengths.

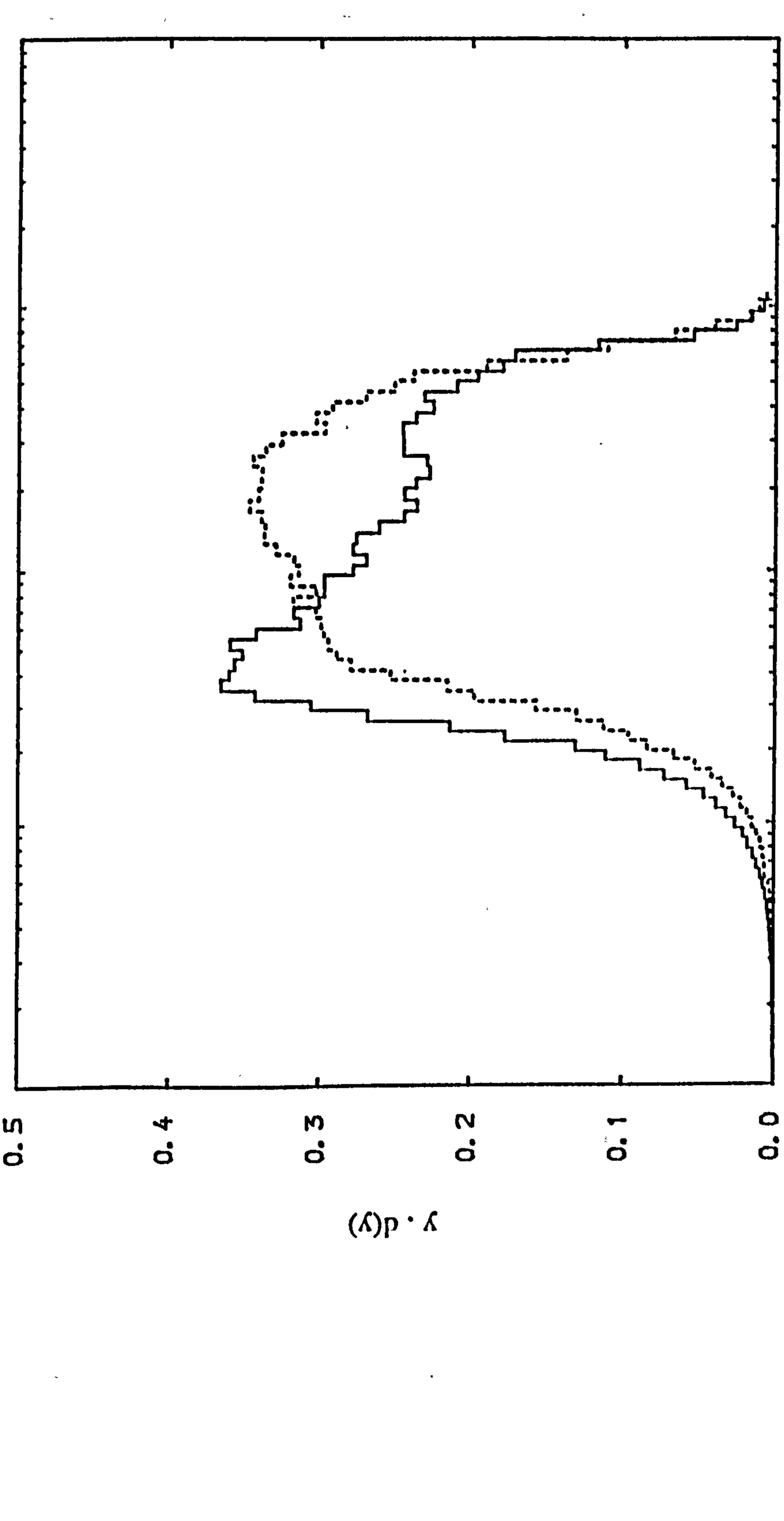

Fig. 6.3 y d(y) spectra of ^{60}Co gamma-rays for co-axial double cylindrical TEPC operated without and with anti-coincidence modes at simulated mean chord length of 0.5 μm.

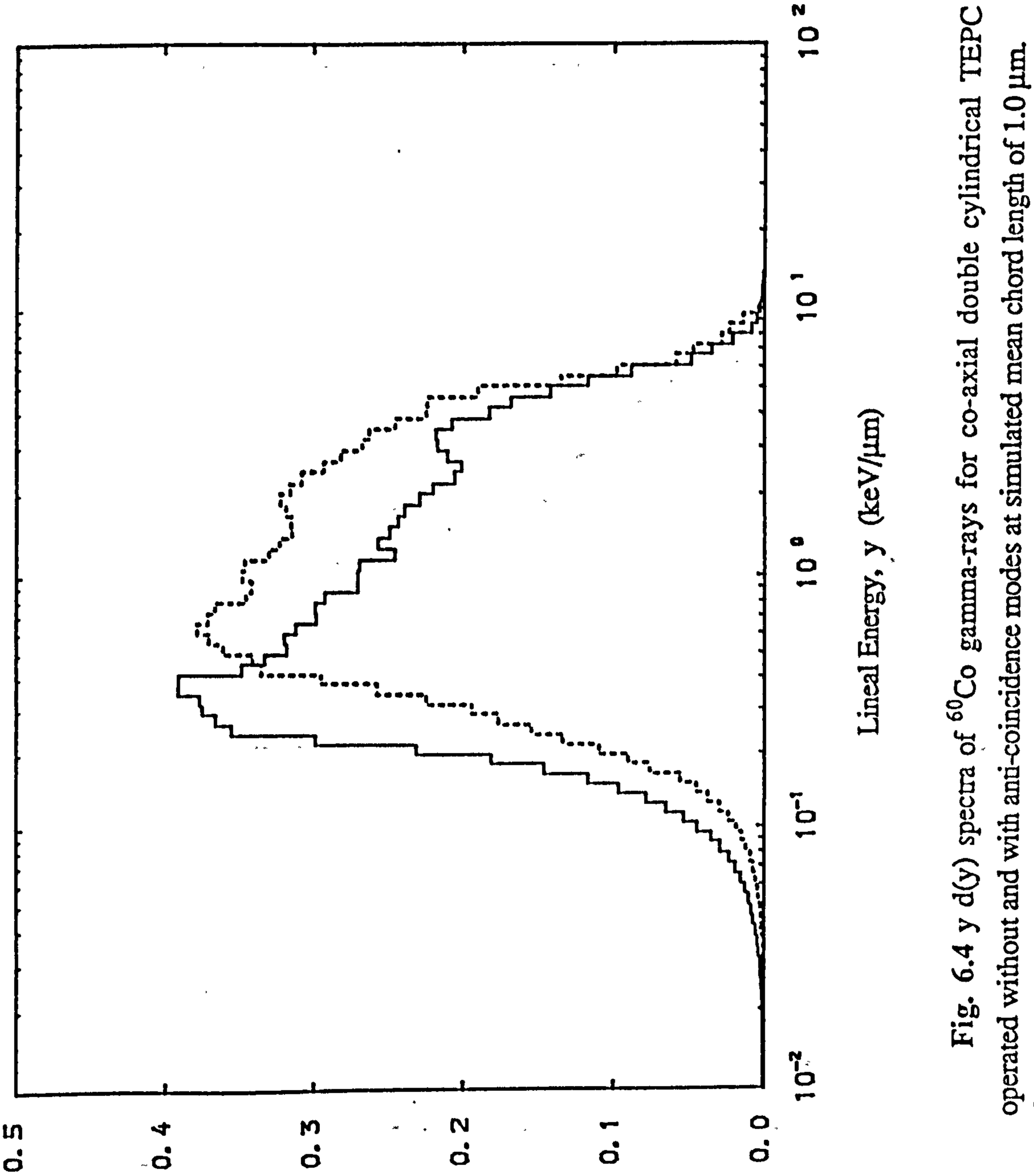

Fig. 6.4 y d(y) spectra of ^{60}Co gamma-rays for co-axial double cylindrical TEPC operated without and with anti-coincidence modes at simulated mean chord length of 1.0 μm.

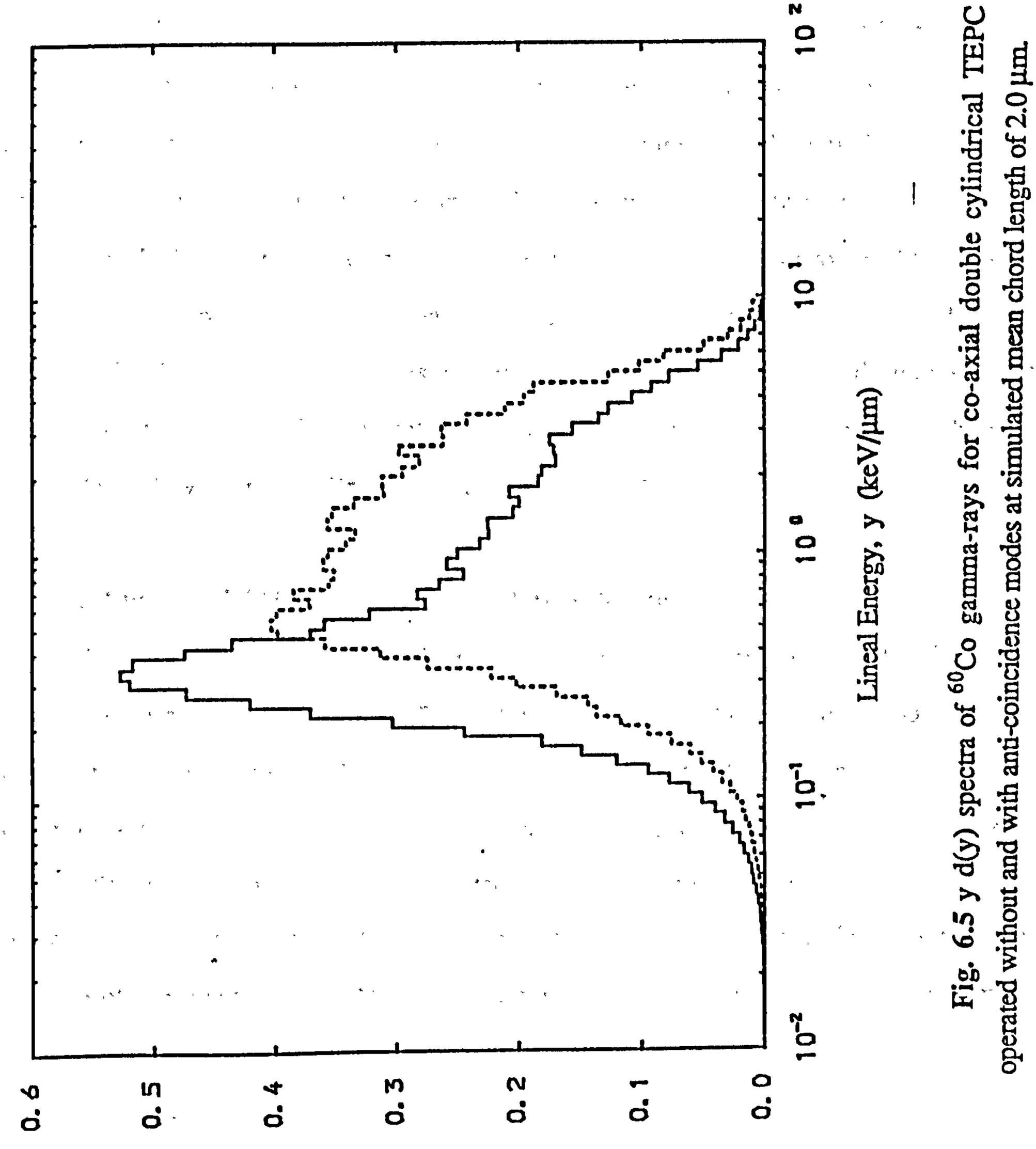

Fig. 6.5 y d(y) spectra of ^{60}Co gamma-rays for co-axial double cylindrical TEP operated without and with anti-coincidence modes at simulated mean chord length of 2.0 μm.

6.3.2 Microdosimetric Spectra of Mixed Fields

Microdosimetric spectra of the mixed fields are shown in **Fig. 6.6 - 6.11** for the counter operated without and with anti-coincidence modes. The spectra are shown in the conventional y.d(y) vs. log y presentation in such a way that equal areas under the curves represent equal contributions to absorbed dose. The underlying physical processes which explain the shape of the spectra have been discussed for instance by Rodgers and Gross (1974). The spectra can be divided into three components. First, the dose fraction at $y \leq 8.0$ keV/μm is due mainly to electrons produced predominantly by photons through Compton scattering and also through photoelectric effect. Second, the dose fraction from y about 8.0 keV/μm to 150 keV/μm is due entirely to the fast and slow protons produced from neutron interactions. Third, the dose fraction at $y \geq 150$ keV/μm due to heavy charged particles which is hardly shown in the measurements. The dose distribution is dominated by the proton events which produce a proton edge at about 150 keV/μm and most of the proton events fall below the proton Bragg peak at about 100 keV/μm.

6.3.2.1 Spectra Without Anti-Coincidence Mode

The spectra without anti-coincidence mode for UTR-300 reactor, ^{252}Cf and ^{241}Am-Be neutrons are shown in **Fig.6.6, 6.7** and **6.8** respectively. Gamma contributions to the dose for each spectrum are 13.2, 26.2 and 41.1% respectively. The shape of the gamma component of the spectra depends on the energy of the gamma ray energy (Coppola *et al* ., 1976). The gamma component is attributed from gamma rays generated by neutrons in the mixed fields from the environment and by hydrogen capture, $H(n,\gamma)D$, which produces photons of energy of about 2 MeV. More gamma contribution in the Am-Be spectrum could be attributed from the scattering gamma radiation in the room.

Neutron contributions to the total dose are due predominantly to the protons. The high energy protons, i.e. crossers deposit energy predominantly at the lower y, while at the higher y the dose distributions are due to slow recoil protons due to crossers, insiders, starters and stoppers. Consequently, the shape of the spectra depends on the composition of

the low and high energy protons. However there is no obvious separation between the low-y and high-y doses.

The difference between the reactor and ^{252}Cf fission neutron spectra is small. However, the Am-Be spectrum is different from the fission neutron spectra, in which more proton event at the lower y are due to the fast protons. This is due to the fact that more high energy neutrons are emitted from the Am-Be neutron source than the others.

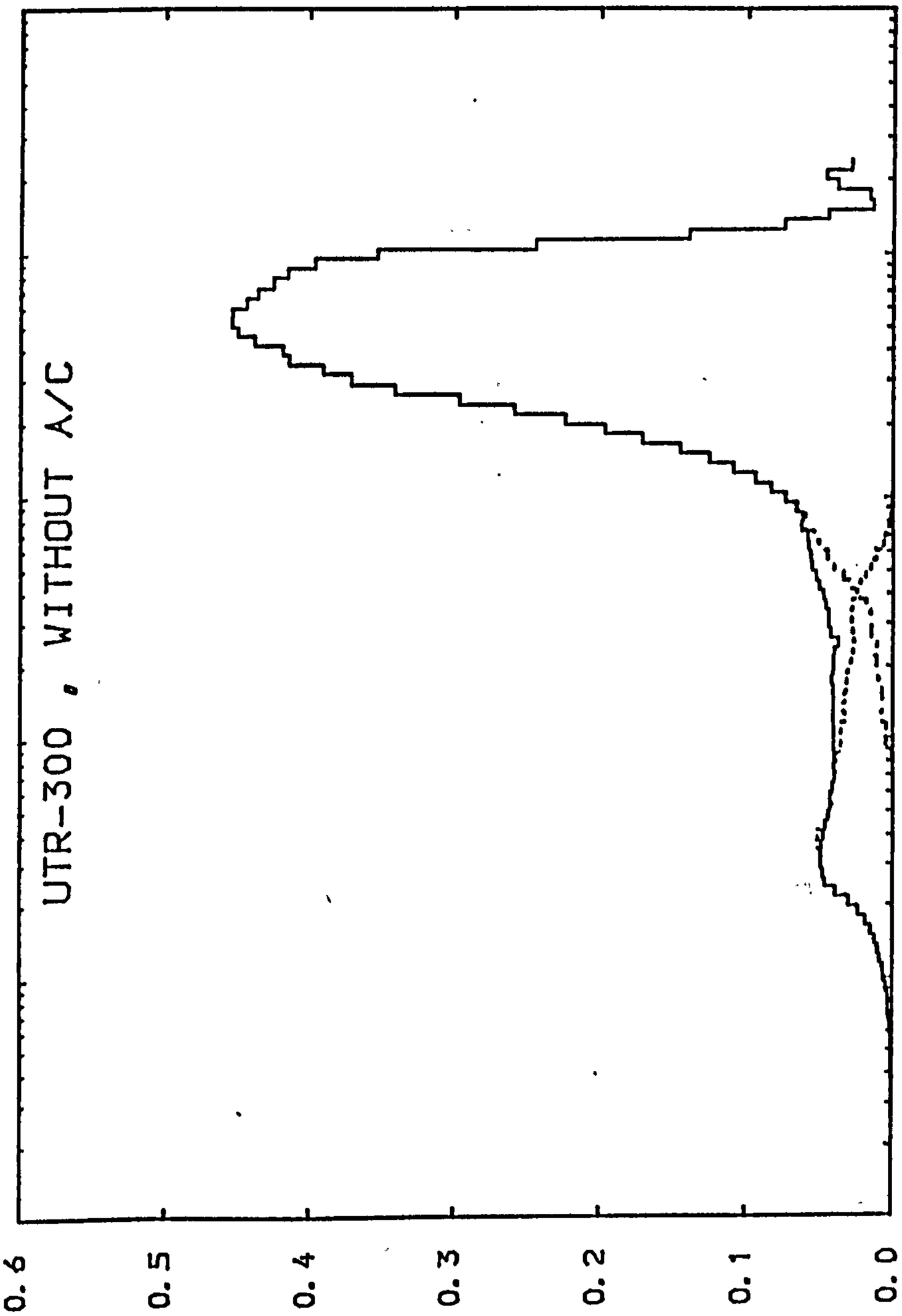

Fig. 6.6 y d(y) spectra of mixed fields of the UTR-300 nuclear reactor for co-axial double cylindrical TEPC operated without anti-coincidence mode at simulated mean chord length of 1.0 µm.

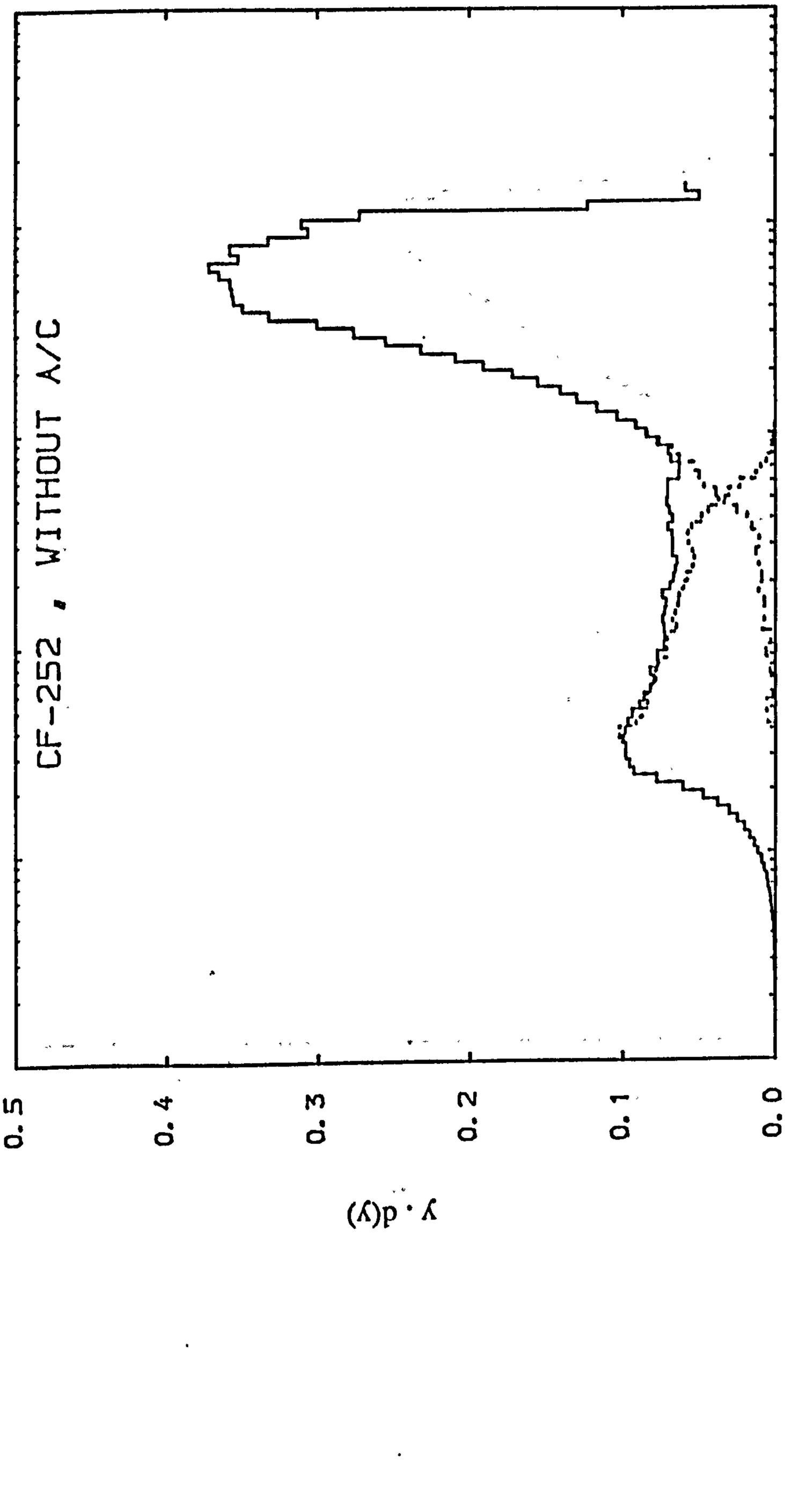

Fig. 6.7 y d(y) spectra of mixed fields of the ^{252}Cf fission neutrons for co-axial double cylindrical TEPC operated without anti-coincidence mode at simulated mean chord length of 1.0 μm.

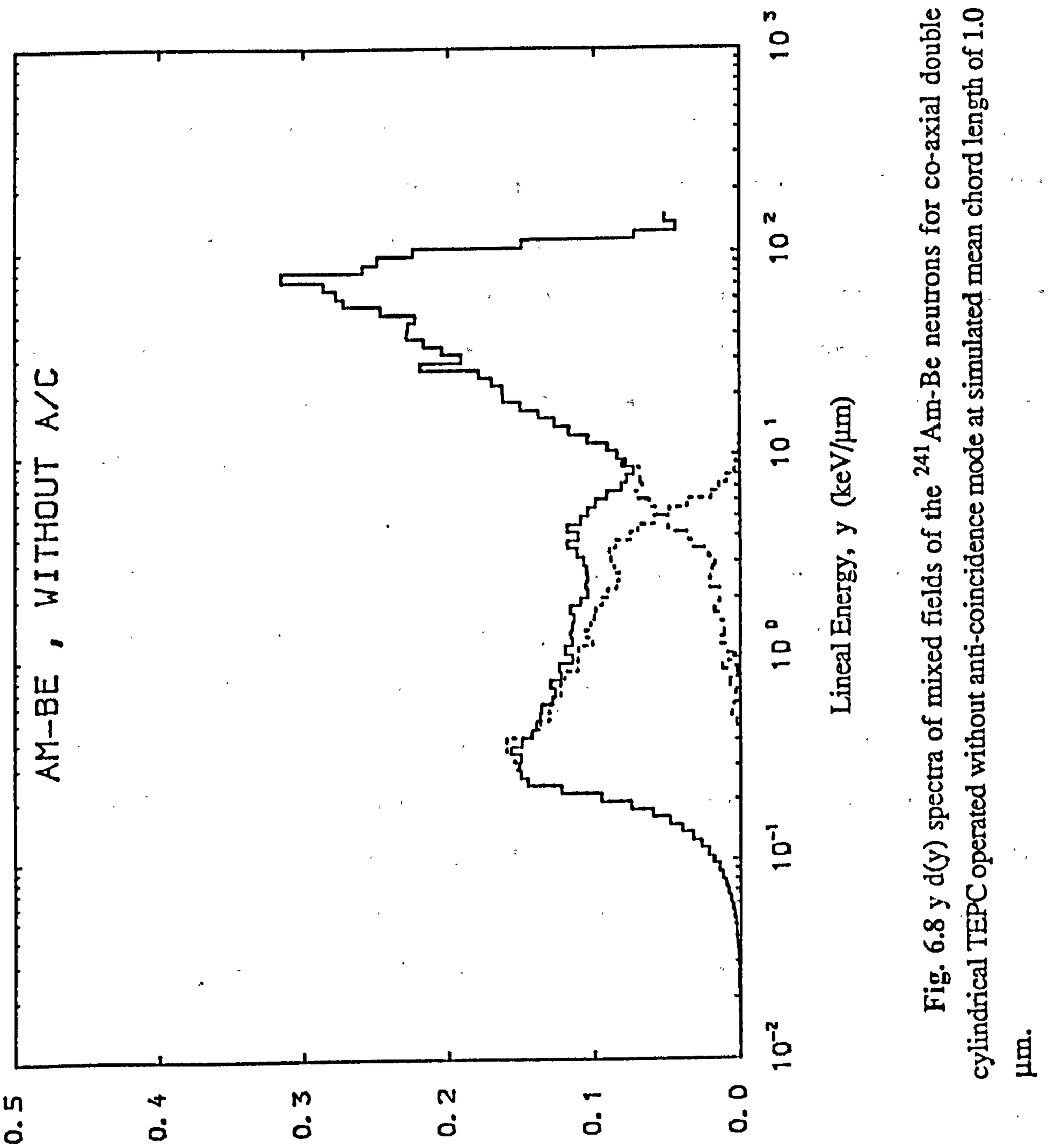

Fig. 6.8 y d(y) spectra of mixed fields of the ^{241}Am-Be neutrons for co-axial double cylindrical TEPC operated without anti-coincidence mode at simulated mean chord length of 1.0 µm.

6.3.2.2 Spectra With Anti-Coincidence Mode

The spectra with anti-coincidence mode for the UTR-300 reactor, ^{252}Cf and ^{241}Am-Be neutrons are shown in Fig. **6.9, 6.10** and **6.11** respectively. The shape of the spectra indicates a significant portion has been vetoed for both the gamma and neutron components when operated in anti-coincidence mode.

Gamma contributions to the absorbed dose are 13.6, 18.2, and 28.0% for UTR-300 reactor, ^{252}Cf and ^{241}Am-Be neutron spectra respectively. Gamma contribution to the absorbed dose for the reactor spectrum is reduced slightly but the percentage of the contribution is about the same value as that of the spectrum without anti-coincidence because more insiders were observed. The spectra obtained from radioactive sources show a considerable drop in the gamma contribution. The underlying physical process have been discussed in section (6.3.1).

The dose fractions due to the high energy protons which occupy the lower y values, i.e. the crossers, in the spectra without anti-coincidence have been removed by the anti-coincidence.Here, the dose fractions are dominated by slow recoil protons due to insiders and those associated with the dividing wall of energy corresponds to the thickness of the dividing wall or less, i.e. crossers, stoppers, and starters which occupy at the lower $y \leq 150$ keV/μm. Note that, slow proton crossers dominate the spectrum with anti-coincidence because protons of energy equivalent to about twice the thickness of the dividing wall can deposit energy in the inner TEPC without being detected by the anti-coincidence arrangement. Therefore, protons of energy ≤ 1.7 MeV can be of crossers, starters and stoppers.

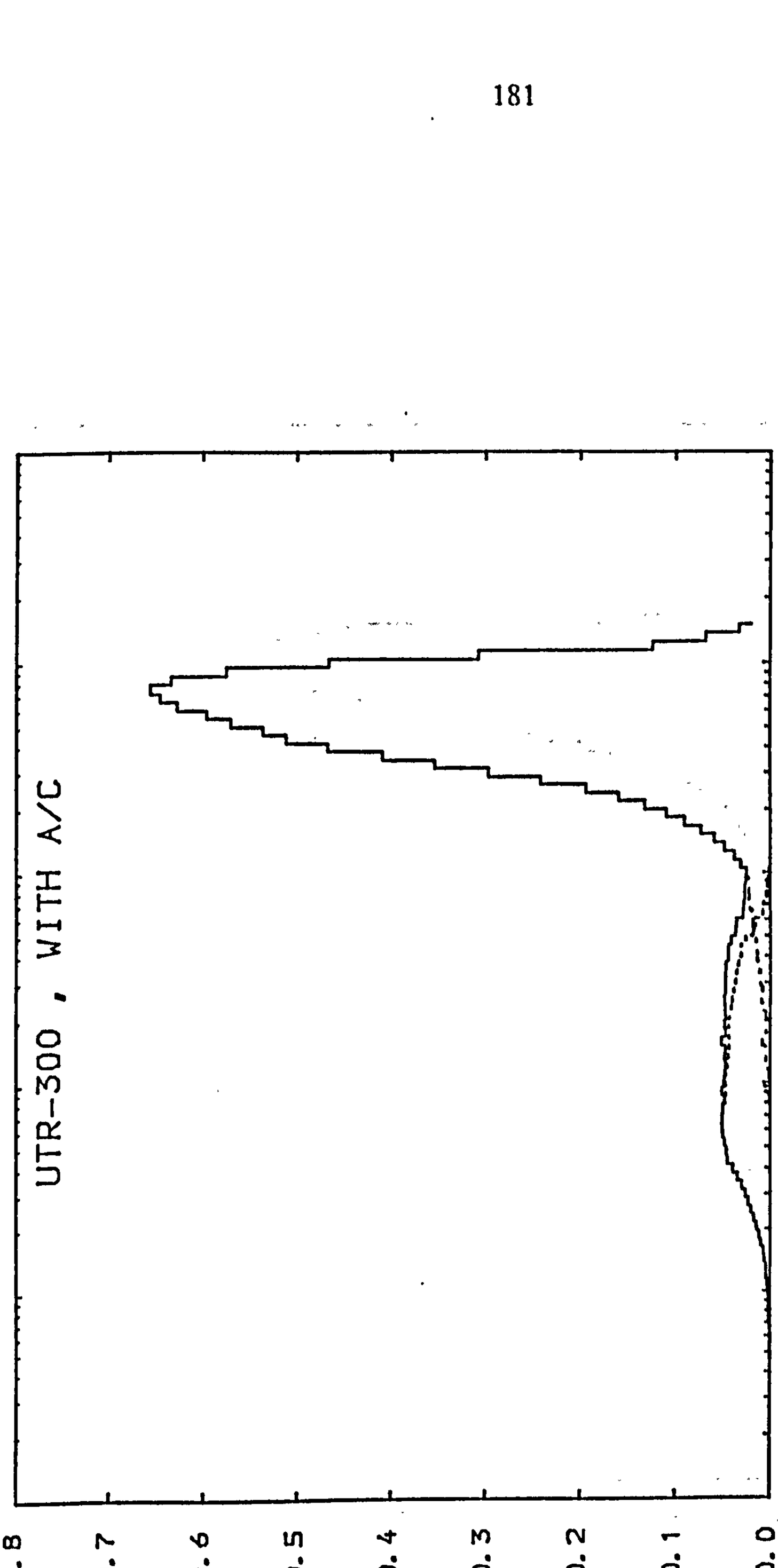

Fig. 6.9 y d(y) spectra of mixed fields of the UTR-300 nuclear reactor for co-axial double cylindrical TEPC operated with anti-coincidence mode at simulated mean chord length of 1.0 μm.

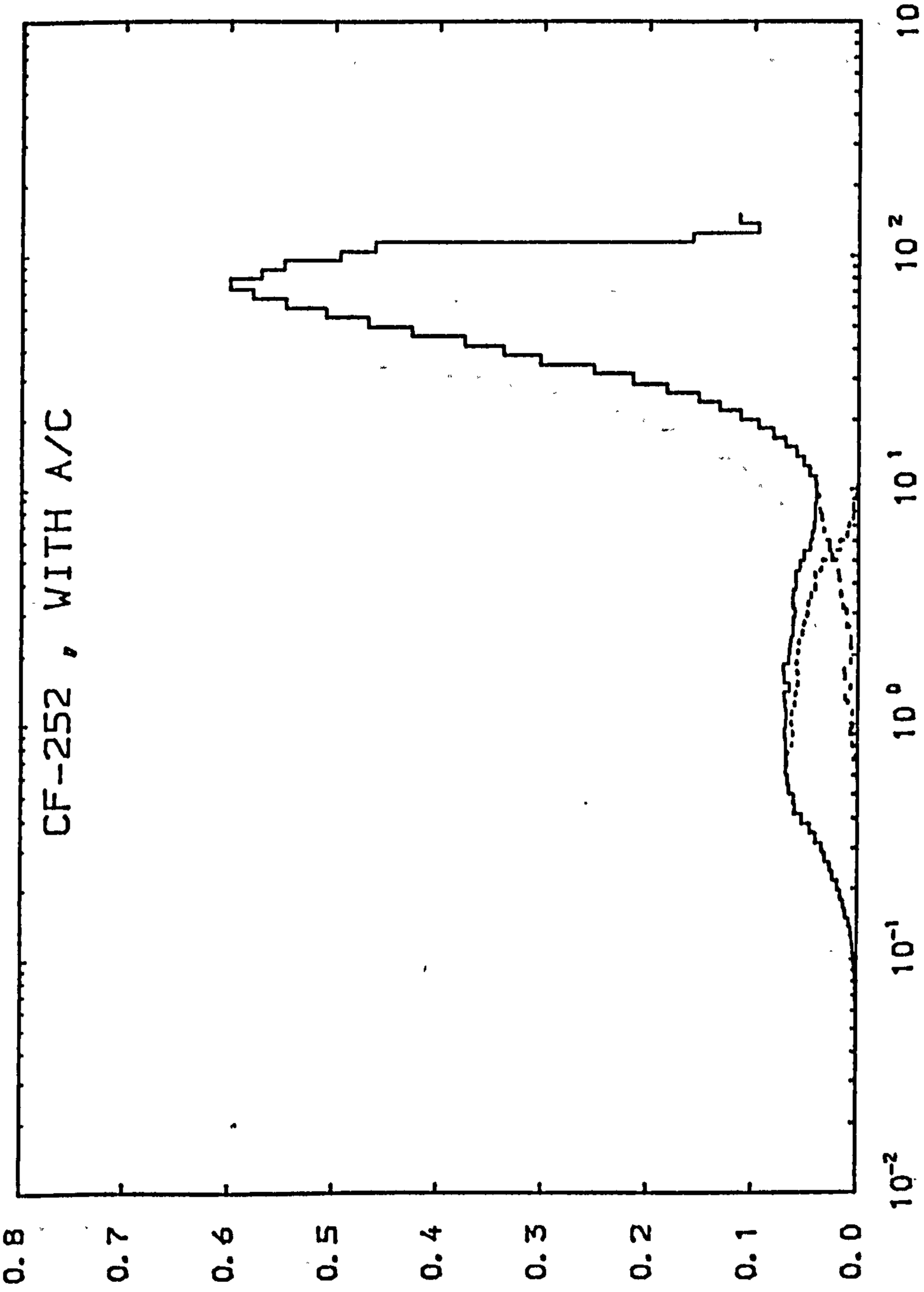

Fig. 6.10 y d(y) spectra of mixed fields of the ^{252}Cf fission neutrons for double cylindrical TEPC operated with anti-coincidence mode at simulated mean chord length of 1.0 μm.

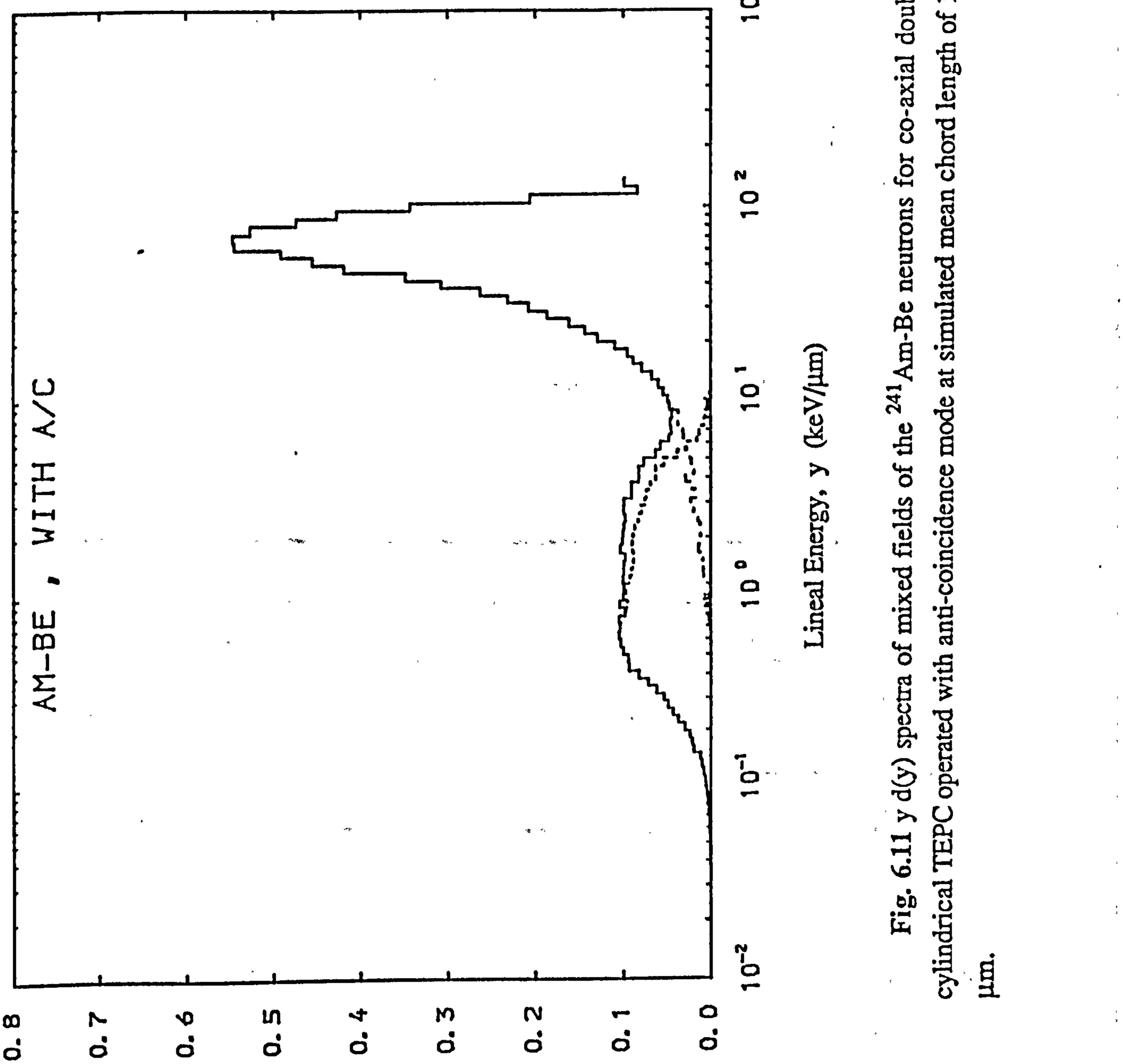

Fig. 6.11 y d(y) spectra of mixed fields of the ^{241}Am-Be neutrons for co-axial double cylindrical TEPC operated with anti-coincidence mode at simulated mean chord length of 1.0 μm.

6.3.3 Mean values of Lineal Energy

6.3.3.1 Low-LET ^{60}Co Gamma Rays

The frequency and dose mean lineal energy for the counter operated with and without anti-coincidence modes are shown in **Table 6.2.** It can be seen that the value of $\bar{y}_F$ increases with the decrease of mean chord length. Also, the value of $\bar{y}_F$ is higher for the dosimeter operated with anti-coincidence than that operated without anti-coincidence mode. This shows that the mean energy deposition per event is higher for the smaller mean chord length than that of the larger mean chord length because more crossers occur for the smaller tissue volume. The higher mean energy deposition per event in anti-coincidence mode is due to the fact that slow electrons dominate the events at higher y-values.

Table 6.2. The frequency and dose mean lineal energies of ^{60}Co gamma rays for co-axial double cylindrical TEPC operated without and with anti-coincidence arrangements.

$\bar{l}$	$\bar{y}_F$ (keV μm^{-1})		$\bar{y}_D$ (keV μm^{-1})	
(μm)	without A/C	with A/C	without A/C	with A/C
0.5	0.549	0.746	1.647	1.933
1.0	0.428	0.635	1.273	1.575
2.0	0.373	0.592	0.962	1.451

Also, it can be seen that the value of $\bar{y}_D$ increases with the decrease of mean chord length and is higher for the dosimeter operated with anti-coincidence mode. This reflects that the dose average energy deposition is higher for the smaller simulated tissue volume and for anti-coincidence mode.

The value of $\bar{y}_F$ is unaffected by the resolution of the counter. However, the value of $\bar{y}_D$ is influenced by the variance due to ionization fluctuation, counter resolution and the

chord length distribution of the counter. The relative variance of the chord length distribution for ^{60}Co in a cylinder is six times greater than that of the sphere (Eickel and Booz, 1976).

The results of the previous measurements using conventional TEPCs are shown in **Table 6.3.** It is not possible on the basis of these measurements to compare with the previous results because the difference obtained by others and by us could be due to the fact that the present counter produced less scattering than the conventional TEPCs. It was found that the extended value of y is about 10 keVμm^{-1} for the mean chord length of 0.5 μm as compared with 20 keVμm^{-1} using conventional cylindrical TEPC for the mean chord length of 0.65 μm (Coppola *et al.*, 1976). Consequently our $\bar{y}_D$ values **(Table 6.2)** are consistently lower than others.

Table 6.3. The frequency and dose mean lineal energies of ^{60}Co gamma rays for conventional TEPC obtained in the previous works.

$\bar{l}$ (μm)	TEPC type	$\bar{y}_F$ (keV μm^{-1})	$\bar{y}_D$ (keVμm^{-1})	References
0.65	Cylinder, wall	0.39	2.78	Coppola *et al.* (1976)
0.65	Cylinder, wall-less	0.373	2.48	-do-
0.65	Sphere, wall	0.326	2.04	-do-
0.67	Cylinder I,wall-less	0.434	2.42	Herskind and Jessen (1981)
0.67	Cylinder II,wall-less	0.386	2.06	-do-
1.33	Sphere, wall	0.41	1.10	Heikkila and Kiviniitty (1981)
1.33	Sphere, wall-less	0.26	1.22	Kliauga and Dvorak (1978)
1.37	Cylinder, wall	0.31	1.86	Coppola *et al.* (1976)
1.37	Cylinder, wall-less	0.318	1.88	-do-
3.0	Cylinder, wall	0.314	1.46	-do-
3.0	Cylinder, wall-less	0.269	1.32	-do-

6.3.3.2 Mixed Radiation Fields

The frequency and dose mean lineal energies derived from the spectra without and with anti-coincidence modes are shown in **Table 6.4** and **6.5** respectively. It can be seen that the value of $\bar{y}_F$ and $\bar{y}_D$ is higher for the spectra with anti-coincidence than the spectra without anti-coincidence indicating higher values of the mean energy deposition per event and the dose average energy deposition in anti-coincidence mode. Fast protons and electrons have been rejected in anti-coincidence arrangements resulting in more energy being deposited by slow recoil protons and electrons. It is a known fact that slow charged particles deposit more energy in tissue than do fast charged particles.

The value of $\bar{y}_F$ obtained with anti-coincidence mode for spectra of the mixed fields is higher than that obtained without anti-coincidence mode by a factor about 2. There is a significant change in the value of $\bar{y}_F$ after gamma subtraction. However, the value obtained after the gamma subtraction are slightly higher for the spectra with anti-coincidence than the spectra without anti-coincidence by a factor of 1.4 for fission neutron spectra and 1.6 for Am-Be neutron spectra.

The value of $\bar{y}_D$ of the mixed fields depends on the dose distributions of gamma-ray and neutron compositions. There is no significant change in $\bar{y}_D$ values of the reactor spectra with and anti-coincidence modes because both spectra having about equal gamma compositions. On the other hand, a significant change in $\bar{y}_D$ values of the Am-Be spectrum without anti-coincidence from the spectrum with anti-coincidence is due to a large difference in the gamma-ray contaminations. Also, the $\bar{y}_D$ value of the neutron component in the anti-coincidence spectrum is slightly higher than the spectrum without anti-coincidence, as expected, because of the significant increase in the relative contribution from slow recoil protons.

Table 6.4. The frequency and dose mean lineal energies of mixed fields for co-axial double cylindrical TEPC operated without anti-coincidence arrangements and the mean values obtained from previous measurements using conventional TEPCs.

Source	$\bar{y}_F$ (keV μm^{-1})		$\bar{y}_D$ (keV μm^{-1})		Reference
	mixed	n-comp.	mixed	n-comp.	
UTR-300	2.90	23.97	48.21	55.35	This Work
Cf-252	1.59	20.05	39.30	52.85	-do-
Am-Be	1.00	14.56	27.40	45.59	-do-
Fission, 10m	3.76	26.99	58.28	59.28	Cousins and Rushton (1985)
Fission, 170m	1.84	23.24	52.70	61.50	-do-
Am-Be	0.81	-	30.66	-	Cowling and Waker (1985)

Table 6.5. The frequency and dose mean lineal energies of mixed fields for co-axial double cylindrical TEPC operated with anti-coincidence arrangements.

Source	$\bar{y}_F$ (keV μm^{-1})		$\bar{y}_D$ (keV μm^{-1})	
	mixed fields	n-component	mixed fields	n-component
UTR-300	4.19	33.29	50.32	57.94
Cf-252	3.15	27.71	52.76	64.19
Am-Be	2.11	24.03	40.70	55.88

6.3.4 Quality Factor and Dose Equivalent of Mixed Fields

The quality factor of ^{60}Co gamma rays derived from various formulae for spectra without and with anti-coincidence modes are shown in **Table 6.6.** $\bar{Q}_1$, $\bar{Q}_2$ and $\bar{Q}_4$ were obtained from equations (2.50), (2.42) and (2.47) respectively. $\bar{Q}_3$ was derived from equation (2.45) with the order changed from 1.5 to 0.6 according to Braby *et al.* (1983).

The quality factor for ^{60}Co gamma rays is high for spectra with anti-coincidence mode and for smaller mean chord length. Note that the differences between the Q-values using different formulae suggest more research is required to establish a unified formula which should include microdosimetric distributions and saturation factors. The values of $\bar{Q}_4$ are consistently higher than others because for an entirely different reason which will be discussed in the following discussion.

Table 6.6. The quality factor of ^{60}Co gamma-rays derived from various formulae for the spectra with and without anti-coincidence modes.

$\bar{l}$ (μm)	$\bar{Q}_1$		$\bar{Q}_2$		$\bar{Q}_3$		$\bar{Q}_4$	
	(a)	(b)	(a)	(b)	(a)	(b)	(a)	(b)
0.5	0.46	0.54	1.03	1.07	1.19	1.35	1.43	1.68
1.0	0.35	0.44	0.98	1.02	1.02	1.09	1.24	1.50
2.0	0.27	0.40	0.93	1.00	0.86	1.14	1.02	1.48

(a) without anti-coincidence mode
(b) with anti-coincidence mode

Table 6.7 tabulates the mean quality factor of neutrons in mixed fields derived from this work using various formulae as described above. The quality factor is higher when the dosimeter in operated with anti-coincidence and for fission neutrons. The values of $\bar{Q}_1$, $\bar{Q}_2$, and $\bar{Q}_3$ are in reasonable agreement among the respective formulae. They represent an approximation of biological effectiveness of mixed radiation fields for a given dose relative to the effectiveness of gamma rays.

The values of $\bar{Q}_4$, on the other hand, are consistently higher than the others by a factor of about 3-4. This is, as expected, because here the approximation of biological effectiveness is independent of parameters based on absorbed dose but depends on the saturation values of LET for different radiation types (Al-Affan and Watt, 1985 and 1987). The saturation lineal energies, y_0, applied are 3.6 keV/μm for electrons at $y \leq 8.0$ keV/μm

and 72 keV/μm for protons at y > 8.0 keV/μm. In this approach, cellular inactivation is determined predominantly by primary ionizations along the particle tracks when the mean spacing corresponds to 2 nm, i.e. equivalent to spacing between the strands in double-stranded DNA (Watt *et al.*, 1985). At first sight the results appear to be consistent with the recent recommendation of the ICRP that the quality factor of fast neutrons be increased by a factor of two, assuming that there is no biological repair for the reference radiation but there are other arguements which dispute this (Watt, 1989).

The calculated values of $\bar{Q}_4$ for 0.5 and 1.0 MeV neutrons are 54.5 and 53.2 respectively (Al-Affan and Watt, 1987). Our results are lower by less than 5 % for neutrons of energy of about 850 keV.

Table 6.7. The quality factor of neutrons derived from various formulae for co-axial double cylindrical TEPC operated without and with anti-coincidence modes in mixed radiation fields.

Source	$\bar{Q}_1$		$\bar{Q}_2$		$\bar{Q}_3$		$\bar{Q}_4$	
	(a)	(b)	(a)	(b)	(a)	(b)	(a)	(b)
UTR-300	14.59	16.80	8.55	8.91	9.17	10.16	42.82	49.17
CF-252	14.40	17.70	8.20	9.79	9.29	10.38	41.93	48.39
Am-Be	13.11	16.00	7.18	8.62	8.85	9.97	39.34	47.03

(a) without anti-coincidence mode

(b) with anti-coincidence mode

Table 6.8 and **6.9** tabulate the dose and dose equivalent rates of spectra without and with anti-coincidence modes for neutron and gamma components respectively. Equation (3.36) was used to calculate the dose received by the counter for the TE gas density corresponds to the mean chord length of 1.0 μm. The dose equivalent rates were calculated using the quality factor formulae of ICRU (1986) and Al-Affan and Watt (1987). Dose

equivalent rates measured using a Sievert meter were 5000, 600 and 60 μSv hr^{-1} for the UTR-300 reactor, ^{252}Cf and ^{241}Am-Be neutrons of mixed fields respectively. Measurement of gamma-ray dose equivalent rate in the room was about 1-3 μSv hr^{-1} for radioactive neutron sources and 50 μSv hr^{-1} at 50 cm from the vertical beam of the reactor at the operating power of 0.5 kW. Both measurements were made using ionization chamber type RO2A.

The results show that the dose and dose equivalent rates of spectra with anti-coincidence are higher than the spectra without anti-coincidence indicating the significant role of slow protons generated form neutrons in the mixed fields.

Dose equivalent rates based on the spacing of the primary ionization is higher than that based on the absorbed dose. These values are thought to be more realistic than the conventional ones for ionizing radiation at low dose and low dose rates as damage occur predominantly for electron tracks which are stoppers and also near the end of proton tracks i.e. when the mean free path of ionization corresponds to the spacing between the strands of the DNA.

Table 6.8. Dose and dose equivalent rates of the neutron component for the co-axial double cylindrical TEPC operated without and with anti-coincidence modes in mixed (n,γ) fields.

Source	Dose Rate, $\dot{D}$ (μGy hr^{-1})		Dose Equivalent Rate, $\dot{H}$ (μSv hr^{-1})			
			ICRU (1986)		Al-Affan and Watt (1987)	
	(a)	(b)	(a)	(b)	(a)	(b)
UTR-300	224.4	311.4	3142	5232	9609	15311
CF-252	18.86	25.93	272	459	791	1255
Am-Be	2.72	4.49	35.6	71.8	107	211

(a) without anti-coincidence mode

(b) with anti-coincidence mode

Table 6.9. Dose and dose equivalent rates of the gamma-ray component for the co-axial double cylindrical TEPC operated without and with anti-coincidence modes in mixed (n,γ) fields.

Source	Dose Rate, $\dot{D}$ (μGy hr^{-1})		Dose Equivalent Rate, $\dot{H}$ (μSv hr^{-1})			
			ICRU (1986)		Al-Affan and Watt (1987)	
	(a)	(b)	(a)	(b)	(a)	(b)
UTR-300	34.3	49.1	11.98	21.4	42.49	72.95
CF-252	6.69	5.79	2.34	2.54	8.29	8.67
Am-Be	1.90	1.75	0.67	0.77	2.36	2.62

(a) without anti-coincidence mode

(b) with anti-coincidence mode

6.4 Some Factors Influencing the Measurements

An attempt to compare our results with those from the conventional TEPC would be premature because much work has still to be done in exploring the capabilities and limitations of the dosimeter. However, it is a great importance to determine and discuss thoroughly all uncertainties involved and all parameters influencing the experimental results.

The counter has been calibrated using internal alpha particles prior to microdosimetric measurements. The calibration was performed by a series of measurements of the calibration peak at the lower electronic gains in order to determine the gradient of the calibration curve. Our data points indicate that the electronic system used has a linear response to the electronic gain. However, in the microdosimetric spectra measurements, the linearity of the electronic system throughout the lower y was assumed by extrapolating the calibration curve to higher electronic gains.

After the measurements the calibration peak at two extreme electronic gains was determined to make sure the linearity of the calibration is maintained. Consequently the gas gain stability was also checked after the measurement by determining the position of the calibration peak with respect to its position prior to the measurement. This was intended to correct system nonlinearities. However no significant change in the gas gain was detected. One or two channel shifting was expected for such a broad calibration peak.

The extrapolation of the measured spectra to zero energy can contribute errors up to about 20% for $\bar{y}_F$ and 1% for $\bar{y}_D$ (Booz, 1976 and ICRU, 1983). Also, the extrapolation to infinite lineal energy can affect the value of $\bar{y}_D$.

The dependence of energy per ion pair (w) on energy of charged particles is worth mentioning because it could introduce error to the measured spectra. However, in this work the energy was calibrated using alpha particles and by assuming a constant w value for both electrons and protons. Also, w taken as the same for alpha particles, protons and electrons.

CHAPTER 7

CONCLUSION AND FUTURE WORK

7.1 Conclusion

The radiation quality of intermediate energy neutrons is not well defined. Nevertheless they are known to be capable of producing serious biological effects because of their interactions with tissue mainly through elastic scattering to produce short-range heavy charged particles. In this region, where the nuclear scattering processes become more dominant than the electronic scattering processes (Al-Kazwini *et al.*, 1988) the stopping process of charged particles in matter is not fully defined. The stopping powers and projected ranges are important quantities for the determination of microdosimetric spectra of neutrons in tissue volumes. Due to lack of experimental data they can only be predicted by calculations (Lindhard *et al.*, 1963, Watt, 1972, Oldenburg and Booz, 1972, Ziegler, 1985 and Burger, 1976) as has been attempted in this work. The discrepancy between the experimental and theoretical results and between the theoretical methods suggests that more research needs to be done if the stopping process in this region is to be understood.

The conventional TEPCs are very useful devices for radiation protection despite the fact that they are incapable of separating the component of neutrons in any desired energy band in mixed fields of fast neutrons. It is very important, therefore, to develope a technique which has high efficiency for the detection of intermediate energy neutrons in mixed fields.This can be achieved using a co-axial double cylindrical TEPC which has a common TE dividing wall of thickness equivalent to the range of protons at the energy of interest and the use of coincidence/anti-coincidence counting arrangements. Events due to intermediate energy neutrons are detected in the inner counter when operated in anti-coincidence with the outer counter. Events due to fast neutrons interacting in both the counters can be removed by the anti-coincidence technique. However, there are some events due to fast neutrons which

deposit energy at the region of interest which must be removed by calculation to determine the necessary correction procedure to the measured spectra with a precision of about 10 %.

In the course of this research, much time and effort have been spent on the design and manufacture of the co-axial double cylindrical proportional counters both in non-TE and TE versions before pulses from ionizing radiation could be seen. Considerable difficulties were experienced in making the counters work mainly associated with the technical problems of electrical sparking due to sharp edges and inadequate insulation. Several methods had been tried before fabrication of the TE dividing wall could be achieved. Now TE films for the common dividing wall can be fabricated from A-150 TE plastic with sufficient homogeneity and conductivity at thicknesses of about 10-20 μm which corresponds to the maximum range of protons of energy 700 keV - 1 MeV. Use of then films of conducting mylar permit selection of neutrons < 100 keV but the degree of pertubation of the equilibrium charged particle conditions due to the non tissue-equivalence has yet to be assessed.

The present co-axial double cylindrical TEPC is capable of selecting the energy deposition spectra of neutrons (≤ 850 keV) in mixed radiation fields of fast neutrons. It is very important for better operating efficiency that the dosimeter should be incorporated with a fast coincidence/anti-coincidence unit having an appropriate threshold voltage. This is necessary in order to remove events from low pulses due mainly to electronic noise which otherwise could affect the gate operation and resulting loss of some of the anti-coincidence events.

The laboratory and field work experiments have confirmed the applicability of the dosimeter for microdosimetric measurements in mixed fields. Discrimination against gamma-rays and fast neutrons are achieved. The radiation quality and dose fraction of neutrons (≤ 850 keV) can be separated from those of fast neutrons which provide useful information for interpretive purposes in radiation protection. There is an increase in the radiation quality of spectra determined in the anti-coincidence mode indicating the greater importance of intermediate energy neutrons in mixed radiation fields.

The specification of radiation quality based on energy deposition is of limited value in defining the ability of ionizing radiation to induce damage. The quality of neutrons to produce biological damage appears to be consistent with the experimental observations if it is based on the mean free path between the primary ionizations, i.e. linear primary ionization (Watt, 1989). However, the quality can be determined approximately using microdosimetic technique by applying appropriate saturation corrections for different radiation types despite the knowledge that site sizes are of nanometer dimensions (Al-Affan and Watt, 1987). The quality factor of neutrons is three times higher than the conventional quality factor which suggest that the current values should be revised in terms of risk assessment.

7.2 Future Work

There are short-term and long-term future works need to be done to explore the practical value of this device for radiation protection.

Laboratory experiments with the dosimeter should be completed for gamma rays of various energies. The discrimination against gamma-ray induced events could be used to explore the differentiation between insiders and crossers, in particular for low-energy gamma rays at the smaller mean chord lengths. Also, the anti-coincidence technique could be used for enhancement of the differentiation between the electrons and low-energy proton events and requires further investigation. It may be possible to use the counter to extract information on the type of photon field.

Measurements with monoenergetic neutrons at various energies must be made to test the theoretical calculations and to improve methods of assessing correction factors for fast neutron effects. This could provide more information on the capabilities and limitations of the device for improvement in the future design of the counter.

To design a counter which can be operated selectively for intermediate energy neutrons (<100 keV) in mixed radiation fields, a uniform TE dividing wall with thickness of about

1.2 μm is required. The present method of preparation, using moulding techniques, was found to be inadquate for production of satisfactory walls with A-150 plastic at thicknesses which were sufficiently homogeneous and conducting. Improved fabrication techniques are required. Alternatively, TE film may be made from other plastic materials in which the conductivity could be increased by 'doping', in the same way as the plastic conductors are prepared. This will remove an excessive use of carbon for conductivity as in the case of A-150 plastic in which it was found difficult to make homogeneous because of the distribution of carbon molecules at film thicknesses of less than about 10 μm.

Recent developments in microelectronics combined with improved techniques for the TEPC construction could make it possible to develop a fully automated portable co-axial double cylindrical TEPC. The coincidence and anti-coincidence modes of operation can be achieved simultaneously using two separate electronic systems incorporated with log amplifiers to cover several decades of the spectra in a single measurement. Software can be written to incorporate into a ROM which would automatically control the system for gas gain, and stability from voltage fluctuation. It could also be made to yield a direct evaluation of ambient dose and dose equivalent immediately after measurement, which would be a necessary procedure if the device is to be of practical use in radiation protection.

Appendix A

Monte Carlo Calculation of Chord Length Distributions in Right Circular Cylinders of Finite Dimension

The pulse height distribution generated in the cylindrical TEPCs depends on the distribution of track lengths of charged particles intercepting the surface of the cylinder. Unfortunately, the analytical calculations are difficult to achieve. By generating a large sample of random tracks, the chord length distribution of the cavity can be determined in a statistical manner using Monte Carlo techniques. We assumed that the cylinder is immersed in a uniform isotropic field of tracks in space. Knowing the distribution of tracks in space and the dimension and orientation of the cylinder, the length of the tracks can be calculated and then tabulated according to the length to obtain the distribution of chord length. This appendix describes the procedure to generate the chord length distribution for circular cylinders of finite dimension.

A.1 Probability of tracks intercepting the cylinder

Consider a particle track intersects the surface of a cylinder at random. It can enter the cavity in two possible ways, i.e. either through the curved surface, denoted by S, or through the circular end surface, denoted by E. Let the finite dimension of the cylinder be specified by the height, H, and the radius, R. Then the probabilities that the track enters the curved surface, P(S), and the circular end, P(E), are given respectively by the ratio of the area $2\pi RH$ and $2\pi R^2$ to the total area of the cylinder $2\pi R(R+H)$. Thus

$$P(S) = \frac{H}{R+H} \qquad \text{(A-1)}$$

$$P(E) = \frac{R}{R+H} \qquad \text{(A-2)}$$

The frequency of tracks that enter the curved surface is constant along the length of the cylinder. On the other hand, the frequency of tracks that enter the circular surface increases

with the distance, r, from the centre of the surface, i.e. $0 \leq r \leq R$. The cumulative probability that a given track occurs at distance r is given by

$$P(r) = \int_0^r \frac{2\pi\ r\ dr}{\pi\ R^2} = \frac{r^2}{R^2} \qquad \text{(A-3)}$$

The direction of tracks in space must have the distribution function which is not biased for any direction. Therefore, the components of an isotropic unit vector are the direction cosine α, β, and γ. If the track enters the top of the cylinder, γ is the polar angle and if it enters the side β is the polar angle. Since, the element of area on the cylinder through which the track enters is not equally accessible to tracks of all direction, the frequency of tracks of a given direction is proportional to the cosine of the polar angle.

A.2 Chord length in circular cylinders

To calculate the length of the tracks intersecting the cylinder through the curved surface, i.e. track 1, and through the circular surface, i.e. track 2, let β_1 and γ_2 be the polar angles for the curve surface and the circular end respectively as shown in the diagram. and z_1 and z_2 are the distances of the tracks intersect the cylinder. It can be shown that the length of track 1 is given by

$$l_1 = \frac{2R \cos \alpha_1}{\cos^2 \beta_1} \qquad \text{(A-4)}$$

or

$$l_1 = \frac{z_1}{\cos \gamma_1} \qquad \text{(A-5)}$$

The length of track 2 is given by

$$l_2 = \frac{r \cos \alpha_2}{\cos^2 \beta_2} + \frac{\sqrt{(R^2 - r^2(1 - \cos^2 \alpha_2 / \cos^2 \beta_2))}}{\cos \beta_2} \qquad \text{(A-6)}$$

or $$l_2 = \frac{z_2}{\cos \gamma_2} \qquad \text{(A-7)}$$

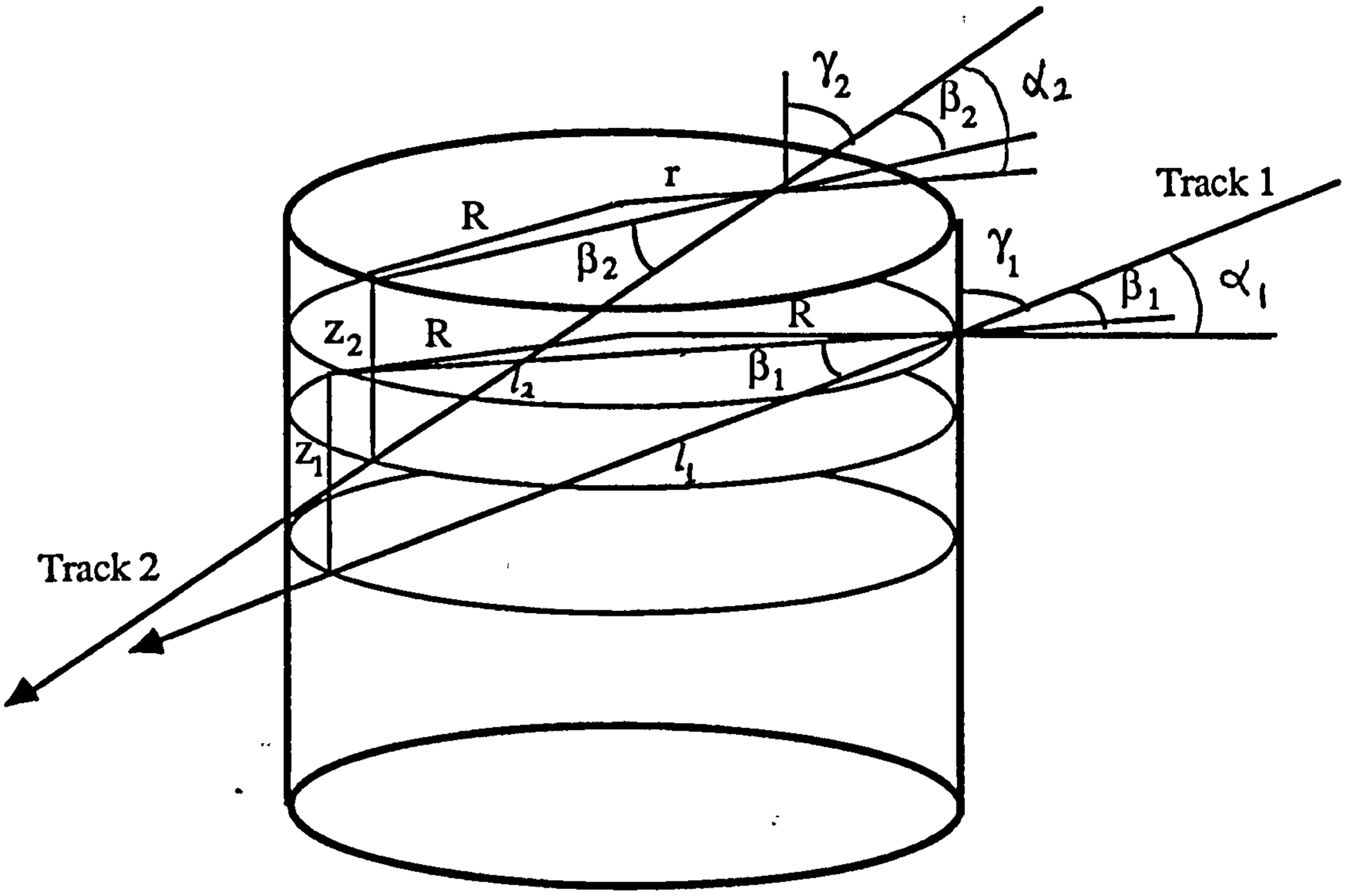

B.3 Monte Carlo computation

For each track we choose a random number p between 0 and 1. To include the probability that the track enters the side or the circular end, we divide the unit interval into two portion. If p falls between 0 and H/(R+H), the track enters the side. On the other hand if p falls between H/(R+H) and 1, the track enters the circular end.

To calculate polar angles we generate the random number x from discrete distribution with the probability density of cos(x). We divided the angle distribution into 100 channels for tracks entering the side and end of the cylinder. Therefore we tally the cosine of the polar angle of the tracks entering S and E surfaces before preceeding to the evaluation of track distributions.

The frequency of tracks entering the side is constant along the length. Because of symmetry, we can choose a distance z from a random number between 0 and H/2. To include the frequency of tracks entering the circular surface which increases with r, we choose a random number q between 0 and 1, such that $r^2 = qR^2$.

The chord length of the tracks is computed and the length is scored in the appropriate channel of equal width. The longest chord length is $l_{max} = \sqrt{(H^2 + 4R^2)}$. The probability density of the cylindrical volume for μ-randomness, $f_\mu(l)$, is calculated according to equation (B-7).

$$f_\mu(l_i) = \frac{N_{max}}{l_{max}} \frac{N_i}{N_T} \qquad \text{(B-7)}$$

where N_{max} is the channel number at the maximum chord length l_{max}, N_i is the number of track at channel i and N_T is the total number of tracks used in the computation. The function $f_\mu(l)$ must be normalized so that

$$\int_0^{l_{max}} f_\mu(l)\, dl = 1 \qquad \text{(B-8)}$$

Since, all the channels have equal width, then dl for each channel is equal to l_{max}/N_{max}.

```
      Program Monte_Carlo
!     Routine for the calculation of chord length distributions of
!     circular cylinder.

!     DECLERATION

      Real*8  p1(1001), r1(2000), x1(101)
      Real*8  p2(1001), r2(2000), x2(101)
      Real*8  H,HT,HT2,DR,TM,TTM,DIM,PI
      Real*8  a1,a2,za1,za2,cza,c11
      Real*8  fn,fm,c2,xr1,xr2,xr3,cz2,c13
      Real*8  teta1,teta2

!     Others if not declare are declared by default

      Integer freq1(1001),freq2(1001)
      Integer NCOUNT1(100),NCOUNT2(100)
      Integer NCOUNT(100),NTOTAL(100),NT
      Integer ND,NS,NE
      Integer i,j,np,ip,nr,ifail

      Logical lp
      Integer  G05EYF
      External G05EYF,G05CAF,G05DAF

      DATA NOUT/6/
      DATA freq1/ 1001*0 /
      DATA freq2/ 1001*0 /

!     State the number of tracks you intended to use
      DATA ND/ 150000 /

!     PROGRAM

!     Dimension of the Cylinder Please !!!
      H=2.0
      H2=H/2.0
      DIM=2.0
      DR=DIM/2.0
      cdmax=sqrt(DIM*DIM+H*H)

!     Probability for the tracks entering the surfaces
      HT=H/(H+DR)
      RT=DR/(H+DR)
      HT2=2.0*H/(2.0*H+DR)
      PI=2.0*ASIN(1.0D0)
      PI2=PI/2.0

!     Calculate the maximum angle for tracks P(S-S) and P(E-S)
      TM=H/DIM
      TTM=ATAN(TM)

!     Calculate the number of tracks intercepting on each surface
!     Note that by multiplication with the above probability you
!     get more or less about the same total as calculated using
!     the following nag routine
!     but with reduce CPU time of course.
      DO I=1,ND
        P=G05CAF(P)
       IF (P.LE.HT) THAN
          NS=NS+1
        ELSE
         NE=NE+1
        ENDIF
      ENDDO
```

```
      WRITE(NOUT,*)ND,NS,NE

!     Calculate Chord length distributions
      np=101
      ip=1
      lp=.true.
      nr=2000
      ifail=0
!     Calculate the distribution of tracks belongs to P(S)
!     Note that x1(j) are the polar angles
       do=j=1, 101
        x1(j)=(dfloat(j)-1)/50.0*atan(1.0d0)
        p1(j)=sin(x1(j))
      enddo
        call G05EXF(p1,np,ip,lp,r1,nr,ifail)

      do i=1,NS
        j=G05EYF(r1,nr)
        freq1(j)=freq1(j)+1
      enddo

      do j=1,101
        do k=1, freq1(j)
10      continue
      a1=0.0
      a2=G05DAF(0.0,PI2)
      teta1=pi2-x1(j)
      za1=G05DAF(0.0,H2)
      za2=h-za1
      cza=za2/cos(teta1)
      cl1=2.0*dr*cos(a2)/cos(x1(j))
       if(cl1.gt.cza)cl1=cza
       if(cl1.gt.cdmax) goto 10
       L=int(100.0*cl1/cdmax)+1
       if(L.gt.100) L=100
       NCOUNT1(L)=NCOUNT1(L)+1
      enddo
    enddo


!     Calculate the distribution of track belongs to P(E)
    do j=1, 101
     x2(j)=(dfloat(j)-1)/50.0d0*atan(1.0d0)
     p2(j)=sin(x2(j))
    enddo
     call G05EXF(p2,np,ip,lp,r2,nr,ifail)

    do i=1, NE
     j=G05EYF(r2,nr)
     freq2(j)=freq2(j)+1
    enddo

    do j=1, 101
     do k=1, freq2(j)
20   continue
      fm=G05CAF(fm)
      fm=dr*dr*fm
      fm=SQRT(fm)
      c2=G05DAF(0.0,PI)
      teta2=pi2-x2(j)
      xr1=xr*cos(c2)/cos(teta2)
      xr2=xr*xr*cos(c2)*cos(c2)
      xr2=xr2/cos(teta2)*cos(teta2)
      xr3=dr*dr-(xr*xr-xr2)
      xr3=SQRT(xr3)
      cl2=(xr1+xr3)/cos(teta2)
```

```
      cz2=h/cos(x2(j))
      if(cl2.gt.cz2) cl2=cz2
      if(cl2.gt.cdmax) goto 20
      L=int(100.0*cl2/cdmax)+1
      if(L.gt.100) L=100
      NCOUNT2(L)=NCOUNT2(L)+1
    enddo
  enddo

  do L=1,100
    NCOUNT(L)=NCOUNT1(L)+NCOUNT2(L)
    NTOTAL(L)=NTOTAL(L-1)+NCOUNT(L)
    if(L.eq.100) NT=NTOTAL(L)
    enddo


    do L=1,100
      tl=float(ncount(l))
      tn=float(nt)
      pl(l)=100.0*tl/(tn*cdmax)
      xl(l)=cdmax*l/100.0
      pp(l)=pl(l)*xl(1)
      pp(l)=pp(l)+pp(l-1)
      if(l.eq.100) ptot=pp(100)
                              enddo

!     PRINT RESULTS

      write(nout,800) (j, freq(j),freq2(j), j=1,101)
      write(nout,700)(l,xl(l),ncount1(l),ncount2(l),ncount(l),pl(l),
     *l=1,100)
      write(nout,*)Nt, ptot
!     check that Nt=ND and ptot=1
700   format(i3,2x,f7.4,3(1x,i6),2x,f7.4)
800   format(1x,i3,2(2x,i5))
      END
```

APPENDIX B

```
      PROGRAM MICRODOSIMETRY

!     Routine for calcualtion microdosimetric distributions, mean values
!     of lineal energy, quality factor.

      IMPLICIT REAL*(A-H,O-Z)

!     Declaration for dimension only. Others are declared by default.
      DIMENSION Y(200),CY(200),FY(200),DY(200),YFY(200),YDY(200)
      DIMENSION CG(200),FG(200),DG(200)
      DIMENSION CP(200),FP(200),DP(200)
      DIMENSION F1(200),F2(200),D1(200),D2(200),YD1(200),YD2(200)
      DIMENSION YR(200),YAW(200)
      DIMENSION QY1(200),QY2(200),QY3(200),QY4(200)
      DIMENSION QNY1(200),QNY2(200),QNY3(200),QNY4(200)

      DATA NOUT/31/

      OPEN(UNIT=30,FILE='MIXED_FIELDS.DAT',STATUS='OLD',ACCESS=
     * 'SEQUENTIAL')
      OPEN(31,FILE='RESULTS.DAT',STATUS='NEW')
      READ(30,*) NMAX
      READ(30,*)  (Y(I),CY(I),CG(I),CP(I),  I=1, NMAX)

      CL=2.3025851
!     PROGRAM
!     Mixed Radiation Fields
!     ----------------------
!     Calculate the sum
      DO I=1, NMAX
         SUM1=SUM1+CY(I)
         SUM2=SUM2+Y(I)*CY(I)
         SUM3=SUM3+Y(I)*Y(I)*CY(I)
      ENDDO

!     Calculate f(y) and frequency mean lineal energy
!     Note that in logrithmic scale f(y) = y.f(y)
      DO I=1,NMAX
         FY(I)=CY(I)/SUM1
         SUMFY=SUMFY+FY(I)
         YFY(I)=Y(I)*FY(I)
         SUMYF=SUMYF+YFY(I)
      ENDDO

!     Calculate d(y) and dose mean lineal energy
      DO I=1,NMAX
         DY(I)=Y(I)*FY(I)/SUMYF
         SUMDY=SUMDY+DY(I)
         YDY(I)=Y(I)*DY(I)
         SUMYD=SUMYD=YDY(I)
      ENDDO

!     Gamma component only
!     --------------------
!     Calculate fg(y) and dg(y)
      DO I=1,NMAX
         SUG1=SUG1+CG(I)
         SUG2=SUG2+Y(I)*CG(I)
      ENDDO
```

```
      DO I=1,NAMX
         FG(I)=CG(I)/SUG1
         SUGFY=SUGFY+FG(I)
         SUGYF=SUGYF+Y(I)*FG(I)
      ENDDO

      DO I=1,NMAX
         DG(I)=Y(I)*FG(I)/SUGYF
         SUGDY=SUGDY+DG(I)
         SUGYD=SYGYD+Y(I)*DG(I)
      ENDDO

!     Neutron component only
!     ----------------------
!     Calculate fn(y) and dn(y)
      DO I=1,NMAX
         SUN1=SUN1+CP(I)
         SUN2=SUN2+Y(I)*CP(I)
      ENDDO

      DO I=1,NMAX
         FP(I)=CP(I)/SUN1
         SUNFY=SUNFY+FP(I)
         SUNYF=SUNYF+Y(I)*FP(I)
      ENDDO

      DO I=1,NMAX
         DP(I)=Y(I)*FP(I)/SUNYF
         SUNDY=SUNDY+DP(I)
         SUNYD=SUNYD+Y(I)*DP(I)
      ENDDO

!     Calculate the composition of gamma-rays and neutrons
!     ----------------------------------------------------

      SUNG=SUG1+SUN1
      DO I=1,NMAX
         F1(I)=CG(I)/SUNG
         F2(I)=CP(I)/SUNG
      ENDDO

      DO I=1,NMAX
         D1(I)=Y(I)*F1(I)/SUMYF
         D2(I)=Y(I)*F2(I)/SUMYF
!     for grapical reprensentation of gamma-ray and neutron component.
         YD1(I)=Y(I)*D1(I)
         YD2(I)=Y(I)*D2(I)
         GAMMA_FRAC=GAMMA_FRAC+YD1(I)/SUMYD
         NEUTRON_FRAC=NEUTRON_FRAC+YD2(I)/SUMYD
      ENDDO

!     Calculate the Quality Factor of Mixed Radiation Fields.
!     -------------------------------------------------------
!     1.Using the formula of ICRU (1986), i.e. Q1
         a1=5510.0
         a2=5.0e-05
         a3=2.0e-07
         DO I=1,NMAX
            QY1(I)=A2*Y(I)**2+A3*Y(I)**3
            QY1(I)=A1*(1.0-QY1(I))/Y(I)
            SUMQ1=SUMQ1+QY1(I)*DY(I)
         ENDDO
         Q1=SUMQ1/SUMDY

!     2. Using the formula of Lindblom and Samuelson (1981), i.e. Q2
         Q2=0.8+0.14*SUMYD
```

```
!     3. Using the formula of Braby et al. (1983) i.e. Q3
        Y0=125.0
        DO I=1,NMAX
           YR(I)=Y(I)/Y0
           YR(I)=(1.0-EXP(-YR(I)**2))
           YR(I)=Y0*Y0*YR(I)/Y(I)
           QY3(I)=DY(I)*YR(I)**0.6
           SUMQ3=SUMQ3+QY3(I)
        ENDDO
        Q3=SUMQ3/SUMDY

!     3. Using the formula of Al-Affan and Watt (1987) i.e. Q4
        DO I=1,NMAX
           if(Y(I).LE.8.0) Y0=3.6
           IF(Y(I).GT.8.0) Y0=72.0
           Yaw(I)=Y(I)/Y0
           Yaw(I)=(1.0-EXP(-Yaw(I)**2))
           Yaw(I)=Y0*Y0*Yaw(I)/Y(I)
           QY4(I)=1.33*Yaw(I)*DY(I)
           SUMQ4=SUMQ4+QY4(I)
        ENDDO
        Q4=SUMQ4/SUMDY


!     Calculate the Quality Factor of Neutrons.
!     -----------------------------------------
!     1.Using the formula of ICRU (1986), i.e. QN1
        a1=5510.0
        a2=5.0e-05
        a3=2.0e-07
        DO I=1,NMAX
           QNY1(I)=A2*Y(I)**2+A3*Y(I)**3
           QNY1(I)=A1*(1.0-QNY1(I))/Y(I)
           SUNQ1=SUNQ1+QNY1(I)*DP(I)
        ENDDO
        QN1=SUNQ1/SUNDY

!     2. Using the formula of Lindblom and Samuelson (1981), i.e. QN2
        QN2=0.8+0.14*SUNYD

!     3. Using the formula of Braby et al. (1983) i.e.QN3
        Y0=125.0
        DO I=1,NMAX
           YR(I)=Y(I)/Y0
           YR(I)=(1.0-EXP(-YR(I)**2))
           YR(I)=Y0*Y0*YR(I)/Y(I)
           QNY3(I)=DP(I)*YR(I)**0.6
           SUNQ3=SUNQ3+QNY3(I)
        ENDDO
        QN3=SUNQ3/SUNDY

!     3. Using the formula of Al-Affan and Watt (1987) i.e. QN4
        DO I=1,NMAX
           if(Y(I).LE.8.0) Y0=3.6
           IF(Y(I).GT.8.0) Y0=72.0
           Yaw(I)=Y(I)/Y0
           Yaw(I)=(1.0-EXP(-Yaw(I)**2))
           Yaw(I)=Y0*Y0*Yaw(I)/Y(I)
           QNY4(I)=1.33*Yaw(I)*DP(I)
           SUNQ4=SUNQ4+QNY4(I)
        ENDDO
        QN4=SUNQ4/SUNDY

!       PRINT RESULTS
!       -------------
```

```
!       Mixed Fields
        WRITE(NOUT,*)SUMYF,SUMYD,Q1,Q2,Q3,Q4
!       Neutron Component
        WRITE(NOUT,*)SUNYF,SUNYD,QN1,QN2,QN3,QN4
```

REFERENCES

AL-AFFAN, I. A. M. (1985) *Studies of Microdosimetry of Intermediate Energy Neutrons*. PhD Thesis, University of Dundee, U.K.

AL-AFFAN, I. A. M., COLAUTTI, P., TALPO, G. and **WATT, D. E.** (1984) *Calculated Microdose Spectra for Intermediate Energy Neutrons (1 to 100 keV)*. **Radiation Protection Dosimetry, 5, 151-157.**

AL-AFFAN, I. A. M. and **WATT, D. E.** (1985) *Saturation Values of Lineal Energies in Microdosimetry; Quality Factor*. **Radiation Protection Dosimetry, 11,** 66-67.

AL-AFFAN, I. A. M. and **WATT, D. E.** (1987) *Determination of Quality Factors by Microdosimetry*. **Nuclear Instruments and Methods in Physics Research, A 255,** 338-340.

Al-KAZWINI, A. T. (1983) *Ranges and Cross-Section for Inactivation of Solid Enzymes by Low Energy H, He and N Ions*. PhD Thesis, University of Dundee. U.K.

AL-KAZWINI, A. T., CANNINGHAM, J. W. and **WATT, D. E.** (1988) *Damage by Nuclear Elastic Scattering (NES) - Forty Years On*. **International Journal of Radiation Biology, 53,** 683-685.

ANDERSEN, H. H. and **ZIEGLER, J. F.** (1977) *Hydrogen Stopping Powers and Ranges in All Elements*. In "***The Stopping and Ranges of Ions In Matter***", **Vol. 3,** Ziegler, J. F., Pergamon Press, New York and London.

ARKHIPOV, E. P. and **GOTT, Y. U.** (1969) *Slowing Down of 0.5-30 keV protons in some materials*. **Soviet Physics JETP, 29,** 615-618.

ATTIX, F. H. (1986) In "***Introduction to Radiological Physics and Radiation Dosimetry***", Wiley-Interscience, New York, pp. 463-503.

AUXIER, J. A., SNYDER, W. S. and **JONE, T. D.** (1968) *Neutron Interactions and Penetration in Tissue*. In "***Radiation Dosimetry***", **Vol. 1,** Attix, F. H. and Roesch, W. C., Eds., 2nd. Edition, Academic Press, New York, pp. 275-316.

AWSCHIALOM, M. and **ATTIX, F. H.** (1980) *A-150 Plastic Equivalent Gas*. **Physics in Medicine and Biology, 25,** 567-569.

BARRUS, D. M. and **BLAKE, R. L.** (1977) *The Method of Streatching Commercially Available Organic Films to Lower Thickness*. **Review Science Instruments, 48,** 116-117.

BELONOGII, P. N., IVANOV, V. I., KUZMIN, E. C., PITKEVICH, V. A. and **TIBANOV, A. P.** (1971) *TE Material Proportional Counters in Microdosimetry*. In Proceedings of a Symposium on Biophysical Aspects of Radiation Quality, (IAEA, Vienna) pp 139-168.

BERGER, M. J. and **SELTZER, S. M.** (1982) *Stopping Powers and Ranges of Electrons and Positrons*. NBSIR 82-2550, National Bureau of Standards, Washingston, DC 20234, USA.

BICHSEL, H. (1968) *Charged-Particle Interactions*. In "***Radiation Dosimetry***", **Vol. 1,** Attix, F. H. and Roesch, W. C. Eds., 2nd. Edition, Academic Press, New York, pp. 157-228.

BICIISEL, II. (1975) *Consideration Concerning Neutron Dosimetry.* In Proceedings of 2nd. Symposium on Neutron Dosimetry in Biology and Medicine, Report No. EUR 5273, Burger, G. and Ebert, H. G. Eds., (CEC, Luxembourg) pp. 191-220.

BIRKHOFF, R. D., TURNER, J. E., ANDERSON, V. E. FEOLA, J. M. and **HAMM, R. N.** (1970) *The Determination of LET Spectra from Energy-Proportional Pulse-Height Measurements I. Track-length Distributions in Cavities.* **Health Physics, 18,** 1-14.

BODDY, K., DENNIS, J. A. and **LAWSON, R. C.** (1969) *Neutron Dosimetry in the Vivo Measurement of Intrathyroidal Iodine in Man by Activation Analysis.* **Physics in Medicine and Biology, 14,** 470-480.

BODDY, K., HOLLOWAY, I., ELLIOTT, B.Sc. CLAROS, D., ROBERTSON, I. and **EAST, B. W.** (1972) *Low-Cost Facilities for Partial Body and Total Body in Vivo Activation Analysis in the Clinical Environment.* Symposium on Nuclear Activation Techniques in Life Sciences. International Atomic Energy Agency, pp. 1-20.

BOHR, N. (1948) *Comprehensive Theory of the Penetration of Atomic Particles Through Matter.* **Kgl. Danske Videnskab. Selskab, Mat.-Fys. Medd., 18,** no. 8, 144.

BOOZ, J. (1976) *Microdosimetric Spectra and Parameters of Low LET-Radiations.* In Proceedings of 5th. Symposium on Microdosimetry, Report No. 5452, Booz, J., Ebert, H.G., Smith, B.G.R. (CEC, Luxembourg) pp. 311-344.

BOOZ, J. (1978) *Mapping of Fast Neutron Radiation Quality.* In Proceedings of 3rd. Symposium on Neutron Dosimetry in Biology and Medicine, Report No. EUR 5848, Burger, G. and Ebert, H. G. Eds., (CEC, Luxembourg), pp. 499-514.

BOOZ, J. (1984a) *Development of Dose Equivalent Meters Based on Microdosimetric Principles.* **Radiation Protection Dosimetry, 23,** 155-170.

BOOZ, J. (1984b) *Advantages of Introducing Microdosimetric Instruments and Methods into Radiation Protection.* **Radiation Protection Dosimetry, 9,** 175-185.

BOOZ, J. and **COPPOLA, M.** (1974) *Energy Deposition by Fast Neutrons to Small Spheres.* In Proceedings of 4th. Symposium on Microdosimetry, Report No. 5122, Booz, J., Ebert, H. G., Eickel, R. and Waker, A., Eds., (CEC, Luxembourg), pp. 983-1000.

BOOZ, J. and **FEINENDEGEN, L. E.** (1988) *A microdosimetric Understanding of Low-Dose Radiation Effects.* **International Journal of Radiation Biology, 53,** 13-21.

BOOZ, J., OLDENBURG, U. and **COPPOLA, M.** (1972) *Das Problem der Gewebeaquivalenz fur Schnelle Neutrone in der Microdosimetrie.* In Proceedings of 1st. Symposium on Neutron Dosimetry in Biology and Medicine, Report No. EUR 4896 Burger, G., Schraube, H. and Ebert, H. G. Eds, (CEC, Luxembourg), pp. 117-134.

BOOZ, J. and **POLI, A.** (1981) *Evaluation of the Mean Quality Factor of Mixed Neutron-Gamma Radiations from Microdosimetric Spectra.* In Proceedings of 4th. Symposium on Neutron Dosimetry, Report No. EUR 7448, Burger, G. and Ebert, H. G., Eds.(CEC, Brussels and Luxembourg) pp. 237-261.

BORGESEN, P. (1985) *Measurements of the Stopping Power for keV Light Ions in Condensed Molecular Gases.* **Nuclear Instruments and Methods in Physics Research, B12,** 73-79.

BOUCLIER, R., CHARPAK, G., DIMCOVSKI, Z., FISCHER, G. and **SAULI, F.** (1970) *Investigation of Some Properties of Multiwire Proportional Chambers.* **Nuclear Instruments and Methods, 88,** 149-161.

BRABY, L.A., RATCLIFFE, C.A. and **METTING, N.F.** (1983) *A Portable Dose Equivalent Monitor Based on Microdosimetry.* In Proceedings of 8th Symposium on Microdosimetry, Report No. EUR 8395, Booz, J. and Ebert, H. G., Eds., (CEC, Luxembourg), pp. 1075-1086.

BREYER, B. and **CIMERMAN, M.** (1971) *Attenuation of Proportional Counter Pulses by Pulse Shaping networks.* **Nuclear instruments and Methods, 92,** 19-20.

BROERSE, J. J. and **BARENDSEN, G. M.** (1973) *Relative Biological Effectiveness of Fast Neutrons for Effects on Normal Tissue.* **Current Topic of Radiation Research, 8,** 305-350.

BURGER, G. (1986) *Proton Stopping-Power and Range Tables.* Stopping Power Committee of the ICRU

CAMPBELL, J. L and **LEDINGHAM, K. N.** (1966) *Pulse Height Distributions from Proportional Counters.* **British Journal of Applied Physics, 17,** 969-774.

CAMPION, P. J. (1971a) *The measurement of Gas Multiplication in Tissue Equivalent Gas.* **International Journal of Applied Radiation and Isotopes, 22,** 703-706.

CAMPION, P. J. (1971b) *The Operation of Proportional Counters at Low Pressures for Microdosimetry.* **Physics in Medicine and Biology, 16,** 611-616.

CASE, K. M., HOFFMANN, F. DE. and **PLACZEK, G.** (1953) *Introduction to the Theory of Neutron Diffusion.* Los Alamos Scientific Laboratory, Los Alamos, New Mexico, USA.

CASWELL, R. S. (1966) *Deposition of Energy by Neutrons in Spherical Cavities.* **Radiation Research, 27,** 92-107.

CASWELL, R. S. and **COYNE, J. J.** (1972) *Interaction of Neutrons and Secondary Charged Particles with Tissue: Secondary Particle Spectra.* **Radiation Research, 52,** 448-470.

CASWELL, R. S. and **COYNE, J. J.** (1976) *Microdosimetric Spectra and Parameters of Fast Neutrons.* In Proceedings of 5th Symposium on Microdosimetry, Report No. EUR 5452, Ebert, H. G. and Smith, B. G. R., Eds., (CEC, Luxembourg), pp. 79-123.

CASWELL, R. S. and **COYNE, J. J.** (1978) *Energy Deposition Spectra for Neutrons based on Recent Cross Section Evaluation.* In Proceedings of 6th Symposium on Microdosimetry, Report No. EUR 6064, Booz. J. and Ebert, H. G., Eds., (CEC, Harwood Academic Publisher, London), pp. 1159-1171.

CASWELL, R. S. and **COYNE, J. J.** (1980) *Kerma Factor Neutron Energies below 30 MeV.* **Radiation Research, 82,** 217-254.

CHARLES, M. W. (1972) *Gas Gain Measurements in Proportional Counters.* **Journal of Physics E: Scentific Instruments, 5,** 95-100.

CLAROS, D (1973) *Partial-Body in Vivo Neutron Activation Analysis- A Technique for Measuring Minerals and Bone.* PhD Thesis, Bioengineering Unit (Wolfson Centre) and Scottish University Research and Reactor Centre, University of Strathclyde.

COCKCROFT, A. L. and **CURRAN, S. C.** (1951) *The Elimination of End Effects in Counters.* **Review Scientific Instruments, 22,** 37-47.

COLE, A (1969) *Absorption of 20 eV to 50,000 eV Electron Beams in Air and Plastic.* **Radiation Research, 38,** 7-33.

COLAUTTI, P., CUTAIA, M., MAKAREWICZ, M., SCHRAUBE, H., TALPO, G. and **TORNIELLI, G.** (1985) *Neutron Microdosimetry in Simulated Volumes Less than 1 μm in Diameter.* **Radiation Protection Dosimetry, 13,** 117-121.

COOK, C. J., JONE, E. JR. and **JORGENSEN, T. JR.** (1953) *Range Energy Resulations of 10-250 keV Protons and Helium Ions in Various Gases.* **Physical Review, 91,** 1417-1421.

COPPOLA, M. and **BOOZ, J.** (1973) *Influence of Energy Straggling on the Shape of Neutron Produced Single Event Spectra.* **Biophysik, 9,** 225-236.

COPPOLA, M., EICKEL, R., FITZGERALD, M., PIRRWITZ, D., PORRO, F. and **BOOZ, J.** (1976) *Experimental Evaluation of the Spectral Energy Deposition in Small Volumes by Low-LET Radiations.* In Proceedings of 5th. Symposium on Microdosimetry, Report No. 5452, Booz, J., Ebert, H.G., Smith, B.G.R. (CEC, Luxembourg) pp. 377-391.

COSACK, M., KUTSCHA, M. and **PAULSEN, A.** (1972) *The Proton Recoil Proportional Counter as Device to Measure Neutron Fluxes at Energies below 100 keV.* In Proceedings of 1st. Symposium on Neutron Dosimetry in Biology and Medicine, Report No. EUR 4896, Burger, G., Schraube, H. and Ebert, H.G., Eds., (CEC, Luxembourg), pp. 267-282.

COUSINS, T. and **RUSHTON, L. P.** (1985) *The Development and Use of a Tissue Equivalent Proportional Counter Analysis System to Measure the Dose Delivered to the Gut of an Anthropomorphic Phantom from a Fission Source.* In Proceedings of 5th. Symposium on Neutron Dosimetry, Report No. EUR 9762, Schraube, H., Burger, G. and Booz, J. Eds. , (CEC, Brussels and Luxembourg) pp. 337-348.

COWLING, A. R. and **WAKER, A. J.** (1985) *Experimental Studies of a Large-Volume Tissue-Equivalent Proportional Counter.* **Radiation Protection Dosimetry, 13,** 353-356.

CUNNINGHAM, J. W. (1982) *Quantitative Analysis of Damage of Enzyme, Viruses, Bacteria and High Cells by Ionising Radiation.* PhD Thesis, University of Dundee, U.K.

CURRAN, S. C. and **CRAGGS, J. D.** (1949) In "***Counting Tubes*** ", Butterworths Scientific Publication, London.

De LUCA, P. M., HIGGINS, P. D., PEARSON, D. W., and **ATTIX, F. H.** (1981) *Neutron and Pohoton Dose Components in a 15 MeV Neutron Beam Determined with a Graphite-Walled Proportional Counter.* In Proceedings of 7th. Symposium on Microdosimetry. Report No. EUR 7147, Booz,J., Ebert, H. G. and Hartfiel, H. D., Eds, (CEC, Harwood Academic Publisher, London), pp. 1159-1169.

De LUCA, P. M., SCHELL, M. C., PEARSON, D. W., and **ATTIX, F. H.** (1982) *Characteristics of Various Tissue and A150-Plastic Equivalent Gas Mixtures for Microdosimetric Application.* USDOE Report No. DOE/EV/01105 289 through 297.

DENNIS, J. A. and **DUNSTER, H. J.** (1985) *Radiation Quality and Radiation Protection: Implications of Changes in Quality Factor.* **Radiation Protection Dosimetry, 13,** 327-334.

DIETHORN, W.A. (1956) *Methane Proportional Counter System for Natural Radiocarbon Measurements*, N.Y.O., 6628, 65.

DIETZE, G., BOOZ, J., EDWARDS, A., GULDBAKKE, S., KLUGE, H., LEROUTZ, J.B., LINDBORG, L., MENZEL,H. G., NGUYEN, V. D., SCHIMITZ, Th. and **SCHUHMACHER,H.** (1988) *Intercomparison of dose equivaqlent meters based on microdosimetric techniques.* **Radiation Protection Dosimetry, 23,** 227-234.

DVORAK, R.F. (1969) Calculation of dE/dx and Energy Loss Distribution in Spherical Cavities for Monoenergetic Neutron Fields. *Health Physics* , **17**, 279-293.

EDWARDS, A.A. and **DENNIS, J.A.** (1975) The Calculation of Charged Particle Fluence and LET Spectra for the irradiation of Biological Significant Materials by Neutrons. *Physics in medicine and Biology* , **20**, 395-409.

EICKEL, R. and **BOOZ, J.** (1976) The Influence of the Counter Wall and the Counter Shape on the Spectral Energy Deposition in Small Volumes by ^{60}Co Gamma-Rays and 200 kV X-Rays. *Radiation and Environmental Biophysics* , **13**, 145-165.

ENDRES, G.M.R. and **BRACKENBUSH, L.W.** (1981) Neutron Dosimetry and Spectra Measurements in PWR Containment.In Proceddings of 4th. Symposium on Neutron Dosimetry, Report No. EUR 7448, Burger, G. and Ebert, H.G., Eds., (CEC, Brussels and Luxembourg), pp. 523-534.

EVANS, R.D. (1968) X-Ray and γ-Ray Interactions. In " Radiation Dosimetry ", **Vol. 1**, Attix, F.H. and Roesch, W.C. Eds., 2nd. Edition, Academic Press, New York, pp. 93-155.

FANO, U. (1954) Note on the Bragg-Gray Cavity Principle for Measuring Energy Dissipation. *Radiation Research* , **1**, 237-240.

FAKUDA, A. (1980) Stopping Powers of a TE-Gas for 40 - 200 keV Protons. *Physics in Medicine and Biology* , **25**, 877-886.

FAKUDA, A. (1981) Stopping Powers of a TE-Gas for 40 - 200 keV He and N. *Physics in Medicine and Biology* , **26**, 623-632.

FAKUDA, A (1982) Stopping Powers of H_2, O_2, C_2H_4 for 40 - 200 keV Protons. *Physics in Medicine and Biology* , **27**, 73-79.

FASTRUP, B., HVELPLUND, P. and **SAUTTER, C.A.** (1966) Stopping Cross-Section of Carbon of 0.1-0.9 MeV atoms with $Z \leq 20$. *Kgl. Danske. Videskab. Selskab. Mat.-Fys. Medd.*, **35**, no. 10,

FIDORRA, J. and **BOOZ, J.** (1978) The Local Distribution of Radiation Quality of a Collimated Fast Neutron Beam from 15 MeV deutrons on Beryllium. In Proceedings of 6th Symposium on Microdosimetry, Report No. EUR 6064, Booz. J. and Ebert, H.G., Eds., (CEC, Harwood Academic Publisher, London), pp. 483-496.

FIDORRA, J., POLI, A. and **BOOZ, J.** (1981) Experimental Microdosimetry Spectra and Parameters of Collimated Fast Neutron Beams in a Whater Phantom for Different Field Sizes. In Proceedings of 7th. Symposium on Microdosimetry. Report No. EUR 7147, Booz,J., Ebert, H.G. and Hartfiel, H.D., Eds, (CEC, Harwood Academic Publisher, London), pp. 1169-1179.

FINK, R.W. (1975) Proportional-Counter Spectrometery in Atomic Inner-Shell Processes, In " Experimental Approaches and Applications ", **Vol II**, Crasemann, B. Ed., Academic Press, New York, pp. 169-186.

GEARY, M.J. and **HAQUE, A.K.M.M.** (1976) The Stopping Power and Straggling for Alpha Particles in Tissue Equivalent Materials. *Nuclear Instruments and Methods* , **137**, 151-155.

GOLD, R. and **BENNETT, E.F.** (1966) Electron Multiplication Process in Proportional Counters. *Physical Review* , **147**, 201-213.

GOODHEAD, D. T (1987) *Relationship of Microdosimetric Techniques to Applications in Biological Systems.* In " *The Dosimetry of Ionizing Radiation* ", Vol II, Kase, K. R., Bjarnagard, B. E. and Attix, F. H. Eds, Academic Press, Inc. pp. 1-89.

GOTT, R. and **CHARLES, M. W.** (1969) *Attenuation of Proportional Counter Pulses by Equal Integrating and Differentating Time Constants.* **Nuclear Instruments and Methods, 72,** 157-160.

HANKINS, D. E. (1963) *Monitoring Intermediate Energy Neutrons.* **Health Physics, 9,** 31-39.

HAQUE, A. K. M. M. and **SAQ'AN, S. A.** (1978) *Microdosimetric Study with Cylindrical Walled and Wall-less Proportional Counters.* In Proceedings of 6th Symposium on Microdosimetry, Report No. EUR 6064, Booz. J. and Ebert, H. G., Eds., (CEC, Harwood Academic Publisher, London), pp. 1185-1202.

HARTMANN, G. MENZEL, H. G. and **SCHUHMACHER, H.** (1981) *Different Approachs to Determine Effective Quality Factor and Dose Equivalent Using the Rossi-Counter.* In Proceedings of 4th. Symposium on Neutron Dosimetry, Report No. EUR 7448, Burger, G. and Ebert, H. G., Eds., (CEC, Brussels and Luxembourg), pp. 225-235.

HARVEY, J. R. and **BENDING, R. C.** (1976) *A Neutron Source with an Effective Energy of 0.5 keV.* **Physics in Medicine and Biology, 21,** 85-97.

HARVEY, J. R. and **MILL, A. J.** (1988) *Progress Towards a European Filtered Neutron Beam Facility.* **Radiation Protection Dosimetry, 23,** 325-328.

HEIKKILA, J. and **KIVINIITTY, K.** (1981) *Microdosimetric Measurements of Gamma Radiation and a Coincidence Measurement System for Them.* In Proceedings of 7th. Symposium on Microdosimetry, Report No. EUR 7147, Booz, J., Ebert, H. G. and Hartfiel, H. D. Eds., (CEC, Harwood Academic Publisher, London), pp. 727-732.

HERSKIND, C. and **JESSEN, K. A** (1981) *Investigation of the Performance of Wall-Less Tissue Equivalent Proportional Counters.* In Proceedings of 7th. Symposium on Microdosimetry, Report No. EUR 7147, Booz, J., Ebert, H. G. and Hartfiel, H. D. Eds., (CEC, Harwood Academic Publisher, London), pp. 733-743.

HOGBERG, G. (1971) *Electronic and Nuclear Stopping Cross Sections in Carbon for Light Mass Ions of 4.5 to 46 keV Energy.* **PhysicsaStatus Solidi B, 48,** 829-841.

HOGEWEG, B. (1978) *Microdosimetric Measurements and Some Applications in Radiobiology and Radiation Protection.* Ph D Thesis, University of Amsterdam, Publication of the Radiobiological Institute of the Organization for Health Research TNO, Rijswijk, Netherlands.

HUGES, S. (1967) *The Range of 5 - 50 keV Heavy Ions in Various Gases.* **Physics in Medicine and Biology, 12,** 565-571.

ICRP (1961) *Measurement of Absorbed Dose of Neutrons and of Mixtures of Neutrons and Gamma Rays.* Report No 25, National Committe and Radiation Protection and Measurements, published as National Bureau of Standards, Handbook 75, U.S. Department of Commence, Washington.

ICRP (1966) Recommendations of the International Commission on Radiological Protection, Publication No. 9, Pergamon Press, Oxford.

ICRP (1977) Recommendations of the International Commission on Radiobiological Protection. ICRU Publication, No. 26, Ann ICRP 1: No 3.

ICRU (1962) *Radiation Quantities and Units*. Report No. 10a, International Commission on Radiation Units and Measurements, Published as National Bureau Standard (U.S., Government Printting Office, Washington, D.C.), Handbook 84.

ICRU (1964) *Physical Aspects of Irradiation*. Report No. 10b, International Commission on Radiation Units and Measurements, Published as National Bureau Standard (US), Handbook 85.

ICRU (1969) *Neutron Fluence, Neutron Spectra and Kerma*. Report No. 13, International Commission on Radiation Units and Measurements, Bethesda, Maryland, U.S.A.

ICRU (1970) *Specification of High Activity Gamma-Ray Sources*. Report No. 18, International Commission on Radiation Units and Measurements, Bethesda, Maryland, U.S.A.

ICRU (1971) *Radiation Protection Instrumentation and Its Applications*. Report No. 20, International Commission on Radiation Units and Measurements, Bethesda, Maryland, U.S.A.

ICRU (1973) *Measurement of Absorbed Dose in a Phantom Irradiated by a Single Beam of X or Gamma Rays*. Report No. 23, International Commission on Radiation Units and Measurements, Bethesda, Maryland, U.S.A.

ICRU (1979) *Average Energy Required to Produced an Ion Pair*. Report No. 31, International Commission on Radiation Units and Measurements, Bethesda, Maryland, U.S.A.

ICRU (1977) *Neutron Dosimetry for Biology and Medicine*. Report No. 26, International Commission on Radiation Units and Measurements, Bethesda, Maryland, U.S.A.

ICRU (1980) *Radiation Quantities and Units*. Report No. 33, International Commission on Radiation Units and Measurements, Bethesda, Maryland, U.S.A.

ICRU (1983) *Microdosimetry*. Report No. 36, International Commission on Radiation Units and Measurements, Bethesda, Maryland, U.S.A.

ICRU (1986) *Quality Factors in Radiation Protection*. Report No. 40, International Commission on Radiation Units and Measurements, Bethesda, Maryland, U.S.A.

IZATT, J. A. and **SCOBIE, J.** (1967) *Characteristics of the UTR-100 Reactor*. **Journal of British Nuclear Energy Society, 6,** 343-353.

JANNI, J. F. (1982) *Proton Range-Energy Tables 1 keV-10 GeV*. **Atomic Data and Nuclear Data Tables, 27,** 147-339.

JUNG, H. and **ZIMMER, K. G.** (1966) *Some Chemical and Biological Effects of Electic Nuclear Collisions*. **Current Topics in Radiation Research, 2,** 69-127.

KAWECKA, B., MORSTIN, K. and **BOOZ, J** (1984) *Optimisation of the Design of Microdosimetric Dose Equivalent Meters*. **Radiation Protection Dosimetry, 9,** 203-206.

KELLERER, A. M. (1970) *Analysis of Patterns of Energy Deposition*. In Proceedings of 2nd. Symposium on Microdosimetry, Report No. EUR 4452, Ebert, H. G., Ed., (EEC, Brussels), pp. 107-134.

KELLERER, A. M. (1971) *Considerations on the Random Traversal of Convex Bodies and Solutions for General Cylinders*. **Radiation Research, 47,**359-376.

KELLERER, A. M. (1976) *A Survey of Approaches to Radiation Biophysics.* In Proceedings of 5th. Symposium on Microdosimetry, Report No. EUR 5452, Booz, J., Ebert, H. G. and Smith, B.G.R. Eds. (CEC, Luxembourg), pp 409-438.

KELLERER, A. M. and **CHMELEVSKY, D.** (1975) *Criteria for the Applicability of LET.* **Radiation Research, 63,** 226-234.

KELLERER, A. M. and **ROSSI, H. H.** (1972) *The Theory of Dual Radiation Action.* **Current Topics in Radiation Research, Quarterly , 8,** 85-158.

KEMSHALL, C. D. BEAUCHAMP, K. G. and **BEJAMIN, P. W.** (1969) *Attenuation of Proportional Counter Pulses by RC Amplifier Time Constants.* **Nuclear Instruments and Methods, 68,** 153-156.

KEY, M. (1971) *Comparative Effects of Neutrons and X-rays on Chinese Hamster Cells.* In Proceedings of Symposium on Biological Aspects of Radiation Quality, Internation Atomic Energy Agency, Vienna, pp. 431-444.

KLIAUGH, P. J. and **DVORAK, R.** (1978) *Microdosemetric Measurements of Ionization by Monoenergetic Photons.* **Radiation Research, 73,** 1-20.

KNOLL, G. F. (1979) *Proportional Counters.* In "***Radiation Detection and Measurement*** ", John Wiley and Sons, New York, pp. 182-217.

KOCHAROV, G. E. and **KOROLEV, G. A.** (1963) *Theory and Operation of Proportional Counters.* Bulletine of Academic of Science of USSR, Physical Series, **27,** 308-314.

KOWALSKI, T. Z. (1985) *Measurement and Parameterisation of Gas Gain in Proportional Counters.* **Nuclear Instruments and Methods in Physics Research, A234,** 521-526.

LINDBLOM, E. and **SAMUELSON, G.** (1981) *Determination of the Quality Factor by the Variance Technique.* In Proceddings of 4th. Symposium on Neutron Dosimetry, Report No. EUR 7448, Burger, G. and Ebert, H. G., Eds., (CEC, Brussels and Luxembourg), pp. 279-288.

LINDHARD, J. and **SCHRAFF, M.** (1961) *Energy Deposition by Ions in the keV Region.* **Physical Review, 124,** 128-130.

LINDHARD, J., SCHARFF, M. and **SCHIOTT, H. E.** (1963) Range Concepts and Heavy Ion Ranges. **Kgl. Danske Videnskab. Selskab, Mat.-Fys. Medd., 33,** no. 14, 39 pp.

MACCABEE, H. D., RAJU, M. R. and **TOBIAS, C. A.** (1968) *Fluctuation of Energy Loss by Heavy Charged Particles in Thin Absorbers.* **Physical Review, 165,** 469-474

MADER, U. (1980) *Chord Length Distributions for Circular Cylinders.* **Radiation Research, 82,** 454-466.

MAIER, E., KNESEWITSCH, P. and **BURGER, G.** (1975) *Mixed Field Dosimetry with Ionization Chambers and Proportional Counters.* In Proceedings of the 2nd. Symposium on Neutron Dosimetry in Biology and Medicine, Report No. EUR 5273, Burger, G. and Ebert, H. G., Eds., (CEC, Luxembourg), pp. 263-304.

MATHIESON, E. and **CHARLES, M. W.** (1969) *Attenuation of Proportional Counter Pulses by Equal Integrating and Differentating Time Constants.* **Nuclear Instruments and Methods, 72,** 155-156.

MENZEL, H. G. (1985) *Practical Implementation of Microdosimetric Counters in Radiation Protections*. In Proceddings of 5th. Symposium on Neutron Dosimetry, Report No. EUR 9762, Schraube, H., Burger, G. and Booz, J. Eds., (CEC, Brussels and Luxembourg) pp. 287-305.

MENZEL, H. G. and **WAKER, A. J.** (1976) *Radiation Quality Studies of a Fast Neutron Threapy Beam.* In Proceedings of 3rd. Symposium on Neutron Dosimetry, Report No. EUR 5452, Booz,J., Ebert, H. G. and Smith, B. G. R. Eds. (CEC, Luxembourg) pp. 591-606.

MILL, A. J. (1986) *Filtered Neutron Beams for Cancer Therapy*. Central Electricity Generating Board (CEGB) **Research**, no. 19, pp. 26-39.

MILL, A. J. and **HARVEY, J. R.** (1978) *Intermediate Energy Neutron Production; A Suevey of Existing Techniques, A Proposed Source and Its Applications*. Central Electricity Generating Board (CEGB) RD/B/N4324, EUR 6107 EN.

MORGAN, K. Z. (1973) *History of Damage and Protection from Ionizing Radiation.* In "***Principle of Radiation Protection*** ", Morgan, K. Z., Turner, J. E., Eds., Robert E. Krieger Publising Co., Huntington, New York, pp 1-75.

MOORHEAD, R. D.(1965) *Stopping Cross Section of Low Atomic Number Materials for He^+, 65-180 keV*. **Journal of Applied Physics, 36,** 391-395.

NCRP (1961) *Measurement of Absorbed Dose of Neutrons, and of Mixtures of Neutrons and Gamma Rays*. National Committee on Radiation Protection and Measurements, NCRP Report No. 25, Published as National Bureau of Standard, Handbook 75, Deprtment of Commerce, Washington, U.S.A.

OLDENBURG, U. and **BOOZ, J.** (1970) *Wall Effects of Spherical Counter*. In Proceedings of 2nd. Symposium on Microdosimetry, Report No. EUR 4452, Ebert, H. G., Ed., (CEC, Brussels), pp. 269-278.

OLDENBURG, U. and **BOOZ, J.** (1971) *A Monte Carlo Analysis of Neutron-Produced Single Event Spectra*. **Biophysik, 8,** 71-80.

OLDENBURG, U. and **BOOZ, J.** (1972) *Mass Stopping Power and Pathlength of Neutron Produced Recoils in Tissue and Tissue Equivalent Materials I. Neutron Energy < 1MeV*. Report No. EUR 4876E (CEC).

ORMROD, J. H. and **DUCKWORTH, H. E.** (1963) *Stopping Cross Sections in Carbon for Low-Energy Atoms with $Z \leq 12$*. **Canadian Journal Of Physics, 41,** 1424-1442.

PHILLIPS, J. A. (1953) *The Energy Loss of Low Energy Protons in Some Gases*. **Physical Review, 90,** 532-536.

PIESCH, E. and **BURGKHARDT, B.** (1981) *Measurement of Stray Neutron Fields in Containment of Nuclear Rectors*. In Proceddings of 4th. Symposium on Neutron Dosimetry, Report No. EUR 7448, Bueger, G. and Ebert, H. G., Eds., (CEC, Brussels and Luxembourg), pp. 549-559.

POWER, D. and **WHALING, W.** (1962) *Range of Heavy Ions in Solids*. **Physical Review, 126,** 61-69.

RAMSEY, W. E. (1940) *Measurements of Discharge Characteristics of Geiger Mueller Counters*. **Physical Review, 57,** 1022-1029.

REYNOLDS, H. K., DUNBAR, D. N. F., WENZEL, W. A. and **WHALING, W.** (1953) *The Stopping Cross Sections of Gases for Protons of 30-600 keV*. **Physical Review, 92,** 742-748.

RICOURT, A., POSNY, F., SOULIE, R., CHEMTOP, M. and **NGUYEN, V. D.** (1981) Possibilitees d'utilidation des techniqus microdosimetrie pour la determination de l'equivalent de dose. In Proceedings of 7th. on Microdosimetry, Report No. EUR 7147, Booz,J., Ebert, H.G. and Hartfiel, H.D., Eds, (CEC, Harwood Academic Publisher, London), pp. 625-636.

RITTS, J.J., SOLOMITO, M. and **STEVENS, P.N.** (1969) Calculation of Neutron Fluence-to-Kerma Factors for Human Body. *Nuclear Applications and Technology* , **7**, 89-99.

RODGER, R.C. and **GROOS, W.** (1974) Microdosimetry of Monoenergetic Neutrons. In Proceedings of 4th. on Microdosimetry, Report No. EUR 5122, Booz, J., Ebert, H.G. and Waker, A., Eds., (CEC, Luxembourg) pp: 1027-1042.

ROSE, M.E. and **KOEFF, S.A.** (1941) The Investigation of Properties of Proportional Counters. *Physical Review* , **59**, 850-859.

ROSSI, B.B. and **STAUB, H.H.** (1949) Ionization Chambers and Counters, McGraw-Hill Book Co., New York.

ROSSI, H.H. (1959) Specification of Radiation Qualiy. *Radiation Research* , **10**, 522-531.

ROSSI, H.H. (1968) Micrscopic Energy Distribution in Irradiated Matter. In " Radiation Dosimetry ", **Vol. 1**, Attix, F.H. and Roesch, W.C. Eds., 2nd. Edition, Academic Press, New York, pp. 43-92.

ROSSI, H.H. (1977) A Proposal for Revision of the Quality Factor. *Radiation and Environment Biophysics* , **14**, 275-283.

ROSSI, H.H., and **FAILLA, G.** (1956) Tissue Equivalent Ionization Chambers. *Nucleonics* , **14**, 32-37.

ROSSI, H.H. and **ROSENWEIG, W.** (1955a) A Device for Measurement of Dose as a Function of Specific Ionization. *Radiology* , **64**, 404-425.

ROSSI, H.H. and **ROSENWEIG, W.** (1955b) Measurement of Neutron Dose as a Function of Lineal Energy Transfer, *Radiation Research* , **2**, 417-425.

ROSSI, H.H., BIAVATI, M.H. and **GROSS, W.** (1961) Local Energy Density in Irradiated Tissues I. Radiobiologocal Significance. *Radiation Research* , **15**, 431-439.

SAION, E.B. and **WATT, D.E.** (1988) Microdosimetry of Intermediate Energy Neutrons in Fast Neutron Fields. *Radiation Protection Dosimetry* , **23**, 265-268.

SAUTER, C.A. and **ZIMMERMANN, E.J.** (1965) Stopping Cross Sections of Carbon and Hydrogen Solids for Low Energy Protons and Helium Ions. *Physical Review* , **140**, A490-A498.

SCHREWE, U.J., PIHET, P. and **MENZEL, H.G.** (1988) On the Calibration of Tissue-Equivalent Proportional Counters with Built-in α-Particles Sources. *Radiation Protection Dosimetry* , **23**, 249-252.

SCHUMMACHER, H., MENZEL, H.G., BUHLER, G. and **ALBERTS, W.G.** (1985) Experimental Basis for Optimization of the Wall Thickness of Microdosimetric Counters in Radiation Protection. *Radiation Protection Dosimetry* , **13**, 341-345.

SCHUMMACHER, H. and **KRAUSS, O.** (1986) *Area Monitoring of Photons and Neutrons from Medical Electron Accelerators Using Tissue-Equivalent Proportional Counters*. **Radiation Protection Dosimetry, 14,** 325-327.

SCHUMMACHER, H., MENZEL, H. G.and **KLUGE, H.** (1987) *Dosimetry of a Bare and D2O Moderated 252Cf Source using Low Pressure Proportional Counters*. **Radiation Protection Dosimetry, 19,** 103-109.

SCHWEAD, P. and **RAY, W. A.** (1960) *Disrtibution of Path Lengths in a Cylindrical Ionization Chamber for a Homogenous Isotopic Flux*. Research Institute of Advance Studies, Baltimore, Maryland, USA.

SHALEV, S. and **HOPSTONE, P.** (1978) *Emprical Expression of Gas Multiplication in ^{3}He Proportional Counters*. **Nuclear Instruments and Methods, 155,** 237-247.

SHONKA, R. F., ROSE, J. E. and **FAILLA, G.** (1958) *Conducting Plastic Equivalent to Tissue, Air and Polystyrene*. Second United Nation International Conference on Peaceful Uses of Atomic Energy, **Vol. 21** (UN, New York) pp. 48.

SMATHERS, J. B., OTTE, V. A., SMITH, A. R., ALMOND, P. R., ATTIX, F. H., SPOKAS, J. J., QUAM, W. M. and **GOODMAN, L. J.** (1977) *Composition of A-150 Tissue Equivalent Plastic*. **Medical Physics, 4,** 74-77.

SRDOC, D. (1970) *Experimental Technique of Measurement of Microscopic Energy Distribution in Irradiated Matter Using Rossi Counters*. **Radiation Research, 43,** 302-319.

SRDOC, D. (1979) *Measurement of the Fano Factor in Tissue Equivalent and Other Gases*. In Radiation Physics, Biophysics and Radiation Biology, Report No. COO-4733-2 (National Technical Information Service, Springfield, Virginia, USA), pp. 58

SRDOC, D. , GOODMAN, L. J., MARINO, S. A., MILLS, R. E., ZAIDER, M. and **ROSSI, H. H.** (1981) *Microdosimetry of Monoenergetic Neutrons Radiation*. In Proceedings of 7th. Symposium on Microdosimetry, Report No. EUR 7147, Booz,J., Ebert, H. G. and Hartfiel, H. D., Eds, (CEC, Harwood Academic Publisher, London), pp. 765-774.

SUTCLIFFE, J. F. and **WATT, D. E.** (1974). *Inactivation cross-sections for ribonuclease irradiated by H, He and H beams at energies less than 10 keV*. In Proceedings of 4th. Symposium on Microdosimetry, Report No. 5122, Booz, J., Ebert, H. G., Eickel, R. and Waker, A., Eds., (CEC, Luxembourg), pp. 477-487.

THWAITES, D. I. and **WATT, D. E.** (1978) *Phase Effects in Stopping Power for Low-Energy Heavy Charged Particles*. In Proceeding of the 6th. Symposium on Microdosimetry, Report no. EUR 6064, Booz, J and Ebert, H. G., Eds., (CEC, Harwood Academic Publisher, London), pp. 777-792.

WAIBEL, E. and **WILLEMS, G.** (1985) *Ionisation Ranges and w Values for Low Energy Protons in Tissue-Equivalent Gas*. **Radiation Protection Dosimetry, 13,** 79-81.

WAKER, A. J. (1988) *Some Electrical and Fabrication Properties of Virgin and Recycled A-150 Tissue Equivalent Plastic*. **Physics in Medicine and Biology, 33,** 157-164.

WATT, D. E. (1967) *Proportional Counter Design in Radiocarbon Dating*. **Nuclear Instruments and Methods, 50,** 353-354.

WATT, D. E. (1972) *Quasi-Elastic Nuclear Interactions in Tissue-Like Media*. **Physics in Medicine and Biology, 17,** 409-415.

WATT, D. E. (1985) *Specification and Measurement of Radiation Effectiveness.* Contract No. B16-A-024-UK, Radiation Protection Research Programe 1985-1989, (CEC) Vol II, July 1987, pp. 56.

WATT, D. E. (1988) *Absolute Biological Effectiveness of Neutrons and Photons.* **Radiation Protection Dosimetry, 23,** 63-67.

WATT, D. E. (1989) *On Absolute Biological Effectiveness and Unified Dosimetry.* **Journal of Radiological Protection, 9,** 33-49.

WATT, D. E., AL-AFFAN, I. A. M., CHEN, C. Z., and **THOMAS, G. E.** (1985) *Identification of Biological Mechanisms of Damage by Ionizing Radiation.* **Radiation Protection Dosimetry, 13,** 285-294.

WATT, D. E. and **RAMSDEN, D.** (1964) *High Sensitive Counting Techniques.* In "*International Series of Monographs on Electronics and Instrumentation*", Pergamon Press, London.

WATT, D. E. and **SUTCLIFFE, J. F.** (1972) *Calculated Stopping Powers, Pathlengths and Projected Ranges of Low Energy Heavy Particles in Soft Tissue and RNA.* In Proceedings of 3rd. Symposium on Microdosimetry, Report No. EUR 4810, Ebert, H. G., Ed., (CEC, Luxembourg), pp. 187-198.

WEYL, P. K. (1953) *The Energy Loss of Hydrogen, Helium, Nitrogen, Neon ions in Gases.* **Physical Review, 91,** 289-296.

WIJNGAARDEN, A. V. and **DUCKWORTH, H. E.** (1962) *Energy Loss in Condensed Matter of ^{1}H and ^{4}He in the Energy Range $4 < E < 30$ keV.* **Canadian Journal of Physics, 40,** 1749-1764.

WILKINSON, D. (1950) *Inization Chambers and Counters,* Cambridge University Press, London.

WILLIAMS, A. and **SARA, R. I.** (1962) *Parameters Affecting the Resolution of Proportional Counter.* **International Journal of Applied Radiation and Isotopes, 13,** 229-238.

WILSON, H. W. (1965) *The Scottish Research Reactor Centre.* **Nature, 205,** 10-14.

WILSON, K. and **EMERY, E. W.** (1968) *Path Length Distributions Within Cylinders of Various Proportions.* In Proceedings of 1st. Symposium on Microdosimetry, Report No. EUR 3747, Ebert, H. G., Ed., (CEC, Luxembourg), pp. 79-89.

YEUNG, T. K. (1981) *Studies in the Energy Loss of Low Energy Ions.* Ph D Thesis, University of Dundee, U.K.

ZAIDER, M. and **BRENNER, D. J.** (1985) *On the Microdosimetric Defination of Quality Factor.* **Radiation Research, 103,** 302-316.

ZASTAWNY, A. (1966) *Gas Amplication in a Proportional Counter with Carbon Dioxide.* **Journal of Scientific Instruments, 43,** 179-181.

ZIEGLER, J. F. (1980) *Stopping Cross-Sections for Energetic Ions in All Elements.* In "*The Stopping and Ranges of Ions in Matter* ", **Vol. 5,** Ziegler, J. F., Ed., Pergamon Press.

ZIEGLER, J. F., BIERSACK, J. P. and **LITTMARK, U.** (1985) *The Stopping and Ranges of Ions in Solids.* In "*The Stopping and Ranges of ions in Matter* ", **Vol. 1,** Ziegelar, J. F., Ed., Pergamon Press, pp. 1-321.